DYNAMIC RESPONSE SENSITIVITY FOR STRUCTURAL CONDITION ASSESSMENT

A Dissertation

by

LU ZHONGRONG

B. Sc., M. Sc.

Submitted to

Department of Civil and Structural Engineering

The Hong Kong Polytechnic University

A thesis submitted in partial fulfillment of the requirements for the

Degree of Doctor of Philosophy

January 2005

STATEMENT OF ORIGINALITY

I hereby declare that this dissertation is my own work and that, to the best of my knowledge and belief, it reproduces no material previously published or written nor material which has been accepted for the award of any other degree or diploma, except where due acknowledgement has been made in the text.

Signed

_____

LU ZHONGRONG

To

My parents,

My wife Huang Min

Abstract of dissertation entitled

DYNAMIC RESPONSE SENSITIVITY FOR STRUCTURAL CONDITION ASSESSMENT

Submitted by

LU ZHONGRONG

For the Degree of Doctor of Philosophy

at the Hong Kong Polytechnic University

January, 2005

ABSTRACT

Assessment of the condition of existing structures is vital for their maintenance and repair. Prestress force has been used widely with long span structure, and it is the most important factor to describe the load-carrying capacity of the structure. Besides, many structural systems are susceptible to damage in their useful lives due to many reasons. A change in the prestress force and structural damages will produce changes in the dynamic characteristics and the dynamic responses of the structure. This is the basis for the vibration-based damage and prestress force identification methods.

In this dissertation, two methods for damage detection are developed. The first method is dynamic response sensitivity-based finite element model updating. Elemental damage is identified from the measured structural dynamic responses. The other approach is parameterization of crack in beam. The parameters of the crack, i.e. the location and the depth of the crack are identified from the measured dynamic structural responses in time domain.

The contributions in this desertation are:

1. Time domain response sensitivity with respect to physical parameters of a structural system is obtained numerically and analytically, and it was used for structural damage detection;

2. Further applications of the dynamic response sensitivity for damage detection are developed, such as structural damage detection taking into account the temperature effect, differentiating different damage types in

structures made of isotropic homogeneous material, prestress force identification and damage detection including the load environment.

3. A method for parameterization of crack in beam is proposed and a method for identifying the crack location and crack depth is developed in time domain using the measured dynamic response;

4. A method for prestress force identification in structures is developed based on modal superposition. The prestress force is identified from the measured dynamic responses of the structure.

PUBLICATIONS ARISING FROM THE WORK

***JOURNAL PAPERS*:**

Lu, Z.R. and Law, S. S. (2004). "System Identification including the Load Environment." *Journal of Applied Mechanics-ASME*, **71**(5), 739-741

Law, S. S., Lu, Z.R. (2005). "Crack Identification in Beam from Dynamic Responses." *Journal of Sound and Vibration*, 285(4-5), 967-987

Law, S. S., Lu, Z.R. (In press). "Time Domain Responses of a Prestressed Beam and Prestress Identification." *Journal of Sound and Vibration*.

Lu, Z.R. and Law, S. S. (Under review). "Numerical Study of Damage Detection by Model Updating with Temperature Effects Removed." *Journal of Sound and Vibration*.

Lu, Z.R. and Law, S. S. (Under review). "Sensitivity of Dynamic Response and its Application in Damage Detection." *Journal of Sound and Vibration.*

Lu, Z.R. and Law, S. S. (Under review). "Force Identification Using Sensitivity in Time Domain." *Journal of Engineering Mechanics-----ASCE*.

Lu, Z.R. and Law, S. S. (Under review). "Simultaneous Identification of System Parameters and Input Force." *Journal of Applied Mechanics-ASME*.

Lu, Z.R. and Law, S. S. (Under review). " Identification of Prestress Force from Measured Structural Responses." *Mechanical Systems and Signal Processing.*

Lu, Z.R. and Law, S.S. (Under review). “Assessment of elemental load resistance from response sensitivity – Part I: Simulations.” *Journal of Engineering Mechanics-----ASCE*.

Lu, Z.R. and Law, S.S. (Under review). “Assessment of elemental load resistance from response sensitivity – Part II: Experimental Verification.” *Journal of Engineering Mechanics-----ASCE*.

Lu, Z.R. and Law, S.S. (Under review). “Dynamic analysis of beam with multiple cracks.” *Computers and Structures.*

***CONFERENCE PAPERS*:**

Law, S. S., Lu, Z.R. (2003). “Study on Different Beam Models in Prestress Force Identification.” *Proceedings of the 10th Asia Pacific Vibration Conference*, Gold Coast, Australia, November 12-14, 2003, pp349-354.

Law, S. S., Lu, Z.R. (2004). “State Space Approach to Calculate Sensitivity of Dynamic Response.” *Proceedings of the 2004 ASME International Mechanical Engineering Congress and Exposition*, Anaheim, California, November 13-19, 2004. Vol. 1.

ACKNOWLEDGEMENTS

I would first like to express my sincerest gratitude and appreciation to Dr. S. S. Law, my chief supervisor, for his guidance, encouragement and kindest friend throughout the course of this research. His valuable suggestions, profound insight and high dedication have been a constant source of inspiration for my study at the Hong Kong Polytechnic University.

I appreciate very much the helpful comments and suggestions from Dr. X. Q. Zhu on the experimental work of this research. I would like to thank Dr. Di. Wu, Dr. Z.Y. Shi, Mr. J.Q. Bu and Miss X.Y. Li for their constructive comments and encouraging discussions.

Special thanks are extended to Mr. T. T. Wai, Mr. H.Y. Yau, Mr. C.W. Liauw and Mr. C.F. Cheung for their assistance in the laboratory work.

I am grateful to the Hong Kong Polytechnic University for the financial support during my graduate study here.

Finally, I would like to express my heartfelt gratitude to my wife, Huang Min for her support, encouragement and patience in these years. Deep gratitude is also devoted to my parents for their constant support and encouragement throughout my study.

TABLE OF CONTENTS

LIST OF FIGURES

LIST OF TABLES

LIST OF NOTATIONS

K = Stiffness matrix of a structure

M = Mass matrix of a structure

C = Damping matrix of a structure

K_g = Geometrical matrix of a structure due to prestress force

k^e = Stiffness matrix of an element

m^e = Mass matrix of an element

ρ = Mass density of material

$F(t)$ = Input excitation force

T = Prestress force

ω_r = r th natural frequency of a structure

λ_r = r th eigenvalue of a structure

$\{\phi\}_r$ = r th mode shape of a structure

Φ = Mode shape matrix of a structure

N = Total number of DOFs in analytical model

NE = Total number of element in a FE model

Q = Total number of measured DOFs

S = Sensitivity matrix

R = General dynamic response

$d(t)$ = Displacement response

$\hat{d}(t)$ = Measured displacement

$\dot{d}(t)$ = Velocity response

$\ddot{d}(t)$ = Acceleration response

$\hat{\ddot{d}}(t)$ = Measured acceleration

$q(t)$ = Modal displacement

$\dot{q}(t)$ = Modal velocity

$\ddot{q}(t)$ = Modal acceleration

$\varepsilon(t)$ = Strain response

$\tilde{\varepsilon}(t)$ = Measured strain

$y(t)$ = Transverse displacement of the beam

$\tilde{y}(t)$ = Measured transverse displacement

$G(t)$ = Orthogonal polynomial function

$\delta(x)$ = Dirac delta function

T_E = Kinetic energy of the system

U_E = Potential energy of the system

W_c = Work done due to viscous damping

$Y(x)$ = Mode shape function

β = Frequency parameter

L = Length of the beam

h_0 = Height of the beam

h_c = Depth of the crack

b = Width of the beam

α_A = Damage index of cross-sectional area

α_E = Damage index of Young's modulus

α_I = Damage index of second moment of area

E = Young's modulus of material

G = Elastic shear modulus of material

A = Area of a frame cross-section or plate

J = Torsional constant of a frame cross-section

I = Moment of inertia of a frame cross-section

v = Poisson’s ratio

Chapter 1

INTRODUCTION

1.1 General Remarks

1.1.1 Background and Motivation of Vibration-Based Damage and Prestress Force Identification

Due to a wide variety of unforeseen conditions and circumstances, it is never possible to design and build a structure that has a zero percentage of probability of failure. Structural aging, environmental conditions, etc. are examples of factors that could affect the reliability and the life of a structure. Regular inspection and condition assessment of engineering structures are necessary so that early detection of any defect can be made and the safety and reliability of the structure can be determined. Early damage detection allows maintenance and repair works to be properly programmed thus minimizing the maintenance cost.

Most systems are subject to damage over their useful lives. Damage may be defined as a change introduced into a system that adversely affects the current or future performance of the system (Doebling et al. 1998). In the past three decades, the research work is focused on identification of damage in structural and mechanical systems in civil, mechanical, and aerospace engineering. Thus, the definition of damage will be confined to the material and/or geometric properties of these systems, including changes to the boundary conditions and system connectivity, which adversely affect the performance of the systems (Farrar et al., 2001).

The increasing interest in monitoring a structure and detecting damage as early as possible results from previous catastrophic failures with great loss of life and property (Lancaster, 2000; Jones, 1998, 2001). Catastrophes due to structural failures, such as the series of Comet I aircraft failures in the 1950s caused by fatigue cracks of the cabin, the capsizing of the Alexander L Kielland rig in 1980 started from fatigue fracture of a brace, the air crash due to in-flight loss of the exterior skin on an Aloha Airlines flight in Hawaii in 1988, focus the public concerns on the safety of structures and mechanical systems. The public concerns, in turn, urge the government for the need of health monitoring the existing but ageing infrastructures. For example, there are over 2500 bridges built in the 1960's and 1970's in the United States, which typically have only two plate girders carrying all the dead and live loads (Drdacky, 1992). It is a real challenge for technology and the economy to monitor them and to carry out proper repair if it is needed.

Visual inspection by an expert has been the only available means of damage detection and structural maintenance during the early years of damage detection. However, many modern structures, such as offshore platforms, long-span bridges and space structures are difficult or inaccessible in their service life. Besides, many failures start from the inside of structural components, thus they cannot be detected by naked eyes at an early damage stage. Therefore, non-destructive evaluation (NDE) techniques are introduced and developed. As we know, most non-destructive damage detection techniques used are local experimental methods, such as acoustic or ultrasonic methods, magnetic field methods, radiography, eddy-current methods, or thermal field methods (Doherty, 1993). All of these experimental techniques require that the location of the damage be known a priori and be readily accessible. Due to these limitations, the application of these methods is far from satisfactory since we are

limited to detect local damage on the surface of the structure and the size of the structure is also practically limited. There is a great need for local damage identification methods that can be applied to complex and large-scale structures. This is the background of vibration-based damage detection that came into being.

The structural damage may be caused by various reasons such as operating loads, impact, fracture, fatigue, corrosion, manufacturing fault etc., in general, producing changes in the structural physical properties (i.e., stiffness, mass, and damping), and these changes will lead to changes in the dynamic characteristics or dynamic response of the structure. This fact has been widely noticed and used by structural engineers for damage detection or health monitoring of a structure. The vibration-based damage detection is found on the basis that the modal parameters (namely frequencies, mode shapes and/or transfer functions, modal damping) are functions of the physical properties of the structure (mass, damping, and stiffness). Recently, with the developments of technology in many areas, such as increase in memory and speed of scientific computing, advances in sensor and experimental techniques, and development of finite element methods, have contributed to the development of the vibration-based damage detection methods.

In recent years, the interest in the safety assessment of existing prestressed concrete bridges increased. Prestress force is introduced to control crack initiation in concrete, to reduce deflections, and to add strength to the prestressed members. Therefore, a substantial difference between the desired and the in-service prestress force can lead to severe and critical serviceability and safety problems (Saiidi et al., 1996; Saiidi et al., 1998). Most concrete bridges consist of prestressed concrete in two predominant construction categories: pre-tensioned and post-tensioned. The bridge deck may lose some of its prestress force due to creep and long period of service under

design or overloaded vehicles. Assessment on the magnitude of the prestress force or the loss of pretress force in the bridge deck is important for its load-carrying capacity assessment. It needs to develop a method that can identify the prestress force or prestress force loss via monitoring changes in dynamic responses.

1.1.2 Vibration-Based Damage and Prestress Force Identification

1.1.2.1 Interpretation of Vibration-Based Damage Detection

In general, the vibration-based damage assessment is an inverse problem to identify the location, pattern and quantity of the loss in system stiffness from the measured structural vibration data. With the discovery of the Fast Fourier Transform (FFT) algorithm (Cooley and Tukey, 1965) and the use of digital computers in laboratory test systems, the development of techniques such as digital signal processing, modal testing and analysis is notably inspired. The advances in these areas in turn allowed researchers to investigate the possibilities for quantitatively measuring the state of a structure by inspecting its vibration characteristics. This encouraging technique has received wide attention throughout the civil, mechanical and aerospace engineering communities due to its potential for solving the aforementioned inaccessibility problem of localized experimental inspection methods. Doebling et al. (1998) provided an excellent summary on research advances in these techniques over the last three decades. A typical scheme of vibration-based non-destructive evaluation procedure is summarized as follows: firstly, the vibration response of the structure is measured. For an ambient vibration test, only the output response of the structure aroused from ambient excitation sources such as wind loads, normal traffic and wave loads is measured. For a forced vibration test, both the input excitation force and output structural response are measured. Secondly, modal analysis is performed to get

modal parameters such as natural frequencies, mode shapes and damping ratios from the measured time histories. Thirdly, a non-destructive detection algorithm is applied to identify damage using the previously estimated modal parameters. An analytical model of the structure and/or its predicted response may also be used as a baseline in the detection process if necessary. Lastly, structural safety and reliability analysis is carried out to direct the future usage of the structure according to the results of damage identification.

1.1.2.2 Four-level Damage Identification

The vibration-based damage detection approaches can be categorized according to various criteria. A well known classification for damage detection methods, proposed by Rytter (1993), defines the following four levels.

- Level 1 (Damage Detection): Determination of the presence of damage in the structure;
- Level 2 (Damage Localization): Level 1 plus determination of the probable location of the damage;
- Level 3 (Damage Quantification): Level 2 plus quantification of the severity of the damage;
- Level 4 (Consequence): Level 3 plus prediction of the remaining useful life of the structure.

The four-level damage identification method provides a sequence to assess the structural damage stage by stage. Since Level 4 prediction requires knowledge associated with other fields such as structural design, fracture mechanics, materials aging studies, and damage mechanism, it is therefore not included in this research.

This dissertation will address only the vibration-based damage identification methods that provide damage information on the first three levels.

1.1.2.3 Linear Damage versus Non-Linear Damage

The damage can be classified as linear or non-linear damage according to its effects on the dynamic response of a structure. A linear damage is defined as the case in which the structure retains its initial linear-elastic property after damage occurrence (Doebling et al., 1998). The damage, in terms of changes in the geometry and/or material properties of the structure, changes the dynamic properties of the structure in a linear or a linear combination manner. Therefore, the response of the damaged structure can still be modeled using linear equations of motion. Up to now, the majority of the research results published in the technical literature address only the linear cases of damage detection.

Non-linear damage is defined as the case when the initially linear-elastic structure behaves in a non-linear manner after the damage has been introduced. (Doebling et al., 1998). These non-linear behaviors in structural response can also be attributed to the changes in geometry and material properties caused by damage. One example of geometrically non-linear damage cases is a crack that subsequently opens and closes under the operating load. Material non-linear damage examples include non-linear behavior exhibited by a damaged concrete beam. If a structure exhibits moderate or severe nonlinearities, conventional damage identification approaches will give results with large error or even wrong results. Some researchers (Topole and Tzvetkova, 1996) try to directly obtain the equations of system physical properties based on the first law of thermodynamics rather than use modal analysis techniques in structural damage prediction. Jin et al. (2000) investigates the possibility of applying an energy

index approach in general nonlinear finite element analysis for damage detection in highway bridge structures. The nonlinear behaviors of the bridges under dynamic loading conditions due to material inelastic deformation and crack damages have been studied. In another study, nonlinear analysis and chaos theory were applied to structural health monitoring (Livingston et al., 2000). Chaotic behavior was observed in the bridge model. They found that the natural frequencies of the structure are not fixed, but wander in time in a characteristic pattern around a central value.

1.1.2.4 Response-Based Approach versus Model-Based Approach

Damage detection using changes in modal data can be classified into two broad categories. The first category is the “response-based approach” in which the loss in stiffness is directly related to the measured modal parameters. Cawley and Adams (1979) proposed a method based on the assumption that the ratio of frequency changes in two modes is related to the location of damage. In this method, theoretical frequency ratios due to damage at different positions on the structure are compared to the measured ones. Salawu (1997b) introduced a global integrity index for detecting damage using a linear combination of the frequencies of both damaged and intact structure. Uzgider et al. (1993) used a technique based on identification of some stiffness parameters by using measured natural frequencies. In their method, vibration modes, for which the stiffness parameters are mostly sensitive, are selected and used to evaluate the magnitude of these parameters. Other applications of the “response-based approach” are due to Zhang et al. (1992, 1993) for detecting structural faults in frame structures and localizing defects in foundation piles. The drawback of most of the methods based on the above approach is that consideration of all possible damage scenarios at different locations on the structure is required. Consequently, excessive computational time is needed especially for large structures.

The second category of damage detection techniques is the “model-based approach” which is based on updating certain physical parameters to get a perfect agreement between the experimentally measured modal parameters and a finite element model. The updated parameters can be interpreted afterwards to evaluate damage and identify its location. Mottershead and James (1997) have used an updating technique to correct the mass and stiffness at the joint of an aluminium space frame. Collins et al. (1972, 1974) have proposed an updating method based on statistical technique. The updated parameters are estimated so that their variance is a minimum. Friswell (1989) has adopted the minimum variance method of Collins et al. (1972, 1974) assuming that the measurement noise and the parameter estimates are not independent. Grossman (1982) has used a penalty function method based on a weighted average of the ratio between the measured and analytical modal data. From a theoretical viewpoint, natural frequencies as well as mode shapes can be used as modal parameters in the updating algorithm. However, in practice the measured mode shapes are normally less accurate than the natural frequencies. Up to 30% measurement error in the eigenvectors may be expected (Dascotte, 1990). On the contrary, the error in the measured natural frequencies is around 1% (Dascotte, 1990). Therefore, the eigenvalues can be used with more confidence than the eigenvectors in the updating procedure. If the quality of the measured mode shapes improves, they can contribute to the updating algorithm more efficiently. Recently, a scanning laser Doppler measurement system (Kochersbergen et al., 1992; Arrunda et al., 1992) has been developed in order to improve the quality of the measured mode shapes.

1.2 Objective and Scope of the Thesis

It is desirable to develop a universal damage detection method that can be successfully used to detect damage in laboratory structure such as truss and frame structures, in practical aerospace and mechanical structures, and further in civil structures such as long-span bridges. And, it is also desirable to develop a robust damage detection method which can be used to classify different types of damage in structural components. Furthermore, it is also preferable to develop a method to identify the prestress force or prestress loss in the prestressed structure.

The primary goal of this dissertation research aims to develop a simple, economical and yet technological feasible vibration-based evaluation procedure to assess damage and prestress force in existing structures using the measured structural dynamic responses. To meet this primary objective, the present thesis aims to complete the following tasks:

1. To develop a methodology of identifying elemental damage using dynamic response;

2. To develop a methodology of identifying structural damage including the load environment;

3. To develop a methodology for damage detection while taking into account the effect of environment, such as temperature difference in the measurements;

4. To develop an approach to identify damage and differentiate the damage type for a structure of isotropic material;

5. To develop a methodology based on sensitivity-based model updating for prestress force identification.

6. To propose a new crack model in beam and to develop a method for identifying the crack location and crack depth in time domain using the measured dynamic response;

7. To develop a methodology of vibration-based prestress force identification in time domain;

8. To developed a methodology of vibration-based prestress force and the moving excitation force(s) identification;

The organization of the remainder of the dissertation is as follows. The literature on the different crack models in beam and damage detection methods developed by various researchers in the past few decades are reviewed and summarized in Chapter Two.

Chapter Three deals with the strategy of structural damage detection from response sensitivity based finite element model updating method. Chapter Four deals with the further application of response sensitivity for damage detection, i.e., damage detection with temperature effect removed, differentiating different damage types in structures, assessment of prestress force and damage detection including the load environment. Chapter Five covers the other developments, i.e. a new crack model in beam is proposed as a delta function in this chapter, a method for identifying the damage location and damage depth is proposed in time domain. A new technique based on modal superposition and optimal technique is proposed to identify prestress force in beam using measured dynamic response in time domain is also included in this chapter.

Conclusions are made for this thesis research and some recommendations for future work are presented in Chapter Six.

Chapter 2

LITERATURE REVIEW

This chapter aims to provide a review on recent research on crack models in beam and recent advances in damage detection methods. As mentioned before, the field of non-destructive damage detection methods is very broad and covers techniques in many engineering disciplines, such as, acoustics, radiology, magnetics, thermodynamics, and structural mechanics. This literature review herein will be limited to methods that estimate damage from the vibration-based approaches. And the literature will also cover vibration-based methods for prestress force identification.

2.1 Crack Modeling in Beam

There are a number of approaches to model cracks in beam structures in the literature. Generally, these methods can be classified into two main groups: the first group is open crack model, in which the crack is assumed to be permanently opened. This crack model mainly falls into three categories: local stiffness reduction, discrete spring models, and crack functions. The second group is opening and closing crack or breathing crack model, in which the crack opens and closes alternately during vibration.

2.1.1 Local Stiffness Reduction

A crack in a structure member introduces a local reduction in stiffness (or local increase in flexibility) that affects its dynamic response. The total flexibility of the cracked region of the structural element was related with the crack stress intensity factor (SIF) (Irwin, 1957; Bueckner, 1958; Westmann and Yang, 1967). The SIFs were obtained in many cases, and a well- founded relationship was discovered between the energy release rate, the SIFs, and the compliance of the cracked member.

Using the fracture mechanics relations between the strain energy release rate, stress intensity factor and the Castigliano theorem, the local flexibility for a cross-section in the crack region is computed as,

$$c = M / \Delta\phi = (6\pi h / bEI) F_I(s) \tag{2-1}$$

where M is the moment acting at the cross-section and $\Delta\phi$ is the relative angle at the cross-section, h is the height , b is the width of the rectangular cross-section, EI is the flexural rigidity, $s=a/h$, a is the crack depth, and

$$F_I(s) = 1.86s^2 - 3.95s^3 + 16.37s^4 + 37.22s^5 + 71.81s^6 + 126.9s^7 + 172s^8 - 144s^9 + 66.6s^{10} \tag{2-2}$$

At present, SIFs have been theoretically obtained for various types of loading and specimen configurations. The formulas for the SIFs as a function of the crack depth can be found in several handbooks (Tada et al., 1985).

Fine-mesh finite element techniques were also used to compute local flexibility of beam type structures (Gudmundson, 1983; Haisty and Springer, 1988; Ostachowicz and Krawczuk, 1990, 1991; Krawczuk and Ostachowicz, 1992, 1993a, 1993b). Qian et al. (1990) derived the stiffness matrix of a beam element with a crack from an integration of the SIFs. A finite element model was established to consider the effect

of crack closure on the modal parameters. Viola et al. (2002) also developed a cracked finite element of a Timoshenko beam.

2.1.2 Discrete Spring Models

There are many existing literatures that model the crack as discrete spring. Gudmundson (1983) used a spring to represent a permanent open crack. Rizos et al. (1990) modeled a beam with an open crack as two undamaged parts connected by a spring. They used the general form of the mode shapes of the two undamaged beams along with the boundary conditions at the crack location to establish equations on either side of the crack. Similar approach was used by Narkis (1994) to relate the natural frequency of the beam with a double-edged crack. The method was extended to a beam later with a series of crack (Shifrin and Ruotolo, 1999). Sundermeyer and Weaver (1995) modeled the crack as a bilinear spring. It showed that the beam was excited at two frequencies simultaneously, and the steady state response signal consists not only of the two driven frequencies, but also a component at a frequency equal to the difference between the two driving frequencies. Ballo (1998) modeled a cracked rotating shaft with a breathing crack as a non-linear spring, but their model was limited to the fundamental mode. The idea of representing a crack as a spring was extended by Neild et al. (2001). The beam was divided into short rigid blocks joined with rotational and transverse springs that represent bending and shear deformation respectively. Any stiffness reduction due to the crack was represented by adjusting the rotational spring stiffness at that position.

2.1.3 Crack Functions

Christides and Barr (1984) developed a cracked Euler-Bernoulli beam theory by deriving the differential equation and associated boundary conditions for a uniform Euler-Bernoulli beam containing one or more pairs of symmetric cracks. Shen and Pierre (1990; 1994) used a two-dimensional finite element approach to determine the parameter that controls the stress concentration profile near the crack tip in the theoretical formulation without experimental verification. The Christides and Barr beam theory is an important step for the development of a rigorous cracked beam vibration theory. However, the assumption of the exponential distribution of the stress field close to the crack is a limitation that can be improved. Chondros et al. (1998) used a similar approach and derived the so called crack functions using fracture mechanics methods. The crack was modeled as a continuous flexibility using the displacement field in the vicinity of the crack. Carneiro and Inman (2002) extended this model to a Timoshenko type cracked beam. Sinha et al. (2002) proposed a simplified crack model in beam structure and used this model to estimate the crack locations and depth by minimizing the difference between the measured and predicted frequencies via model updating method. Abdel et al. (1999) used this approach in reinforced concrete beam. A damage function was presented for damaged concrete beam. This damage function is characterized by three parameters, namely, the length of the damage zone, the magnitude of the damage and the damage pattern. The damage pattern and its magnitude can be successfully determined by updating the three parameters in the inverse problem.

2.1.4 Opening and Closing (Breathing) Crack Model

The non-linearity from a breathing crack has an important effect on the structural health monitoring, and the bilinear stiffness model is the most simple non-linear crack model and it is usually used to model the behavior of the crack opening and closure. A larger stiffness value corresponds to the state of crack closure, and a smaller stiffness value corresponds to crack opening. In fact, partial crack closure often exists due to 1) roughness interference; 2) wedging by corrosion or wear debris; 3) elastic constraint in the wake of the plastic zone. “Breathing” cracks have been investigated by Gudmundson (1983), who studied the effects of closing cracks on the dynamic characteristics of an edge cracked cantilever beam. Later, an experimental work was used to confirm by Ibrahim et al. (1987), who modeled a crack as a bilinear spring. Qian et al. (1990) used a finite element model to analyze the effect of crack closure on the vibration of a beam. The stiffness matrix of the system, derived from the stress intensity factors, was given two values; one for closing crack and the other for open the crack. The sign of stress on the crack faces was used to determine whether the crack was open or closed at each time step. Ostachowz and Krawczuk (1990) studied the influence of a closing crack using a special finite element in the contact area. Shen and Chu (1992) developed a “breathing crack” model, which opens when the normal strain near the crack tip is positive and otherwise when it closes. A more general approach, employing many terms of a Fourier series to simulate the continuous change of stiffness in crack breathing, was proposed by Abraham and Brandon (1995) and Brandon and Abraham (1995). Brandon and Mathias (1998) investigated strongly non-linear displacement by experiments. Brandon et al. (1999) acquired the spectral signatures for open the crack, closing crack and breathing conditions using a pre-loaded cracked cantilever beam in laboratory. Zhang and Testa (1999) investigated the

closure effects of the vibration responses of a fatigue cracked beam using experiments. Kisa and Brandon (2000) developed a finite element scheme for computing the eigen-parameters for a cracked beam for different degrees of closure. Bovsunovsky and Matveev (2000) presented an analytical method to determine the dynamic characteristics of a beam with a closing crack. This method was used to detect the fatigue crack in beam-like structure by Matveev and Bovsunovsky (2002).

2.2 Vibration-Based Damage Detection Methods

2.2.1 Vibration-Based Damage Identification with Model Updating

The approach that solves for the updated matrices by forming a constrained optimization problem based on the equations of motion, the original model and the measured data, is the well-known model updating approach. There is a large amount of literature on damage assessment methods based on the modification of a structural model matrices such as mass, stiffness, and damping to reproduce as closely as possible the measured static or dynamic responses from the data. Comparisons of the updated matrices to those of the original model corresponding to the intact structure give an indication of the location and extent of damage. Many algorithms can be found in the literature, and the differences in the algorithms can be classified as

- Objective functions to be minimized;
- Constraints placed on the problem;
- Numerical method used to implement the optimization.

It should be noted that the model updating algorithms are usually applied in both damage detection applications and model refinement applications in a similar way,

namely, to seek an analytical model that is as close to the real structure as possible. However, considering the difference in application objectives between model improvement and damage detection, attention should be paid to some particular issues for discriminating and relating the usage of model updating methods in the two fields mentioned above.

The purpose of model improvement is to modify the system stiffness, mass matrix and damping parameters of the numerical model so that better agreement between the numerical results and measured data can be obtained. In the construction of the original finite element model, it is usual to make some simplifications and reasonable assumptions. But sometimes, there are small features in the geometric representation of the structure that cannot be modeled in detail by a computational economical finite element mesh, and also, the boundary conditions and joints between components (such as bolted joints, welds, etc.) are hard to be fully understood. In such cases, engineers may, according to their engineering judgments, try to find a compromise with acceptable results. According to Mottershead and Friswell (1993), there are three forms of model errors: 1) model structure errors, which are likely to occur when there is uncertainty concerning the governing physical equations; 2) model parameter errors, which typically include inappropriate boundary conditions and inaccurate assumptions used in order to simplify the model; and 3) model order errors, which often arise when discretizing the complex structures and can result in a model of insufficient order. These model errors may exist only in a few locations or be extensively distributed in the structure (Law et al., 2001).

On the other hand, the damage detection applications aim to identify changes in stiffness, mass and damping matrices due to damage excluding the modeling errors. It is known that the damage only causes loss in local stiffness of the structure. To

distinguish damage from previously mentioned artificial errors in model construction, a good quality original model that accurately represents the structure of intact stage is necessary. Usually, a two-stage damage detection algorithm is adopted, firstly, *a prior* model refinement procedure is conducted to obtain this model by correlating erroneous initial model to the intact structure, and secondly, another model updating process solves subsequently for the updated matrices that correlated to the damaged structure. Comparisons of the updated matrices to the correlated original ones provide an indication of damage location and extent.

The finite element model updating methods, either for model improvement application or for damage detection application, could be generally classified into the following three categories: 1) Optimal matrix updating methods; 2) Eigenstructure assignment methods; and 3) Sensitivity-based updating methods. The following sections review the techniques in these three categories and discuss their applications in damage detection and finite element model improvement.

2.2.1.1 *The Optimal Matrix Updating Methods*

Optimal matrix updating methods include methods that use a closed-form direct solution to find the updated model matrices (stiffness and/or mass) to produce the measured modal data as closely as possible. Several reviews on these methods have been published (Smith and Beattie, 1991; Zimmerman and Smith, 1992; Hemez, 1993). The problem is generally formulated by Lagrange multiplier and penalty-based optimization, which can be expressed as

$$\min_{\Delta M,\Delta C,\Delta K} = \{J(\Delta M,\Delta C,\Delta K) + \lambda R(\Delta M,\Delta C,\Delta K)\} \tag{2-3}$$

where J is the objective function, R is the constrain function, λ is the Lagrange multiplier or penalty constant.

Earlier work on optimal matrix updating using measured modal data was proposed by Rodden (1967), who used the measured vibration modes to determine the structural influential coefficients of an effectively unconstrained structure. Hall (1970) presented an approach to optimize the stiffness matrix by minimizing the least-squares formed difference between the analytical modes and experimental modes based on an assumption that the mass matrix is exact. A similar procedure was given by Ross (1971) and Zak (1983).

Constrained minimization theory has also been applied to the optimal matrix updating algorithms. Brock (1968) presented an approach to optimize linear structural matrices by minimizing modal force errors with a property matrix symmetry constraint, which helps to preserve the reciprocity condition in the updated model. Baruch (1978) made an assumption that the mass matrix is correct and formulated a stiffness optimization method to acquire improved eigenvectors by minimizing the mass-weighted Frobenius norm of perturbations to global modal parameter matrix. Lagrange multipliers are used to enforce the constraints of zero modal force error and stiffness matrix symmetry. Berman (1979) questioned the assumption of the exact mass matrix, and proposed a so-called analytical model improvement (AMI) procedure to adjust the stiffness and mass matrix simultaneously (Berman and Nagy, 1983). In their method, the measured modes, in turn, are treated as exact data and the mass orthogonality constraint is satisfied by using Lagrange multiplier. Based on Baruch and Berman's work, researchers believed that one of three quantities, the analytical mass, stiffness and the measured modes, should be assumed as the reference, and then the other two can be updated. A new class of structural matrix updating methods, named the model-reference-based methods, is subsequently introduced and attracted considerable attention in structural dynamics.

The previous approaches will produce a model where the analytical modes agree exactly with the measured ones. However, Chen (1983) demonstrated the updated mass and stiffness matrices can be dramatically modified, e.g., a stiffness coefficient of zero value in original matrix could be altered to a very large number. The load paths that do not exist in real structure are hence introduced by these undesirable alterations. This is because that the constraints mentioned above still lack adequate mechanism to control parameter changes in the procedure of matrix updating.

Kabe (1985) introduced a method that uses structural connectivity information as constraint to optimally adjust the stiffness matrix. The adjustment is such performed that the percentage change to each stiffness matrix coefficient is minimized. The physical configuration is preserved by keeping the sparsity pattern of the original stiffness matrix and the updated model exactly reproduces the measured modes used. Smith and Beattie (1991) extended Kabe's formulation and solve the problem as the minimization of both the perturbation matrix norm and the modal force error subject to symmetry and sparsity constraints. McGowan et al. (1990) also used structural connectivity information in their stiffness adjustment algorithms applied to damage identification, in which mode shape expansion algorithms are employed to extrapolate the incomplete measured mode shapes to be comparable with analytical predicted modes. Smith (1992) presents an iterative technique to the optimal update problem that enforces the sparsity of the matrix at each iteration. The sparsity is enforced by multiplying each entry in the stiffness update by either one or zero, depending on the correct sparsity pattern.

Zimmerman and Kaouk (1994) noticed the fact that perturbation matrices tend to be of small rank because damage is usually located in a few structural members rather than distributed all over the structure. They presented an algorithm based on the basic

minimum rank perturbation theory (MRPT) that a unique minimum rank matrix solution for an underdetermined structure exists. Further research is extensively conducted by them and their colleagues to extend and improve the algorithm (Kaouk and Zimmerman 1994a, 1994b, 1994c, 1995; Zimmerman et al., 1995).

A method was presented by Doebling (1996) to calculate a minimum-rank update on the elemental parameter vector rather than for the global or elemental stiffness matrices. This method also uses the same basic formulation as the MRPT, which constrains the global stiffness matrix perturbation to be an explicit function of the diagonal elemental stiffness parameter perturbation matrix that preserves the finite element strain-displacement relations. A limitation of this method as with all minimum-rank procedures is that the rank of the perturbation is always equal to the number of modes used in the computation of the modal force error.

The optimal matrix updating methods with constraints based on structural vibration mechanics and physical connectivity may be useful for the model improvement problem to obtain improved modal responses from analytical prediction. However, its capability for damage detection is doubtful. This is because damage typically causes local changes in structural stiffness matrix, whereas the matrix update methods tend to make modification throughout the entire matrices. Therefore, the results of damage identification suffer from a lack of persuasive proves with physical meaning.

2.2.1.2 *The Eigenstructure Assignment Methods*

Another matrix updating method, known as eigenstructure assignment is based on the design of a fictitious controller which would minimize the modal force error. The controller gains are then interpreted as parameter matrix perturbations to the undamaged structural model.

In eigenstructure assignment approaches, the model updating problem is formulated as a closed loop system, in which the state feedback describes the right hand side of the equation of motion in terms of the displacement and velocity variables. The feedback gain matrix is determined so that the output eigenvalues and eigenvectors correlate the measured eigen-data very well. This procedure will result in modifications to the stiffness and damping matrices but the mass matrix remains unchanged. The updated stiffness and damping matrices are given by

$$[K]=[K_A]+[B][G][C_o], \quad [C]=[C_A]+[B][G][C_s] \qquad \textbf{(2-4)}$$

where $[G]$ is the feedback gain matrix determined by the eigenstructure assignment method. $[B]$ is an input distribution matrix which may be chosen arbitrarily. $[K]$ and $[C]$ are the updated stiffness and damping matrices respectively, $[K_A]$ and $[C_A]$ are the orignal stiffness and damping matrices respectively. $[C_o]$ and $[C_s]$ are the matrices relating the outputs and states. Because the obtained correction matrix $[B][G][C_o]$ and $[B][G][C_s]$ are generally non-symmetric, a further process of determining the matrices $[C_o]$ and $[C_s]$ iteratively may be needed until symmetric correction matrices are acquired.

Minas and Inman (1990) proposed two model updating methods based on eigenstructure assignment technique. The first method formulates the problem as a non-linear optimization procedure with enforced symmetry constraint. Both eigenvalues and eigenvectors are assigned to produce the updated stiffness and damping matrices. The second method uses only the eigenvalue information incorporating with a state-space formulation to determine the state matrix. Zimmerman and Widengren (1990) also presented a symmetric eigenstructure assignment approach

in which a generalized algebraic Riccati equation is used to calculate the stiffness and damping correction matrices.

Damage detection by using eigenstructure assignment technique was pioneered by Zimmerman and Kaouk (1992). They used a subspace rotation algorithm to improve the assignability of the eigenvectors and preserve matrix sparsity in the updated model. Lindner and Goff (1993) used an eigenstructure assignment technique to identify the damage coefficient defined for each structural member. A numerical simulation is performed to detect damage in the finite element model of a ten-bay truss structure. Lim (1994, 1995) applied a constrained eigenstructure assignment technique to process the measured incomplete modal data from a twenty-bay planar truss. The feedback gain matrix is diagonalized, and the diagonal members are interpreted as element-level perturbations to the stiffness matrix so that the damage is localized directly.

Lim and Kashangaki (1994) introduced the best achievable eigenvectors into structural damage detection, as a derivative of eigenstructure assignment technique. They chose the control gain matrix that eliminates the modal force errors between the original structural model and the damaged structure. The best achievable eigenvectors, written in terms of measured eigenvectors, are then related to the measured eigenvectors as indicators of damage location. The localized damage is quantified using eigenstructure assignment technique so that the best achievable eigenvectors, intact structural matrices and the control gains satisfy the modal force error equation.

A technique similar to eigenstructure assignment known as FRF assignment is presented by Schulz et al. (1996). The authors formulate the problem as a linear solution for element-level stiffness and mass perturbation factors. They illustrate that using FRF measurements directly to solve the problem is more straightforward than extracting mode shapes. This technique is applied to a finite element model of a bridge

structure. Cobb and Liebst (1997) also presented another eigenstructure assignment-based method for structural damage detection.

2.2.1.3 *The Sensitivity-Based Updating Methods*

Another class of matrix updating methods is based on the solution of a first-order Taylor series that minimizes a function of residual errors caused by structural matrices perturbations. The residual r_i characterising the differences between the damaged and undamaged state can be formulated for real eigenvalues λ_i, time response $d(t)$ or frequency response functions (FRFs, FRF represents the steady state transfer function of a dynamic system and describes the relation between an input and an output as a function of frequency in terms of gain and phase.) $H_{st}(\omega)$, etc., i. e.

$$r_k = w_k(\lambda_i^{dam} - \lambda_i^0) \tag{2-5}$$

$$r_k = w_k(d_i^{dam}(t_j) - d_i^0(t_j)) \tag{2-6}$$

$$r_k = w_k(H_{st}^{dam}(\omega_p) - H_{st}^0(\omega_p)) \tag{2-7}$$

where w_k is an individual weighting factor for the *kth* residual.

A linear or sequentially linearised relation is required of the form

$$\{r\} = [S]\{\Delta p\} \tag{2-8}$$

$\{\Delta p\}$ is the perturbation in the unkowns. Equation (2-8) expresses the effects of parameter changes due to changes of the measured data included in the residual vector. $[S]$ is the sensitivity matrix, which is used here in a general sense. Usually, $[S]$ is calculated from the partial derivatives of residuals with respect to the parameters

$$S_{ij} = \frac{\partial r_i}{\partial p_j} \tag{2-9}$$

An exhaustive classification of various sensitivity-based updating techniques is given by Hemez (1993). Jahn (1948) derived the complete formulae for eigenvalue and eigenvector sensitivities in a first-order Taylor series for a standard eigen-problem. The theory is then extended by Fox and Kappor (1968) in structural dynamics to solve the eigen-derivatives of a generalized symmetric eigen- problem with respect to physical variable changes. Some efforts have been devoted to improve the accuracy of the obtained approximate eigen-sensitivities in case where measurements are incomplete in modal orders (Yu et al., 1996). To essentially avoid such difficulties, Nelson (1976) developed an effective algorithm to compute eigen-derivatives of single mode by just using the modal data of that mode. Considering the difficulty of matrix inverse of system dimension involved with Nelson's method, Lim et al. (1987) proposed an approximate modal method and Ting (1992) suggested an accelerated subspace iteration method to improve computational efficiency. For eigen-sensitivities of repeated modes, discussions and solutions can be referred to the published work by Dailey (1988) and Lee and Jung (1997).

The earliest application of eigen-sensitivity analysis to finite element model updating is proposed by Collins et al. (1974). They generally formulated the inverse problem as a linear approximation below by using the truncated Taylor series of the modal data.

$$\delta\{z\} = [S]\delta\{p\} \qquad \textbf{(2-10)}$$

where $\delta\{p\}$ is the incremental vector to the updating physical parameters, $\delta\{z\}$ is the residual vector of the measured modal data, and $[S]$ is the eigen-sensitivity matrix.

Chen and Garba (1980) then modified the method proposed by Collins by introducing matrix perturbation technique to avoid the eigen-solution required for each

iteration. Zhang et al. (1987) further improved the solution condition of the inverse problem by reducing the number of unknowns through early localization of the significant model errors. Lin et al. (1995) suggested employing both analytical and experimental modal data to calculate the eigen-sensitivities. Such accurately determined eigen-sensitivity coefficients are then used in the classical model updating procedure to overcome the existing difficulties of identifying small magnitude model errors and slow convergence. Jung and Ewins (1992) suggested dividing the model updating procedure into two sessions, with the first session to locate major errors in grouped macro elements, then to refine the analytical model in the second session. Law et al. (2001) applied the super-element modeling technique to improve the finite element model of a bridge deck structure based on a similar consideration. The large number of DOFs in the original analytical model is dramatically reduced and the solution condition is improved.

The major difference between the various sensitivity-based methods is the modal parameters used to estimate the sensitivity matrix. In addition to the most popular natural frequencies and mode shapes, other types of data, e.g., frequency response functions (FRFs), time histories of response, or combination of these, can also be used. Abdel Wahab (2001) presented a damage detection method based on model updating, in which the sensitivity of the natural frequencies, mode shapes and modal curvatures to damage are combined to construct the sensitivity matrix. Fritzen et al. (1998) developed another model updating based damage detection method using the sensitivity of FRFs with respect to damage. The sensitivity of the modal strain energy (MSE) to damage was also derived and used in damage identification (Shi et al., 2000b). The technique was even extended to static data. Sanayei and Onipede (1991) presented an approach for updating the stiffness parameters of FEM using the results

of a static load-displacement test. A sensitivity-based updating scheme of element-level parameters is used to minimize the errors between the applied forces and forces produced by applying the measured displacements to the stiffness matrix. This technique was further extended to sensitivity analysis of static strain by the authors (Sanayei and Saletnik, 1996a, 1996b).

A structural damage detection method through the sensitivity-based finite element model updating procedure was presented by Hemez and Farhat (1995). They formulated the sensitivities at the element level. This allows the identification to focus on the structural members susceptible to damage, thus improves the computational efficiency comparing with the sensitivity analysis in structure level. Fritzen et al. (1998) studied the problem of identifying damage in a rectangular plate and beam structure using sensitivity-based model updating methods. Their discussion focuses on two problems: modeling errors in undamaged finite element model and their influence on damage localization accuracy, and the solution of the ill-posed equation system. A *prior* updating of the analytical model is suggested to improve the robustness of the damage localization procedure. By using a QR orthogonal decomposition algorithm to acquire the accurate solution for the ill-conditioned inverse problem, they made the conclusion that the sensitivity-based model updating methods are, in principle, suitable tools to deal with the problem of damage detection.

2.2.2 Damage Index Methods

Damage index method is another group of damage detection approaches, which utilize modal data (such as natural frequencies, mode shapes, modal damping, etc.) as damage indicators to identify the structural damage location and extent. The methods

are relatively simple and straightforward, but generally they do not provide quantitative information about the structural damage. In many practical applications, however, it is sufficient that the location of damage is indicated and this damage can be further investigated subsequently by visual inspection or other non-destructive test methods for damage quantification.

The existing approaches may be classified into the following categories based on the modal parameters used for the damage location process: 1) damage index based on modal frequency changes; 2) damage index based on mode shape changes; 3) damage index based on mode shape curvatures / strain mode shapes; 4) damage index based on strain energy changes; and 5) damage index based on modal flexibility changes.

2.2.2.1 *Damage Index from Modal Frequency Changes*

In the early stage of modal experiment, the technique and equipment for modal testing is not sophisticated and accurate enough, therefore, the most effective damage detection methods at that time are those using changes in natural frequencies. It is because frequency measurement can be obtained cheaply and reliably. There is a large amount of literature related to damage detection using shifts in vibration frequencies. Salawu (1997a) presented a comprehensive review on the use of modal frequency changes in damage detection.

Cawley and Adams (1979) presented a formulation to detect the possible damage location in composite materials from frequency changes only. In their method, the change in the jth natural frequency of a structure is a function of the damage position vector $\{s\}$ only, but not the damage extent, and the changes in stiffness matrix due to the damage δK so that

$$\delta\omega_j = f\left(\delta K, \{s\}\right) \qquad \textbf{(2-11)}$$

Expanding this function for a little-damaged state ($\delta K \approx 0$), and ignoring the higher order terms, we have

$$\delta\omega_j = f(0,\{s\}) + \delta K \frac{\partial f(0,\{s\})}{\partial(K)} \qquad \textbf{(2-12)}$$

Assuming the extent of damage is independent of frequency, and noticing that $f(0,\{s\}) = 0$ for all possible $\{s\}$ since there is no frequency change without damage, the ratio of the frequency change between two modes j and k is verified to be a function of damage location only

$$\frac{\delta\omega_j}{\delta\omega_k} = \frac{\delta K g_j(\{s\})}{\delta K g_k(\{s\})} = h(\{s\}) \qquad \textbf{(2-13)}$$

Therefore the simulated damage position, from which the analytical predicted ratio $\delta\omega_j / \delta\omega_k$ equals the experimentally measured ratio, is indicated as possible damage site. The formulation does not account for possible case of multiple-damage locations.

Some researchers (Penny et al., 1993; Messina et al., 1996) found the previous method sensitive to measurement errors. Friswell et al. (1994) presented a damage detection method based on a known catalogue of likely damage scenarios. They assume that there exists a precise model of the structure, and compute the ratios of the frequency changes for several lower modes using the model of intact state and all the postulated damage scenarios. The same ratios are also calculated for the inspected structure. A power law relation is used to fit these two sets of values. When damage scenario of the structure lies in the set of assumed damages, the correct type of damage will produce a fit depicted by a unity-slope line. For all other types of damage, the fit will be inexact. Williams et al. (1996) proposed another approach for improving damage localization using natural frequency sensitivity.

Another pattern recognition method for detecting structural defects in frame structures was proposed by Zhang et al. (1992). The method is based on the fact that the ratios of relative change in natural frequency between any two modes is approximately equal to the ratio of the squares of the corresponding modal strain values at the damage position. Since this method is sensitive to experimental and strain analysis errors, two parameters are introduced to control the damage identification process. A similar approach is also applied to detect faults in foundation piles (Zhang et al., 1993).

Messina et al. (1996) proposed a statistical-based assurance criterion from natural frequency change for detecting single damage location. Let $\{\Delta f\}$ be the measured frequency change vector for a structure with a single defect, and $\{\delta f_j\}$ be the theoretical frequency change vector for a damage of a known size at location j, the Damage Location Assurance Criterion (DLAC) for location j can be defined as

$$DLAC(j) = \frac{|\{\Delta f\}^T \cdot \{\delta f_j\}|^2}{(\{\Delta f\}^T \cdot \{\Delta f\}) \cdot (\{\delta f_j\}^T \cdot \{\delta f_j\})} \qquad \textbf{(2-14)}$$

DLAC values lies in the range of 0 to 1. The location j giving the highest DLAC value shows the best match to the measured frequency change pattern and is therefore taken as the predicted damage site. Later, they extended this method to multiple damage detection and introduce two algorithms for quantifying the extent of the damage (Contursi et al., 1998; Messina et al., 1998). The approach, titled the Multiple Damage Location Assurance Criterion (MDLAC), is formulated as

$$MDLAC(\{\delta D\}) = \frac{|\{\Delta f\}^T \cdot \{\delta f(\{\delta D\})\}|^2}{[\{\Delta f\}^T \cdot \{\Delta f\}] \cdot [\{\delta f(\{\delta D\})\}^T \cdot \{\delta f(\{\delta D\})\}]} \qquad \textbf{(2-15)}$$

δD is the perturbation in the stiffness reduction vector. Other approaches using changes in natural frequencies to the forward problem of damage detection include the work reported by Gudmundson (1982), Tracy and Pardoen (1989), and Biswas et al. (1990). The common basis of these methods is that it is required to consider all possible damage scenarios at different locations in the structure. However, the number of combinations of all damage scenarios could be tremendous for a practical structure. Therefore, excessive computational time is needed especially for large-scale structures.

Lifshitz and Rotem (1969) treated the damage detection as an inverse problem so that the damage state parameters are calculated directly from measured frequency changes. It may be reported the first journal article on detect damage via vibration measurements. They found the change in the dynamic modulus, which is related to the frequency change, could be used as an indicator of damage in particle-filled elastomer. The dynamic modulus is computed by using curve fitting of the measured stress-strain relationships at various levels of filling.

Stubbs and Osegueda (1990) developed a method for detecting damage in structure using modal frequency sensitivity based on the work by Cawley and Adams (1979). They assumed that damage occurs at only one member of the structure, and computed an error function for each mode and each structural member based on sensitivity analysis of modal frequency to damage. This method is demonstrated producing more accurate results than their previous methods, and is most useful for skeletal structures where the damage affects one significant stiffness component. However, the accuracy of this method is dependent on the quality of the finite element model (or other analytical model) used to compute the sensitivities.

Salawu (1997b) proposed a global integrity index for detecting reduction or increase in the global stiffness of a structure. The index is obtained from a linear

combination of the frequencies from the undamaged and damaged structures respectively. The method has been successfully applied to assess the integrity of a full-scale concrete highway bridge (Salawu, 1995). Other examples of inverse methods for detecting damage via modal frequency changes are reported by Adams et al. (1978), Wang and Zhang (1987), Hearn and Testa (1991), Koh et al. (1995), Morassi and Rovere (1997).

The advantages of frequency-based damage detection approaches lie in: 1) since the frequency information is independent of the sensor position, few measuring points are required; 2) the resonant frequency has less statistical variation from random error sources than other modal parameters; 3) the methods can be implemented to continuously health monitoring a structure, since usually ambient vibration induced by normal traffic, is sufficient to extract the resonant frequencies.

Because modal frequencies are a global property of the structure, it is not clear that shifts in this parameter can be used to identify more than the mere existence of damage. In other words, the frequencies generally cannot provide spatial information on the structural changes. In the case of a symmetrical structure, the changes in natural frequencies due to damage at two symmetric locations are exactly the same. One may expect that higher modal frequencies are associated with local responses, or that multiple frequency shifts can provide spatial damage information because structural changes at different locations will cause different combination of frequency changes. Unfortunately, there is often insufficient number of frequencies with significant changes to uniquely determine the damage location because of the practical limitations in modal test and analysis involved with excitation, modal density, etc.

2.2.2.2 *Damage Index from Mode Shape Changes*

Mode shapes inherently contain the spatial information about structural changes. With the development of modal testing techniques, many researchers devoted their efforts in detecting damage with measured mode shape information. Many early works are based on direct comparison of mode shapes obtained before and after the structure is damaged.

West (1984), who might be reported the first systematic use of mode shape information for locating structural damages, proposed the Modal Assurance Criteria (MAC) to determine the level of correlation between the modes measured from undamaged and damaged structures. The MAC, generally, is defined as

$$MAC(\phi_r, \phi_s) = \frac{\left|\phi_r^T \phi_s\right|^2}{\phi_r^T \phi_r \phi_s^T \phi_s} \qquad \textbf{(2-16)}$$

where ϕ_r and ϕ_s are any two eigenvectors of a structural system. It stands for correlation level between the two modes on a scale from 0 to 1, with a value of 1 to indicate identical mode shapes and 0 for orthogonal ones. For the application of damage detection, the eigenvectors ϕ_r and ϕ_s are often replaced by a pair of mode shape vectors measured from the structure before and after damage occur. In model updating cases, however, the mode shape pairs respectively from a tested structure and its corresponding analytical model are used instead to calculate the MAC values. In West's method, a structure and its mode shapes are partitioned using sub-structure schemes, and the changes in MAC across the sub-structures are used to localize the structural damage.

Yuen (1985) used finite element analysis to obtain the natural frequencies and the mode shapes of the damaged structure in a numerical study. A systematic approach was used to determine the changes in mode shape due to the presence of structural

damage. The study showed that a normalized set of eigenparameters describing the changes in the fundamental mode shape of the cantilever model possess definitive characteristics with respect to the location and extent of damage.

Fox (1992) showed experimentally that measurement of mode shape changes for a single vibration mode, such as the MAC, are relatively insensitive to the saw cut damage in a beam. This problem could be highlighted if too much data compression is caused due to incomplete measurement. “Node line MAC”, a specific MAC obtained by putting measurement points close to a node for a particular mode, is proposed and found to be a more sensitive indicator of mode shape changes caused by damage. To locate the damage, the relative mode shape changes at node points (in modes that show little change in natural frequencies) are related with the corresponding peak amplitude points (in modes that show relatively large changes in natural frequencies) by a simple graphical comparison method. A method of scaling the relative changes in mode shapes for better damage localization is also proposed by Fox.

As a development to the MAC techniques, Lieven and Ewins (1988) proposed another correlation criteria using mode shape information for damage localization, named the Coordinate Modal Assurance Criterion (COMAC), which is defined as

$$COMAC(k) = \frac{[\sum_{r=1}^{N} \left| \phi_{k,r}^{A} \phi_{k,r}^{B} \right|]^2}{\sum_{r=1}^{N} (\phi_{k,r}^{A})^2 \sum_{r=1}^{N} (\phi_{k,r}^{B})^2} \qquad \textbf{(2-17)}$$

where subscripts k and r stand for coordinate index and mode index respectively, and superscripts A and B indicate the state after and before the structural damage has occurred. This correlation value is related to structural degrees-of-freedom (DOFs) rather than to mode indices and this is obviously more helpful to show the sites of defects in the structure than the MAC.

Mayes (1992) developed a method, known as the Structural Translational and Rotational Error Checking (STRECH) for structural model error localization based on mode shape changes. By taking the relative ratios of modal displacements, the method assesses the accuracy of structural stiffness between two different DOFs in a finite element model. The STRECH method can be applied to model improvement problems, as reported by Mayes, to compare the results from a modal test with the ones of an original finite element model. It can also be used in damage detection cases to compare the results from two tests, which are performed at different stages in the service life of a structure.

Other studies that examine the mode shape changes to identify damage are also briefly reviewed. Skjaeraek et al. (1996) presented a structural damage detection method based on changes in the natural frequencies and mode shapes using a substructure iteration technique. The optimal sensor placement issue for the method is also examined. Cobb and Liebst (1997) and Shi et al. (2000a) separately proposed a sensor location optimization method for their structural damage approaches based on eigenvector sensitivity analysis. Ratcliffe (1997) developed an approach, which uses a finite difference approximation of a Laplacian operator on mode shape measures, to localize the damage in a beam. Other examples primarily focus on the use of MAC and COMAC can be found in reports by Rizos et al. (1990), Kim et al. (1992), Salawu and Williams (1994).

2.2.2.3 *Damage Index from Mode Shape Curvatures / Strain Mode Shapes*

An alternative to using mode shapes to obtain spatial information about changes in structural vibration characteristics is to use mode shape derivatives such as curvatures. The mode shape curvature of a structure can be computed from the modal displacement or accelerations. For beams, plates, and shells, which have a direct

relationship between curvature and bending strain, some researchers also examine the practical possibility to obtain the curvature by measuring strain directly.

Pandey et al. (1991) demonstrated that absolute changes in the mode shape curvatures could be a good damage recognition index for the finite element modeled beam structure. In their method, the curvature values are computed from displacement mode shape using central difference operator. Chance et al. (1994) found that numerically calculated curvature for mode shapes could introduce unacceptable errors. Instead of measuring or computing curvature directly, they used measured strains and achieved dramatic improvement in the results of damage identification.

Measuring the rotation of mode shapes is more difficult than measuring the translational mode shapes in the past. Recently, Abdo and Hori (2002) forecasted that the rotation of mode shapes might be feasible to be measured in the near future, as major advances have been made in the field of structural dynamics and mechanical vibration testing. They investigated the application of the rotation of mode shapes to detect and locate structural damage, and they found it is a sensitive indicator of damage. The study illustrates that the rotation of mode shapes has the ability to localize the damaged region when displacement modes fail.

Despite the advantage of providing spatial information on the structural damage, methods using mode shapes and their derivatives suffer from several drawbacks in practical applications: 1) a large number of measuring points are needed in order to obtain the mode shapes for a complex structure; 2) mode shape measurements are sensitive to random errors and show more statistical variation than resonant frequencies; 3) rotational mode shapes, though more sensitive to structural changes than translational mode shapes, are still difficult to obtain with existing modal test

techniques; 4) the mode shape based methods, especially the curvature techniques, are not generally applicable to a structure of any shape.

2.2.2.4 *Damage Index from Modal Strain Energy Changes*

To further seek an effective approach to localize structural damage, some researchers start to make use of mode shapes correlated with information of finite element model to implement a new damage indicator. Some studies (Chen and Garba, 1988; Kashangaki et al., 1992) illustrated that the strain energy is very useful in identifying structural damage. The general definition of modal strain energy of a structure with respect to the *ith* mode can be expressed as

$$MSE_i = \frac{1}{2}\{\phi\}_i^T K \{\phi\}_i \qquad \textbf{(2-18)}$$

where $\{\phi\}_i$ is the modal displacement shape of the *ith* mode, and K is the stiffness matrix of a structure.

Stubbs et al. (1992) proposed a method based on examining the decrease in modal strain energy between two structural DOFs, as defined by the curvature of the measured mode shapes. Later, Topole and Stubbs (1995) investigated the feasibility of using limited set of modal parameters for structural damage detection. Stubbs and Kim (1996) improved the method by using the modal strain energy to localize and estimate the severity of the damage without baseline modal parameters.

Another development on the use of modal strain energy is presented by Law et al. (1998), named Elemental Energy Quotient (EEQ). The EEQ of the j th element and the r th mode is defined as

$$EEQ_{rj} = \frac{\{\phi\}_r^T k_j^e \{\phi\}_r}{\{\phi\}_r^T m_j^e \{\phi\}_r} \qquad \textbf{(2-19)}$$

where k_j^e is the *j*th elemental stiffness matrix, m_j^e is the *j*th mass matrix. Shi et al. (1998) proposed the concept of the Elemental Modal Strain Energy (EMSE), the MSE of the *jth* element and the *rth* mode before and after the occurrence of damage is defined as

$$MSE_{rj} = \{\phi\}_r^T k_j^e \{\phi\}_r, \quad MSE_{rj}^d = \{\phi_d\}_r^T k_j^e \{\phi_d\}_r \tag{2-20}$$

With damage occurring in an element, the EMSE changes little in the intact elements, but there will be a larger change in the damaged elements. The Modal Strain Energy Change Ratio (MSECR) defined as

$$MSECR_j^r = \frac{\left|MSE_{rj}^d - MSE_{rj}\right|}{MSE_{rj}} \tag{2-21}$$

could be a meaningful indicator for damage localization. The authors also presented two damage quantification algorithms based on sensitivity analysis of MSE (Shi et al., 2000b; Shi et al., 2002).

2.2.2.5 *Damage Index from Modal Flexibility Changes*

Lin (1990) observed that higher modes contribute more to the stiffness matrix of a structure than the lower modes based on governing equations of structural dynamics. Hence, it is needed to measure all the modes of the structure, especially the higher frequency modes in order to obtain a good estimate of the stiffness matrix, or its change as required in damage detection. However, due to practical limitations in experimental modal test, it is much difficult to measure higher frequency response data. To overcome this difficulty, another class of damage detection methods uses flexibility matrix to estimate changes in structural stiffness. Because the flexibility

matrix is the inverse of the stiffness matrix, it is most sensitive to changes in the lower frequency modes of the structure which can be practically measured in test.

Generally the flexibility matrix can be estimated from the mass-normalized measured mode shapes and frequencies. The formulation of the flexibility by this method is called modal flexibility. A commonly accepted feature of modal flexibility, related to vibration-based damage detection, is the fact that modal flexibility can be approximately estimated from a few of lower modes of the structure. As this feature inherently overcomes the shortcoming of mode incompleteness of measured modal data, many research efforts have been conducted on this subject.

Doebling et al. (1996) proposed a technique to estimate unmeasured residual flexibility matrix. The residual flexibility matrix represents the difference between the exact flexibility matrix and the measured dynamic flexibility matrix, which is contributed from modes outside the measured bandwidth. The proposed technique completes the reciprocity of the residual flexibility matrix so that it can be used in computation of measured modal flexibility. It is demonstrated that the introduction of residual flexibility into the computation of the modal flexibility gives a more accurate estimation of the static flexibility matrix, hence improves the results of damage localization.

Raghavendrachar and Aktan (1992) examined the application of modal flexibility for a three span concrete bridge. In their comparison, the modal flexibility is found to be more sensitive to local damages than natural frequencies or mode shapes. Toksoy and Aktan (1995) conducted a modal testing with eleven accelerometers on an existing three-span reinforced concrete bridge. In contrast with frequencies and mode shapes, there are significant differences caused by damage in modal flexibility. Zhao and Dewolf (1999) presented a sensitivity study theoretically comparing the use of natural

frequencies, mode shapes, and modal flexibilities for structural monitoring. The results demonstrate that modal flexibilities are more likely to indicate damage than either the other two.

Pandey and Biswas (1994, 1995) proposed a damage location method based on directly examining the changes in the measured flexibility of the structure. This method is applied to a simple analytical beam model and a wide-flange steel beam. Results from the numerical and experimental examples show that location of the damage could be predicted from a few of the lower modes of the structural vibration. Lu et al. (2002) pointed out that Pandey and Biswas's method is difficult to locate multiple damages, and recommend the modal flexibility curvature for multiple damage localization due to its high sensitivity to closely distributed structural damages.

Zhang and Aktan (1998) studied the modal flexibility and its derivative, called the Uniform Load Surface (ULS), which is defined as the deformed shape of the structure when subjected to a uniform unit load. After investigating their truncation effect and sensitivity to experimental errors, they suggested that ULS has much less truncation effect and is least sensitive to experimental errors, while keeping good sensitivity to local damage. The ULS is calculated using the uniform load flexibilities constructed by summing the columns of the measured flexibility matrix. The ULS curvature is then estimated using a central difference operator and used as an indicator to local damage (Zhang and Aktan, 1995).

Wu and Law (2004a) discussed the damage indices based on changes in modal flexibility, Uniform Load Surface (ULS) and their curvatures and extended to two-dimensional space for localizing damage in plate structures. Furthermore, a new approach to estimate the ULS curvature is proposed based on the Chebyshev

polynomial approximation, instead of commonly used the finite central difference method.

Wu and Law (2004b) extended the previous study on damage localization in plate structures with ULSC index to quantitatively identifying damage with a sensitivity-based method. The Uniform Load Surface (ULS) is obtained from measured incomplete modal data and formulated in the two-dimensional space for a plate structure. For each plate element, a parameter is defined and related to the isotropic reduction in stiffness due to damage. The sensitivity of the ULS curvature with respect to the elemental stiffness parameters is derived analytically. Damage can then be located and quantified from the iteratively updated parameter changes from the intact state to the damaged state.

A model updating method aiming to model error correction is developed based on modal flexibility sensitivity to the elemental generic parameters (Wu and Law, 2004c). The European Space Agency Structure is studied in a numerical example to validate the method. Furthermore, to interpret the physical meaning of generic element parameters, the concept of elemental eigen-parameters is derived from generic element theory. An experiment was carried out to further verify the proposed method in the laboratory (Wu and Law, 2004d).

The main advantage of the methods using modal flexibility attributes to the fact that the flexibility matrix can be approximately synthesized from a few lower natural frequencies and mode shapes. Furthermore, the flexibility matrix is insensitive to mass changes compared to the stiffness matrix (Berman and Flannelly, 1971). Computation of damage index based on modal flexibility is simple, fast and inexpensive through direct comparison of difference in modal flexibility before and after damage without the requirement of an analytical model of the structure. The disadvantage lies in:

modal mass or mass-normalized mode shapes are required to estimate the modal flexibility. Thus, for ambient vibration tests from which the mass-normalized mode shapes cannot be extracted, there is no way to estimate the modal flexibility from the output-only measurements without certain assumptions or approximations.

2.2.3 Non-linear Methods

In contrast with the large amount of literature on linear damage detection methods, non-linear vibrational properties are much less investigated.

Sundermeyer and Weaver (1995) utilize the nonlinear behavior of a breathing crack to detect the existence of the crack. It is illustrated that the predicted steady state response of the cracked beam shows the effect of the opening and closing of the crack and clearly reveals the presence of a bilinear spring even though the difference between the compressive and tensile stiffness is small. The prominence of this non-linear effect is then related to the crack depth and location.

Van De Abeele and De Visscher (2000) studied the amplitude dependency of the dynamic behavior of a gradually damaged reinforced concrete (RC) beam. The non-linearity is quantified as a function of the damage and the proposed nonlinear damage detection method is compared with linear damage assessment approach.

A time stepping model is proposed by Nield (2001) to study the non-linearity in the vibration characteristics. This model is able to include damage in the form of a moment-rotation relationship over the crack region. Beam test showed that there is a change of non-linear behavior with damage. The change is greatest at low damage levels. Four possible non-linear mechanisms are discussed: 1) crack closure leading to a bilinear stiffness mechanism; 2) friction across the crack due to matrix aggregate

interaction; 3) slip between steel and concrete; and 4) the non-linear behavior of concrete in compression.

Owen et al. (2002) states that a suitable phenomenological model for the non-linear behavior assumes that the stiffness transition from open to closed cracks follows a hyperbolic tangent form. The resulting model is used to model the response of RC beams at different damage levels. They found that the cracks do not fully close during the vibration cycle.

Vanlanduit et al. (2002) use vibration characteristics to detect cracks during a fatigue test on a steel bar. To perform this test, an experiment setup is developed to simultaneously estimate static and dynamic response, as well as linear and non-linear vibration features. In this test, it turned out that the non-linear dynamic response is more sensitive to damage than the static non-linear and linear-elastic response. Also a double crack could be detected near fatigue failure using a non-linear identification method.

2.2.4 Review on Time Domain Damage Identification Methods

The damage detection methods reviewed above are all in frequency domain. There are also many publications on damage detection in time domain using structural dynamic response. Seibold and Weinert (1996) proposed a method to localize cracks in rotating machinery based on measured vibrations. This method used a time domain identification algorithm: the Extended Kalman Filter (EKF). The localization is performed by designing a bank of EKFs, in which each filter is tuned to a different damage hyposis. By calculating the probabilities of different hypotheses, the crack can be localized and its depth can be determined.

Majumder and Manohar (2003) proposed a time domain approach for damage detection in bridge structures using ambient vibration data. The vibration induced by a moving vehicle on the bridge is taken to be the excitation force. It was assumed that a validated finite element model for the bridge structure in its undamaged state is available. Alterations to be made to this initial model, to reflect the changes in bridge behaviour due to occurrence of damage, are determined using a time domain approach.

Recently, Shi et al. (2000) and Chen and Li (2004) presented methods to identify structural parameters and input time history simultaneously from output-only measurements. The structural parameters and the input time history are obtained in an iterative manner. Law and Zhu (2004) proposed an approach for damage detection in a concrete bridge structure in time domain. Both the damage and moving vehicular loads are identified successfully.

Ling and Haldar (2004) proposed a system identification procedure for nondestructive damage detection of structures, which is a finite element based time-domain linear system identification technique capable of identifying structures at element level. The proposed algorithm can identify a structure without using input excitation information and can consider both viscous and Rayleigh type proportional damaping in the dynamic model.

2.3 Vibration-Based Prestress Force Identification

In recent years, the interest in the safety assessment of existing prestressed concrete bridges increases. Prestress force is introduced to control crack initiation in concrete, to reduce deflections, and to add strength to the prestressed members. Therefore, a substantial difference between the desired and the in-service prestress force can lead to severe and critical serviceability and safety problems (Saiidi et al.,

1996; Saiidi et al., 1998; Aalami, 2000; Miyamoto et al., 2000). Most concrete bridges consist of prestressed concrete in two predominant construction categories: pre-tensioned and post-tensioned. It is known that the loss of pretress force occurs due to elastic, creep and shrinkage of concrete, steel relaxation, anchorage slip, and frictional loss between tendon and it surrounding materials. And sometimes damage or severing of prestress strands will also cause loss of prestress force. Assessment on the magnitude of the prestress force or the loss of pretress force in the bridge deck is important for its load-carrying capacity assessment. It is desirable to develop a method that can identify the prestress force or prestress force loss via monitoring changes in dynamic responses.

Unless a prestressed structure is instrumented at the time of construction, the existing prestress force cannot be directly measured. Based on previous works, nondestructive evaluation methods using vibration test data can be used to estimate the loss of prestress force in the prestressed structure due to the following reasons: 1) the loss of the prestress force in the structure is related to the change in structural stiffness(Lin, 1963; Saiidi et al., 1994); 2) the loss of prestress force changes vibration characteristics of the structure(Saiidi et al. 1994; Miyamoto et al., 2000); and 3) the change in structural stiffness can be estimated by monitoring the changes in vibration characteristics of the structure(Kim and Stubbs, 1995; Stubbs and Kim, 1996;Kim and Stubbs, 2002; Kim et al., 2003). Miyamoto et al. (2000) studied the behaviour of a beam with unbonded tendons, and a formula was proposed for the prediction of the modal frequency for a given prestress force with laboratory and field test verifications. Saiidi et al, (1994) reported a study with modal frequency due to the prestress force with laboratory test results. Several researchers (Abraham et al, 1995b) tried to predict

the loss of prestress based on a damage index derived from the derivatives of mode shapes without success.

Very recently, Kim et al. (2004) reported a method to identify prestress loss in prestressed concrete (PSC) bridges using modal information. In the method, an analytical model is formulated to estimate changes in natural frequencies of the PSC bridges under various prestress forces. Then an inverse solution algorithm is proposed to detect prestress loss by measuring the changes in natural frequencies.

2.4 Critical Issues and Shortcomings in Existing Methods

Vibration-based structural damage assessment has been an attractive subject in structural engineering for more than two decades. Research in vibration-based damage detection has been rapidly expanding in recently years. All the aforementioned damage detection methods have been studied in details by their authors and achieved their specific objectives either by numerical simulations or experiments on simple structures, e. g. beams, truss structures and planar frames. However, due to many reasons, it is still difficult, sometimes even impossible to apply many of these approaches for damage detection to practical engineering structures, especially for large-scale or complex engineering structures.

It is known that the global dynamic properties of the structure may not be sensitive enough to the local changes in stiffness or mass due to structural damage. This is the first obstacle to prevent vibration-based damage detection methods from successfully applying to engineering problems. Kashangaki et al. (1992) indicated that damage detection is more feasible for the structural members that contribute significantly to the strain energy of the measured modes, but most structural members have only small contributions to the strain energy of a structure. Thus it is difficult to detect local

damage in its early stage or localize small model errors. For instance, Creed (1987) shows that it would be necessary for a natural frequency to change by about 5% for damage to be detected with confidence. However, judging from significant frequency changes alone, one is not sure the existence of damage since frequencies may shift (exceeding 5%) due to other reasons, say, changes in ambient conditions, etc. The modeling errors and measurement errors also play a significant role in vibration-based damage detection. It is noticed that there is usually 1% to 2% errors in measured natural frequencies and up to 30% measurement errors in the mode shapes. This also has adverse effects on the accuracy of the identified results.

Another major problem in damage detection is the reliance on the finite element model. There will undoubtedly be errors even in the model of the undamaged structure. Thus if the measurements on the damaged structures are used to identify damage locations, the methods will have great difficulty in distinguishing between the actual damage sites and the location of errors in the original model. If suitable parameters are not included in to allow for the undamaged model errors, then there will be a systematic error between the model and the data. It is very likely that the original errors in the model will produce frequency changes that are far greater than those produced by the damage. There are two approaches to reducing this problem, but both rely on having measured data from an undamaged structure. The first is to update the finite element model of the undamaged structure to construct a reliable model. The second alternative uses differences between the damaged and undamaged response data in the damage location algorithm. This does rely on the structure not changing, except for the damage, between the two sets of measurements.

The number and location of measurement sensors is another important issue. Many approaches work well in computation simulations but perform poorly due to the

measurement limitations imposed by practical testing. These limitations usually arise, because the number of measurement stations is limited by commercial consideration, and that the rotational DOFs usually cannot be measured, and that some DOFs in the structures are inaccessible. As far as damage index method is concerned, the derived equations can only be used to localize the damage at those measured DOFs or the defects in the structural members connected to them. There is no way to find the faults at other sites of the structure, which are not measured in the test. For the damage detection based on model updating techniques, since the finite element models for modern civil engineering structures, e. g. long-span bridges and tall buildings, involve a large number of DOFs by assembling all the critical and uncritical structural components, the number of DOFs in the model will be much greater than the number of measured DOFs. To deal with the spatially incomplete modal data, the modal reduction or modal expansion techniques are often used. However, when the measured DOFs are far less than the analytical model DOFs, both the techniques lead to remarkable additional errors and seriously degrade the accuracy of damage detection results. In some cases when the number of equations is smaller than that of unknown model parameters, this even results in an ill-conditioned and underdetermined inverse problem, to which one can not find a unique solution.

There is an issue that has received almost no attention in the previous technical literature when applying model updating methods to damage detection problem, which can be generalized as the ability to differentiate the damage patterns and then identify them. The damage may be caused by different factors such as operating loads, impact, fatigue, corrosion, etc., and therefore various damage patterns may occur. Damage of typical patterns, such as crack, delamination and aging, affects the structures'

behaviors very differently. Therefore how to model the damage itself plays a significant role in the detection procedure.

Most of the existing approaches simply limit structural damages as isotropic reduction in local stiffness, usually involving a scalar parameter such as Young's modulus. Subsequently two questions are often asked: where is the location of damage and what is its extent. As this over-simplified model could lead to significant different modal response from the real damaged structure, additional errors is introduced into model updating process and the accuracy of the detection results is decreased subsequently. A more satisfactory procedure to detect damage should orderly answer the following questions: where is the location of damage; what kind of damage it is; then what is its extent. Although some efforts have been made to build a more refined model for damage, such as the crack model in a beam (Christides and Barr, 1984), and to apply the model to damage identification (Sinha et al., 2002), research work in this area is still limited.

One important issue is the dependence on prior analytical models and/or prior test data for the damage detection. Many of the existing algorithms need access to a detailed finite element model of the structure, while others assume that a data set from the undamaged structure is available. Usually, the lack of availability of this type of data makes an approach impractical for certain applications.

An issue that has received almost no attention in the literature is the ability to discriminate changes in the modal properties resulting from occurrence of damage from those resulting from variations in measurements due to changing environmental and/or test conditions and from the repeatability of the test. High level of uncertainty in the measurements will prevent the early damage detection when the damage in the

structure is small. Very few studies report the results of false-positive study, i.e. applying the damage detection method to two sets of data from the undamaged structure to verify that the method does not falsely identify damage. Doebling et al. (1997) and Farrar and Jauregui (1996) have started to examine this issue.

Chapter 3

SENSITIVITY OF DYNAMIC RESPONSE AND ITS APPLICATION IN DAMAGE DETECTION

3.1 Introduction

In recent years, many researchers have presented different methods for damage identification using natural frequencies and mode shapes, including the sensitivity methods (Farhat and Hemez, 1993; Shi et al., 2000; Wu and Law, 2004), optimization methods(Hassiotis and Jeong, 1993), modal residual methods (Kabe, 1985; Lim and Kashangaki, 1994) and modal force error methods (Zimmerman and Kaouk, 1994). More recently, Liu and Chen (2002) presented a computational inverse technique for identifying stiffness distribution in structures using structural dynamics response in the frequency domain, where the sensitivity matrix of displacement amplitude with respect to the stiffness factor was calculated by solving a set of linear algebraic equations.

In the damage identification of structures, the damage parameters are generally related to the stiffness reduction as discussed by Araujo dos Santos et al. (2000), Bicanic and Chen (1997) and Chen and Bicanic (2000). When discretizing the structure into a number of finite elements, the stiffness distribution in the structures can then be expressed in terms of the stiffness parameter. The difficulty in identifying the stiffness parameter lies in the large number of unknowns. When solving an inverse

problem of parameter identification, it is usually formulated as an objective function of a weighted sum of squared difference between the measured value and the corresponding simulated value of the dynamic properties of the structures. The inverse reconstruction can then be solved by means of optimization methods to minimize the objective function. Genetic algorithms (GAs) have been widely used as a searching technique for such non-linear problem. The advantages of GAs lie in, (1) they do not need the sensitivity analysis and initial guess (Cunha et al., 1999; Liu and Chen, 2001); and (2) they converge to the global optimal of the solution. However, the disadvantage of GAs is computationally extensive and they suffer from slow convergence at the later stage due to the nature of random searching. Thus, for problems with large number of parameters to be identified, using GA becomes impractical.

In this chapter, the sensitivity matrices of dynamic responses (displacement, velocity and acceleration) with respect to the elastic modulus are calculated. An error function is defined in a set of non-linear implicit equations of unknown parameters in the form of the difference between the calculated responses and measured dynamic responses of the structure. In the present study, measured displacements and accelerations are used in the identification of the elemental Young's modulus, and penalty function method is used iteratively. After the dynamic responses of the structure are obtained, the sensitivities of the dynamic responses with respect to the unknown parameters are then calculated to form the sensitivity matrix. Computation simulations show the high efficiency and accuracy of the proposed method. Satisfactory results can be obtained even when the measured data is polluted with noise when regularization technique is used in the solution process. A frame structure and the European Space Agency Structure with single and multiple damages are used

as numerical examples to illustrate the proposed method, and it is further verified by experimental results obtained from a free-free supported steel beam in the laboratory.

3.2 Forward Problem

3.2.1 Dynamic Responses of the Structure

For a general finite element model of a linear-elastic time-invariant structure, the dynamic governing equation is given by

$$[M]\{\ddot{d}\}+[C]\{\dot{d}\}+[K]\{d\}=\{F(t)\} \tag{3-1}$$

where [M], [C] and [K] are the system mass, damping and stiffness matrices respectively. As we know, Rayleigh damping is the most popular damping model for structural dynamic analysis. In this thesis, Rayleigh damping model is taken, which is of the form: $[C]=a_1[M]+a_2[K]$, where a_1 and a_2 are constants to be determined from two given damping ratios that corresponding to two unequal frequencies of vibration. If a more accurate estimation of the actual damping is required, a more general form of Rayleigh damping, the Caughey damping model (Bathe, 1982) can be adopted. $\{\ddot{d}\}$, $\{\dot{d}\}$ and $\{d\}$ are the acceleration, velocity and displacement vectors of the structure, $\{F(t)\}$ is the nodal force vector.

For an isotropic elastic material, the elemental stiffness matrix is proportional to the elastic modulus of the material and the geometric coefficient such as the length of the element, cross sectional area, etc., which are usually taken as the unknown parameters to be identified in the inverse problem. The stiffness matrix of the structure is expressed as the summation of the elemental stiffness matrices as,

$$[K] = \sum_{i=1}^{NE} [k]_i^e \tag{3-2}$$

where *NE* is the number of the elements. Damage in the *i*th element is modeled as a reduction in the average elastic modulus E^i. Substituting Equation (3-2) into Equation (3-1), we have

$$[M]\{\ddot{d}\} + [C]\{\dot{d}\} + \sum_{i=1}^{NE} [k]_i^e \{d\} = \{F(t)\} \tag{3-3}$$

The dynamic responses of the structures can be obtained from Equation (3-3) by direct numerical integration method, say, the well-known Newmark-β method.

3.2.2 The Sensitivity of Responses in Time Domain

We can now derive the response sensitivity with respect to the physical parameters. Performing partial differentiations on both sides of Equation (3-3) with respect to the elastic modulus of the *ith* element, we have,

$$[M]\{\frac{\partial \ddot{d}}{\partial E^i}\} + [C]\{\frac{\partial \dot{d}}{\partial E^i}\} + [K]\{\frac{\partial d}{\partial E^i}\} = -\frac{\partial [k]_i^e}{\partial E^i}\{d\} - a_2 \frac{\partial [K]}{\partial E^i}\{\dot{d}\} \quad (i=1,2,\ldots NE) \tag{3-4}$$

where $\{\frac{\partial d}{\partial E^i}\}$,$\{\frac{\partial \dot{d}}{\partial E^i}\}$,$\{\frac{\partial \ddot{d}}{\partial E^i}\}$ are the displacement, velocity and acceleration sensitivities with respect to the unknown parameter. Note that Equation (3-4) is in the same form as Equation (3-3). Since the displacement and velocity responses have been obtained from Equation (3-3), the right hand side of Equation (3-4) serves as the equivalent force input, and similarly, the sensitivities can also be obtained numerically by direct integration. The dynamic response sensitivities of the initial conditions usually vanish this is because the initial conditions are independent of the system parameters. In the case when a structure is suddenly released from a static equilibrium state, the sensitivity of the initial displacement to the elemental Young's modulus

exists, and thus the sensitivity of initial velocity has a non-zero value. In this case, the sensitivity of initial displacement is obtained from the direct differential of the static equilibrium equation.

3.3 Inverse Problem

In the forward analysis, the dynamic responses and their sensitivity with respect to the elastic moduli of a finite element system can be obtained from Equations (3-3) and (3-4) for a given set of parameters E^i ($i=1, 2, \ldots, NE$). In the inverse problem, however, these parameters are required to be identified from the measured responses. In other words, the parameters are chosen to best fit the experiment data. There are in general two ways to fit the data: one is simply using the least-squares method which minimizes the sum of squared errors; the other is the sensitivity-based analysis method which has different formulation for different problems, and it is often obtained approximately by neglecting the higher order of the formulation. The latter approach is adopted in this study. The objective function is defined as

$$g(E) = \sum_{j=1}^{l} \sum_{i=1}^{nt} \{\hat{R}_{ij} - R_{ij}\}^T [W] \{\hat{R}_{ij} - R_{ij}\} \qquad (3\text{-}5)$$

where l is the number of measurement locations, nt is the number of time instances to provide the measured data. $\{E\}$ is the vector of unknown elastic moduli $(E^1, E^2, ..., E^{NE})^T$ to be identified, R is the vector of calculated dynamic response of the structure from a known set of $\{E\}$, which can be displacement response, acceleration response, etc, and $\hat{R}$ is the corresponding vector of measured response. $[W]$ is the weight matrix. In this thesis, it is taken as a unity matrix.

3.3.1 Penalty Function Methods

Penalty function method is generally used for modal sensitivity with a truncated Taylor series expansion in terms of the unknown parameters (Friswell and Mottershead, 1995). The truncated series of the dynamic responses in terms of the stiffness parameter E^i of an element is used to derive the sensitivity-based formulation from the general dynamic responses. The identification problem can be expressed as follows to find the vector $\{E\}$ such that the calculated response best matches the measured response, i.e.

$$[Q]\{R\} = \{\hat{R}\} \tag{3-6}$$

where the selection matrix $[Q]$ is a constant matrix with elements of zeros or ones, matching the degrees-of-freedom corresponding to the measured response components. Vector $\{R\}$ can be obtained from Equation (3-3) for a given set of $\{E\}$.

Let

$$\{\delta z\} = \{\hat{R}\} - [Q]\{R\} = \{\hat{R}\} - \{R_{cal}\} \tag{3-7}$$

In the penalty function method, we have,

$$\{\delta z\} = [S]\{\delta E\} \tag{3-8}$$

where $\{\delta z\}$ is the error in the measured output and $\{\delta E\}$ is the perturbation in the parameters, $[S]$ is the two-dimensional sensitivity matrix which is one of the matrices at time *t* in the three-dimensional sensitivity matrix shown in Figure 3-1. For a finite element model with *NE* elements, the number of unknown elemental elastic modulus is *NE*, and only *NE* equations are needed to solve the parameters. Matrix $[S]$ is on the Parameter-*t* plane in Figure 3-1, and we can select any row of the three-dimensional sensitivity matrix, say, the *i*th row corresponding to the *i*th measurement for the purpose. When writing in full, Equation (3-7) can be written as,

$$\{\delta z\} = \begin{Bmatrix} \hat{R}(t_1) \\ \hat{R}(t_2) \\ \vdots \\ \hat{R}(t_l) \end{Bmatrix} - \begin{Bmatrix} R_{cal}(t_1) \\ R_{cal}(t_2) \\ \vdots \\ R_{cal}(t_l) \end{Bmatrix}$$

with $l \geq NE$ to make sure that the set of equation is over-determined. Equation (3-8) can be solved by the standard simple least-squares methods as follows,

$$\{\delta E\} = [S^T S]^{-1} S^T \{\delta z\} \tag{3-9}$$

or

$$E_{j+1} = E_j + [S_j^T S_j]^{-1} S_j^T (\hat{R} - R_{cal}) \tag{3-10}$$

The subscript "*j*" indicates the iteration number at which the sensitivity matrix is computed.

3.3.2 Regularization

Like many other inverse problems, Equation (3-9) is an ill-conditioned problem. In order to provide bounds to the solution, the damped least-squares method (DLS) (Tikhonov, 1963) is used and singular-value decomposition is used in the pseudo-inverse calculation. Equation (3-9) can be written in the following form in the DLS method:

$$\{\delta E\} = (S^T S + \lambda I)^{-1} S^T \{\delta z\} \tag{3-11}$$

where λ is the non-negative damping coefficient governing the participation of least-squares error in the solution. The solution of Equation (3-11) is equivalent to minimizing the function

$$J(\{\delta E\}, \lambda) = \left\| S\{\delta E\} - \{\delta z\} \right\|^2 + \lambda \left\| \{\delta E\} \right\|^2 \tag{3-12}$$

with the second term in Equation (3-12) provides bounds to the solution. When the parameter λ approaches zero, the estimated vector $\{\delta E\}$ approaches to the solution

obtained from the simple least-squares method. Matlab Regularization toolbox (Hansen, 1992) is used in this thesis to obtain the optimal regularization parameter λ.

3.3.3 Procedure of Iteration

Starting with an initial guess $\{E_0\}$ for the unknown vector *E*, usually, $\{E_0\}$ is taken as the original elemental Young's modulus, the procedure of iteration is given as:

Step 1: Solve Equation (3-3) at the *(k+1)th iteration* with known $\{E_k\}$ for $\{R\}$ and compute the value $\{\delta z_k\}$.

Step 2: Solve Equation (3-4) at the *(k+1)th iteration* with known $\{E_k\}$ for $\{\frac{\partial R}{\partial E^i}\}$ to get the sensitivity matrix.

Step 3: Find E_{k+1} from Equation (3-9) or Equation (3-10).

Step 4: Repeat Steps 1 to 3 until $\left\| \frac{E_{k+1} - E_k}{E_{k+1}} \right\| \le tolerance$. The tolerance equals to 1.0×10^{-8} in this chapter unless otherwise states.

3.4 Numerical Examples

3.4.1 A Plane Frame Structure

A plane frame structure as shown in Figure 3-2 is studied to illustrate the proposed method. It is discretized into eleven Euler beam elements with twelve nodes. The frame is fixed at nodes *1* and *12*. Each node has three degrees-of-freedom. There are eleven unknown elastic moduli in the inverse analysis. The mass density

is $\rho = 2.7 \times 10^3 \ \ kg/m^3$, the original Young's modulus of the material is $E = 69 \times 10^9 \ N/m^2$, the height and width of the frame are respectively 1.2 m and 0.6 m, and the cross-section dimensions are $b = 0.01m$ and $h_0 = 0.02m$ with the second moment of inertia equals $6.67 \times 10^{-9} \ m^4$. The first five natural frequencies of the undamaged frame are 13.095, 57.308, 76.697, 152.410 and 196.485Hz. Rayleigh damping model is taken, in this numerical study, the damping ratios of the first two modes are taken equal to 0.01.

Sinusoidal, impulsive and random excitations are studied to calculate the dynamic responses and their sensitivities with respect to the stiffness parameter of the frame. The sinusoidal force is taken as $F(t) = 10\sin(2\pi ft)$ where f is the frequency of excitation. The force is applied at node *2* along the *x*- direction. The impulsive force is applied at the same node as the sinusoidal force with 0.1 second duration. It is expressed in the following form with a magnitude of 10 *N*.

$$F(t) = \begin{cases} 200(t - 0.05) & 0.05 \le t \le 0.1 \\ 200(0.15 - t) & 0.1 \le t \le 0.15 \end{cases} \tag{3-13}$$

Uniformly distributed random force between +10 *N* and -10 *N* and normal random force between 0 to 10 *N* are also applied separately at node *2* along the *x*-direction.

The response is measured along the *x*-direction at node *9* with a sampling rate of 500 Hz including the first five modes of the structure.

3.4.1.1 *Features of the Response Sensitivities*

Figures 3-3 to 3-8 shows the time histories of the excitation force, the displacement response, its sensitivity, velocity and acceleration response sensitivities with respect to the elastic modulus in element 1 for each type of the forces described above. Since the

magnitudes of all the excitation forces are equal, a comparison of the responses and their sensitivities is possible.

The displacement sensitivity is less noisy than the acceleration sensitivity, while the latter is much larger than the former. The shapes of the three types of sensitivities in time are similar for each type of excitation, but it is different for different excitation. The sensitivities increase with time under excitation in general, except with the impulsive and sinusoidal excitations at 25 Hz where the sensitivities have the largest value at around 1.5s from the beginning of excitation. This observation cannot be explained and is believed to be dependent on the interaction between the excitation and the structural system.

A comparison of the sensitivities shows that sinusoidal excitation at the first modal frequency would give higher sensitivities than random force excitations while those from impulsive excitation exhibit the smallest sensitivity. This may be due to the reason that there is only one impact hit acting on the frame during the time history, while the other excitations acting at the frame during the whole time history. The sensitivities from excitation at lower modal frequency of the structures are larger than those from a higher modal frequency. But the sensitivities from excitation at a lower frequency which is not a modal frequency are very small. These observations show that the sensitivities are dependent somewhat on the displacement response of the structure. This can be further explained from the point of energy input: the most energy is inputted to the structure from the sinusoidal excitation force at the first modal frequency, so the sensitivities are the largest from this excitation; the least energy is inputted from the impulsive force and thus the sensitivities are the smallest.

Figures 3-7 and 3-8 show the sensitivities obtained from random excitations. The sensitivities from the two types of excitation are very similar and they are smaller

compared to those from sinusoidal excitations but they are larger compared to those from the impulsive excitations.

Figure 3-9 gives the displacement sensitivities with respect to damage in elements 3 and 6 of the frame from sinusoidal excitation at the first modal frequency. Damage in element 3, which is vertical, is found to be more significant to the horizontal response at node *9* than element *6* which is horizontal.

3.4.1.2 *Damage Detection Studies*

Several studies of single and multiple damages in the frame are studied and they are shown in Table 3-1. In the present study, the damage is simulated by assuming a reduction in the elastic modulus of an element. Both sinusoidal and impulsive excitations are used for the identification. The impulsive force as shown above but repeating at one second interval is used, while the sinusoidal excitation is defined as $F = 10 sin(12\pi t)$ at a frequency of 6 Hz. The sampling rate is 1000 Hz and 200 time steps are used in the identification. The relative percentage error is defined as following

$$\text{Error}(\%) = \frac{E_{id} - E_{true}}{E_{true}} \times 100\% \qquad (3\text{-}14)$$

and they are shown in Table 3-2 for the following study cases.

Study case 1: Initial finite element model updating

No damage is simulated in the structure, but the initial elastic moduli of all the elements are taken 5% under-estimation from the original value to simulate modeling error in the finite element model. The displacement response collected along the *x*-direction at node *9* is used for the model updating. The solution converges to the true value in 271 iteration steps and 322 iteration steps for both sinusoidal excitation and impulsive excitation respectively with the maximum error of 0.02% and 0.1% for the

sinusoidal and impulsive excitations respectively at element 7 indicating that sinusoidal excitation gives better results. The optimal regularization parameters are $\lambda_{opt} = 7.8\times10^{-15}$ and 2.4×10^{-15} for the two excitation forces respectively. This study shows the accuracy of the proposed approach in the system updating. In the following scenarios, only sinusoidal force is used in the identification.

Study cases 2 and 3: Single damage identification

Single damage in the frame is considered in elements 3 and 6 separately for Study cases 2 and 3 respectively. The same displacement measurement as Study case 1 is used in the identification. The damage magnitude is 20% reduction in the elastic modulus in the Study case 2 and 5% in the Study case 3. The initial guesses on the elastic moduli are taken as the original values. The sinusoidal excitation sensitivity leads to correct elastic modulus in the elements after 22 and 13 iterations with a maximum error of 0.19% at element 9 and 0.1% at element 5 respectively, and the corresponding optimal regularization parameters are $\lambda_{opt} = 8.2\times10^{-15}$ and 8.6×10^{-15} respectively. This indicates the effectiveness of the proposed approach in detecting both small and mediate damages.

Study case 4: Study on the frequency of the excitation force

Here, Study case 2 is re-studied, but the frequency of the sinusoidal force is taken as 25 Hz. The same displacement measurement as Study case 1 is utilized. Under this sinusoidal excitation force, correct elastic modulus in each element is obtained after 24 iterations with a maximum error of 0.15% at element 9, and the corresponding optimal regularization parameter is $\lambda_{opt} = 5.5\times10^{-15}$. This study indicates the frequency of the excitation force has little effect on the damage detection.

Study case 5: Multiple damages identification

Multiple damages in the frame are considered to occur in elements 3 and 6 simultaneously with 20% and 5% reduction in the elastic modulus respectively. The same sinusoidal excitation force as Study case 1 is used and the same displacement measurement as Study case 1 is utilized. Again very good results are obtained after 25 iterations, and Table 3-2 gives the error of identification in all the elements with a maximum error of -0.41% in element 9. The optimal regularization parameter is $\lambda_{opt} = 7.4 \times 10^{-15}$.

Study case 6: Study on different kinds of measurements

This study case gives a comparison of different kinds of measurements on the damage detection. The last Study case is re-studied, but here, acceleration measurement is used. Again very good results are obtained after 18 iterations with a maximum error of 0.13% in element 5. The identified results are also listed in Table 4-2. The optimal regularization parameter is $\lambda_{opt} = 3.0 \times 10^{-10}$. Comparing with the last Study case, this study shows the acceleration measurement seems to give better identification results. This indicates acceleration measurement is more suitable for damage detection for damage detection when there is no measurement noise.

Study case 7: Study on multiple measurements

All the studies above use only one displacement or acceleration measurement. This study aims to discuss the effects of multiple measurements on the results of damage detection. The last Study case is re-studied, but here, two displacement measurements are used. The first one locates at node 9 in global x-direction and the second one locates at node 5 in global y-direction. Better results are obtained in comparison with Study case 5 using only one displacement measurement after 23 iterations with a maximum error of -0.21% in element 9. The identified results are also listed in Table 3-2. The optimal regularization parameter is $\lambda_{opt} = 1.6 \times 10^{-15}$. Comparing with Study

case 5, this study shows two displacement measurements seems to give better identification results with a relative smaller errors in all elements. It is interesting to find that relative identified error reduced about 50%. This indicates that more measurements should be used for practical damage detection to reduce the identification error.

Study case 8: Study on measurement noise

The effect of measurement noise on the identification is studied. A normally distributed random error with zero mean and a unit standard deviation is added to the measured displacement as

$$\hat{d} = d_{cal} + Ep \times N_{oise} \times \mathrm{var}(d_{cal}) \qquad (3\text{-}15)$$

where $\hat{d}$ is the vectors of polluted displacement; E_p is the noise level ; N_{oise} is a standard normal distribution vector with zero mean and unit standard deviation; var(•) is the variance of the time history; d_{cal} is the vector of calculated displacement. Damage Study case 3 is again studied but with 1% and 10% noise included in the measurements. Again satisfactory results are obtained after 32 iterations and 41 iterations for the two noise levels respectively, and the errors of identification are shown in Table 3-2 with a maximum error of 0.7% and 2.5% in elements 8 and 6 respectively for the cases with 1% and 10% noise respectively. The optimal regularization parameter are $\lambda_{opt} = 2.2 \times 10^{-14}$ and 6.3×10^{-14} respectively. Higher relative errors are found in the identified results in comparing with noise free studies.

3.4.2 The European Space Agency Structure

The European Space Agency Structure (ESAS) is studied as another numerical example to validate the effectiveness of the proposed method. The finite element

model (FEM) of the structure ESAS is shown in Figure 3-10. The structure is modeled by 48 frame elements and 44 nodes with three DOFs at each node for the translation and rotational deformations. Each frame element is constructed by integrating an Euler-Bernoulli beam element with a rod element. The modulus of elasticity of material is assumed to be $E = 7.5 \times 10^{10}\ N/m^2$ and the density is $\rho = 2800\, kg/m^3$. The total number of DOFs specified in the analytical finite element model is 132. The first eight natural frequencies of the undamaged ESAS structure are 16.86, 63.13, 80.05, 131.34, 173.33, 196.23, 201.73 and 214.42Hz. Rayleigh damping model is used for constructing the damping matrix and the modal damping ratios of the first two modes are taken as 0.01 and 0.02 respectively.

3.4.2.1 *Damage Detection Studies*

Damage in the structure is introduced as a reduction in the stiffness of individual elements (a reduction of the elastic modulus of material), but the other properties remain unchanged. This damage model agrees with others found in the literature (Zimmerman and Kaouk, 1994; Pandey and Biswas, 1995; Topole and Stubbs, 1995; Messina et al., 1998). Four damage cases are considered and details of the damages are given in Table 3-3.

One sinusoidal force is used to excite the structure and the dynamic responses and their sensitivities with respect to the elemental Young's modulus are calculated by Newmark method. The sinusoidal force is taken as $F = 5000\sin(22\pi t)$. The force is applied at node *26* along the global negative y-direction.

Study case9: Study on Multiple damages near the supports

In this study, two local damages are introduced in elements 1 and 13, which are adjacent to the support of the structure. It is assumed that there is a 10% reduction in Young's modulus in each of these two elements. The sampling rate is 500 Hz.

Acceleration response is used for damage detection and the first five hundred data points are used. Only one accelerometer is used and it locates at the 5^{th} node in the global y-direction. First of all, it is assumed that there is no modeling error in the finite element model. The response of the damaged structure is used as the "measured" response. The local damages are identified from the finite element model updating in an iterative manner as shown in the *Procedure of Iteration* (See Section 3.3.3). The damages are identified after 25 steps of iteration. The optimal regularization parameter is found to be 1.2×10^{-10} . Figure 3-11 shows the identified results. From this figure one can see, the two local damages are identified very accurately with maximum relative error less than 0.1%, while there is no error in all other elements. This shows the efficiency and the accuracy of the proposed method.

Study case10: Study on Sampling Rate

In this study, six local damages are introduced in elements 20, 21, 35, 36, 37 and 40, these six elements are adjacent to each other as Figure 3-10 shows. It is assumed that there is a 10%, 7%, 15%, 10%, 10% and 10% reduction in Young's modulus in these seven elements respectively. This scenario is to simulate damage spreading over several members of the structure. Two sampling rates are studied: (1) 500 Hz, which includes the first 10 modes of the structure; (2) 200 Hz, which includes the first 3 modes. Acceleration response is used for damage detection and the first five hundred data points are used. Two accelerometers are used, the first one locates at the 5^{th} node along the global y- direction, and the second one locates at the 18^{th} node along the global y-direction. The required iteration numbers are 26 and 29 for sampling rates (1) and (2) respectively and the regularization parameters are found to be 1.24×10^{-10} and 1.31×10^{-10} for the two sampling rates respectively. Figure 3-12 shows the identified results. The local damages are identified very accurately with maximum relative error

less than 0.1% in these two cases. This shows the sampling rate has little effect on the accuracy of the identified results.

Study case11: Study on Data Points

Study case 10 is re-examined here. Two more local damages are introduced to the structure in elements 1 and 13 with a 10% reduction in Young's modulus besides the local damages in Study case 10. In this case the sampling rate is 500 Hz. Two different lengths of data are studied: (a) 200 data points; (b) 500 data points. The accelerometers are located at the same places as Study case 10. The required iteration numbers are 27 and 30 for cases (a) and (b) respectively and the regularization parameters are 1.26×10^{-10} and 1.34×10^{-10} respectively. Figure 3-13 shows the identified results. The local damages are identified with a maximum error less than 0.1% in element 12 in cases (a) and (b). This shows the number of data points has little effect on the accuracy of the identified results when it is larger than the number of the unknowns.

Study case12: Study on measurement noise

The last Study case is re-examined here. The sampling rate is 500 Hz and 500 data points are used in the identification. The accelerometers are located at the same places as Study case 10. Two different noise levels are studied: 1% and 10%. The required iteration numbers are 31 and 35 for the cases with 1% and 10% noise level respectively and the regularization parameters are found to be 1.36×10^{-10} and 1.41×10^{-10} respectively. Figure 3-14 shows the identified results. From this figure, one can see that the measured noise has large effect on the identified results in comparison with the noise free studies above. The maximum relative error for 1% noise level is -3% in element 20 and for 10% noise level is 5.1% in element 14. Thus, in real application, the measured noisy data has to be de-noised before it can be used for damage detection.

3.5 Experimental Verification

The proposed method is further verified by experiment on a steel beam conducted in the laboratory. The length, width and height of the beam are respectively 2.1 *m*, 0.025 *m* and 0.019 *m*, and the elastic modulus and mass density of the material are $2.07\times10^{11}\ \ N/m^2$ and $7.83\times10^{3}\ \ kg/m^3$ respectively. The beam is suspended at its two ends as shown in Figure 3-15. It is discretized into twenty Euler beam elements with two degrees-of-freedom at each node. The elastic moduli of all the elements are taken as the unknowns to be identified in the inverse analysis. The first five natural frequencies of the intact beam are 22.87, 62.76, 123.05, 203.24 and 303.45 Hz from modal test of the beam. A sinusoidal force at the frequency of half of the first natural frequency of the beam was applied at the nodal point of the first vibration mode of the beam 480mm from the left free end with an exciter model LDS V450. The lateral acceleration obtained with a B&K 4370 accelerometer at the middle of the beam was used to identify these unknown elastic moduli. The sampling frequency is 2000Hz. Time history of the input sinusoidal force was also recorded as the input force for calculating the numerical response of the beam. Newmark method was used for the numerical solution of the system dynamic equations. Rayleigh damping model is adopted and the modal damping ratios were taken as 0.007 and 0.01 for the first two mode. The acceleration response data of the first second, i. e., 2000 time steps, were used for the damage detection.

In the identification, the high frequency measurement noise in the measured acceleration was removed by using 21-points moving average.

It is known that the finite element modeling error in the intact structure has significant effect on the accuracy of the damage identified results. In most cases, the initial finite element is updated first to obtain a good representation of the intact

structure. Table 3-4 lists the first five frequencies of the intact beam from eigenvalue analysis and the experimental frequencies. From this table, one can see, these two sets of frequencies match each other well, indicates the finite element model of the beam is good enough to use for damage detection.

Study case 13: Experimental study on single damage identification

Two cracks are introduced at 1.66 *m* and 1.72 *m* from the left free end with 3*mm* and 9*mm* crack depth respectively, and they are created using a machine saw with 1.3mm thick cutting blade. Since the two cracks are close to each other and they are in the same element *17* of the finite element model. The crack damage is modeled as a reduction in the flexural rigidity of this element. The measured first five natural frequencies of the damaged beam are 22.74, 61.77, 119.75, 198.49 and 299.5 Hz respectively. The average equivalent damage is calculated as 12.8% reduction in the flexural rigidity of the cracked element by the crack model (Sinha et al. 2002), such that the first five calculated modal frequencies are: 22.71, 62.25, 120.73, 200.55 and 301.37 Hz matching closely with the experimental modal frequencies. The convergence tolerance equals 5.0×10^{-7} in this case and Study case 14.

Good results are obtained after 54 iterations. Errors in the identified results are shown in Table 3-5 with a maximum error of 7.15% at element *17*. The optimal regularization parameter is $\lambda_{opt} = 2.3\times10^{-9}$.

Study case 14: Experimental study on multiple damage identification

The two cracks studied in Study case 13 increase to 12*mm* each. Another two cracks are introduced at 1.49 *m* and 1.52 *m* from the left free end of the beam with 9*mm* and 6*mm* depth respectively. The latter two cracks are in the same element *15*. The first five experimental natural frequencies of the damaged beam are 21.97, 56.58, 110.96, 189.33 and 289.06 Hz. The average equivalent damage is calculated as 37.4%

and 57.6% reduction in the flexural rigidity of the cracked elements 15 and 17 respectively, such that the first five calculated modal frequencies are: 21.96, 56.94, 111.82, 190.01 and 288.33 Hz matching closely with the experimental modal frequencies.

Good results are obtained after 67 iterations of identification. The errors of identification are shown in Table 3-5 with a maximum error of -9.54% at element 17. The corresponding optimal regularization parameter is $\lambda_{opt} = 5.4 \times 10^{-9}$. This experimental work showed that the proposed method is capable to identify multiple damages at close spacing with acceptable errors.

3.6 Comparison with Other Time Domain Approaches

Several other time domain damage detection methods are available in the literature. Seibold and Weinert (1996) developed a method to localize cracks in rotating machinery based on the time domain measurements. This method used a time domain identification algorithm: the Extended Kalman Filter (EKF). The localization is performed by designing a bank of EKFs. By calculating the probabilities of different hypotheses, the crack can be localized and its depth can be determined. In developing a time-domain damage detection algorithm, the incomplete measurements in space and state should be considered in addition to measurement noise. The incompleteness in space occurs when structural responses are not measured at all degrees-of-freedom (Dofs) corresponding to its numerical model. Some algorithms circumvent this diffculty by including the unmeasured dof as system parameters to be estimated in damage detection (Seibold and Weinert 1996). The incompleteness in state also occurs in most dynamic measurements because only one state of acceleration, velocity, or

displacement time history is usually measured. Numerical schemes for integrating or differentiating the measured state vector are applied to compute unmeasured state vectors. Since the numerical schemes naturally develop computational error and amplify noise in measured responses, the most desirable way may be to avoid computing unmeasured responses using measured data in formulating a damage detection algorithm. Cattarius and Inman (1997) proposed a method using time histories of vibration response to detect the presence of damage. The beat phenomenon is used to look for small changes in response frequencies due to the existence of structural damage. This method is limited to detect the existence of damage without knowing the location and extent of the damage.

This chapter presents a new time-domain damage detection algorithm using an output error estimator based on general measurement (displacement, acceleration, etc.). The proposed damage detection algorithm estimates structural parameters through the minimization of an error function defined by the weighted least-squared error between the measured and the calculated dynamic responses. Since the error function is defined only with the time history of acceleration (displacement) measured at a few locations, the algorithm does not require any other measured information other than acceleration (displacement).

In comparison with other time domain damage detection methods, the proposed method has the following advangtages: (1) the number of measurements can be very small; (2) the identification process is fast and the identified results are accurate; (3) the number of identification equation can be adjusted according to the duration of time, this indicates that the identification equation can always be over-determined; (4) several types of measurements can be used for the damage detection, i. e., displacement, acceleration, strain measurement etc, or any combination of these

measurements can be used; (5) only a short duration of dynamic response measurement is needed in the identification; (6) the proposed method has the potential for identifying large number of structural parameters.

3.7 Concluding Remarks

A novel damage identification method based on dynamic response sensitivity is proposed in this chapter. The sensitivity matrices of the dynamic displacement, velocity and acceleration with respect to elemental stiffness parameter are calculated, and they are used in a sensitivity-based method to update the stiffness parameters. This approach only involves measurement error while the different modeling errors of the system can be updated iteratively taking advantage of the plentiful measured data. Although only one response measurement is required for the updating of a large number of system parameters theoretically, and good identified results can be obtained from one measurement, when more measurements are taken in the identification, the identified results can be improved as shown in this chapter. This study also shows that acceleration measurement seems to give better identified results than displacement measurement when there is no measurement noise. Both computation simulations and laboratory work show the high efficiency and accuracy of the proposed method. Satisfactory results can be obtained even when the measured data is polluted with noise when regularization technique is employed in the solution. One limitation of the proposed method in this chapter is that the time history of the excitation force has also to be measured.

Table 3-1–Case studies for plane frame structure

Study Cases	Damage location (Element(s))	Reduction in elastic modulus	Noise	Measurement
1	No damage	Nil	Nil	Displacement
2	3	20%	Nil	Displacement
3	6	5%	Nil	Displacement
4	3	20%	Nil	Displacement
5	3 and6	20% and 5%	Nil	Displacement
6	3 and 6	20% and 5%	Nil	Acceleration
7	3 and 6	20% and 5%	Nil	Displacement
8a	6	5%	1%	Displacement
8b	6	5%	10%	Displacement

Table 3-2– Error (%) in the identified results of Study cases 1 to 8

Study cases	Noise	Error (%) in each element										
		1	2	3	4	5	6	7	8	9	10	11
1a	-	0.0	0.0	0.0	0.0	0.0	0.0	0.02	0.0	0.0	0.0	0.0
1b	-	0.0	0.0	0.0	0.0	0.0	0.0	0.1	0.0	0.0	0.0	0.0
2	-	0.0	0.0	0.0	0.0	0.0	0.0	0.0	0.0	0.19	0.0	0.0
3	-	0.0	0.0	0.0	0.0	0.1	0.0	0.0	0.0	0.0	0.0	0.0
4	-	0.0	0.0	0.0	0.0	0.0	0.0	0.0	0.0	0.15	0.0	0.0
5	-	-0.04	-0.08	0.24	-0.31	0.26	-0.02	0.12	0.25	-0.41	0.13	-0.02
6	-	0.01	-0.02	-0.03	0.01	0.13	-0.01	-0.12	0.01	0.03	0.02	-0.02
7	-	-0.02	-0.04	0.12	-0.16	0.13	-0.01	0.06	0.12	-0.21	0.06	-0.01
8a	1%	-0.06	0.11	0.18	-0.08	-0.07	0.17	-0.14	0.7	-0.03	-0.08	0.06
8b	10%	0.93	1.32	-0.82	1.18	-0.96	2.50	-1.91	1.11	0.85	1.43	-1.05

Note: Case 1a denotes sinusoidal excitation force; Case 1b denotes impulsive excitation force

Table 3-3 –Case studies for ESAS structure

Study Cases	Damage location (Element(s))	Reduction in elastic modulus	Noise	Measurement
9	1 and 13	10%	Nil	Acceleration
10	20, 21, 35, 36, 37, and 40	10%, 7%, 15%, 10%, 10% and 10%	Nil	Acceleration
11	1, 13,20, 21, 35, 36, 37, and 40	10%, 10%, 10%, 7%, 15%, 10%, 10% and 10%	Nil	Acceleration
12	1, 13,20, 21, 35, 36, 37, and 40	10%, 10%, 10%, 7%, 15%, 10%, 10% and 10%	1% and 10%	Acceleration

Table 3-4- The measured and the analytical Natural frequencies (Hz) and the relative error (%) of the steel free-free beam with multiple cracks

Crack Scenarios		Mode				
		1	2	3	4	5
No crack	Experimental	22.87	62.76	123.05	203.24	303.45
	Analytical	22.83/-0.18	62.74/-0.03	123.04/-0.0	203.03/-0.12	302.86/-0.2
Two cracks	Experimental	22.74	61.77	119.75	198.49	299.50
	Analytical	22.71/-0.22	62.25/-0.03	120.73/0.82	200.55/1.04	301.37/0.62
Four cracks	Experimental	21.9 7	56.58	110.96	188.38	289.87
	Analytical	21.96/0.0	56.94/0.64	111.82/0.78	190.01/0.87	288.33/-0.53

Note: •/• denotes the modal frequency/relative error;

Table 3-5– Error (%) in the identified results of Study cases 13 and 14

Study Cases	Error (%) in each element																			
	1	**2**	**3**	**4**	**5**	**6**	**7**	**8**	**9**	**10**	**11**	**12**	**13**	**14**	**15**	**16**	**17**	**18**	**19**	**20**
13	**2.32**	**3.24**	**-2.22**	**-3.43**	**-4.01**	**2.61**	**3.15**	**-3.08**	**-1.03**	**-2.47**	**-3.55**	**-4.21**	**3.45**	**2.21**	**-1.59**	**-4.35**	**7.15**	**-5.03**	**3.37**	**3.45**
14	**4.13**	**3.61**	**-4.24**	**3.64**	**4.83**	**3.67**	**5.62**	**-4.33**	**-2.58**	**-3.83**	**-2.76**	**-4.68**	**5.73**	**4.54**	**-6.81**	**5.42**	**-9.54**	**6.11**	**-4.83**	**-1.07**

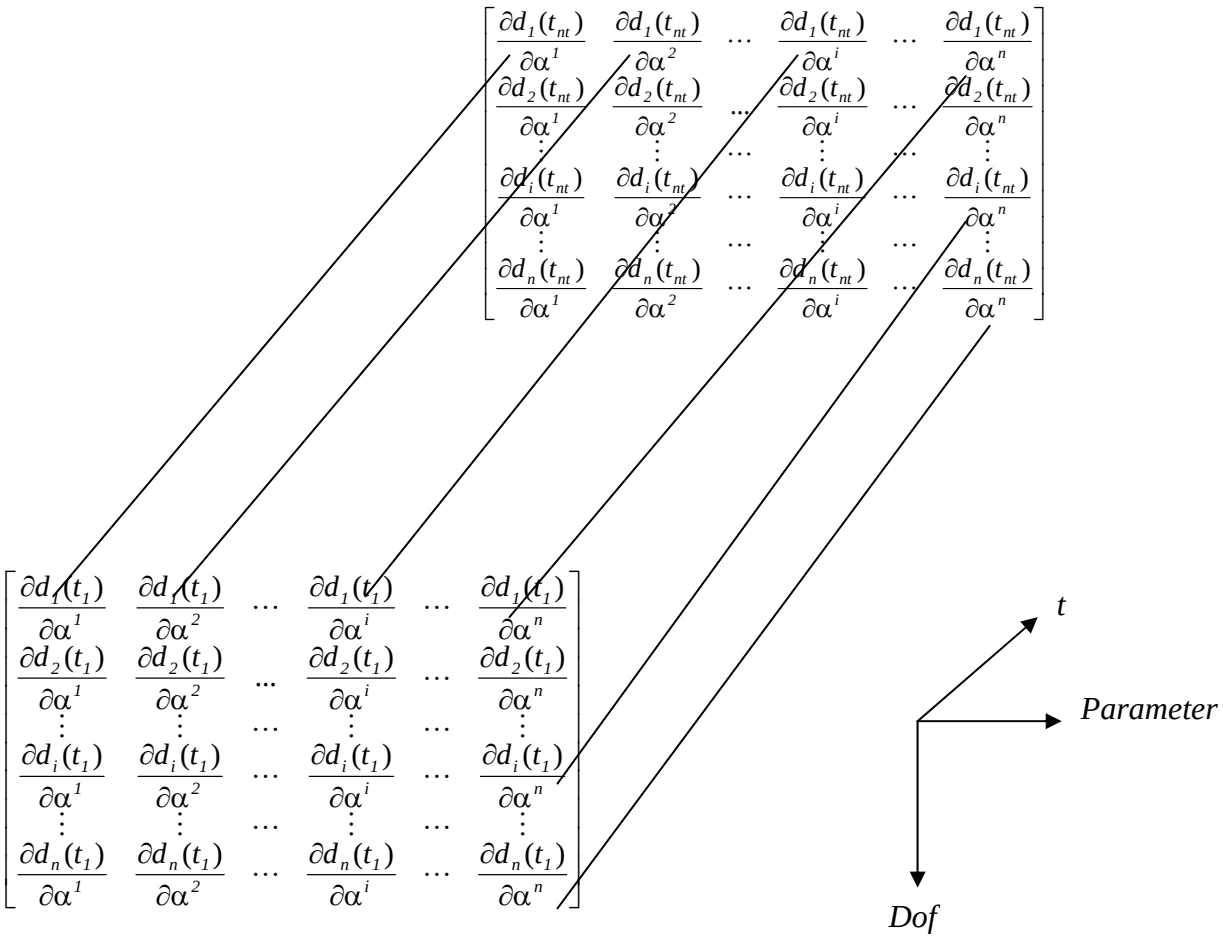

Figure 3-1- Three-dimensional sensitivity matrix

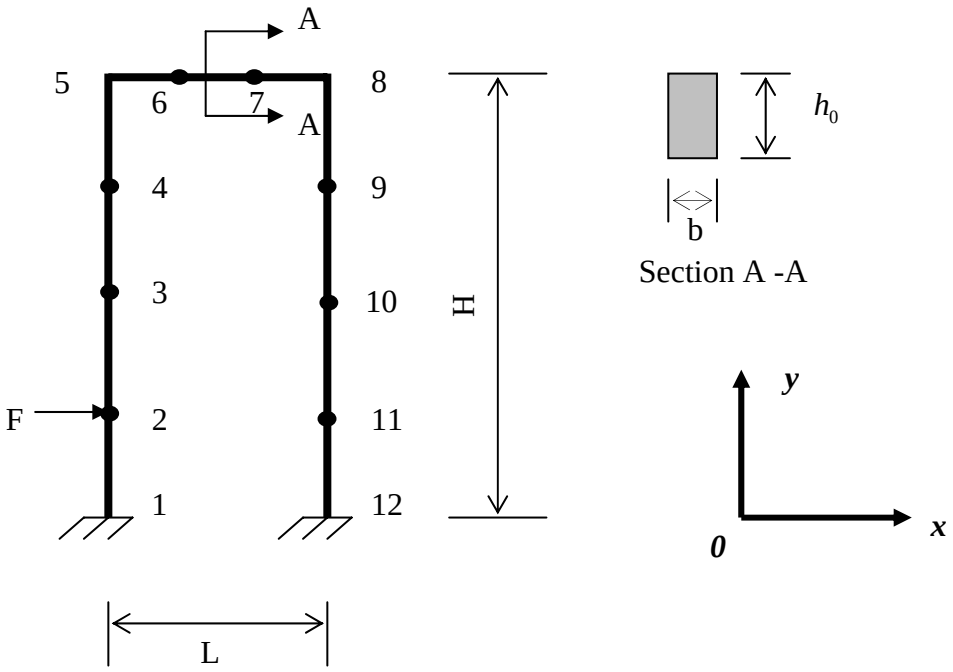

Figure 3-2- The plane frame structure

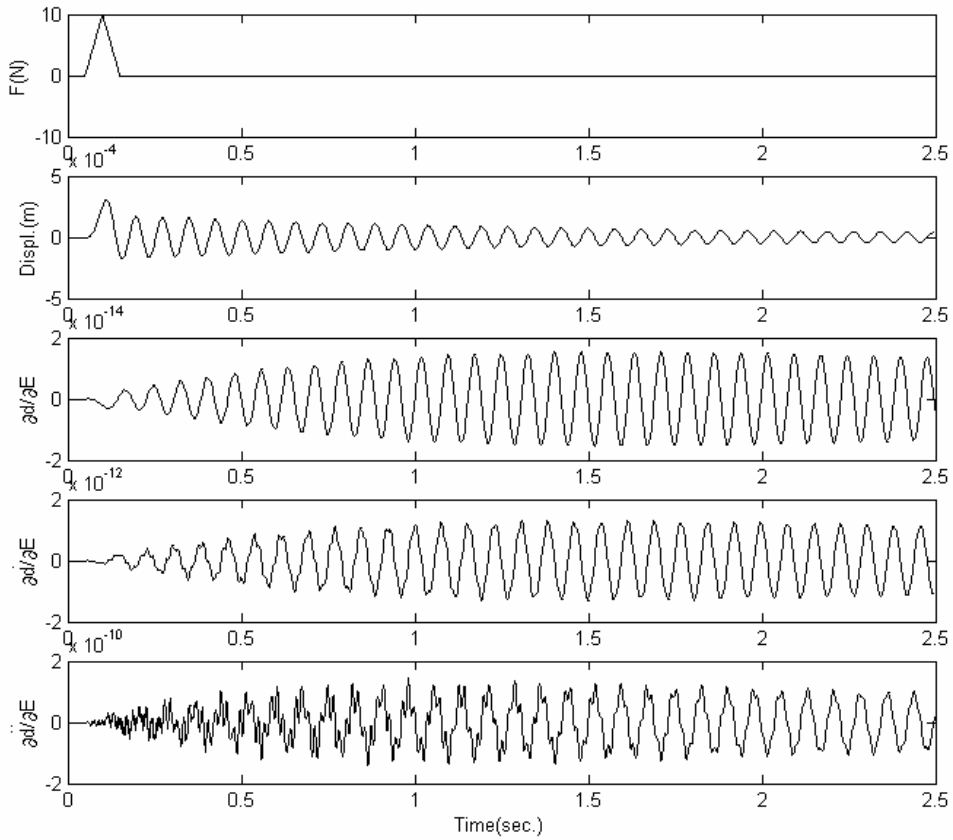

Figure 3-3- Response sensitivity from impulsive force

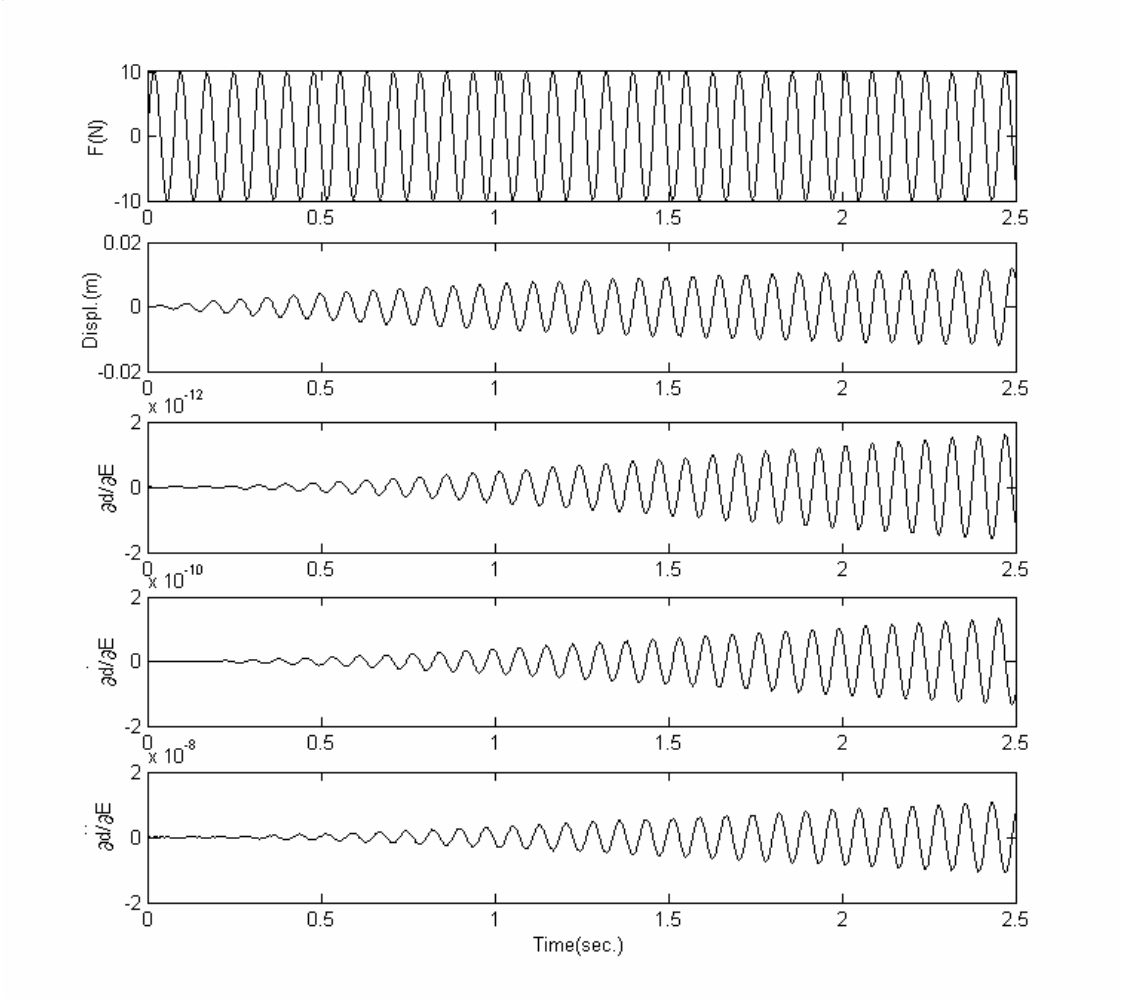

Figure 3-4- Response Sensitivity from sinusoidal force at the 1st natural frequency of the frame

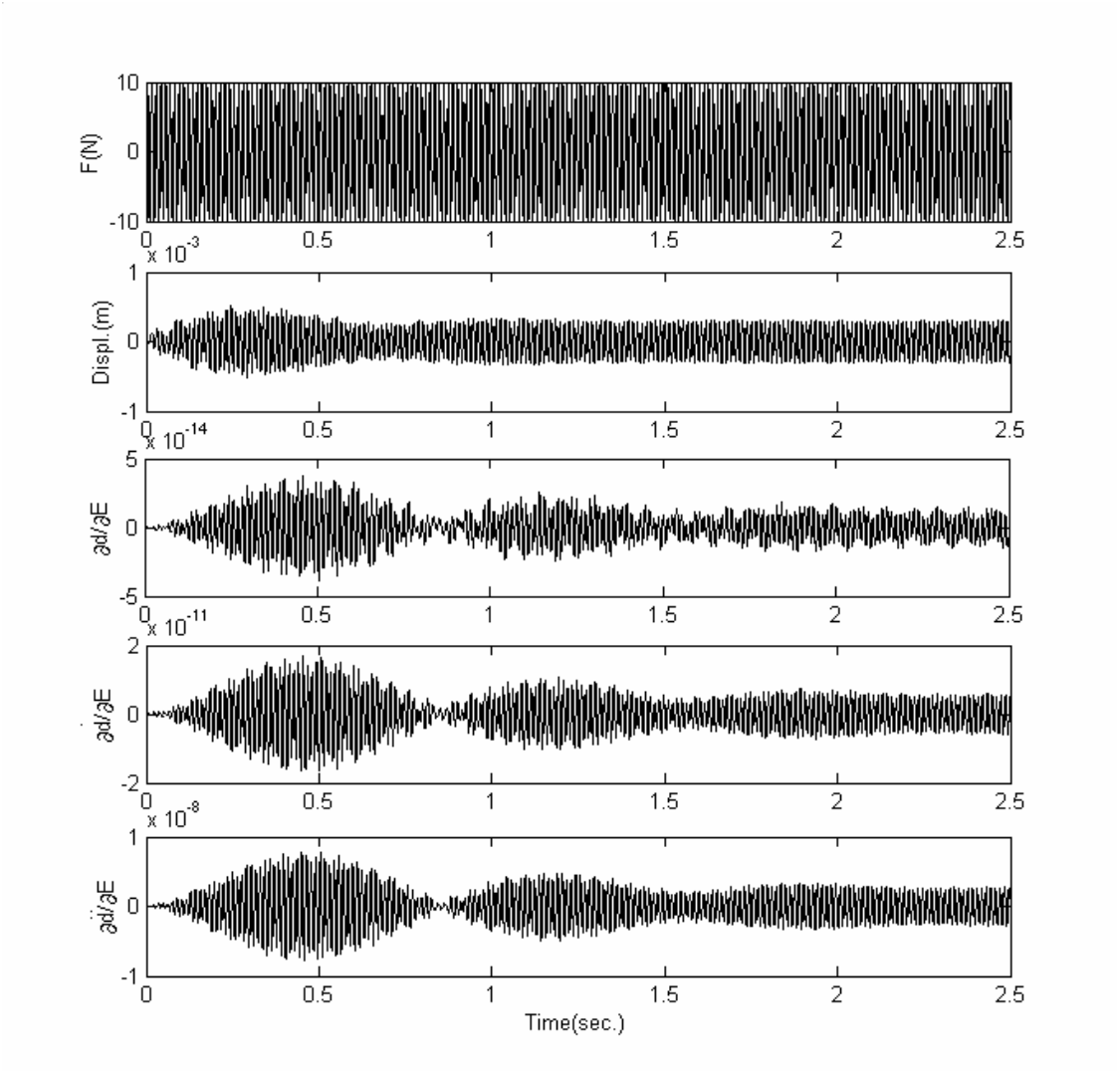

Figure 3-5- Response Sensitivity from sinusoidal force at the 3rd natural frequency of the frame

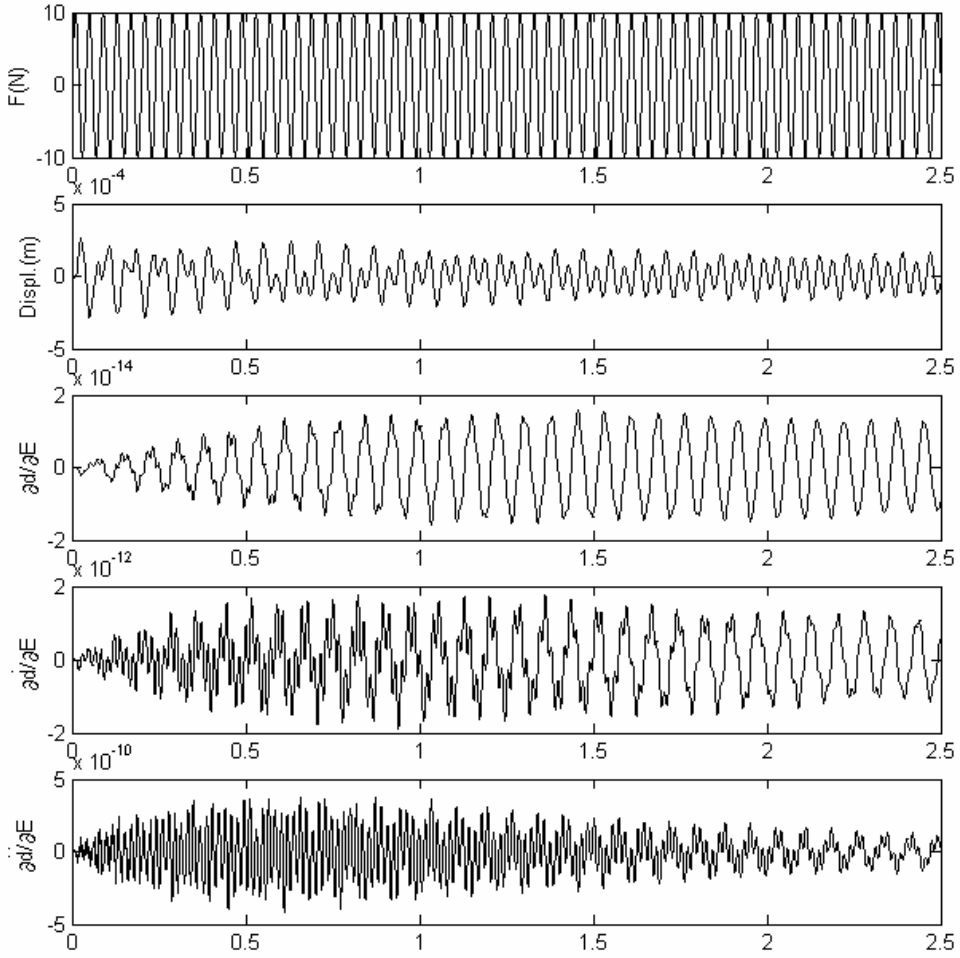

Figure 3-6- Response sensitivity from sinusoidal force at 25 Hz

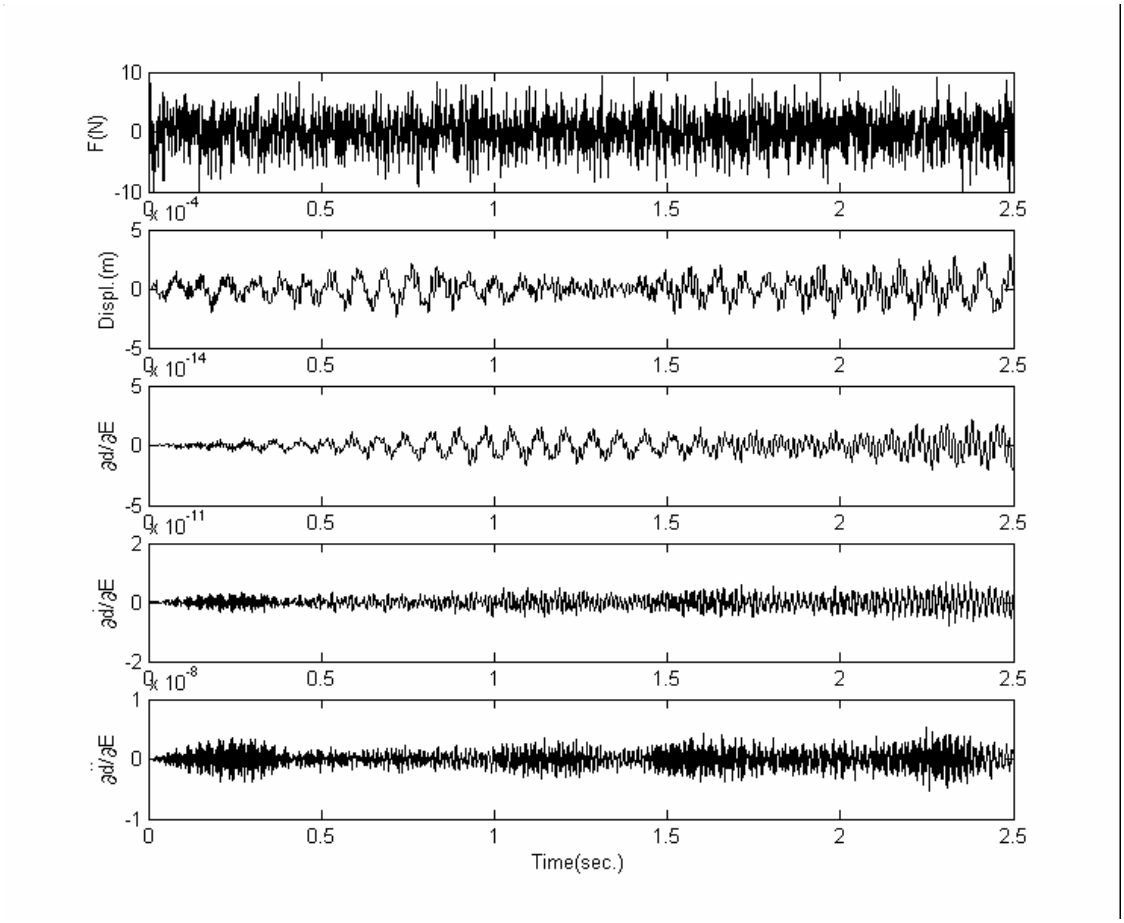

Figure 3-7- Response sensitivity from uniformly distributed random noise excitation

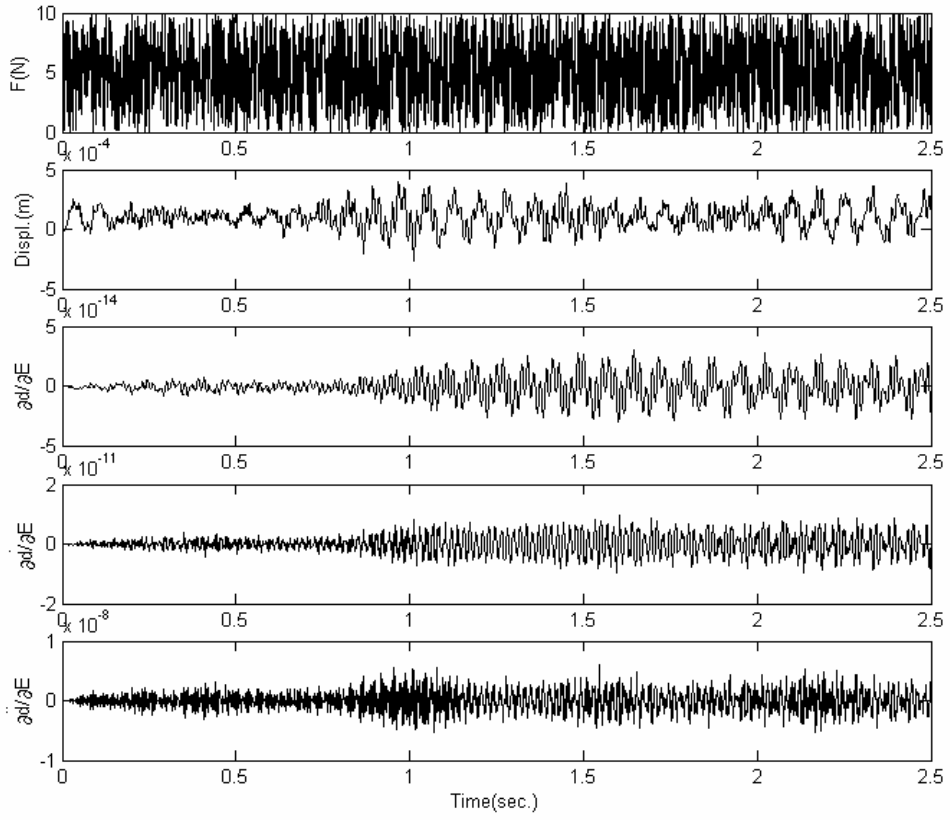

Figure 3-8- Response sensitivity from normal random noise excitation

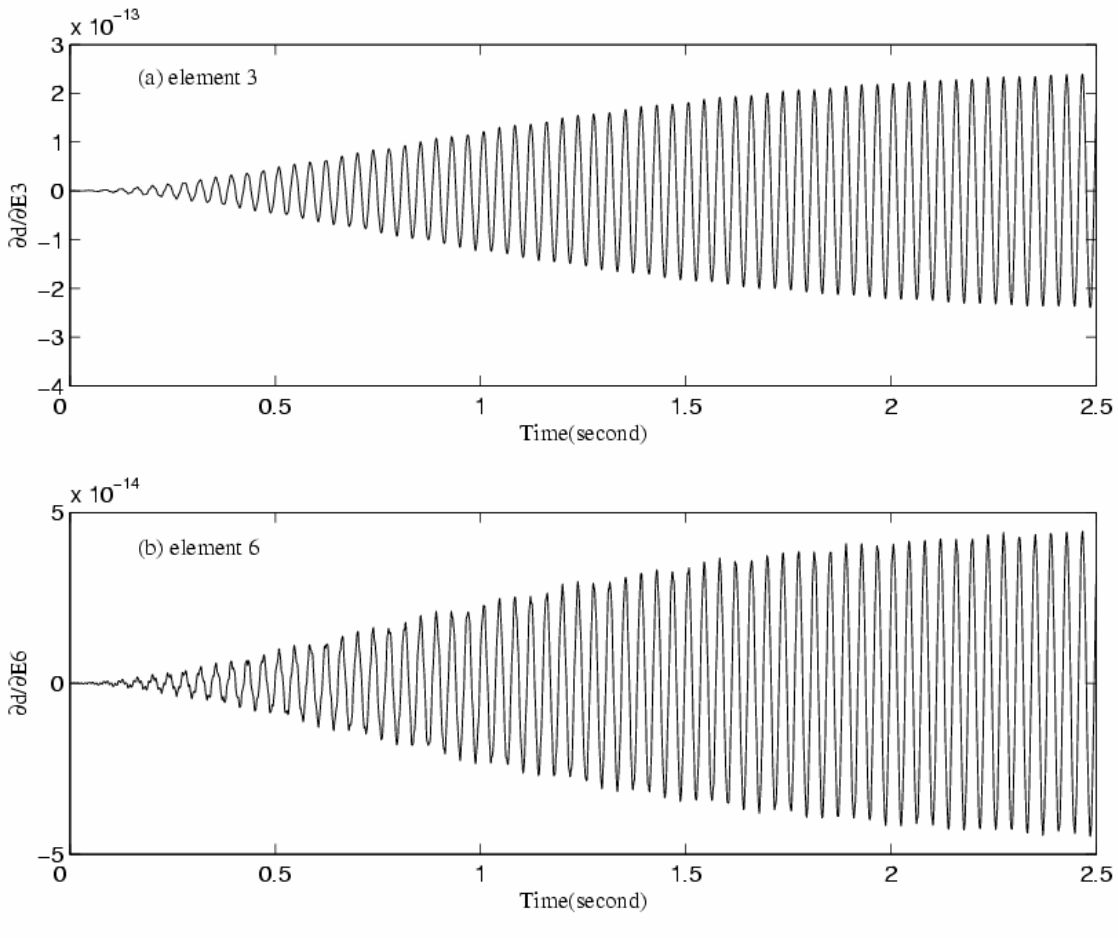

Figure 3-9- Displacement sensitivity with respect to different elemental elastic modulus

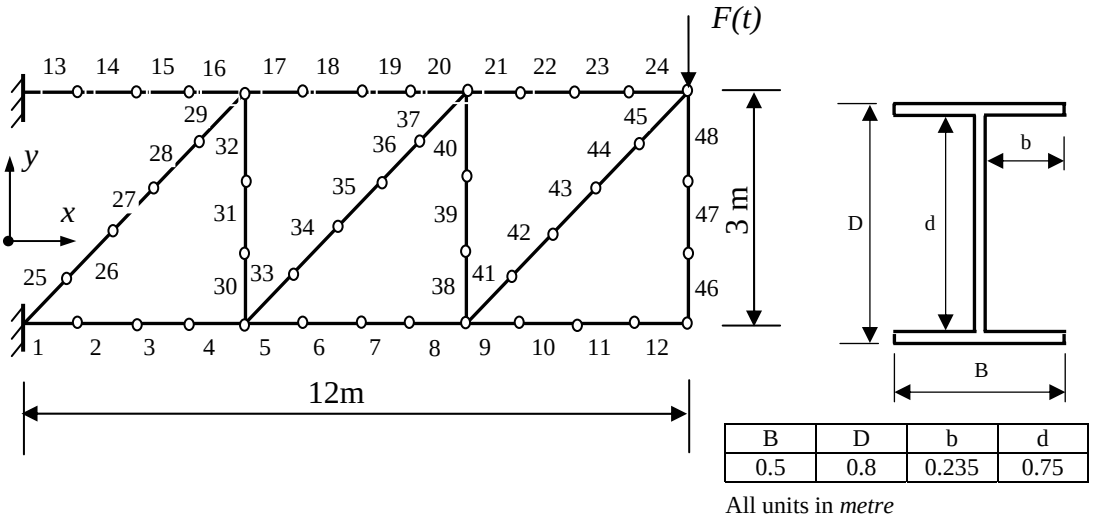

B	D	b	d
0.5	0.8	0.235	0.75

All units in *metre*

Figure 3-10- Finite element model of the European Space Agency Structure

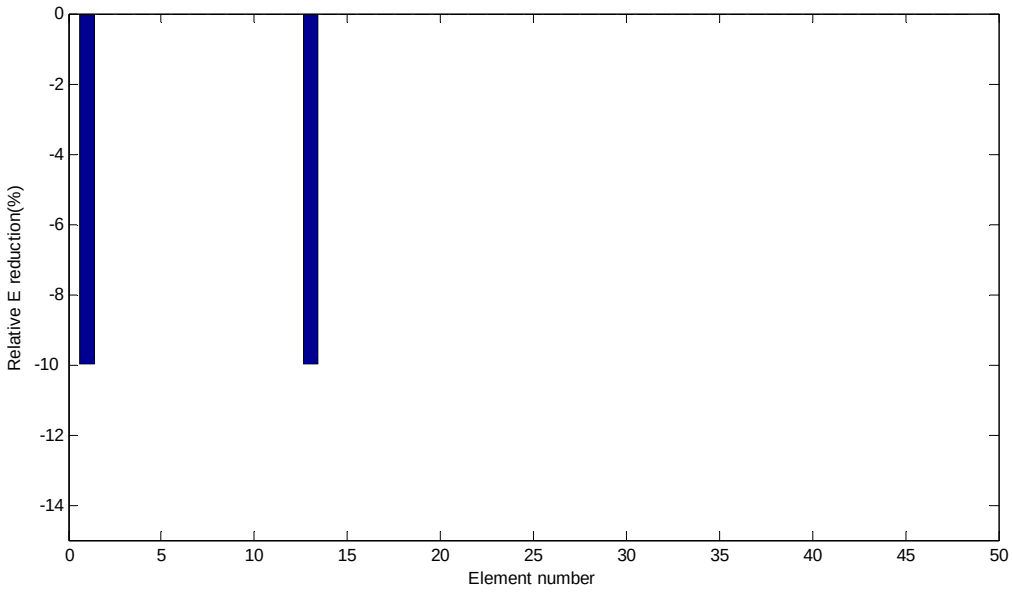

Figure 3-11- Identification of multiple damages near the supports

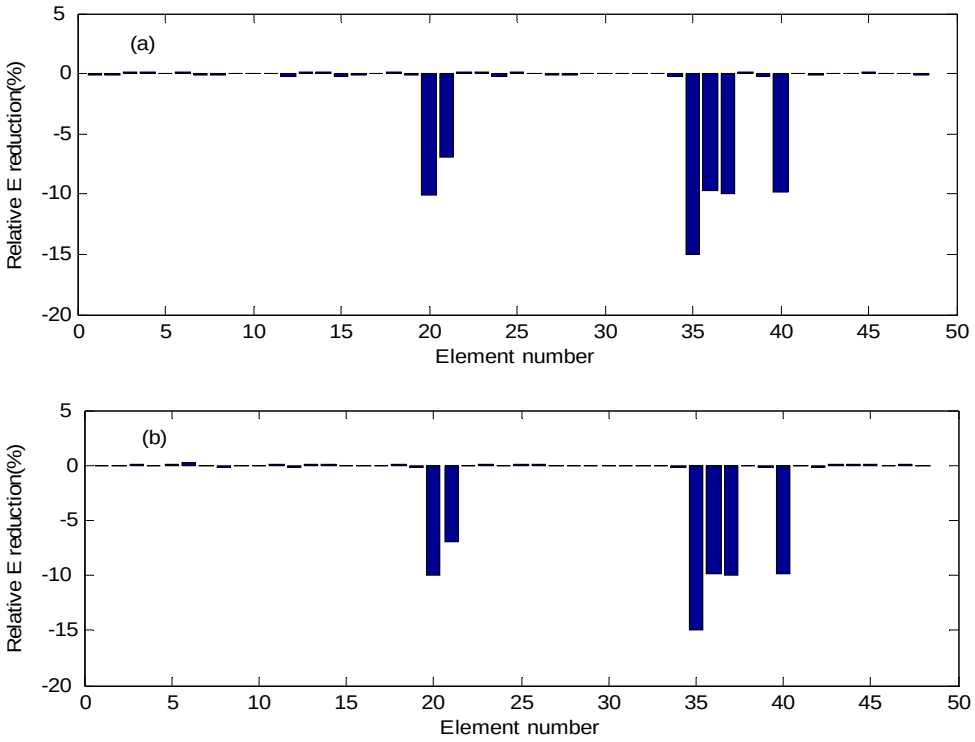

Figure 3-12- Identification of damages from different sampling rates (a) sampling rate= 500 Hz; (b) sampling rate = 200 Hz

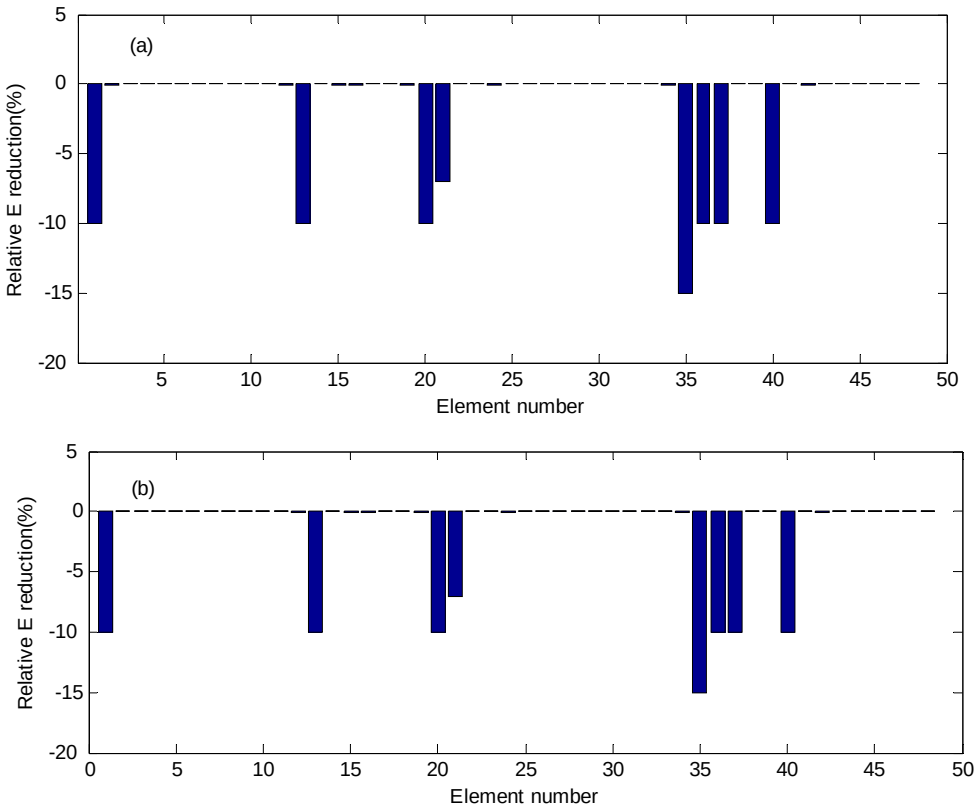

Figure 3-13- Identification damages from different data points
(a) data points=200; (b) data points=500

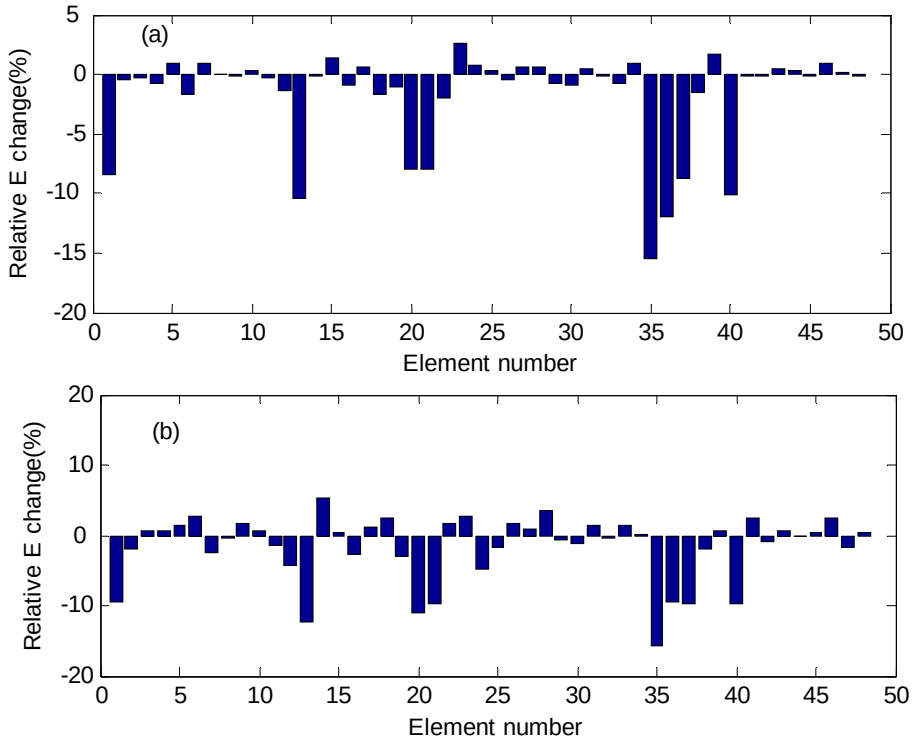

Figure 3-14- Identification of damages from different noise levels (a) noise level=1%; (b) noise level=10%

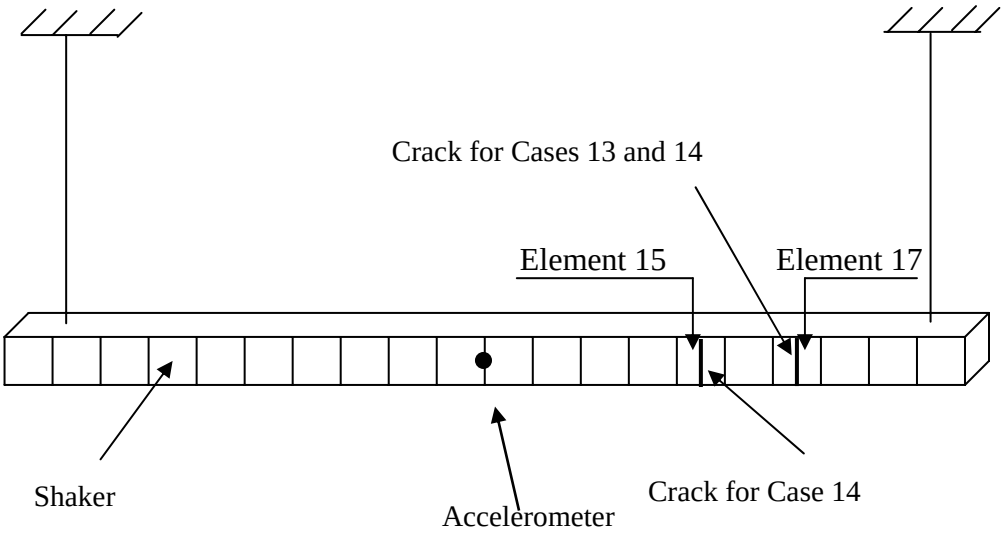

Figure 3-15- Forced vibration test of free-free steel beam

Chapter 4

FURTHER APPLICATIONS OF RESPONSE SENSITIVITY FOR STRUCTURAL DAMAGE DETECTION

This chapter extends the proposed dynamic response sensitivity-based finite element model updating damage detection method in the last chapter for further applications. Four more applications are developed, namely, the structural damage detection taking into account the effects of temperature difference, differentiating different types of damage in structure, identifying the prestress force in prestressed structures and damage detection including the load environment.

4.1 Numerical Study of Damage Detection by Model Updating with Temperature Effects Removed

4.1.1 Introduction

Damage detection based on a reference set of measured data usually has the problem of different environmental temperature in the two sets of measurements, and this temperature effect is usually ignored in the subsequent model updating. This section investigates the effect of this factor on the damage detection results with a combination of modeling errors and measurement noise. A method is then proposed to

remove the temperature effect prior to model updating. Local damages are identified in a gradient-based model updating method based on dynamic response sensitivity. The sensitivities of dynamic responses with respect to the system parameters and temperature difference are calculated by direct integration of the equation of motion. The dynamic responses are used to identify the damage location and extent. A single degree-of-freedom mass-spring system and a more complicated plane truss structure are studied to illustrate the effectiveness of the proposed method. The effect of temperature difference on the accuracy of results for the damaged elements is found not significant, but it would cause a spread of errors to other elements which may lead to false warnings in the case of identifying small damages particularly in a large-scale structure.

4.1.2 Sensitivity in Time Domain

4.1.2.1 *Dynamic Response of the System*

For an *N* degree-of-freedom time-invariant discrete system with *NP* nodal points and *NE* finite elements, the governing equation of motion is given by

$$[M]\{\ddot{d}\}+[C]\{\dot{d}\}+[K]\{d\}=\{F(t)\} \tag{4.1-1}$$

where [*M*], [*C*] and [*K*] are the system mass, damping and stiffness matrices respectively, $\{\ddot{d}\}$, $\{\dot{d}\}$ and $\{d\}$ are the acceleration, velocity and displacement vectors of the structure, $\{F(t)\}$ is a vector of nodal forces. For a known force vector and a given set of system matrices, the dynamic responses of the structures can be obtained from this equation by direct numerical integration method, e.g. the Newmark-β method.

4.1.2.2 *Sensitivity of Response with respect to System Parameters*

The mass matrix can be formulated from either the consistent mass matrix or the lump mass matrix. When the consistent mass matrix is adopted, differentiating both sides of Equation (4.1-1) with respect to the mass coefficient of the system will give

$$[M]\{\frac{\partial \ddot{d}}{\partial m_{ij}}\}+[C]\{\frac{\partial \dot{d}}{\partial m_{ij}}\}+[K]\{\frac{\partial d}{\partial m_{ij}}\}=-\frac{\partial [M]}{\partial m_{ij}}\{\ddot{d}\}-a_1\frac{\partial [M]}{\partial m_{ij}}\{\dot{d}\}$$

(i=1,2,…6;j=1,2…6) (4.1-2)

where $\{\frac{\partial d}{\partial m_{ij}}\}$,$\{\frac{\partial \dot{d}}{\partial m_{ij}}\}$,$\{\frac{\partial \ddot{d}}{\partial m_{ij}}\}$ are the displacement, velocity and acceleration sensitivities, a_1 is the coefficient of the Rayleigh damping. Note that Equation (4.1-2) is of the same form as Equation (4.1-1). Since the dynamic responses have been obtained from Equation (4.1-1), the right-hand-side of Equation (4.1-2) serves as the equivalent force input, and the sensitivities can then be obtained numerically by direct integration. The sensitivities of response with respect to each damping and stiffness coefficients can be similarly obtained. This response sensitivity approach, theoretically, could be used to update all the system parameters of the structure from measured dynamic responses.

4.1.2.3 *Sensitivity of Response with respect to Change of Temperature*

A plane truss element is taken to illustrate the proposed approach. The elemental stiffness matrix is

$$[k^e]_0=\frac{EA}{l_0}\begin{bmatrix}1 & 0 & -1 & 0\\ 0 & 0 & 0 & 0\\ -1 & 0 & 1 & 0\\ 0 & 0 & 0 & 0\end{bmatrix} \quad (4.1\text{-}3)$$

where l_0 is the original element length. When taking into account the temperature difference ΔT , we have the elemental stiffness matrix as

$$[k^e]_{\Delta T} = \frac{EA}{l}\begin{bmatrix} 1 & 0 & -1 & 0 \\ 0 & 0 & 0 & 0 \\ -1 & 0 & 1 & 0 \\ 0 & 0 & 0 & 0 \end{bmatrix} \tag{4.1-4}$$

$$l = l_0 + \alpha \Delta T l_0 = l_0(1 + \alpha \Delta T) \tag{4.1-5}$$

where α is the thermal expansion coefficient, and equals $12.5 \times 10^{-6} / ^{o}C$ for steel. Since $\alpha \Delta T << 1$, we have

$$\frac{1}{l} = \frac{1}{l_0(1 + \alpha \Delta T)} \approx \frac{1}{l_0}(1 - \alpha \Delta T) \tag{4.1-6}$$

Equation (4.1-4) can be rewritten as

$$[k^e]_{\Delta T} = \frac{EA(1\text{-}\alpha \Delta \mathrm{T})}{l_0}\begin{bmatrix} 1 & 0 & -1 & 0 \\ 0 & 0 & 0 & 0 \\ -1 & 0 & 1 & 0 \\ 0 & 0 & 0 & 0 \end{bmatrix} \tag{4.1-7}$$

with the temperature effect on the member area of the cross-section ignored. Performing differentiation on both sides of Equation (4.1-1) with respect to the temperature difference ΔT_j for the *jth* member, we have

$$[M]\{\frac{\partial \ddot{d}}{\partial \Delta T_j}\} + [C]\{\frac{\partial \dot{d}}{\partial \Delta T_j}\} + [K]\{\frac{\partial d}{\partial \Delta T_j}\} = -\frac{\partial [K]}{\partial \Delta T_j}\{d\} - a_2 \frac{\partial [K]}{\partial \Delta T_j}\{\dot{d}\} \tag{4.1-8}$$

where a_2 is the Rayleigh damping coefficient.

The sensitivity of response with respect to the temperature difference can be obtained from Equation (4.1-8) by direct integration. It is common in large-scale structure to find visco-elastic materials, which can drastically change with temperature affecting not only the stiffness, but also the damping of the structure. It is assumed that the materials we have in the following studies are non-viscoelastic, and thus the system mass and damping will not be affected by this temperature difference.

4.1.3 The Damage Detection Algorithm with Removal of Temperature Effect

The difference of responses at time t_i obtained from the analytical model and the simulated "measurements" of the damaged structures, ΔR_{t_i}, can be expressed as a first order differential equation with respect to the system coefficients of all the DOFs of the system. The differential of response with respect to the temperature difference can also be calculated for each finite element. When writing in the form of Taylor first order approximation,

$$\Delta R_{t_i} = \sum_{k=1}^{NE}\sum_{i=1}^{6}\sum_{j=1}^{6}\frac{\partial R_{t_i}}{\partial m_{ijk}}\Delta m_{ijk} + \sum_{k=1}^{NE}\sum_{i=1}^{6}\sum_{j=1}^{6}\frac{\partial R_{t_i}}{\partial c_{ijk}}\Delta c_{ijk} + \sum_{k=1}^{NE}\sum_{i=1}^{6}\sum_{j=1}^{6}\frac{\partial R_{t_i}}{\partial k_{ijk}}\Delta k_{ijk} + \sum_{j=1}^{NE}\frac{\partial R_{t_i}}{\partial \Delta T_j}\Delta T_j$$

(4.1-9)

The pattern of temperature distribution in a structure can be obtained from temperature sensors or from theoretical model on the temperature distribution. The temperature differences in all members are assumed equal for simplicity in this study, i.e. $\Delta T_1 = \Delta T_2 = ... = \Delta T_{NE}$. The terms on the temperature difference can then be moved to the left-hand-side of Equation (4.1-9) as

$$\Delta R_{t_i} - \sum_{j=1}^{NE}\frac{\partial R_{t_i}}{\partial \Delta T_j}\Delta T_j = \sum_{k=1}^{NE}\sum_{i=1}^{6}\sum_{j=1}^{6}\frac{\partial R_{t_i}}{\partial m_{ijk}}\Delta m_{ijk} + \sum_{k=1}^{NE}\sum_{i=1}^{6}\sum_{j=1}^{6}\frac{\partial R_{t_i}}{\partial c_{ijk}}\Delta c_{ijk} + \sum_{k=1}^{NE}\sum_{i=1}^{6}\sum_{j=1}^{6}\frac{\partial R_{t_i}}{\partial k_{ijk}}\Delta k_{ijk}$$

or

$$\Delta R'_{t_i} = \sum_{k=1}^{NE}\sum_{i=1}^{6}\sum_{j=1}^{6}\frac{\partial R_{t_i}}{\partial m_{ijk}}\Delta m_{ijk} + \sum_{k=1}^{NE}\sum_{i=1}^{6}\sum_{j=1}^{6}\frac{\partial R_{t_i}}{\partial c_{ijk}}\Delta c_{ijk} + \sum_{k=1}^{NE}\sum_{i=1}^{6}\sum_{j=1}^{6}\frac{\partial R_{t_i}}{\partial k_{ijk}}\Delta k_{ijk} \qquad (4.1\text{-}10)$$

When lump mass matrix is adopted, Equation (4.1-10) becomes

$$\Delta R_{t_i}^{'} = \sum_{k=1}^{NE} \frac{\partial R_{t_i}}{\partial m_k} \Delta m_k + \sum_{k=1}^{NE} \sum_{i=1}^{6} \sum_{j=1}^{6} \frac{\partial R_{t_i}}{\partial c_{ijk}} \Delta c_{ijk} + \sum_{k=1}^{NE} \sum_{i=1}^{6} \sum_{j=1}^{6} \frac{\partial R_{t_i}}{\partial k_{ijk}} \Delta k_{ijk}$$

where Δm_k is the kth lump mass and $\Delta R_{t_i}^{'}$ is the difference of dynamic response from the two damage states of the structure with the temperature effect removed. The sensitivity $\{\frac{\partial R_{ti}}{\partial k_{ijk}}\}$ is assumed not affected by the temperature difference in this study.

It is noted that the first order differential equation can be written in terms of the physical parameters of the structural system, i.e. the modulus of elasticity of material, Poisson ratio, mass density, cross-sectional area of member, dimensions, second moment of area of cross-section, polar moment of area and damping ratio, etc. and Equation (4.1-10) will take up a different form.

If there are N_t ($N_t > 3\times6\times6\times NE$) time steps in a single measured response, Equation (4.1-10) is over-determined, and it can be written as

$$\begin{bmatrix} \frac{\partial R_{t_1}}{\partial m_{111}} & \cdots & \frac{\partial R_{t_1}}{\partial m_{66NE}} & \frac{\partial R_{t_1}}{\partial c_{111}} & \cdots & \frac{\partial R_{t_1}}{\partial c_{N66NE}} & \frac{\partial R_{t_1}}{\partial k_{111}} & \cdots & \frac{\partial R_{t_1}}{\partial k_{66NE}} \\ \frac{\partial R_{t_2}}{\partial m_{111}} & \cdots & \frac{\partial R_{t_2}}{\partial m_{66NE}} & \frac{\partial R_{t_2}}{\partial c_{111}} & \cdots & \frac{\partial R_{t_2}}{\partial c_{66NE}} & \frac{\partial R_{t_2}}{\partial k_{111}} & \cdots & \frac{\partial R_{t_2}}{\partial k_{66NE}} \\ \vdots & \cdots & \vdots & \vdots & \cdots & \vdots & \vdots & \cdots & \vdots \\ \frac{\partial R_{t_i}}{\partial m_{111}} & \cdots & \frac{\partial R_{t_i}}{\partial m_{66NE}} & \frac{\partial R_{t_i}}{\partial c_{111}} & \cdots & \frac{\partial R_{t_i}}{\partial c_{66NE}} & \frac{\partial R_{t_i}}{\partial k_{111}} & \cdots & \frac{\partial R_{t_i}}{\partial k_{66NE}} \\ \vdots & \cdots & \vdots & \vdots & \cdots & \vdots & \vdots & \cdots & \vdots \\ \frac{\partial R_{t_{Nt}}}{\partial m_{111}} & \cdots & \frac{\partial R_{t_{Nt}}}{\partial m_{66NE}} & \frac{\partial R_{t_{Nt}}}{\partial c_{111}} & \cdots & \frac{\partial R_{t_{Nt}}}{\partial c_{66NE}} & \frac{\partial R_{t_{Nt}}}{\partial k_{111}} & \cdots & \frac{\partial R_{t_{Nt}}}{\partial k_{66NE}} \end{bmatrix} \begin{Bmatrix} \Delta m_{111} \\ \vdots \\ \Delta m_{66NE} \\ \Delta c_{111} \\ \vdots \\ \Delta c_{66NE} \\ \Delta k_{111} \\ \vdots \\ \Delta k_{66NE} \end{Bmatrix} = \begin{Bmatrix} \Delta R'_{t_1} \\ \Delta R'_{t_2} \\ \vdots \\ \Delta R'_{t_i} \\ \vdots \\ \Delta R'_{t_{Nt}} \end{Bmatrix}$$

or

$$S\Delta P = \Delta R \qquad (4.1\text{-}11)$$

where S is the response sensitivity matrix and ΔP and ΔR are the vectors of unknown parameter increments and incremental measured responses respectively. For the case of using lump mass matrix, $N_t > 2\times6\times6\times NE + N$ is required to make Equation (4.1-

10) over-determined. Equation (4.1-11) can be solved by the damped least-squares method (DLS) and singular-value decomposition is employed in the pseudo-inverse calculation.

The solution of Equation (4.1-11) is equivalent to minimizing the function

$$J(\{\Delta P\}, \lambda) = \left\| S\Delta P - \Delta R \right\|^2 + \lambda \left\| \Delta P \right\|^2 \qquad (4.1\text{-}12)$$

with the second damping term providing bounds to the solution. The parameter λ is the non-negative damping coefficient governing the participation of the least-squares error in the solution. When parameter λ approaches zero, the estimated vector $\{\Delta P\}$ approaches the solution obtained from the simple least-squares method. Other formulation on the damping terms can also be found in (Tarantola, 1987).

4.1.4 Procedure of Computation

A two-stage approach is adopted with the first stage to update the analytical finite element model and the second stage to identify local damages in the structure. When measurement from the undamaged state of the structure is obtained, the response and its sensitivity to a system parameter are first computed basing on the analytical model of the structure and the measured input force. The error vector ΔR is computed from the calculated responses of the analytical model and the simulated "measured" responses, and the vector of parameter increment is then obtained from Equation (4.1-12). The analytical model is then updated and the response and its sensitivity are again computed for the next iteration. Convergence is considered achieved when the following criterion is met: $\left\| \frac{P_{k+1} - P_k}{P_{k+1}} \right\| \le tolerance$, where $\{P_k\}$ is the vector of the

unknown parameters, *k* denotes the *kth* iteration. The *tolerance* is taken as 1×10^{-5} in this section.

When measurement from the damaged state is obtained, the updated analytical model is used in the iteration in the same way as that using the measurement from the undamaged state. The final set of identified parameter increments correspond to the changes occurred in between the two states of the structure. In the present case, the set of increment of system parameters in all the elements form the vector of unknown parameters, and is initially set equals to a null vector.

4.1.5 Numerical Example

4.1.5.1 *Single Degree-of-Freedom System*

Figure 4-1(a) shows a simple system in which the stiffness is distributed but the mass and damping are localized. It consists of a light cantilever beam of flexural rigidity EI, to the end of which is attached a point mass *m* and a damper *c*. Figure 5-10(b) shows its equivalent model of a single degree-of-freedom system. The mass and damping of the system is *m* and *c* respectively, and the spring coefficient equals to $k = 3EI/L^3$. Parameters of the system are: $m = 2\ Kg$, $c = 1.1\ N\cdot s/m$, $k = 500\ N/m$, and $L = 1\ m$. The equation of motion of the system is

$$m\ddot{d} + c\dot{d} + k(1-\alpha\Delta T)d = F(t) \qquad (4.1\text{-}13)$$

Differentiating both sides of Equation (4.1-13) with respect to the mass, damping, spring stiffness of the system and ΔT, we have,

$$m\frac{\partial \ddot{d}}{\partial m} + c\frac{\partial \dot{d}}{\partial m} + k(1-\alpha\Delta T)\frac{\partial d}{\partial m} = -\ddot{d} \qquad (4.1\text{-}14)$$

$$m\frac{\partial \ddot{d}}{\partial c}+c\frac{\partial \dot{d}}{\partial c}+k(1-\alpha\Delta T)\frac{\partial d}{\partial c}=-\dot{d} \qquad (4.1\text{-}15)$$

$$m\frac{\partial \ddot{d}}{\partial \Delta T}+c\frac{\partial \dot{d}}{\partial \Delta T}+k(1-\alpha\Delta T)\frac{\partial d}{\partial \Delta T}=\alpha kd \qquad (4.1\text{-}16)$$

$$m\frac{\partial \ddot{d}}{\partial k}+c\frac{\partial \dot{d}}{\partial k}+k(1-\alpha\Delta T)\frac{\partial d}{\partial k}=-(1-\alpha\Delta T)d \qquad (4.1\text{-}17)$$

The coupling effect between the flexural rigidity and temperature difference has been neglected.

Responses from two measurement states are used for the identification. The beam is subject to a transverse excitation of $F = 4\sin 16\pi t\ N$ along the local *y*-axis and the beam is assumed to be initially at rest. Sampling rate is 200 Hz and the first second measured acceleration response along the *y*-axis is used for the identification. Figure 4-2 shows the sensitivity of transverse displacement with respect to the three system parameters *m, c, k* and the temperature increment ΔT. It is noted that the dynamic response is more sensitive to the mass parameter and the damping than the flexural rigidity and temperature difference. The following studies are made with the above references.

Study case 1: Effect of temperature difference

The set of damaged system parameter is taken to be $m = 2\ Kg$, $c = 1.2N\cdot s/m$, $k = 450\ N/m$, and assuming that there is a temperature difference of $+20\ ^oC$ between the two sets of measurements. Table 4-1 gives results for Cases *A* and *B* with and without taking the temperature difference into consideration respectively in the identification. The number of iteration required for convergence is 12 for both cases, and the optimal regular parameters are 1.25×10^{-3} and 3.12×10^{-3} respectively. Table 4-1 shows that an error of 0.22% in the stiffness occurs when the temperature

difference is neglected, but the stiffness will converge to the true value when the temperature effect is removed.

Study case 2: Effect of additional mass from sensors

The same single DOF system as for last study is used. A sensor of mass 0.01 *Kg* is added to the system. Table 4-2 gives the identified results with (Case *A*) and without (Case *B*) considering the additional mass. The required number of iteration for convergence is 18 for both cases, and the optimal regularization parameters are *0.009* and *0.008* respectively. Results from Table 4-2 show that the omission of 0.01 *Kg* in the system mass leads to a spread of errors of 0.5%, 1.7% and 0.3% in the identified system mass, damping and stiffness respectively.

Study case 3: Modeling error

The intact and damaged sets of parameters of the system are the same as those in Study 1. The system parameters are taken as: $m = 1\ Kg$, $c = 0.8\ N \cdot s/m$, $k = 300\ N$ to simulate the errors in the initial model. The identified results converge to the "true" damaged system parameters after 22 iterations, and the optimal regularization parameter is *0.024* . Table 4-3 shows the identified results.

Study case 4: Model error and measurement noise

Measurement noise exists in the measured responses in practice, and therefore the effect of 1%, 5% and 10% noise level on the measurements is investigated. A normally distributed random error with zero mean and unit standard deviation is added to the measured acceleration as

$$\hat{\ddot{d}} = \ddot{d}_{cal} + Ep \times N_{oise} \times \mathrm{var}(\ddot{d}_{cal}) \qquad (4.1\text{-}18)$$

where $\hat{\ddot{d}}$ is the vector of polluted acceleration, E_p is the noise level, N_{oise} is a standard normal distribution vector with zero mean and unit standard deviation, var(•) is the variance of the time history, $\ddot{d}_{cal}$ is the vector of calculated acceleration. 2000 data points from 10 second measured responses are used in the study. Table 4-4 shows the identified results. The number of iteration required for convergence is 24, 27 and 28 respectively for the three noise levels, and the corresponding optimal regularization parameters are 0.015, 0.024 and 0.031. Results in Table 4-4 show that the identified results are satisfactory when the noise level is under 10% with a maximum error of 3.42% in damping. This error can in fact be further reduced when more measured data points are used in the analysis. Damping is noted to be more sensitive to random noise than the mass and stiffness.

4.1.5.2 *A Plane Truss Structure*

This numerical study is extended to a more complicated five-bay plane truss structure as shown in Figure 4-3, and the effect of temperature increment, modeling error and measurement noise on the identified results is studied. It is assumed that there is no change in the mass and the damping with the occurrence of damage in the structure and there is no moment constraint between elements at the joints. The material parameters are: mass density is $7860\ Kg/m^3$ and Young's modulus is $200\ GPa$. The finite element model of the structure consists of nineteen two-dimensional truss elements with eleven nodes and twenty-two DOFs. The geometrical data of the structure in the initial finite element model are also shown in Figure 4-3. The external and internal diameter of the hollow circular section member are 0.6 *m* and 0.4 *m* respectively. An excitation force of $F = -10000\sin 20\pi t$ is acting at the 8th node in the negative direction of the global *y*-axis. Two accelerometers are used to collect

the acceleration responses at the 4^{th} node along the global *y*-axis, and at the 10^{th} node along the global *x*-axis. Five damage scenarios as shown in Table 4-5 are studied. Measurements from the first sensor are for the study of the first two damage scenarios, while those from the second sensor are for the study of damage Scenarios *3* and *4*. Measurements from both sensors are used for the study of the last damage scenario. Sampling frequency is 1000 Hz, and 1800 time steps data are used for the identification.

The first damage scenario involves 5% reduction in the axial stiffness in elements 2, 5 and 19 while damage Scenario *2* involves 5% reduction in the axial stiffness in elements 2, 5 and 19 and with a temperature difference of $+40^{o}C$ between the two measurement states. The first eight natural frequencies of the intact structure and the structure with the two damage scenario are shown in Table 4-6. It is noted that the change in the natural frequencies due to the temperature difference is not significant.

Damage Scenario *3* is for the study of the effect of temperature difference on the damage identification and the identified relative reduction in the axial stiffness for each of the elements are shown in Figure 4-4 for the cases with and without removing the temperature effect before the damage identification. It is noted that the local damage in element 5 can be identified very accurately with or without consideration of the temperature effect.

Damage Scenario *4* is for the study of noise effect on the damage identification, and the identified relative reduction in the axial stiffness is shown in Figure 4-5. The results show that the local damage at element 12 can be accurately identified even under 10% measurement noise level, and an increase in the noise level from 5% to 10% lead to an error of approximately +1% in the magnitude of the identified local damage.

Damage Scenario *5* is for the study of a combination of local damages in element 2, 5 and 19, temperature effect, 10% noise level and 3% under estimation in the axial stiffness of all the members in the initial FEM. The use of 1800 data from the first sensor alone has been checked to give accurate results on the local damage for this combination when only 3% modeling error is used, and the computation fails to converge for a larger modeling error. Therefore 4000 data points from both sensors are used for this study. The identified results from the cases with and without the temperature effect removed from the time responses are shown in Figure 4-6. The identified results for the three damaged elements are very close to the true values in both cases. But there is a smearing of errors throughout the structure to other undamaged elements when the temperature effect has not been removed prior to the damage detection.

Given the complexity of this damage scenario, the proposed damage detection method is considered effective in locating and quantifying small local damages with an incorrect initial model and noisy measurement. The number of iteration required for convergence is 33 and the regularization parameter is 2.5×10^{-10}. Good identified results are also obtained for other combinations of damages in different elements. Results in Figure 4-6 also indicate that the temperature effect would not have too much effect on the accuracy of identified damages but it would cause a spread of errors in other elements which may lead to false warnings in the case of identifying small damages.

4.1.6 Concluding Remarks

A damage detection method is proposed making use of the dynamic response sensitivity with respect to the different parameters of a structural system and the

temperature effect in measurement. The measured response can be obtained from as few as a single sensor. The effect of temperature difference between two measurements states is removed in the first stage of pre-processing of the measured data in the proposed algorithm. All the system parameters including the system mass, damping and stiffness can be updated successfully using noisy measurements. Numerical simulations using a single DOF system and a medium span plane truss show that: (1) the effect of temperature difference on the accuracy of results for the damaged elements is not significant, but it would cause a spread of errors to other elements which may lead to false warnings in the case of identifying small damages. (2) the effect of initial finite element model error on the accuracy of identification is significant, and more measured data is required for an accurate updating. The proposed method is limited to two-dimensional elements in this section and further research is required for application to structure consists of three-dimensional elements. And only numerical simulation is given to illustrate the proposed approach due to the limitation of experiment condition in our university. Further research is needed to carry out experimental study on real large-scale structures.

4.2 Assessment of Elemental Load Resistance from Response Sensitivity

4.2.1 Introduction

Damage is idealized as an overall reduction in local stiffness in most of the existing approaches in the literature. But there may be many types of damage throughout the service life of the structure affecting the structural dynamic response and characteristics differently. Engineers would like to know the load resistance of each structural component after an occurrence of damage incidence. For structures constituted of isotropic homogeneous material, such capacity would depend on the different physical and geometric properties of the component, viz. the cross-sectional area, second moment of area and torsional moment of area of cross-section, etc. Therefore, a more satisfactory procedure to approach the damage detection problem should give answers on the location and magnitude of the damage as well as the type of damage affecting the load-carrying capacity of the structure. One approach was developed by Wu and Law (2002) who had differentiated the damage type in a structure using a vector of sensitivities from the eigen-parameters of each structural member recently.

This section provides an assessment on the load resistance of structural elements as discussed in last paragraph. The sensitivities of dynamic response with respect to different damage indices of a structure are analytically obtained. The problem of coupling between these indices is addressed and solved. The local damages are identified in a gradient-based model updating method based on the dynamic response

sensitivity. This section covers the derivation of formulations, numerical simulations and an experiment verification of the proposed method. A plane frame and a plane truss structures are studied in the numerical simulations to illustrate the effectiveness of the proposed damage detection method. Studies show that the proposed method is insensitive to model errors in the identification using short duration of measured data from as few as two sensors. The magnitude of damage is known directly from the actual amount of changes in the vector of damage indices.

4.2.2 Forward Problem

4.2.2.1 *Dynamic Responses Sensitivities with respect to Different Damage Indices from Newmark Method*

For a general finite element model of a linear elastic time-invariant structure with *N* degrees-of-freedom and *NE* elements, the dynamic governing equation is given by

$$[M]\{\ddot{d}\}+[C]\{\dot{d}\}+[K]\{d\}=\{F(t)\} \qquad (4.2\text{-}1)$$

where [M], [C] and [K] are the system mass, damping and stiffness matrices respectively. Also, Rayleigh damping is adopted in this chapter. $\{\ddot{d}\}$, $\{\dot{d}\}$ and $\{d\}$ are the acceleration, velocity and displacement vectors of the structure, $\{F(t)\}$ is a vector of applied nodal forces. The dynamic responses of the structures can be obtained from this equation by direct numerical integration using the well-known Newmark- β method.

For a planar beam-column element, let E^i, I^i and A^i be the Young's modulus of material, the second moment of area of cross-section and the sectional area of the *ith* element respectively. A physical damage affects the different physical parameters of an element differently, and these physical parameters become

$$E_d^i = E_0^i(1+\alpha_E^i) \qquad (-1 \le \alpha_E^i \le 0) \tag{4.2-2}$$

$$I_d^i = I_0^i(1+\alpha_I^i) \qquad (-1 \le \alpha_I^i \le 0) \tag{4.2-3}$$

$$A_d^i = A_0^i(1+\alpha_A^i) \qquad (-1 \le \alpha_A^i \le 0) \tag{4.2-4}$$

where E_0^i, I_0^i, A_0^i are the parameters of the intact structure, E_d^i, I_d^i, A_d^i are the parameters of the damaged structure, α_E^i, α_I^i and α_A^i represent the damage indices for the Young's modulus of material, the second moment of area and area of the cross-section respectively. Equations (4.2-2) to (4.2-4) give

$$E_d^i I_d^i = E_0^i I_0^i(1+\alpha_E^i+\alpha_I^i+\alpha_E^i\alpha_I^i) \tag{4.2-5}$$

$$E_d^i A_d^i = E_0^i A_0^i(1+\alpha_E^i+\alpha_A^i+\alpha_E^i\alpha_A^i) \tag{4.2-6}$$

Performing differentiations on both sides of Equation (4.2-1) with respect to the different damage indices, e.g. the damage index on the elastic modulus of the *ith* element, we have,

$$[M]\{\frac{\partial \ddot{d}}{\partial \alpha_E^i}\}+[C]\{\frac{\partial \dot{d}}{\partial \alpha_E^i}\}+[K]\{\frac{\partial d}{\partial \alpha_E^i}\} = -\frac{\partial [k]_i^e}{\partial \alpha_E^i}\{d\} - a_2\frac{\partial [k]_i^e}{\partial \alpha_E^i}\{\dot{d}\} \quad (i=1,2,\ldots NE) \tag{4.2-7}$$

where $\{\frac{\partial d}{\partial \alpha_E^i}\}$,$\{\frac{\partial \dot{d}}{\partial \alpha_E^i}\}$,$\{\frac{\partial \ddot{d}}{\partial \alpha_E^i}\}$ are the displacement, velocity and acceleration sensitivities with respect to the unknown index α_E^i. The terms on the right-hand-side of Equation (4.2-7) can be obtained once the displacement and velocity are obtained from Equation (4.2-1) using Newmark method. The sensitivities can then be obtained by direct integration. The sensitivities with respect to other parameters, i.e. $\{\frac{\partial d}{\partial \alpha_A^i}\}$, $\{\frac{\partial \dot{d}}{\partial \alpha_A^i}\}$, $\{\frac{\partial \ddot{d}}{\partial \alpha_A^i}\}$, $\{\frac{\partial d}{\partial \alpha_I^i}\}$, $\{\frac{\partial \dot{d}}{\partial \alpha_I^i}\}$ and $\{\frac{\partial \ddot{d}}{\partial \alpha_I^i}\}$ can similarly be obtained.

The indices α_E^i, α_I^i and α_A^i are used in this study instead of the original physical parameters E_i, I_i and A_i in the formulation of the sensitivity in previous works. This approach has the advantage of yielding sensitivities which are larger than those from the original parameters by several orders as seen in Figure 4-7 where the different sensitivity curves are calculated for Example 1.

4.2.2.2 *Dynamic Responses and Response Sensitivities from the State-Space Method*

The dynamic responses and response sensitivities with respect to the damage indices from the state-space method are derived as follows. The equation of motion can be written as the following first order differential equation by state space method:

$$\dot{X} = K^* X + \overline{F} \tag{4.2-8}$$

where $X = \begin{bmatrix} d \\ \dot{d} \end{bmatrix}_{2N\times 1}$, $K^* = \begin{bmatrix} 0 & I \\ -M^{-1}K & -M^{-1}C \end{bmatrix}_{2N\times 2N}$, $\overline{F} = \begin{bmatrix} 0 \\ M^{-1}F \end{bmatrix}_{2N\times 1}$.

where X represents a vector of state variables with a length $2N$ containing the displacements and velocities of the nodes. These differential equations can then be discretized using exponential matrix representation.

$$X_{k+1} = AX_k + \overline{D}\overline{F}_k \tag{4.2-9}$$

$$A = e^{K^* h}, \quad \overline{D} = K^{*-1}(A - I)$$

where A is the exponential matrix, $(k+1)$ denotes the $(k+1)th$ time step of computation, the time step h represents the time difference between the variable states X_k and X_{k+1} in the computation. I is the unit matrix. The dynamic response of the system can be obtained from Equation (4.2-9). Once the displacement and velocity

responses are obtained, the acceleration response can be obtained by directly differentiating the velocity response.

The sensitivity of the dynamic response with respect to the damage index can be derived as follows. Performing differentiation on both sides of Equation (4.2-8) with respect to the *ith* damage index α_E^i, we have,

$$\frac{\partial \dot{X}}{\partial \alpha_E^i} = K^* \frac{\partial X}{\partial \alpha_E^i} + \frac{\partial K^*}{\partial \alpha_E^i} X$$

$$= K^* \frac{\partial X}{\partial \alpha_E^i} + \begin{bmatrix} 0 \\ -M^{-1} \frac{\partial K}{\partial \alpha_E^i} d \end{bmatrix} + \begin{bmatrix} 0 \\ -a_2 M^{-1} \frac{\partial K}{\partial \alpha_E^i} \dot{d} \end{bmatrix} \quad (i=1,2,\ldots NE) \qquad (4.2\text{-}10)$$

Let $Y = \frac{\partial X}{\partial \alpha_E^i}$, and $G = \begin{bmatrix} 0 \\ -M^{-1} \frac{\partial K}{\partial \alpha_E^i} d \end{bmatrix} + \begin{bmatrix} 0 \\ -a_2 M^{-1} \frac{\partial K}{\partial \alpha_E^i} \dot{d} \end{bmatrix}$

where Y is the vector of displacement and velocity sensitivities with respect to the damage index in time domain. Equation (4.2-10) can be rewritten as

$$\dot{Y} = K^* Y + G \qquad (4.2\text{-}11)$$

It is noted that Equation (4.2-11) has the same form as Equation (4.2-8). The displacement and velocity response sensitivities can similarly be obtained as follows,

$$Y_{k+1} = AY_k + \overline{D} G_k \qquad (4.2\text{-}12)$$

The initial conditions of these response sensitivities have been discussed in Chapter four. In this chapter, they are also taken as zeros. Then the acceleration response sensitivity can be obtained by directly differentiating the velocity sensitivity. Similarly, the dynamic response with respect to the *ith* damage index α_A^i and α_I^i can be obtained by performing differentiations on both sides of Equation (4.2-8) with respect to α_A^i and α_I^i respectively.

$$\frac{\partial \dot{X}}{\partial \alpha_A^i} = K^* \frac{\partial X}{\partial \alpha_A^i} + \frac{\partial K^*}{\partial \alpha_A^i} X$$

$$= K^* \frac{\partial X}{\partial \alpha_A^i} + \begin{bmatrix} 0 \\ -M^{-1} \frac{\partial K}{\partial \alpha_A^i} d \end{bmatrix} + \begin{bmatrix} 0 \\ -a_2 M^{-1} \frac{\partial K}{\partial \alpha_A^i} \dot{d} \end{bmatrix} \quad (i=1,2,\ldots NE) \quad (4.2\text{-}13)$$

$$\frac{\partial \dot{X}}{\partial \alpha_I^i} = K^* \frac{\partial X}{\partial \alpha_I^i} + \frac{\partial K^*}{\partial \alpha_I^i} X$$

$$= K^* \frac{\partial X}{\partial \alpha_I^i} + \begin{bmatrix} 0 \\ -M^{-1} \frac{\partial K}{\partial \alpha_I^i} d \end{bmatrix} + \begin{bmatrix} 0 \\ -a_2 M^{-1} \frac{\partial K}{\partial \alpha_I^i} \dot{d} \end{bmatrix} \quad (i=1,2,\ldots NE) \quad (4.2\text{-}14)$$

4.2.3 Inverse Problem

The identification problem is addressed as: to find the vector of unknown damage indices $(\alpha_E^1, \alpha_E^2, \ldots \alpha_E^{NE}, \alpha_I^1, \alpha_I^2, \ldots \alpha_I^{NE}, \alpha_A^1, \alpha_A^2, \ldots \alpha_A^{NE})^T$ such that the calculated responses best match the measured responses, i.e.

$$[Q]\{R\} = \{\hat{R}\} \quad (4.2\text{-}15)$$

where the selection matrix [Q] is a constant matrix with elements of zeros and ones, which maps the degrees-of-freedom of the system to the measured degrees-of-freedom. { R } and { $\hat{R}$ } are the vectors of calculated and measured dynamic responses of the system respectively. The inverse problem is to minimize the error between the calculated and measured responses as

$$\{\delta R\} = \{\hat{R}\} - [Q]\{R\} = \{\hat{R}\} - \{R_{cal}\} \quad (4.2\text{-}16)$$

In the gradient-based method, the error vector is expressed as the first order Taylor expansion of the dynamic response,

$$\{\delta R\} = [S]\{\delta \alpha\} \quad (4.2\text{-}17)$$

where $\{\delta\alpha\}$ is the vector of perturbation of the damage indices, $\{\delta R\}$ is the error vector in the measured output, and $[S]$ is the sensitivity matrix. Equation (4.2-16) can be written in full as,

$$\{\delta R\} = \begin{Bmatrix} \hat{R}(t_1) \\ \hat{R}(t_2) \\ \vdots \\ \hat{R}(t_p) \end{Bmatrix} - \begin{Bmatrix} R_{cal}(t_1) \\ R_{cal}(t_2) \\ \vdots \\ R_{cal}(t_p) \end{Bmatrix} \tag{4.2-18}$$

with the number of time data points equal or larger than the number of unknown damage indices to have Equation (4.2-17) over-determined. Equation (4.2-17) can be solved by the damped least-squares method with bounds to the solution,

$$\{\delta\alpha\} = (S^T S + \lambda I)^{-1} S^T \{\delta R\} \tag{4.2-19}$$

where λ is the non-negative damping (regularization) coefficient governing the participation of least-squares error in the solution.

4.2.4 Computation Simulation

4.2.4.1 *A Plane Frame Structure*

The same plane frame structure as shown in Figure 3-2 is re-studied with the proposed method. It is discretized into eleven Euler beam elements with twelve nodes. The frame is fixed at nodes *1* and *12*. Each node has three degrees-of-freedom. The mass density and the Young's modulus of material are respectively $2.7\times10^{3}\ kg/m^{3}$ and $69\times10^{9}\ N/m^{2}$. The height and width of the frame structure are respectively 1.2 m and 0.6 m, and the cross-sectional dimensions are $b=0.01m$ and $h=0.02m$. The second moment of area is calculated as $6.67\times10^{-9}\ m^{4}$. The first five natural frequencies of the frame are 13.095, 57.308, 76.697, 152.410 and 196.485Hz.

Sensitivity to different type of damage index

First of all, the response and response sensitivity are calculated using both Newmark method and the state-space method demonstrated in Section 4.2.2. A sinusoidal excitation force of $F(t) = 10\sin(8\pi t)$ N is used to excite the structure. The time duration under study is 5 seconds. The force is applied at node *2* along the global *x*- direction. Damping ratio is taken equal to 0.01 for the first two modes. Two values of time increment are studied: 0.01s and 0.001s. Figure 4-8(a) shows the horizontal displacement response at node 10, and Figure 4-8(b) shows the sensitivity of this horizontal displacement response with respect to the damage index of the second moment of area of the first element. A close inspection of this figure shows that there is no obvious difference between the response and response sensitivity calculated from two different time increments by the state-space method. The response curves calculated by Newmark method from the above two different time increments do not match each other well at the first two seconds but match very well when the responses are stable. But the response sensitivity calculated by Newmark method from the above two time increments does not match each other well all the time. This shows that state-space method is better than the Newmark method with a better numerical stability. The response and response sensitivity in the following numerical simulation are calculated by the state-space method. Figure 4-9 shows the sensitivities of displacement response with respect to the three types of damage indices of the first element. It is noted that the displacement response is much more sensitive to damage indices α_E and α_I than damage index α_A (sensitivity of α_E is larger than that of α_A by two orders).

Procedure of Iteration

A check on the sensitivities of the four sets of damage indices show that the sensitivities with respect to α_E^i and α_I^i are much larger than those with respect to α_A^i. A two-stage iterative algorithm is therefore adopted here (Wu and Law, 2004). The

initial set of damage indices $\{\alpha_E\}$, $\{\alpha_I\}$, $\{\alpha_A\}$ are set to be zero, and the iteration process is divided into two stages:

Stage 1: Fix α_A^i and update the indices α_E^i and α_I^i.

Step 1: Solve the response vector $\{R\}$ from Equation (4.2-8) at *(k+1)th* iteration with known $(\alpha_E^i, \alpha_I^i)_k^T$ and compute the error vector $\{\delta R_k\}$.

Step 2: Solve Equation (4.2-10) and Equation (4.2-14) at *(k+1)th* iteration with known $(\alpha_E^i, \alpha_I^i)_k^T$ for the sensitivity $\{\frac{\partial R}{\partial \alpha_E^i}\}$ and $\{\frac{\partial R}{\partial \alpha_I^i}\}$ to form the sensitivity matrix.

Step 3: Find $(\alpha_E^i, \alpha_I^i)_{k+1}^T$ from Equation (4.2-19).

Step 4: Repeat Steps 1 to 3 until $\left\|(\alpha_E^i, \alpha_I^i)_{k+1}^T - (\alpha_E^i, \alpha_I^i)_k^T\right\| \le tolerance1$. The *tolerance1* equals 1.0×10^{-6} in this chapter.

Stage 2: Fix the updated values of α_E^i and α_I^i obtained from Stage 1 and update α_A^i.

Step 1: Solve the response vector $\{R\}$ from Equation (4.2-8) at *(k+1)th* iteration with known $(\alpha_A^i)_k^T$ and compute the error vector $\{\delta R_k\}$.

Step 2: Solve Equation (4.2-13) at *(k+1)th* iteration with known $(\alpha_A^i)_k^T$ for the sensitivity $\{\frac{\partial R}{\partial \alpha_A^i}\}$ to form the sensitivity matrix.

Step 3: Find $(\alpha_A^i)_{k+1}^T$ from Equation (4.2-20).

Step 4: Repeat Steps 1 to 3 until $\left\|(\alpha_A^i)_{k+1}^T - (\alpha_A^i)_k^T\right\| \le tolerance2$. The *tolerance2* is set to 1.0×10^{-6} in this chapter.

Repeat stages 1 and 2 in the next iteration until $\|R_{k+1} - R_k\| \le 10^{-5}$.

The convergence of this computation strategy has been proved by Li and Chen (1999) in the estimation of wind load and system parameters at the same time. While the uniqueness of the solution is not checked in this work, this and other algorithms for solving both the unknown forces and system parameters, such as Ling and Haldar (2004) and Shi et al. (2000), do not guarantee a unique solution. They all depend on the effectiveness of minimization of the objective function not falling into the local minimum. And the uniqueness of the algorithms remains to be an unsolved problem for further research.

Identification of different damage indices

A damage is simulated at the third element. The depth of the cross-section is assumed to be reduced by 1mm over the full width and length of the finite element. This is equivalent to a 14% reduction in the second moment of area of element 3 and 5% reduction in its cross-sectional area, i.e. $\alpha_I^3 = -0.14$ and $\alpha_A^3 = -0.05$. The Young's modulus of all elements is also assumed to be under-estimated by 5%, i.e. $\alpha_E^i = -0.05$, (i = 1,2,…,11). The damping ratios for the first two modes are taken equal to 0.01.

A sinusoidal excitation force of $F(t) = 10\sin(8\pi t)$ N is applied at node 2 along the global *x*-direction. Two acceleration measurements located at node 6 along the global *y*-direction and at node 9 along the global *x*-direction are collected. The sampling rate is 1000 Hz and data from the first two seconds after the application of force are used in the damage detection.

To assess the effect of measurement noise on the proposed method, white noise is added to the calculated acceleration responses of the beam to simulated the noisy measurement data with

$$acc_{measured} = acc_{calculated} + E_p \times N_{noise} \times \sigma(acc_{calculated}) \qquad \textbf{(4.2-20)}$$

where E_p is the noise level, N_{noise} is a standard normal distribution vector with zero mean value and unit standard deviation, $\sigma(acc_{calculated})$ is the standard deviation of the original acceleration response. The effect of 10% noise in the calculated response is studied.

Table 4-7 shows the iteration number and the optimal regularization parameter for convergence in the identification. Table 4-8 shows the results of damage detection in all the finite elements for the cases with and without noise. It is noted that not only the location of the damage is accurately identified; the damage pattern is also accurately classified. The distribution of damage can be read off directly from the table. For the case with 10% measurement noise, the identified indices α_I, α_E and α_A of the third element are respectively –0.06, –0.155 and –0.056 which are close to the true values. It may be concluded that the proposed method is not sensitive to measurement noise since the number of iteration required for convergence does not significantly increase as shown in Table 4-7.

4.2.4.2 *A Planar Truss Structure*

The same five-bay plane truss structure as shown in Figure 4-3 is re-studied as a numerical example here. Effects of modeling error in combination with measurement noise on the identified results are studied in this example. The mass density and Young's modulus of material are $7860\ Kg/m^3$ and $200\ GPa$ respectively. The finite element model of the structure consists of nineteen two-dimensional truss elements with eleven nodes and twenty-two degrees-of-freedom. An excitation force of $F = -10000 \sin 20\pi t\ N$ is acting at node 8 in the negative direction of the global *y*-axis. Two acceleration measurements located at node 4 along the global *y*-axis and node 10 along the global *x*-axis are collected. The damping ratios for the first two

modes are taken equal to 0.01 and 0.02 respectively. The sampling frequency is 1000 Hz and the first 2000 time steps data are used for the identification. Four damage scenarios as shown in Table 4-9 are studied.

Table 4-10 summarized the number of iteration and the optimal regularization parameter for convergence of the identification in each Scenario. Table 4-11 shows the identified results on Scenarios 1 and 3. The damage location and extent are identified with high accuracy even with 10% noise level.

Damage Scenario 4 is a multi-damage case in combination with modeling error and 10% measurement noise. Figure 4-10 indicates that accurate results are obtained for the damaged elements while there are false alarms in other elements with a maximum of 2.2% reduction in index α_A in element 13. From Table 4-10 one can see, more iteration steps are needed with modeling error. This indicates computation with modeling error require a longer computer time for convergence of the identification.

The above studies show finite element modeling error has larger effect on damage identification results than the random noise. A relatively accurate initial model of the structure is therefore required for correct representation of the structure in order to obtain accurate damage detection results, and this can be accomplished by updating the intact structure as illustrated in the section of experimental verification.

4.2.5 Experimental Verification

4.2.5.1 *Description of the Test Structure*

A five-bay three-dimensional frame structure was assembled using Meroform M12 construction system as shown in Figure 4-11(a). The structure consists of thirty-seven 22 *mm* diameter alloy steel tubes jointed together by 17 standard Meroform ball nodes.

Each tube is fitted with a screwed end connector which, when tightened into the node, also clamps the tube by means of an internal compression fitting. All the connection bolts are tightened with the same torsional moment to avoid asymmetry or nonlinear effects caused by man-made assembly errors. The length of all the horizontal, vertical and diagonal tube members between the centers of two adjacent balls is exactly 0.5 m after assembly. The structure orientates horizontally and is fixed into a rigid concrete support at three nodes at one end. Table 4-12 gives a summary of the main material and geometrical properties of the components of the test structure.

4.2.5.2 *Finite Element Modeling of the Test Structure*

In the finite element model of the structure, each ball joint is regarded as a node and each bar as a beam element. The finite element model consists of 37 three-dimensional Euler beam elements and 17 nodes as shown in Figure 4-11(b) and the dimensions of the structure are also shown in this figure. Each node has six DOFs, and altogether there are 102 DOFs for the whole structure. Appendix A shows the elemental mass stiffness and stiffness for finite element analysis.

The total weight of the ball and half weight of the bolt, which connects the ball with the beam elements, are placed on each node as the lump mass. Another half of the weight of the bolt is included as part of the beam element. Each ball node and bolt weighs 230 gram and 90 gram respectively. An additional mass of 72 gram weight is added to each joint to balance the mass of the accelerometers.

4.2.5.3 *Test Procedure on Structure*

Dynamic modal test was conducted on the undamaged structure first. The beam was excited with impacts from a B&K Type 8202 force hammer. A commercial data logging system INV303E and the associated signal analysis package DASP2003 were

used in the data acquisition. The sampling rate was 2020 Hz. Natural frequencies, modal damping and mode shapes were extracted from the measured data. The first eleven measured natural frequencies are listed in Table 4-13, and Figure 4-12 plots the corresponding mode shapes of the intact structure from the modal test. In order to reduce the finite element modeling error of the intact structure, the finite element model needs to be updated. The measured dynamic response from the intact structure is used to update the original finite element model. Due to the limitation of the computer, the measured acceleration data was re-sampled and the sampling rate reduces to one fourth of the original one, that is, 505 Hz. Only data from the first three seconds from two accelerometers (node 3, *z*-direction and node 4, *z*-direction) are used.

4.2.5.4 *Iteration Procedure*

The iteration procedure given for the simulation studies refers only to the treatment of indices with a wide range of sensitivities. The practical case of identification basing on two different states of the structure is discussed below.

When measurement from the undamaged state of the structure is obtained, the response and its sensitivity to a damage index are first computed basing on the analytical model of the structure and the measured input force. The analytical model is then updated and the response and its sensitivity are again computed for the next iteration.

When measurement from the damaged state is obtained, the updated analytical model is used in the iteration in the same way as that using the measurement from the undamaged state. The final set of identified damage indices correspond to the changes occurred in between the two states of the structure. In the present case, the damage

indices of all the elements form the vector of unknown parameter, which is initially set equals to a null vector.

4.2.5.5 *Initial Finite Element Model Updating*

On looking back on the finite element modeling of the structure, the modeling errors may come from two sources: the first one is the lump mass at each node of the structure. Since half weight of each bolt is assumed at the related node as lump mass, and this may be incorrect. Another possible source is the Young's modulus of the material. Therefore the proportion of weight of each bolt at the related node and the Young's modulus of material are taken as the design parameters for model updating. Three seconds response data obtained in the modal test of the intact structure is used to update the finite element model of the original structure. Results show that 62.5% of the weight of each bolt should be placed at the related node as lump mass and the Young's modulus is 99.3% of the original value. The first eleven calculated natural frequencies of the structure after updating are also shown in Table 4-13. The updated natural frequencies agree well with the measured natural frequencies with maximum relative error of 1.86%. The calculated and the measured modeshapes are checked by Modal Assurance Criteria (MAC) as shown in Table 4-14. The two mode shapes are observed matching each other very well. These show that the updated finite element model can represent accurately the intact structure for the next stage of damage detection.

4.2.5.6 *Damage Scenarios*

Several local faults are then introduced into the test structure by replacing two intact members with damaged ones. Damage Scenario E1 has the fourth beam element in the finite element model replaced by a damaged member. Damage was introduced

by grinding away a layer of material from the surface of the beam. Figure 4-13 gives a close view of this damaged member. The external diameter of the tube is reduced from 22.02 *mm* to 21.47*mm*, and the length of the weakened section is 202 *mm*, which locates in the middle of the beam with 99mm and 75mm length of original tube cross-section at both ends.

Damage scenario E2 includes two damage members. Apart from the damage member in Scenario 1, the second beam element in the finite element model was also replaced by a damaged member. The artificial damage is a perforated slot cut in the central length of the beam. The length of slot is 134.77mm, and the remaining depth of the tube in the cut cross-section is 14. 75mm. The slot opens vertically (global *z*-direction). Figure 4-14 gives a close view of this damaged member. Damage scenario E3 is similar to the last scenario but with the slot in element two opened horizontally (global *y*-direction).

4.2.5.7 *Damage Detection*

The perturbed modal properties corresponding to each damaged state of the test structure are obtained in another modal test, and the experimental modal frequencies are shown in Table 4-13. A falling weight test was then conducted on the structure afterwards for each damage scenario. A 5.15 kg mass was hung at node 17. Free vibration was introduced by the sudden release of the mass. The time histories from five accelerometers located at node 2 (global *z*-direction), node 3 (both *z*- and *y*-directions) and node 11(both *z*- and *y*-directions) were recorded for Damage Scenario 1. For Damage Scenarios 2 and 3, the time histories from five accelerometers located at node 14 (global *z*-direction), node 9 (both *z*-and *y*-directions) and node 11 (both *z*- and *y*-directions) were recorded. These responses were selected not in close proximity to the damaged elements. The sampling rate is 2020 Hz and the time duration is 8

seconds for each test covering the whole duration of vibration caused by the falling mass excitation.

Damage Scenario E1

This scenario has four types of damage in the beam element, i.e. a reduction in cross-sectional area *A*, the polar moment of area *J*, the second moments of area I_z and I_y. The analytical reduction in the parameters of the damaged element are estimated approximately by the Guyan reduction method, which are, 6.75%, 3.25%, 3.25% and 2.32% for the polar moment of inertia *J*, the second moments of inertia I_y and I_z, and the cross-sectional area *A* respectively. The measured acceleration data was re-sampled at 505 Hz. Orthogonal polynomial function (Law and Zhu, 2000) was utilized here to remove the measurement noise in the acceleration data. Only two seconds measured data from two accelerometers (node 3, *z*-direction and node 11, *z*-direction) were used for the damage identification. Four sets of damage indices, namely, α_J, α_{I_y}, α_{I_z}, and α_A are updated. The total number of unknown for updating is $37 \times 4 = 148$. And the number of equations is $505 \times 2 \times 2 = 2020$, the number of equations is much greater than the number of unknowns. The required iteration number for convergence and the optimal regularization parameter are 17 and 0.0025 respectively for updating α_A, and those for updating the remaining sets of indices are 23 and 0.0033 respectively. Table 6-7 shows the first eleven natural frequencies calculated for the updated damaged structure, and they are found matching the experimental values very well. Figure 4-15 shows the identified changes in the four sets of physical parameters. It is noted that both the location and the pattern of damage were identified successfully.

Damage Scenario E2

The analytical reduction in the parameters of the damaged element 2 are estimated approximately by the Guyan reduction method, which are, 26.65%, 6.74%, 23.25% and 8.76% for the polar moment of inertia *J*, the second moments of inertia I_y and I_z, and the cross-sectional area *A* respectively. Data in the first two seconds measurement from two accelerometers (node 9, *z*-direction and node 11, *z*-direction) were used for the damage identification. Figure 4-16 shows the identified results. The location of the damage and the damage patterns were identified correctly, except with some false alarms in I_y where elements 3, 5, 21, 27 and 30 are incorrectly identified to have a change larger than 1%. The required iteration number for convergence and the optimal regularization parameter are 19 and 0.0029 respectively for updating α_A and those for updating the remaining sets of damage indices are respectively 25 and 0.0053. The first eleven natural frequencies calculated for the updated damaged structure are shown in Table 4-13, and they are found matching the corresponding experimental values very well.

Damage Scenario E3

The analytical reduction in the parameters of the damaged element 2 are estimated approximately by the Guyan reduction method, which are, 26.65%, 23.25%, 6.74% and 8.76% for the polar moment of inertia *J*, the second moments of inertia I_y and I_z, and the cross-sectional area *A* respectively. Data in the first two seconds of measurement from two accelerometers (node 9, *z*-direction and node 11, *z*-direction) were used for the damage identification. Figure 4-17 shows the identified results. The location of the damage and the damage patterns were identified correctly, except with some false alarms in I_z where elements 16, 18, 23, 26 and 30 are incorrectly identified to have a change larger than 1.0%. The required iteration number for convergence and

the optimal regularization parameter are 18 and 0.0027 respectively for updating α_A and those for updating the remaining sets of damage indices are respectively 26 and 0.0054. The first eleven natural frequencies calculated for the updated damaged structure are shown in Table 4-13, and they are found matching the corresponding experimental values very well.

Identified Damage Values

The identified values for all the three Scenarios are given in Table 4-15. The damage in element 4 is identified with consistently values in all the Scenarios. Damage in element 2 with the major axis in the horizontal or vertical directions is also identified with consistently values. The values are all smaller than the predicted values from the approximate Guyan reduction method.

4.2.6 Concluding Remarks

A new approach for differentiating different types of load resistance of elements in a structure is proposed in this chapter. A method is proposed to calculate the sensitivities of dynamic response with respect to different types of damage indexes by both Newmark method and state-space method. Numerical study shows that state-space is more computational stable than Newmark method. And these damage indexes are used to detect both the location of damage, the extent of damage and type of damage as well. Two numerical simulations and a laboratory work show that the proposed method is effective and robust in both identifying damage and classifying the damage pattern. Studies show the proposed method is insensitive to measurement noise, but like many other damage detection methods, the finite element modeling error has larger effect on the accuracy of damage detection, so a relatively accurate

initial finite element model of the structure is required and thus a two-stage damage detection method is adopted to avoid large error in the damage detection results.

4.3 Identification of Prestress Force from Measured Structural Responses

4.3.1 Introduction

In this section, a method was proposed for identification of prestress force in structures based on structural dynamic response sensitivity. The sensitivity of dynamic responses (displacement, velocity and acceleration) with respect to a system parameter is derived by state space method.

An inverse problem to identify the prestress force is then presented taking the prestress force in all the elements as the unknown parameters in the identification with both sinusoidal and impulsive excitation. The sensitivities of acceleration or strain with respect to the unknown system parameter are used in the identification. The sensitivity-based finite element model updating method is adopted and very good results are obtained. The effect of measurement noise and model errors on the identification result is discussed. Computation simulations and laboratory test on a prestressed concrete beam show that the prestress force can be effectively identified from a short duration of measurement from as few as a single sensor.

4.3.2 Forward Problem

4.3.2.1 *Structural dynamic responses*

Figure 7-15 shows a two spans simply-supported, rectangular prestressed concrete bridge with a prestressing tendon. The equation of motion of the bridge deck modeled as an Euler-Bernoulli beam with N degrees-of-freedom can be written as

$$[M]\{\ddot{d}\}+[C]\{\dot{d}\}+[\overline{K}]\{d\}=\{F(t)\} \tag{4.3-1}$$

where d is the displacement vector, $\dot{d}$ and $\ddot{d}$ are the first and second derivative of d with respect to time t respectively. M is the mass matrix, C is the damping matrix. Here, Rayleigh damping is used, $\{F(t)\}$ is a vector of the nodal forces. $\overline{K}=K-K_g$ is the global stiffness matrix of the structure. K is the global stiffness matrix without prestress force, and K_g is the global geometrical stiffness matrix expressed as,

$$[K_g]=\sum_{i=1}^{NE}[k_g]^i$$

where NE is the total number of element of the finite element. The geometrical stiffness matrix of each element can be written as:

$$[k_g]^i=\frac{T^i}{30l}\begin{bmatrix} 30 & 0 & 0 & -30 & 0 & 0 \\ 0 & 36 & 3l & 0 & -36 & 3l \\ 0 & 3l & 4l^2 & 0 & -3l & -l^2 \\ -30 & 0 & 0 & 30 & 0 & 0 \\ 0 & -36 & -3l & 0 & 36 & -3l \\ 0 & 3l & -l^2 & 0 & -3l & 4l^2 \end{bmatrix}, \quad (i=1,2,...,NE)$$

where T is the uniform axially prestress force and l is the length of the element.

Writing Equation (4.3-1) in the state-space formulation,

$$\dot{X}=K^*X+\overline{F} \tag{4.3-2}$$

where $X=\begin{bmatrix} d \\ \dot{d} \end{bmatrix}_{2N\times 1}$, $K^*=\begin{bmatrix} 0 & I \\ -M^{-1}\overline{K} & -M^{-1}C \end{bmatrix}_{2N\times 2N}$, $\overline{F}=\begin{bmatrix} 0 \\ M^{-1}F \end{bmatrix}_{2N\times 1}$.

where X represents a vector of state variables with a length $2N$ containing the displacements and velocities at the nodes. These differential equations are then discretized using the exponential matrix representation,

$$X_{k+1} = AX_k + \overline{D}\overline{F}_k \tag{4.3-3}$$

$$A = e^{K^* h}, \qquad \overline{D} = K^{*-1}(A - I)$$

where A is the exponential matrix, $(k+1)$ denotes the value at the $(k+1)th$ time step of computation, and h represents the time increment between the variable states X_k and X_{k+1} in the computation. I is a unit matrix. The dynamic response of the system can be obtained from Equation (4.3-3), and the acceleration response can be obtained by directly differentiating the velocity response.

4.3.2.2 *The Strain Responses*

For a two-dimensional finite beam element of length l with deformation described by the deformation vector $(u_r, v_r, \theta_r, u_s, v_s, \theta_s)^T$ at its two ends r and s. The strain at any cross-section distance y from the left end of the element can be obtained in terms of the deformations at its two ends as

$$\varepsilon_x = \frac{u_s - u_r}{l} + \left(\frac{-z}{l^3}\right)[(12y - 6l)v_r + l(6y - 4l)\theta_r - (12y - 6l)v_s + l(6y - 2l)\theta_s] \tag{4.3-4}$$

where z is the distance from the neutral axis of the beam to the strain gauge.

4.3.2.3 *Sensitivity formulation in time domain*

The sensitivity of the dynamic response with respect to a physical parameter of the system, α_i, such as the prestress force, support stiffness and the flexural rigidity of a finite element, etc., can be obtained by differentiating both sides of Equation (4.3-2) with respect to parameter α_i of an element,

$$\frac{\partial \dot{X}}{\partial \alpha_i} = K^* \frac{\partial X}{\partial \alpha_i} + \frac{\partial K^*}{\partial \alpha_i} X$$

$$= K^* \frac{\partial X}{\partial \alpha_i} + \begin{bmatrix} 0 \\ -M^{-1} \frac{\partial \overline{K}}{\partial \alpha_i} d \end{bmatrix} + \begin{bmatrix} 0 \\ -a_2 M^{-1} \frac{\partial \overline{K}}{\partial \alpha_i} \dot{d} \end{bmatrix}, \quad (i=1,2,\ldots NE) \quad (4.3\text{-}5)$$

where a_2 is the coefficient of the Rayleigh damping as shown in Chapter 3.

Let $Y = \partial X / \partial \alpha_i$, where Y is the vector of displacement and velocity sensitivities with respect to parameter α_i.

Put $\overline{P} = \begin{bmatrix} 0 \\ -M^{-1} \frac{\partial \overline{K}}{\partial \alpha_i} d \end{bmatrix}$, and $\overline{G} = \begin{bmatrix} 0 \\ -a_2 M^{-1} \frac{\partial \overline{K}}{\partial \alpha_i} \dot{d} \end{bmatrix}$

Equation (4.3-5) can be rewritten as

$$\dot{Y} = K^* Y + \overline{P} + \overline{G} \quad (4.3\text{-}6)$$

It is noted that Equation (4.3-6) has the same form as Equation (4.3-2). The displacement and velocity response sensitivities can be obtained in a discretized form similar to Equation (4.3-3) as,

$$Y_{k+1} = AY_k + \overline{D}(\overline{P_k} + \overline{G_k}) \quad (4.3\text{-}7)$$

The acceleration response sensitivity can then be obtained by directly differentiating the velocity sensitivity.

4.3.2.4 *Strain Response Sensitivity*

Differentiating both sides of Equation (4.3-4) with respect to parameter α_i, we have

$$\frac{\partial \varepsilon_x}{\partial \alpha_i} = \frac{1}{l}\left(\frac{\partial u_s}{\partial \alpha_i} - \frac{\partial u_r}{\partial \alpha_i}\right) + \left(\frac{-z}{l^3}\right)\left[(12y-6l)\frac{\partial v_r}{\partial \alpha_i} + l(6y-4l)\frac{\partial \theta_r}{\partial \alpha_i} - (12y-6l)\frac{\partial v_s}{\partial \alpha_i} + l(6y-2l)\frac{\partial \theta_s}{\partial \alpha_i}\right]$$

(4.3-8)

which is a function of the displacement sensitivities at the two ends of the element.

4.3.3 Inverse Problem

The identification problem is to find the vector of prestress force $\{T\}$ such that the calculated responses best match the measured responses, i.e.

$$[Q]\{R\} = \{\hat{R}\} \tag{4.3-9}$$

where the selection matrix $[Q]$ is a constant matrix with elements of zeros or ones, which maps the degrees-of-freedom of the system to the measured degrees-of-freedom. $\{R\}$ and $\{\hat{R}\}$ are the vectors of calculated and measured dynamic responses of the system respectively. The inverse problem is to minimize the error between the calculated and measured responses as

$$\{\delta R\} = \{\hat{R}\} - [Q]\{R\} = \{\hat{R}\} - \{R_{cal}\} \tag{4.3-10}$$

In penalty function method, the error vector is expressed as the first order Taylor expansion of the dynamic response,

$$\{\delta R\} = [S]\{\delta T\} \tag{4.3-11}$$

where $\{\delta T\}$ is the vector of perturbation of the parameters, $\{\delta R\}$ is the error vector in the measured output, and $[S]$ is the sensitivity matrix. For a finite element model with *NE* elements, *NE* equations are needed to solve the unknown vector of prestress force in the elements. Equation (4.3-10) can be written in full as,

$$\{\delta R\} = \begin{Bmatrix} \hat{R}(t_1) \\ \hat{R}(t_2) \\ \vdots \\ \hat{R}(t_p) \end{Bmatrix} - \begin{Bmatrix} R_{cal}(t_1) \\ R_{cal}(t_2) \\ \vdots \\ R_{cal}(t_p) \end{Bmatrix} \tag{4.3-12}$$

with $p \geq NE$ to make sure that the equation is over-determined. Equation (4.3-12) can be solved by the damped least-squares method with bounds to the solution,

$$\{\delta T\} = (S^T S + \lambda I)^{-1} S^T \{\delta R\} \tag{4.3-13}$$

where λ is the non-negative damping (regularization) coefficient governing the participation of least-squares error in the solution.

4.3.3.1 *Procedure of Iteration*

When measurement from the non-prestressed state of the structure is obtained, the response and its sensitivity to a system parameter are first computed basing on the analytical model of the structure and the measured input force. The error vector is computed from Equation (4.3-10), and the vector of parameter increment is then obtained from Equation (4.3-13) or (4.3-14). The analytical model is then updated and the response and its sensitivity are again computed for the next iteration. Convergence is considered achieved when the following criterion is met:

$$\frac{\left\|T_{k+1} - T_k\right\|}{\left\|T_{k+1}\right\|} \leq tolerance \tag{4.3-14}$$

where *k* denotes the *kth* iteration. The *tolerance* is taken as 10^{-6} in this section.

When measurement from the prestressed state is obtained, the updated analytical model is used in the iteration in the same way as that using the measurement from the non-prestressed state. The final set of identified parameter increments correspond to the changes occurred in between the two states of the structure. In the present case, the prestress force in all the elements form the vector of unknown parameters, and is initially set equals to a null vector.

4.3.4 Computation Simulation

4.3.4.1 *Prestress Force Identification in a Single Span Beam*

A 30 metres long single span simply supported Euler-Bernoulli beam with a uniform 1.2×10^6 *N* axial prestress force is studied. The mass density and Young's

modulus of material are $2.5\times10^{3}\,kg/m$ and $3.5\times10^{10}\,N/m^{2}$ respectively, and the width and depth of beam are 0.6*m* and 1.2*m* respectively. The prestressed beam is modeled with ten equal Euler-Bernoulli beam elements with three degrees-of-freedom at each node. The first five natural frequencies are: 1.81, 8.27, 19.93, 35.76 and 56.16 Hz. Rayleigh damping is adopted, and the modal damping ratios for the first and second modes are assumed to be 0.02 and 0.04 respectively.

4.3.4.2 *Under Sinusoidal Excitation*

An external sinusoidal force $F(t)=8000[1+0.1\sin(4\pi t)+0.05\sin(15\pi t)]\ N$ is applied at 12 metres from the left support. The frequency components of the force are close to the first two modal frequencies of the beam. Vertical acceleration at 6 meters from the left support and strain measurement at the bottom of the beam 9 metres from the left support are recorded. The sampling rate is 200 Hz which is larger than two times the highest frequency of interest at 56.16 Hz. The beam is assumed initially at rest, and data recorded in the first two seconds after the application of the excitation force is used in the identification.

The identification is performed with three types of measured data: acceleration data or the strain data alone and then with both types of data. The number of iteration required for convergence and the optimal regularization parameters are respectively 24 and 5.21×10^{-9}, 38 and 2.08×10^{-11} and 30 and 1.33×10^{-10} for the three types of measured data. The identified prestress force in each element of the beam almost matches the true value perfectly with a maximum error of 0.25 %.

4.3.4.3 *Under Impulsive Excitation*

An impulsive force is applied at 12 meters from the left support for a short duration of 0.1 second. The magnitude of the force is 9500 N and it is expressed as

$$F(t)=\begin{cases}190000(t-0.05) & N \quad (0.05\le t\le 0.1)\\ 190000(0.15-t) & N \quad (0.1\le t\le 0.15)\end{cases} . \qquad (4.3\text{-}15)$$

Vertical acceleration at 6 meters from the left end is used for the prestress force identification. The sampling rate and number of data points are the same as for the last study. The iteration number for convergence of result and the optimal regularization parameter are 36 and 6.4×10^{-8} respectively. The identified prestress force in each beam element matches the true value excellently with a maximum error of 0.08%.

Results from the studies in this example indicate that the prestress force can be identified accurately from the measured dynamic responses either from acceleration response or strain response or their combination from as few as a single sensor. Identification from acceleration alone is more efficient than from the measured strain with fewer number of iteration for convergence.

4.3.4.4 *Prestress Force Identification in Two- Span Continuous Beam*

A two equal spans prestressed continuous beam as shown in Figure 4-18 is studied. The total length of the beam is 48 meters with the two ends on rigid support and the middle support modeled with a stiff linear spring of vertical stiffness of 1.5×10^{15} *N/m*. The finite element model of the prestressed beam consists of sixteen equal Euler-Bernoulli beam elements with three degrees-of-freedom at each node. The Young's modulus and mass density of material are 3.3×10^{10} N/m^2 and 2500 kg/m^3 respectively. Due to friction loss at the anchorage and friction (Eugene and Andrew, 1995), non-uniform distribution of the prestress is considered. Assuming the beam is jacked from both ends to a tension of 40000 *kN*, the final prestress forces in the elements are listed in Table 4-16. The first five natural frequencies of the prestressed beam are: 3.83, 6.36, 16.69, 21.29 and 28.05 *Hz*. Modal damping ratios for the first and second modes are taken to be 0.02 and 0.04 respectively.

The same sinusoidal excitation as used for the single span beam is used. It is applied at a point 15 *m* from the left support. The sampling rate is 200 *Hz*. The following cases of using two seconds of different type and combination of measured information are studied.

- Case 1 – Acceleration at 18 *m* from the left support.
- Case 2 – Acceleration at 18*m* and strain at 30 *m* from the left support.
- Case 3 – Acceleration at both 18*m* and 30*m* from the left support.
- Case 4 – Strain at both 6 *m* and 30 *m* from the left support.
- Case 5 – Acceleration at both 18*m* and 30*m* from the left support contaminated with 1% or 10% noise.

To simulated the effect of measurement noise, a normally distributed random error with zero mean and a unit standard deviation is added to the calculated displacement as

$$\hat{R} = R_{cal} + Ep \times N_{oise} \times \text{var}(R_{cal}) \qquad (4.3\text{-}16)$$

where $\hat{R}$ is the vectors of measured structural response; E_p is the noise level; N_{oise} is a standard normal distribution vector with zero mean and unit standard deviation; var(•) is the variance of the time history.

The identified prestress force is shown in Table 4-16 together with the required number of iteration and the optimal regularization parameter for each Case. Case 1 fails to identify the prestress force. This may be due to the fact that the sensor is located at the nodal point of the third mode of vibration, and the first three modes contribute greatly to the vibrational response of the beam. Results with an error of identification larger than 1% are highlighted. The error in all cases is very small with a maximum of -1.87%. Acceleration data is found to be more effective than strain data with a smaller number of iteration for convergence and the proposed method is not sensitive to random measurement noise. It is concluded that two second of measured

data from a strain gauge and an accelerometer could in general identify the prestress force distribution along a beam with good accuracy.

4.3.4.5 *Effect of Model Errors*

The effect of different possible model errors is studied with measured acceleration at both 18*m* and 30*m* from the left support. The excitation force, sampling rate and the number of data used for the identification are the same as for last study.

- Case 6 – with 5% under-estimation in the flexural rigidity of the beam
- Case 7 – with reduction of support stiffness to $1/10^{th}$ of the original
- Case 8 – with 3% under-estimation in the mass density of material
- Case 9 – with a change in Rayleigh damping coefficients: the two coefficients a_1 and a_2 are changed from 0.02 and 0.04 to 0.04 to 0.08
- Case 10a – with all the above mentioned model errors together
- Case 10b – with all the above mentioned model errors together plus 10% random noise in the measurements

The identified results for all the above Cases are shown in Table 4-17. The two largest errors in each case are highlighted. The errors for Cases 6 to 9 are very small, while Case 8 with a model error in the mass density shows a slightly larger error than the other cases. This is because the sensitivity of response to a perturbation in the prestress force is very large compared with a small change in other physical parameters of the structural system, e.g. support stiffness, flexural stiffness of the beam, material constants and mass density. This is further confirmed in the results for Case 10 where the error of identification is dominated by the 10% noise effect rather than the combination of different types of model errors.

The relatively small error in the identification is due to the large response sensitivity when compared with sensitivities with respect to other physical parameters

of the structural system, e.g. support stiffness, flexural stiffness of the beam as shown in Figure 2. The curves in Figure 2 are from the case with a sinusoidal excitation force of 20000 *N* at 2*Hz* acting at 21 metres from the left end of the single span beam in the first example. The acceleration response is measured at a point 15 metres from the left support. A beating phenomenon is observed due to the close proximity of the excitation frequency to the fundamental frequency of the structure. The shapes of the sensitivity curves are similar to the dynamic response with similar phase, but there is a phase reversal in the case of the sensitivity with respect to the prestressing force. It should be noted that these observations are only specific to this type of structure and the type of excitation used, but there is a clear dependence between the sensitivities and the original dynamic response.

4.3.5 Experimental Verification

The proposed method is further verified with a simple prestress concrete beam in the laboratory. Figure 4-20(a) shows the experiment setup of the beam. The experimental setup is shown diagrammatically in Figure 4-20(b). It is 4.0 meters long with a $150mm \times 200mm$ uniform cross-section and a clear span of 3.8 meters. A seven-wire straight strand was placed in a 57*mm* diameter duct located at the centre of gravity of the beam cross-section throughout the length of the beam. The duct remains ungrouted such that the prestress force can be monitored as a reference. The elastic modulus of concrete and the steel strand are respectively 31.5×10^9 N/m^2 and 194×10^9 N/m^2 and the mass density of concrete is $2.398 \times 10^3 kg/m^3$. The yield strength of the strand is 192 *kN*. The beam is instrumented with seven equally spaced accelerometers to measure the vertical acceleration responses of the beam. Seven strain gauges are also instrumented on the upper surface of the beam; they locate at L/16, 3L/16, 5L/16, 7L/16, 9L/16, 11L/16, and 13L/16 from the left end.

4.3.5.1 *Modal Tests*

Dynamic modal test is conducted on the concrete beam without prestress force first. The beam is excited with impacts from a Dytran Instruments 12 *lb* instrumented impulse hammer, model 5803A in the vertical direction at a fixed point 3L/8 from the left support. A commercial data logging system INV303E and the associated signal analysis package DASP2003 are used in the data acquisition. One load cell is located at one end of the strand to measure the magnitude of prestress force applied on the concrete beam. The load cell is calibrated before it was installed on the prestress tendon. During the test, once we measured the strains of the lead cell, the prestress force can be calculated from the strain values. After 100 *KN* prestress force is applied to the prestressing strand, another modal test is conducted on the prestressed beam. The frequencies are found increased after prestressing. This seems to contradict with the prediction from the theoretical formula (Kim et al., 2004)

$$\omega_n^2 = \left(\frac{n\pi}{L}\right)^4 \frac{E_c I_c}{\rho_c A_c} - \left(\frac{n\pi}{L}\right)^2 \frac{T}{\rho_c A_c} \tag{4.3-17}$$

where $E_b I_b$ is equivalent flexural rigidity of the beam section, $\rho_c A_c$ is the mass of beam per unit length. T is the magnitude of the prestress force. Equation (4.3-17) shows that an increase in the axial compressive force reduces the modal frequency and vice versa. But on further checking on the experimental system, we found that the equivalent flexural rigidity of the beam without prestress force is 3.13×10^3 *kN-m*^{2}, and it increases to 3.20×10^3 *kN-m*^{2} after prestressing. Also the equivalent mass per unit length of the beam is increased by 1.49% after prestrsssing. This is due to the presence of the additional equivalent flexural rigidity and the mass of the prestressing strand. Thus the physical presence of the prestressing tendon has dual effects on the natural frequency of the beam. The prestressing tendon itself increases the flexural rigidity and

hence the natural frequency of the beam, but the self weight and compressive axial force it carries reduce the frequency of the beam. However, the stiffening effect from the increase in the equivalent flexural rigidity is greater than the softening effect due to the compressive axial force and the additional inertia effect due to its self weight. And this results in a net increase in the natural frequency. Other effect such as an increase in the dynamic modulus of concrete is considered small and is therefore not discussed.

4.3.5.2 *Identification of Prestress Force*

The initial finite element model of the beam before prestressing consists of sixteen two-dimensional Euler-Bernoulli beam elements with three degrees-of-freedom at each node. Impulsive force is applied with the impact hammer at *1/4L* from the left support of the beam. The sampling rate is 2000 Hz. Time histories of both the excitation force and the accelerations are recorded, and data obtained from the third and fourth accelerometers are used in the prestress force identification.

The initial finite element model of the beam before prestressing consists of sixteen two-dimensional Euler-Bernoulli beam elements with three degrees-of-freedom at each node. The flexural rigidity of the beam is calculated as 3.13×10^3 *kN-m*^{2}. The support stiffnesses are updated using the proposed sensitivity approach with 1 second measured data from the two accelerometers, and the left and right support stiffnesses are revised to 8.9×10^7 *N/m* and 9.4×10^7 *N/m* respectively. Rayleigh damping model is adopted in calculating the structural response, and the measured modal damping ratios for the first three modes are respectively 0.028, 0.15 and 0.11. The analytical modal frequencies are shown in Table 4-18.

After the beam is prestressed, the flexural rigidity of the beam section is calculated to be 3.20×10^3 *kN-m*^{2}. The prestress force is identified using data from 0.2 second to 1.0 second after the hammer impact. The first 0.2 second data is skipped because of the

many high frequency components in the response caused by the impulsive force created by the hammer. The orthogonal polynomial function is used to remove the measurement noise. The measured modal damping ratios for the first three modes are respectively 0.022, 0.14 and 0.08. The load cell at the end of the strand shows that the prestress force is 66.7 KN. The identified prestress force and error are shown in Table 4-19, and they are very close to the true force with a maximum error of 10.9% close to one end of the beam. The relative error reduced much compared with the results from the last section. 56 iterations are required for convergence of the results and the corresponding optimal regular parameter is 1.03×10^{-8}. Figure 4-21 shows the curve of convergence and Figure 4-22 shows the reconstructed acceleration responses and the corresponding measured ones. It is noted that these two sets of time histories match each other very well.

4.3.6 Concluding Remarks

A method based on response sensitivity is proposed for identification of prestress force in this section. The sensitivities of dynamic responses with respect to physical system parameters are analytically derived. The sensitivity-based method is used to update the prestress force in an Euler-Bernoulli beam. Both sinusoidal and impulsive excitations from an impact hammer are used, and the effectiveness of both acceleration and strain responses for the identification are studied. Very good identified results can be obtained from a very short duration of 2 seconds from as few as a single measuring point. Numerical simulations and experimental results from a prestressed concrete beam in the laboratory show that the proposed method is insensitive to different types of model errors and measurement noise, but a combination of these two factors would give significant error in the identified result.

4.4 Simultaneous Identification of System Parameters and Input Force

4.4.1 Introduction

In Chapter 3, a method for damage detection based on response sensitivity is proposed and it can be used to identify structural damage successfully. It is assumed that the excitation force can be measured and it is known *a priori*. But in practice, sometimes the excitation force cannot be measured. This section deals with a more general problem when the excitation force is unknown and thus we need to identify the excitation force and the structural damage simultaneously. This research topic has been explored by other researchers. Chen and Li (2004) and Shi et al (2000) presented methods to identify structural parameters and input time history simultaneously from output-only measurements. The structural parameters and the input time history are obtained in an iterative manner. Law and Zhu (2004) also proposed an approach for damage detection in a concrete bridge structure in time domain. Both the damage and moving vehicular loads are identified successfully.

In this section, Newmark method is used in the computation of dynamic response and the sensitivities of dynamic response with respect to the structural physical parameters. The parameter changes are identified simultaneously using an iterative algorithm. A notable advantage of the proposed method is that as few as one dynamic response measurement of the structure is needed in the inverse analysis. A prestressed single-span concrete beam and a two-span continuous beam are used as numerical example to illustrate the effectiveness of the proposed method. Computation

simulations show that the proposed method is not sensitive to measurement noise. Experimental results obtained from a simply supported steel beam with damage excited by a releasing a dead weight demonstrate that the proposed method can successfully identify both the unknown excitation and physical parameters simultaneously.

4.4.2 The Dynamic Response and Response Sensitivity

Figure 4-23 shows a simply supported rectangular prestressed concrete beam with a straight tendon passing through the centroid of the cross-section. The equation of motion by finite element representation can be written as

$$[M]\{\ddot{d}\}+[C]\{\dot{d}\}+[\overline{K}]\{d\}=[B]\{F\} \qquad (4.4\text{-}1)$$

where d is a vector of displacement, $\dot{d}$ and $\ddot{d}$ are the first and second derivatives of d with respect to time t respectively, M is the mass matrix, C is the damping matrix, as in last chapter, Rayleigh damping model in utilized in this section. $\{F\}$ is the vector of input excitation forces and $[B]$ maps these forces to the associated degrees-of-freedom of the structure. $\overline{K}$ is the global stiffness matrix of the prestressed beam with $\overline{K} = K - K_g$, where K is the global stiffness matrix without prestress force. K_g is the global geometrical stiffness matrix, $K_g = \sum_{i=1}^{NE}[k_g]_e^i$, NE is the total number of element, and k_g is the elemental geometrical stiffness matrix.

The *j*th input force is represented by

$$F^j(t) = \sum_{l=1}^{n}(F_0^j + F_l^j \sin \omega_l{}^j t) \qquad (j=1,2,\ldots,N_f) \qquad (4.4\text{-}2)$$

where, F_0^j F_l^j, ω_l^j are parameters of the *jth* force, N_f is the total number of excitation force and *n* is the number of terms in the series. They are taken as the unknown force parameters to be identified in the inverse problem.

Expressing the stiffness matrix of the structure as the summation of the elemental stiffness matrices, and substituting Equation (4.4-2) into Equation (4.4-1), we have

$$[M]\{\ddot{d}\}+[C]\{\dot{d}\}+(\sum_{i=1}^{NE}[k]_i^e-[K_g])\{d\}=[B]\{\sum_{l=1}^{n}(F_0^j+F_l^j\sin\omega_l^j t)\} \qquad (4.4\text{-}3)$$

where $[k]_i^e$ is the *i*th elemental stiffness matrix. The dynamic response can be obtained from Equation (4.4-3) using Newmark method.

The response sensitivity with respect to the parameters of force and system parameters is derived as follows.

Performing differentiation to both sides of Equation (4.4-3) with respect to the parameters of the *jth* excitation force, we have,

$$[M]\{\frac{\partial\ddot{d}}{\partial F_0^j}\}+[C]\{\frac{\partial\dot{d}}{\partial F_0^j}\}+(\sum_{i=1}^{NE}[k]_i^e-[K_g])\{\frac{\partial d}{\partial F_0^j}\}=[B] \qquad (4.4\text{-}4)$$

$$[M]\{\frac{\partial\ddot{d}}{\partial F_l^j}\}+[C]\{\frac{\partial\dot{d}}{\partial F_l^j}\}+(\sum_{i=1}^{NE}[k]_i^e-[K_g])\{\frac{\partial d}{\partial F_l^j}\}=[B]\sin\omega_l^j t \qquad (4.4\text{-}5)$$

$$[M]\{\frac{\partial\ddot{d}}{\partial \omega_l^j}\}+[C]\{\frac{\partial\dot{d}}{\partial \omega_l^j}\}+(\sum_{i=1}^{NE}[k]_i^e-[K_g])\{\frac{\partial d}{\partial \omega_l^j}\}=[B]F_l^j t\cos\omega_l^j t \qquad (4.4\text{-}6)$$

Performing differentiation to both sides of Equation (4.4-3) again with respect to the *jth* physical parameter, P_{Sj}^i , of the *i*th element, we have,

$$[M]\{\frac{\partial\ddot{d}}{\partial P_{Sj}^i}\}+[C]\{\frac{\partial\dot{d}}{\partial P_{Sj}^i}\}+(\sum_{i=1}^{NE}[k]_i^e-[K_g])\{\frac{\partial d}{\partial P_{Sj}^i}\}=-\frac{\partial[k]_i^e}{\partial P_{Sj}^i}\{d\}-a_2\frac{\partial[K]}{\partial P_{Sj}^i}\{\dot{d}\} \qquad (4.4\text{-}7)$$

where a_2 is the coefficient for Rayleigh damping. Note that Equations (4.4-4) to (4.4-7) have the same form as Equation (4.4-3). The response sensitivities can also be

obtained by Newmark method. The initial values of the dynamic responses and sensitivities are all taken equal to zero. In the case of non-zero initial conditions, the sensitivities obtained would be a little different from those with zero initial conditions, but such differences would diminish very rapidly since their effects are transient occurrences. Furthermore if the non-zero effects have to be quantified, the transient responses due to them can be computed as well as their sensitivity with respect to the required physical parameter or force parameter, and they can be identified together in the same iterative process as shown below.

4.4.3 Identification of Excitation Force and Damage

The identification problem is to find the vectors of the force parameters $\{P_F\}$ and the physical parameters of the system $\{P_S\}$ such that the calculated acceleration $\{\ddot{d}\}$ best matches the measured response $\{\hat{\ddot{d}}\}$, i.e.

$$[Q]\{\ddot{d}\} = \{\hat{\ddot{d}}\} \tag{4.4-8}$$

$$\{P_F\} = [F_0^1,...,F_n^1,\omega_1^1,...,\omega_n^1,F_0^2,...,F_n^2,\omega_1^2,...,\omega_n^2,F_0^{Nf},...,F_n^{Nf},\omega_1^{Nf},...,\omega_n^{Nf}]^T$$

$$\{P_S\} = [EA^1,EI_y^1,EI_z^1,GJ^1,L^1,P^1,...,EA^{NE},EI_y^{NE},EI_z^{NE},GJ^{NE},L^{NE},P^{NE},K_V^1,K_R^1,...,K_V^{ns},K_R^{ns}]^T$$

where the selection matrix $[Q]$ matches the degrees-of-freedom corresponding to the measured acceleration components. Vector $\{P_S\}$ gives all the physical parameters for the set of beam-column two-dimensional finite element member, and *ns* is the number of supports. L^i, P^i are the length and axial prestress of the *i*th element, and K_V^i, K_R^i are the translational and rotational stiffness of the *i*th support. Let the error vector be

$$\{\delta z\} = \{\hat{\ddot{d}}\} - [Q]\{\ddot{d}\} \tag{4.4-9}$$

The identification problem can be accomplished in the following two stages.

4.4.3.1 *Input Force Identification*

In the penalty function method, we have,

$$\{\delta z\} = [S_F]\{\delta P_F\} \tag{4.4-10}$$

The physical parameters of the intact structure are used in calculating the matrix $[S_F]$ as we are not certain about the true state of the damage structure. $[S_F]$ is the two-dimensional sensitivity matrix, which is the change of acceleration response with respect to the force parameters in time domain. $\{\delta P_F\}$ is the vector of perturbation in the force parameters. Substituting Equation (4.4-9) and rewriting Equation (4.4-10) in full, we have

$$\begin{Bmatrix} \hat{\ddot{d}}(t_1) \\ \hat{\ddot{d}}(t_2) \\ \vdots \\ \hat{\ddot{d}}(t_m) \end{Bmatrix} - [Q] \begin{Bmatrix} \ddot{d}\ (t_1) \\ \ddot{d}(t_2) \\ \vdots \\ \ddot{d}(t_m) \end{Bmatrix} = [S_F]\{\delta P_F\} \tag{4.4-11}$$

where m is the number of time steps, which should be larger than the number of unknown force parameters to make sure that the set of equation is over-determined. Equation (4.4-10) can be solved by the damped least-squares method (DLS) as follows,

$$\{\delta P_F\} = ((S_F)^T (S_F) + \lambda I)^{-1} (S_F)^T \{\delta z\} \tag{4.4-12}$$

where λ is the non-negative regularization parameter governing the participation of least-squares error in the solution. The solution of Equation (4.4-12) is equivalent to minimizing the function

$$J(\{\delta P_F\}, \lambda) = \left\| (S_F)\{\delta P_F\} - \{\delta z\} \right\|^2 + \lambda \left\| \{\delta P_F\} \right\|^2 \tag{4.4-13}$$

with the second term in Equation (4.4-13) providing bounds to the solution. When the parameter λ approaches zero, the estimated vector $\{\delta P_F\}$ approaches to the solution obtained from the simple least-squares method.

4.4.3.2 *Damage Identification*

Once the forces have been obtained from above, we can move on to the local damage identification. Again by using the penalty function method, we have,

$$\{\delta z\} = [S_S]\{\delta P_S\} \tag{4.4-14}$$

The physical parameters of the intact structure are used in calculating the matrix $[S_S]$. $[S_S]$ is the two-dimensional sensitivity matrix, which is the change of acceleration response with respect to the physical parameter in time domain. $\{\delta P_S\}$ is the vector of perturbation of the parameter. The physical parameter can also be obtained from

$$\{\delta P_S\} = ((S_S)^T(S_S) + \lambda I)^{-1}(S_S)^T\{\delta z\} \tag{4.4-15}$$

or

$$(P_S)_{j+1} = (P_S)_j + ((S_S)_j^T(S_S)_j + \lambda I)^{-1}(S_S)_j^T\{\delta z_j\} \tag{4.4-16}$$

where subscript "*j*" indicates the iteration number.

4.4.3.3 *Algorithm of Iteration*

Since both the excitation force and the damaged structure are unknown, the following iterative algorithm is used in the identification:

(A) Iteration for the excitation force parameters

Starting with a set of given initial values on the unknown force parameter vector $\{(P_F)_0\}$ and the intact set of physical parameter $\{(P_S)_0\}$, the procedure of iteration is given as:

Step 1: With the initial force vector and vector of the undamaged system, Equation (4.4-3) is solved at *j=k+1* iteration step for the acceleration $\{\ddot{d}\}$ and the error vector $\{\delta z_k\}$ is computed.

Step 2: Solve Equations (4.4-4) to (4.4-6) at *j=k+1* iteration step with known $\{(P_F)_k\}$ for the sensitivity matrix $[\partial\ddot{d}/\partial(P_F)_k]$.

Step 3: Find $\{(P_F)_{k+1}\}$ from Equation (5-12) .

Step 4: Repeat Steps 1 to 3 until $\left\|\frac{\{(P_F)_{k+1}\}-\{(P_F)_k\}}{\{(P_F)_{k+1}\}}\right\| \le$ *convergence* limit1.

(B) Iteration for the elemental flexural rigidity

With the modified excitation force parameter vector $\{P_F\}$ obtained from (A) above, and take the intact vector of physical parameter as initial value of $\{P_S\}_0$,

Step 5: Equation (4.4-3) is solved at *j=k+1* iteration step for the acceleration $\{\ddot{d}\}$ and the error vector $\{\delta z_k\}$ is computed.

Step 6: Solve Equation (4.4-7) at *j=k+1* iteration step with known $\{(P_S)_k\}$ for the sensitivity matrix $[\partial\ddot{d}/\partial(P_S)_k]$.

Step 7: Find $\{(P_S)_{k+1}\}$ from Equation (4.4-16).

Step 8: Repeat Steps 5 to 7 until $\left\|\frac{\{(P_S)_{k+1}\}-\{(P_S)_k\}}{\{(P_S)_{k+1}\}}\right\| \le$ *convergence* limit2 .

The identified excitation force obtained in (A) can be further improved using the updated physical parameters obtained in (B) and repeating Steps 1 to 4. On the other hand, the vector of physical parameters can also be further improved using the modified excitation force and repeating Steps 5 to 8. In the simulation examples of this

section, the convergence limit is 1.0×10^{-6} in both the force and parameter identification.

4.4.4 Computation Simulations

4.4.4.1 *Study Case 1 - One impulsive force on a single span beam with one local damage*

A 20 metres long single span simply supported Euler-Bernoulli beam as shown in Figure 4-23 with a constant axial prestress force of $1.0\times10^{6}\,N$ is studied, the prestess tendon is assumed to be unboned. The physical parameters of the beam are: mass density $\rho = 2.5\times10^{3}\,kg/m^{3}$, Young's modulus $E = 3.3\times10^{10}\,N/m^{2}$, length $L = 20\,m$, width $b = 0.6\,m$ and height $h_0 = 1.0\,m$.

The impulsive force is assumed to act on the beam at 8 metres from the left support at time 0.05 second and lasting for 0.05 second. It is assumed to be a constant in such a small time interval, and is expressed mathematically as,

$$F(t) = \begin{cases} 8000\,N & 0.05 \le t \le 0.1 \\ 0 & 0 \le t < 0.05 \text{ or } t > 0.1 \end{cases} \qquad (4.4\text{-}21)$$

White noise is added to the calculated responses of the beam to simulate the noisy measured data with

$$\hat{\ddot{d}} = \ddot{d} + E_p \times N_{noise} \times \sigma(\ddot{d}) \qquad (4.4\text{-}22)$$

where E_p is the noise level, N_{noise} is a standard normal distribution vector with zero mean value and unit standard deviation, $\sigma(\ddot{d})$ is the standard deviation of the calculated acceleration response. The effect of 1%, 5% and 10% measurement noise on the identified result is studied.

The finite element model of the beam consists of ten equal Euler-Bernoulli beam elements with three degrees-of-freedom at each node. The first five natural frequencies of the intact beam are: 4.07, 16.42, 37.03, 65.93 and 103.25 Hz. The damping ratios for these five modes are all equal to 0.02. The local damage is simulated by a 10% reduction in the flexural rigidity of the 3rd element from the left. The force is modeled with five sinusoidal terms plus a constant term as shown in Equation (4.4-2), and the initial set of force parameters is chosen as (1000, 1000, 1000, 1000, 1000, $1000, 2\pi, 4\pi, 6\pi, 8\pi, 10\pi)^T$, where the first six values are the amplitudes, and the last five values are the circular frequencies of the force. Since Equation (4.4-10) is a linear approximation, the parameters of the force are obtained in an iterative manner. It is noted that the force parameters are updated from minimizing a non-linear function using an iterative approach, a local rather than a global minimum maybe found. This may be checked by using a number of the different initial values for the unknown force parameters. In the present numerical example, study shows that when the magnitudes of the force parameters are less than 1000, the constructed force will fail to converge to the true force whereas the magnitudes of the force parameters are equal or greater than 1000 will converge to the true value. Thus the magnitudes of the force are all set to 1000. The time step is *0.001 s* and the response for 2 seconds is calculated. One vertical acceleration measurement at 12 metres from the left support is collected and 2000 data are used. The required number of iteration for convergence for the force with 1, 5 and 10% noise is 70, 72 and 78 respectively, and that for the local damage is 36, 40 and 47 respectively. The optimal regularization parameter λ_{opt} corresponding to 1, 5 and 10% noise level are 0.003, 0.005 and 0.006 respectively for the force and 6.5×10^{-7}, 1.18×10^{-6} and 1.22×10^{-6} respectively for the damage. Table 4-20 summarized the iteration steps required and the optimal regularization parameters corresponding to

different noise levels. Figures 4-24 and 4-25 give the identified results of the impulsive force and the damage. From these figures, the following observations can be obtained:

- The identified impulsive force and the local damage are all close to the true values. This shows that the proposed method is correct and effective to identify iteratively both the excitation force and damage in the beam from noisy dynamic response measurement.
- The identified results are similar and the required number of iteration for convergence is also similar for different noise level under study. This indicates that the present method is relatively insensitive to noise in the measurement.
- The sensitivities of the force parameters, especially the frequency components, have been checked to be much larger than those of the physical parameters. This leads to a much larger regularization in the identified results in the force identification compared with the physical parameters as seen in the two sets of optimal regularization parameters. This will be further studied below.

4.4.4.2 *Study Case 2 – One sinusoidal excitation force on a two-span beam with four local damages*

A 30 metres long simply supported two-span continuous Euler-Bernoulli beam with a constant axial prestress force of $1.2\times10^{6}\ N$ is studied. The physical parameters of the beam are: mass density $\rho = 2.5\times10^{3}\ kg/m^{3}$, Young's modulus $E = 3.3\times10^{10}\ N/m^{2}$, length $L = 30\ m$, width $b = 0.6\ m$ and height $h_0 = 1.0\ m$. The finite element model of the beam consists of sixteen equal Euler beam elements with three degrees-of-freedom at each node. The first five natural frequencies of the intact beam are: 7.26, 11.39, 29.23, 37.00 and 65.90 Hz. The damping ratios for these five modes are all equal to 0.02. The external excitation force

is $f(t) = 16000 \times (1 + 0.1\sin 12\pi t + 0.05\sin 50\pi t)$ *N* and it is applied at the 3rd nodes from the left support. The time step is *0.001 s* and the response for 2 seconds is calculated. One vertical acceleration measurement at the 7th node from the left support is used and 2000 data points are used in the identification. 10% noise is added to the calculated acceleration to simulate the measured response.

The purpose of this study is on the resolution capability of the proposed method for damages at close proximity to each other and on the effect of model error on the identification. The local damages are simulated by assuming 5%, 10%, 5% and 8% reduction in the flexural rigidity of elements 5, 6, 14 and 15 respectively. No model error is assumed in Scenario 1, while 5 % reduction in the flexural rigidity of all the beam elements is assumed in Scenario 2.

Again, the excitation force is modeled with five sinusoidal terms plus a constant term. Since the sensitivity of response to the frequency component of the force is much higher than that for the amplitude of the force, a two-step strategy is adopted in the force updating to avoid large error in the identified force when both types of force parameters are identified simultaneously. The first step updates the frequency components with the initial vector of the force amplitude which have been all initially set at *1000 N*. The initial set of circular frequency of the force is $(14\pi, 22\pi, 30\pi, 40\pi, 60\pi)^T$. The first two frequency components are selected near the first two natural frequencies of the bridge. The other three components are arbitrarily chosen, there is no obvious different in the final results for different values of these three components. The second step adopts the identified frequency components as the true values and updates the force amplitudes. The same set of measured data points are used in the iteration.

The final identified force time histories shown in Figure 4-26 almost overlap each other indicating a high accuracy in the force identification. The identified damages are shown in Figure 4-27 after the second cycle of iterations. The identified reductions in Scenario 1 are 4.8%, 9.5%, 5.3% and 7.5% in elements 5, 6, 14 and 15 respectively. The required number of iteration in the second cycle for the forcing frequency, the magnitude and the damage are respectively 23, 36 and 32. The optimal regularization parameters are respectively 0.08, 6.3×10^{-4} and 8.5×10^{-9}. The identified reductions in Scenario 2 are 4.4%, 9.3%, 5.6% and 7.4% in elements 5, 6, 14 and 15 respectively. The required number of iteration in the second round for the forcing frequency, the magnitudes and the damage are respectively 30, 45 and 40. The optimal regularization parameters are 0.11, 4.5×10^{-4} and 6.7×10^{-9} respectively. Table 4-21 summarized the iteration steps required and the optimal regularization parameters for Study case 2. The two sets of results are very close to each other and to the true value. The following observations are noted:

- Only two seconds of measured data from one accelerometer is required in the identification. Both the excitation force and damages can be identified accurately indicating the proposed method can provide a good resolution on damages at close proximity to each other.
- It is noted that only two cycles of successive iterations are required. The proposed two-steps strategy for the force identification is shown effective to circumvent the usual problem we have in optimization when we have large difference in the sensitivities of the different parameters in the problem.
- The model error of a uniform reduction in the flexural stiffness does not have significant effect on the identified results.

4.4.5 Laboratory Work

The proposed method is further demonstrated with laboratory results from a simply supported single span steel beam as shown in Figure 4-28. The parameters of the beam are: length 2.0 *m*, width 0.0254 *m* and height 0.0194 *m*, the elastic modulus and mass density of the material are $2.065\times10^{11}\ N/m^2$ and $7.761\times10^{3}\ kg/m^3$ respectively. It is discretized into sixteen equal Euler beam elements with three degrees-of-freedom at each node. A mass of *2.61 kg* is hung by a fine nylon rope at node 11 of the beam, and the excitation force generated by cutting the rope will serve as the input force. The true value of the force is *25.58 N* and is an "impulsive force" acting at the initial time *t=0*. Mathematically, it is expressed as

$$f(t)=\begin{cases}-Mg & t=0\\ 0 & t>0\end{cases}$$

The flexural rigidities of all the elements and the assumed impulsive force are taken as the unknowns in the inverse analysis. The initial values for the damage parameters are all zero. The initial vector of the force parameters is $\{(P_F)_0\}=[0,0,0,0,0,0,2\pi,4\pi,6\pi,8\pi,10\pi]^T$. In this case, the magnitude of the force parameters can be all set to zeros.

The sampling frequency is 2000Hz. Acceleration responses collected by B&K 4370 accelerometers from nodes 7 and 9 are used for the identification. A commercial data logging system INV303E and the associated signal analysis package DASP2003 are used in the data acquisition. The data acquisition lasts for 2 seconds. The first 0.5 second data is skipped and only data from 0.5 to 1.5 second are used in the identification. The damage is introduced by removing *1.0* mm thick of material over a length of *9 mm* in element 13 with one edge of the damage zone starting at node 13. The material is removed on both sides of the beam to produce a symmetric change in

the section property. The equivalent reduction in the second moment of inertia of element 13 is found to be 11.3 % after reducing the middle degrees-of-freedom to the two end nodes 13 and 14, by Guyan reduction. The first five natural frequencies of the undamaged beam are 10.523, 41.316, 92.615, 165.353, and 254.625 Hz, and those for the damaged beam are 10.282, 40.508, 91.264, 164.695 and 250.583 Hz obtained from modal test.

The required number of iteration for convergence in the second cycle of iteration is 19 and 154 for the force and the damages, and the corresponding optimal regularization parameter is 6.02 and 13.74 respectively. Figure 4-29 shows the identified damage after the second iteration. The identified damage in element 13 is 13.5% which is close to the true value. But there is a large false identification in element 12. This observation is also commonly found with other damage identification algorithm since element 12 is in immediate adjacent to the damage element and the vibration energy in the element would be much more disturbed than those in other elements as discussed by Shi and Law(2000b). Figure 4-30 shows the identified time history of the force with a peak of *25.6* N at *t=0* which is very close to the true value. Figure 5-9 shows the time histories of the calculated acceleration using the identified input force and the corresponding measured acceleration after using the orthogonal polynomial function (Law and Zhu, 2000) to remove the measurement noise. The two time series match each other very well. The natural frequencies of the beam calculated with the identified parameters are 10.271, 40.744, 92.258, 164.703 and 253.328 Hz which also match the experimental frequencies very well indicating the success of the identification.

4.4.6 Concluding Remarks

This section presented a method for identifying the input excitation force and the physical parameters of a structure simultaneously. Newmark method is used to calculate the structural dynamic responses and their sensitivities with respect to the parameters of force and system parameters. The changes in the force and physical parameters are identified in a gradient-based model updating method based on dynamic response sensitivity. The problem with different sensitivity of parameters in the identification is addressed in the solution process. The proposed method has the advantage that only short duration of dynamic response measurement from only one sensor is needed in the inverse analysis. Laboratory study shows that we do not need to use the measured time response data from the beginning of the time in the identification. This indicates that the proposed method has the potential for the application of practical damage detection.

Table 4-1- Identified results with temperature difference between two measurement states

	Updated mass(*Kg*)	Updated damping(*N.s/m*)	Updated stiffness*(N/m)*
Case *A*	2.0/(0.0)	1.2/ (0.0)	450.0/(0.0)
Case *B*	2.0/(0.0)	1.2/(0.0)	449.0/(0.22)

Note: (•) percentage error in identification

Table 4-2- Identified results with an additional mass

	Updated mass(*Kg*)	Updated damping(*N.s/m*)	Updated stiffness*(N/m)*
Case *A*	2.01/(0.0)	1.2/(0.0)	450.0/(0.0)
Case *B*	2.0/(0.5)	1.22/(1.7)	448.5/(0.3)

Note: (•) percentage error in identification

Table 4-3- Identified results with modeling error

Identified results with modeling error

	Updated mass(*Kg*)	Updated damping(*N.s/m*)	Updated stiffness*(N/m)*
True	2.0	1.2	450.0
Identified	2.0/(0.0)	1.2/(0.0)	450.0/(0.0)

Note: (•) percentage error in identification

Table 4-4- Identified results with measurement noise

Noise Level	Updated mass(*Kg*)	Updated damping(*N.s/m*)	Updated stiffness*(N/m)*
1%	1.998/(0.1)	1.197/(0.25)	450.5/(0.11)
5%	1.987/(0.65)	1.227/(2.25)	448.54/(0.32)
10%	1.97/(1.5)	1.241/(3.42)	446.9/(0.69)

Note: (•) percentage error in identification

Table 4-5- Damage scenarios on the plane truss

Damage Scenario	Damage Location	Reduction in *EA*	$\Delta T\ (^{o}C)$	Noise level	Model error
1	Elements 2, 5,19	5%	Nil	Nil	Nil
2	Element 2, 5, 19	5%	+40	Nil	Nil
3	Element 5	10%	+40	Nil	Nil
4	Element 12	5%	Nil	5%, 10%	Nil
5	Elements 2, 5 and 19	5% each	+40	10%	3% under estimation in all *EA*

Table 4-6- Natural Frequency Changes due to local damage and temperature

	Natural Frequencies (Hz)		
Mode order	Intact	Scenario *1*	Scenario *2*
1	*6.957*	*6.916*/(0.58)	*6.914*/(0.61)
2	*14.406*	*14.328*/(0.54)	*14.325*/(0.57)
3	*23.367*	*23.222*/(0.62)	*23.216*/(0.64)
4	*41.475*	*41.328*/(0.35)	*41.318*/(0.38)
5	*45.123*	*44.931*/(0.43)	*44.919*/(0.45)
6	*64.213*	*63.770*/(0.69)	*63.754*/(0.71)
7	*72.028*	*71.723*/(0.42)	*71.705*/(0.45)
8	*74.486*	*74.284*/(0.27)	*74.2654*/(0.30)

Note : (•) frequency change percentage with respect to the intact structure.

Table 4-7- Iteration number and regularization parameter required for convergence

	Damage indices	without noise	10% noise
Iteration number	α_E and α_I	20	24
	α_A	17	20
λ_{opt}	α_E and α_I	1.71	2.84
	α_A	1.93	2.61

Table 4-8– Identified results for the Plane Frame with and without noise

Damage indices		Element number										
		1	2	3	4	5	6	7	8	9	10	11
α_E (%)	Without noise	-5.3	-5.1	-4.9	-5.0	-4.8	-4.7	-4.7	-4.9	-5.0	-4.7	-4.8
	With noise	-5.6	-4.4	-6.0	-4.7	-4.3	-4.5	-4.4	-4.4	-4.3	-5.5	-4.7
α_I (%)	Without noise	1.3	-0.9	-14.6	-1.1	1.2	-0.7	-0.3	1.1	-0.8	0.2	0.1
	With noise	1.8	-1.3	-15.5	-1.4	-0.6	-0.8	-0.3	2.5	-0.9	-0.7	-0.4
α_A (%)	Without noise	0.1	-1.0	-5.3	-0.9	0.1	-0.7	-0.3	-0.5	-0.3	0.3	0.1
	With noise	1.3	-1.2	-5.6	-1.1	1.3	-0.9	-0.7	1.5	-1.3	0.7	-0.6

Table 4-9– Damage Scenarios for the plane truss

Damage Scenario	Damage Location	Reduction in		Noise level	Model error
		Young's modulus	Area		
1	Element 5	10%	5%	Nil	Nil
2	Element 5	10%	5%	10%	Nil
3	Element 2	5%	10%	10%	Nil
	Element 5	10%	15%		
4	Element 2	5%	10%	10%	5% and 2% under-estimation of Young's modulus and mass density in all elements respectively
	Element 5	10%	15%		
	Element 16	15%	5%		

Table 4-10 - Iteration number and regular parameters for different study cases

Study Case	Iteration number		Regularization parameter	
	for E	for A	for E	for A
1	17	21	0.001	0.003
2	20	23	0.098	0.011
3	22	24	0.01	0.015
4	35	38	0.05	0.07

Note: E denotes Young's modulus of material; A denotes cross-sectional area.

Table 4-11– Identified results for the Damage Scenarios in the Plane Truss

Damage Scenario	Damage Location	Identified Value (%)		Noise level
		Young's modulus	Area	
1	Element 5	-9.9	-5.1	Nil
2	Element 5	-9.5	-4.5	10%
3	Element 2	-4.4	-10.5	10%
	Element 5	-9.4	-13.5	
4	Element 2	-4.1	-11	10%
	Element 5	-9.1	-13.3	
	Element 16	-15.7	-4.3	

Table 4-12- Material and geometrical properties of the test structure

Properties	Beams	Bolts	Balls
Young modulus [N/m^2]	2.10E11	2.10E11	2.10E11
Area [m^2]	6.597E-5	--	--
Density [kg/m^3]	1.2126E4	1.2126E4	1.2126E4
Mass [kg]	0.32	0.09	0.23 + 0.072 *
Poisson ratio	0.3	--	--
Moment of area I_y [m^4]	3.645E-9	--	--
Moment of area I_z [m^4]	3.645E-9	--	--
Torsional rigidity J [m^4]	7.290E-9	--	--

* 0.072 kg additional mass was added to each joint to balance the mass of the accelerometer

Table 4-13– The calculated and experimental natural frequencies of the test structure

Mode	Intact (Hz)		Scenario E1 (Hz)		Scenario E2 (Hz)		Scenario E3 (Hz)	
	Exp.	FEM	Exp.	FEM	Exp.	FEM	Exp.	FEM
1	9.25	9.23/-0.19	9.22	9.19/-0.33	9.13	9.17/0.44	9.16	9.13/-0.32
2	28.27	28.32/0.18	28.20	28.26/0.21	28.04	28.12/0.29	28.17	28.23/0.21
3	33.15	33.77/1.86	33.00	33.64/1.94	32.99	33.51/1.58	32.98	33.61/1.91
4	49.11	49.20/0.2	49.01	49.12/0.22	48.84	49.02/0.37	48.88	49.09/0.43
5	50.52	50.10/-0.82	50.47	49.87/1.19	50.24	50.12/-0.22	50.43	50.14/-0.58
6	70.43	71.18/1.07	70.43	70.94/0.72	70.03	70.51/0.69	70.24	70.86/0.88
7	89.02	89.94/1.03	88.19	89.46/1.44	87.85	88.27/0.48	87.93	89.24/1.49
8	156.15	154.71/-0.92	154.62	154.86/0.16	154.22	154.61/0.25	154.36	154.84/0.31
9	192.79	196.29/1.81	191.28	195.64/2.28	190.45	194.38/2.06	190.87	194.82/2.07
10	258.99	256.79/-0.85	258.48	256.96/-0.59	257.64	255.21/-0.94	257.94	256.73/-0.47
11	276.90	276.17/-0.26	275.23	276.02/0.29	274.48	275.36/0.32	274.68	275.29/0.22

Note: •/• denotes the calculated value/percentage error;

Table 4-14– The diagonal MAC values between the calculated and measured mode

Shapes

	1	2	3	4	5	6	7	8	9	10	11
MAC	1.00	0.99	0.98	0.99	0.99	0.98	0.97	0.96	0.98	0.99	0.98

Table 4-15– Identified values for the Experimental Truss

Damage Scenario	Damage Location	Identified Values of damage indices (%)			
		α_J	α_{I_y}	α_{I_z}	α_A
E1	Element 4	4.5	2.5	2.7	1.8
E2	Element 4	4.4	2.3	2.8	1.6
	Element 2	24.5	1.7	21.8	7.8
E3	Element 4	4.2	2.6	2.9	1.5
	Element 2	24.6	21.5	1.4	7.5

Table 4-16– Identified results for the two-span bridge

		Prestress force (10^7) N					
		True	*Case 2*	*Case 3*	*Case 4*	*Case 5 1% noise*	*Case 5 10% noise*
Iteration No.		-	300	193	326	324	388
λ_{opt}		-	6.2×10^{-8}	3.5×10^{-9}	5.45×10^{-9}	5.7×10^{-9}	7.4×10^{-9}
Element no.	1	3.985	3.984/-0.03	4.000/0.38	3.978/-0.18	3.976/-0.23	3.967/-0.45
	2	3.956	3.957/0.03	3.918/-0.96	3.964/0.20	3.977/0.53	3.998/1.06
	3	3.926	3.926/0.00	3.955/0.74	3.928/0.05	3.911/-0.38	3.895/-0.79
	4	3.897	3.901/0.10	3.863/-0.87	3.906/0.23	3.920/0.59	3.940/1.10
	5	3.854	3.854/0.00	3.888/0.88	3.853/-0.03	3.836/-0.47	3.878/0.62
	6	3.800	3.802/0.05	3.768/-0.84	3.806/0.16	3.818/0.47	3.836/0.95
	7	3.746	3.746/0.00	3.784/1.01	3.748/0.05	3.725/-0.56	3.705/-1.09
	8	3.692	3.691/-0.03	3.658/-0.92	3.688/-0.11	3.710/0.49	3.728/0.98
	9	3.692	3.693/0.03	3.725/0.89	3.692/0.00	3.674/-0.49	3.656/-0.98
	10	3.746	3.745/-0.03	3.708/-1.01	3.743/-0.08	3.767/0.56	3.787/1.09
	11	3.800	3.799/-0.03	3.833/0.87	3.786/-0.37	3.783/-0.45	3.765/-0.92
	12	3.854	3.853/-0.03	3.821/-0.86	3.856/0.05	3.782/-1.87	3.891/0.96
	13	3.897	3.900/0.08	3.936/1.00	3.889/-0.21	3.880/-0.44	3.860/-0.95
	14	3.926	3.927/0.03	3.898/-0.71	3.936/0.25	3.942/0.41	3.957/0.79
	15	3.956	3.955/-0.03	3.993/0.94	3.951/-0.13	3.935/-0.53	3.915/-1.04
	16	3.985	3.987/0.05	3.969/-0.40	3.994/0.23	3.995/0.25	4.004/0.48

Note: •/• denotes the identified value/percentage error.

Table 4-17– Identified results including model errors

		Prestress force (10^7) N						
		True	*Case 6*	*Case 7*	*Case 8*	*Case 9*	*Case 10a*	*Case 10b*
Iteration No.		-	198	203	232	196	243	258
λ_{opt}		-	3.7×10^{-9}	3.8×10^{-9}	5.1×10^{-9}	3.6×10^{-9}	7.8×10^{-9}	2.4×10^{-8}
Element no.	1	3.985	4.050/1.63	4.005/0.50	4.120/3.38	4.080/2.38	4.10/2.91	4.127/3.56
	2	3.956	3.868/-2.22	3.916/-1.01	3.968/0.30	3.902/-1.37	3.92/-0.96	3.718/-6.01
	3	3.926	3.975/1.25	3.958/0.82	3.875/-1.30	3.961/0.89	3.87/-1.55	3.665/-6.64
	4	3.897	3.843/-1.39	3.861/-0.92	3.923/0.67	3.852/-1.15	3.91/0.23	4.306/10.5
	5	3.854	3.881/0.7	3.884/0.78	3.782/-1.87	3.968/2.96	3.78/-1.89	3.581/-7.08
	6	3.800	3.748/-1.37	3.763/-0.97	3.718/-2.16	3.749/-1.34	3.76/-1.16	3.656/-3.79
	7	3.746	3.788/1.12	3.781/0.93	3.834/2.35	3.853/2.86	3.94/5.21	3.945/5.31
	8	3.692	3.654/-1.03	3.654/-1.03	3.538/-4.17	3.636/-1.52	3.71/0.51	3.741/1.33
	9	3.692	3.732/1.08	3.721/0.79	3.665/-0.73	3.731/1.06	3.56/-3.52	3.26/-11.65
	10	3.746	3.702/-1.17	3.702/-1.17	3.641/-2.80	3.684/-1.66	3.61/-3.58	3.542/-5.45
	11	3.800	3.853/1.40	3.838/1.00	3.963/4.29	3.881/2.13	3.89/2.24	3.685/-3.03
	12	3.854	3.817/-0.96	3.825/-0.75	3.894/1.04	3.805/-1.27	3.90/1.14	3.998/3.74
	13	3.897	3.943/1.18	3.931/0.87	3.986/2.28	3.976/2.03	3.95/1.44	4.053/4.00
	14	3.926	3.868/-1.5	3.891/-0.89	3.763/-4.15	3.792/-3.41	3.85/-1.88	3.752/-4.43
	15	3.956	4.013/1.44	3.997/1.03	4.053/2.45	4.031/1.90	3.89/-1.79	3.845/-2.80
	16	3.985	3.949/-0.90	3.961/-0.60	3.875/-2.76	4.090/2.63	4.10/2.99	4.204/5.50

Note: •/• denotes the identified value/percentage error.

Table 4-18–Modal Frequencies (Hz) of the non-prestressed and Prestressed Beam

	unprestressed		*prestressed*	
	FEM	*Experimental*	*FEM*	*Experimental*
Mode 1	23.10	23.21	23.47	23.31
Mode 2	85.62	86.17	86.54	87.98
Mode 3	184.53	183.29	187.12	185.93

Table 4-19- The Identified Prestress Force in Experiment

Element No	1	2	3	4	5	6	7	8	9	10	11	12	13	14	15	16
Prestress (kN)	66.6	69.4	63.6	65.8	72.3	61.1	67.6	70.1	63.3	65.8	68.9	63.0	68.0	68.6	59.4	71.7
Error (%)	0.1	-4.0	4.7	1.3	-8.4	8.4	-1.3	-5.1	5.1	1.3	-3.3	5.5	-2.0	-2.9	10.9	-7.5

Table 4-20- Iteration number and optimal regularization parameters corresponding to different noise levels

		1% noise	5% noise	10% noise
Iteration number	Force	70	72	78
	Damage	36	40	47
λ_{opt}	Force	0.003	0.005	0.006
	Damage	6.5×10^{-7}	1.18×10^{-6}	1.22×10^{-6}

Table 4-21 -Iteration number and optimal regularization parameters for Study Case 2

	Iteration number			λ_{opt}		
	ω_i	F_i	Damage	ω_i	F_i	Damage
Scenario 1	23	36	32	0.08	6.3×10^{-4}	8.5×10^{-9}
Scenario 2	30	45	40	0.11	4.5×10^{-4}	6.9×10^{-9}

Table 4-22-Calculated and measured natural frequencies of the test beam (Hz)

		1st	2nd	3rd	4th	5th
Intact	Measured	10.523	41.316	92.615	165.353	254.625
	Calculated	10.459	41.423	93.116	165.274	256.242
Damaged	Measured	10.282	40.508	91.264	164.695	250.583
	Calculated	10.271	40.744	92.258	164.703	253.328

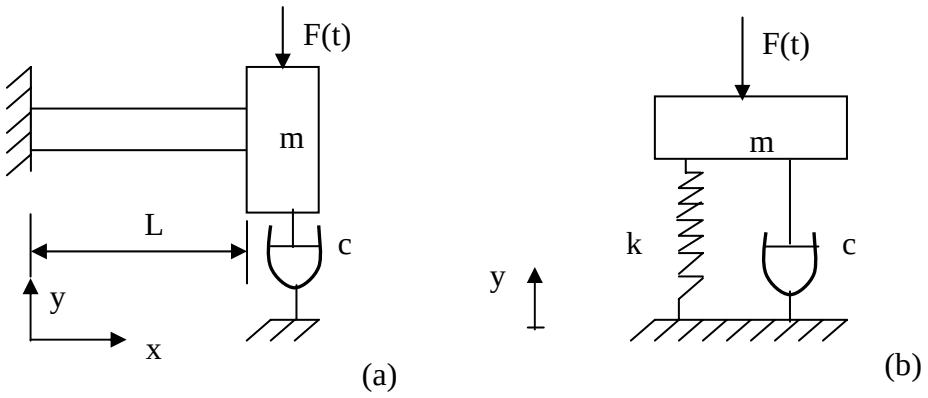

Figure 4-1- (a) The cantilever beam, (b) The equivalent single DOF system

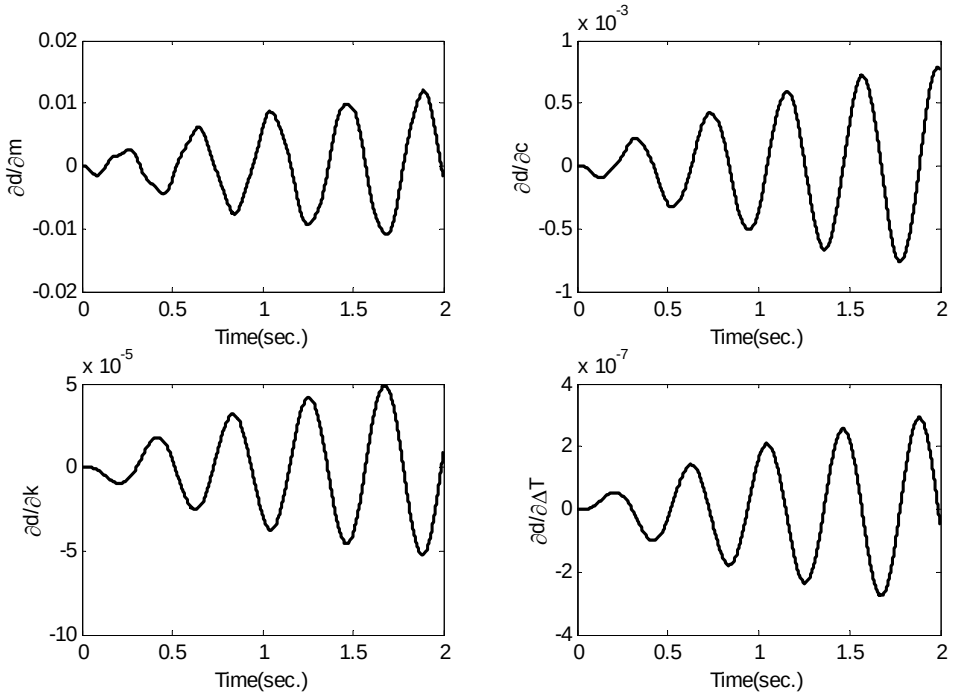

Figure 4-2- Sensitivity of displacement with respect to different parameters

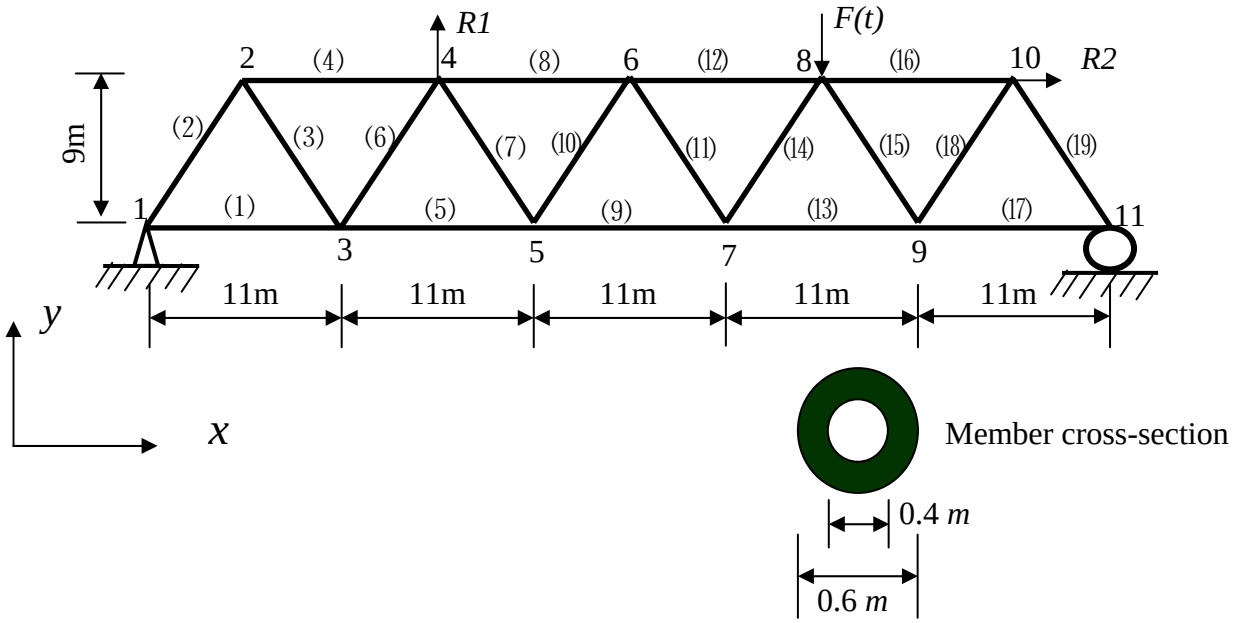

Figure 4-3- The plane truss structure

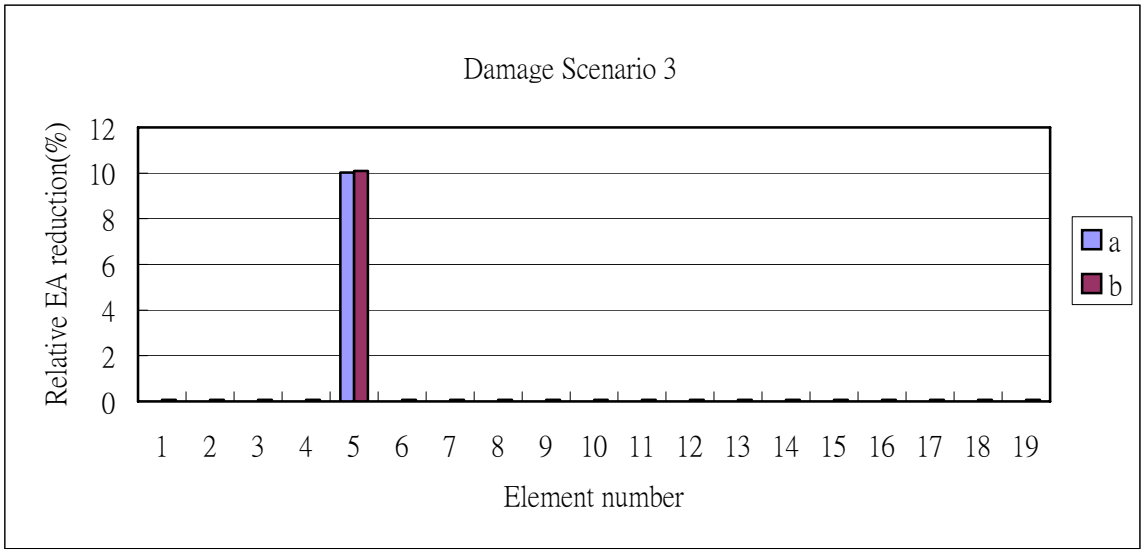

Figure 4-4- Identified Elemental local damage in element 5
(a) With the temperature effect removed;
(b) Without removing the temperature effect

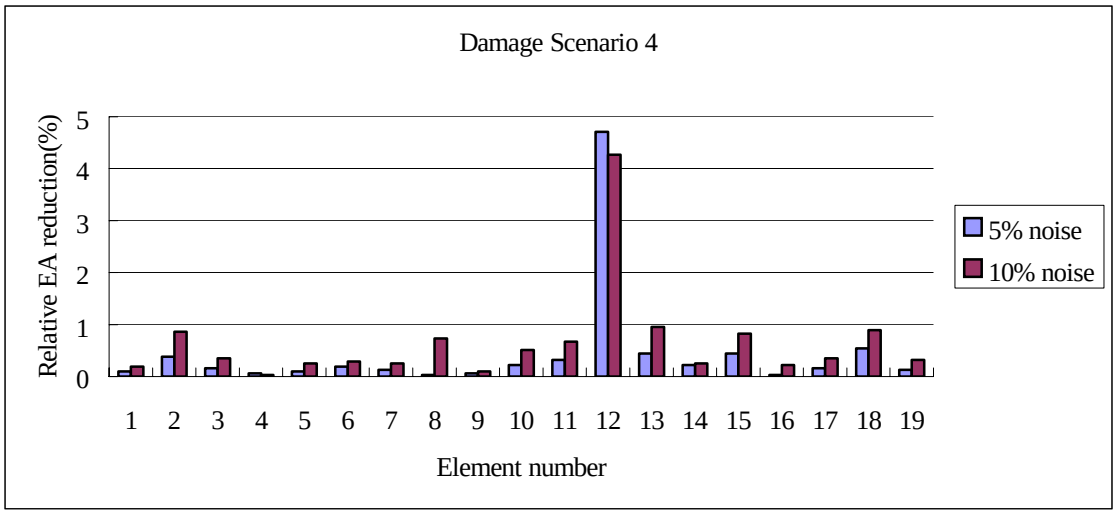

Figure 4-5- Damage detection under different noise level

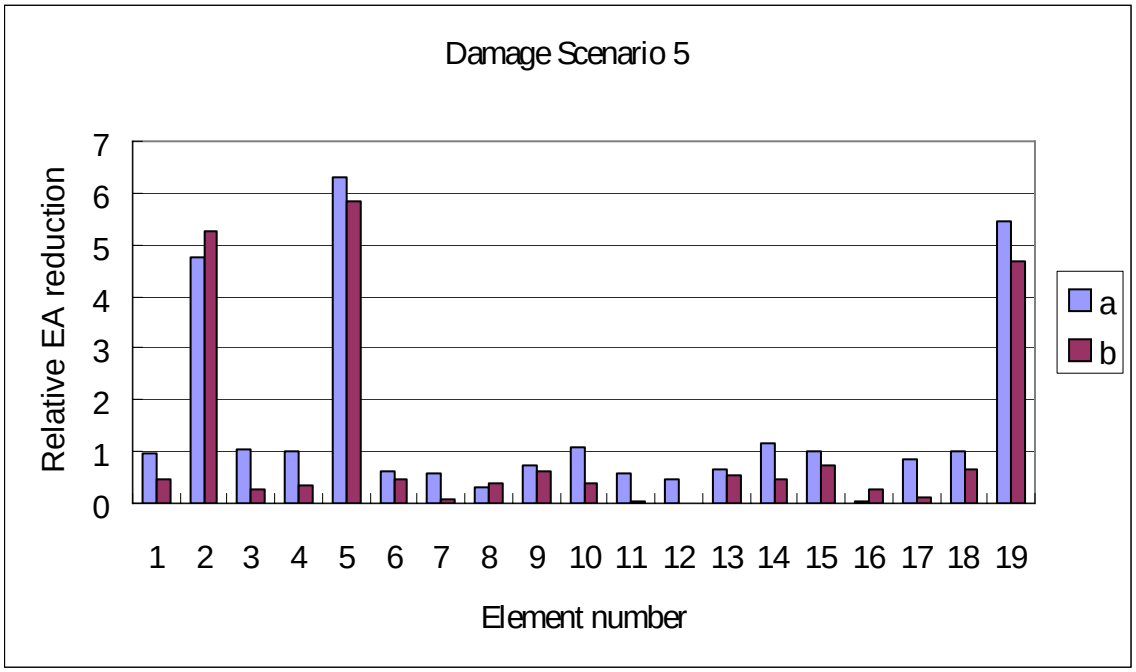

Figure 4-6- Multiple damage detection with modeling error
(a) Without removing the temperature effect
(b) With the temperature effect removed.

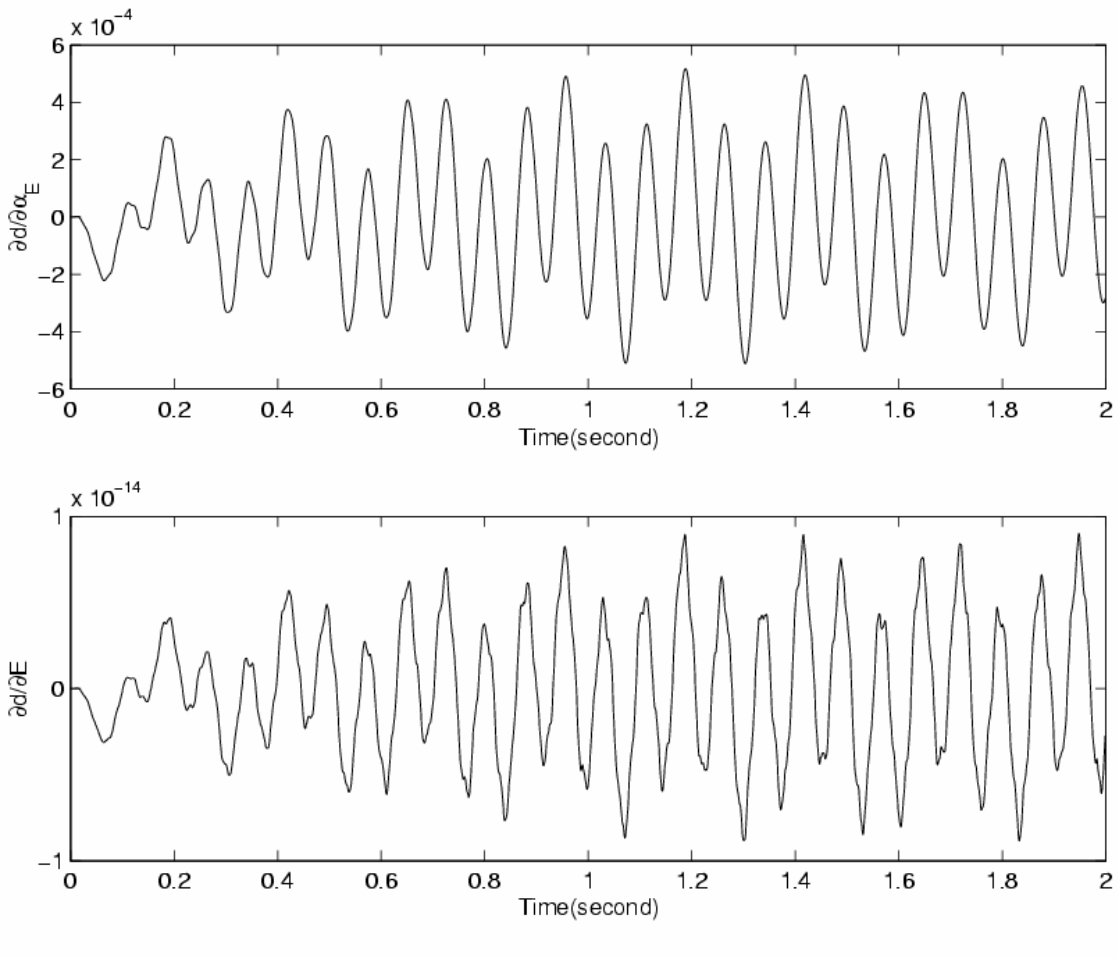

Figure 4-7- Displacement sensitivity with respect to damage index α_E and Young's modulus E

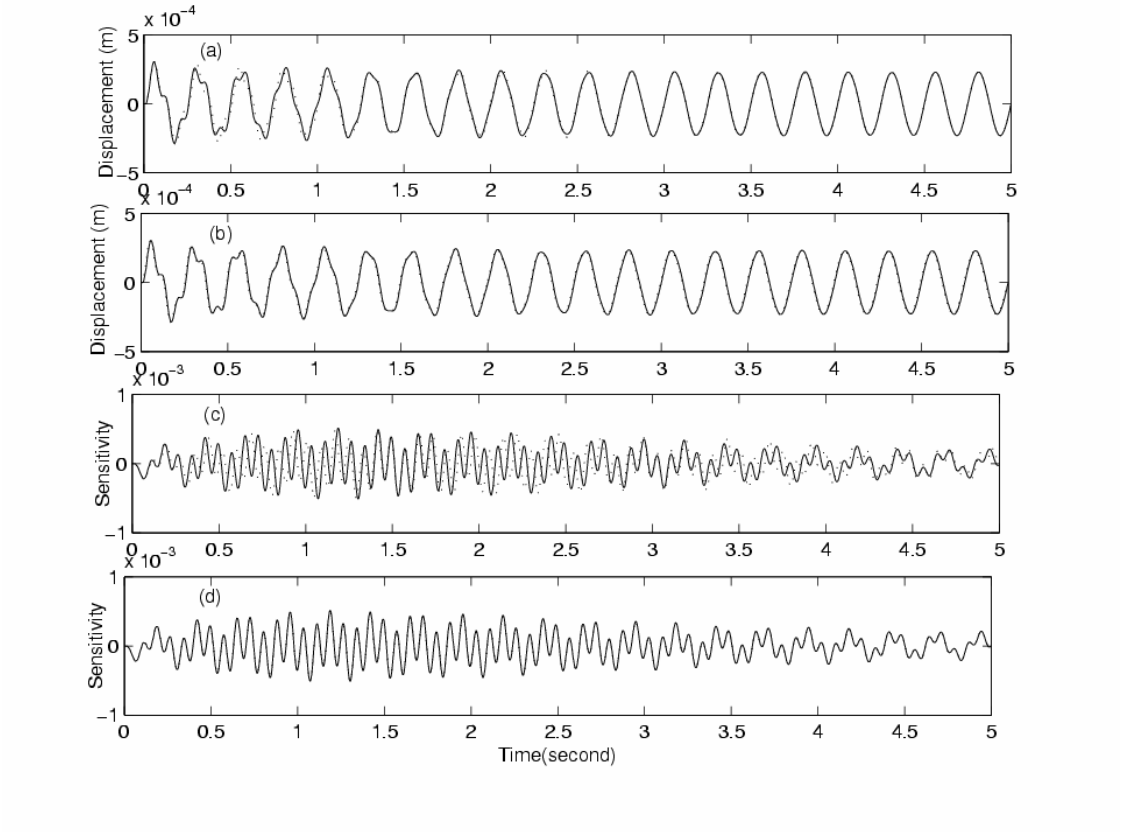

Figure 4-8- Response and response sensitivity (__ dt=0.001s, ... dt=0.0.01s) (a) Response from Newmark method; (b)Response from State-Space) (c) Sensitivity from Newmark method; (d)Sensitivity from State-Space)

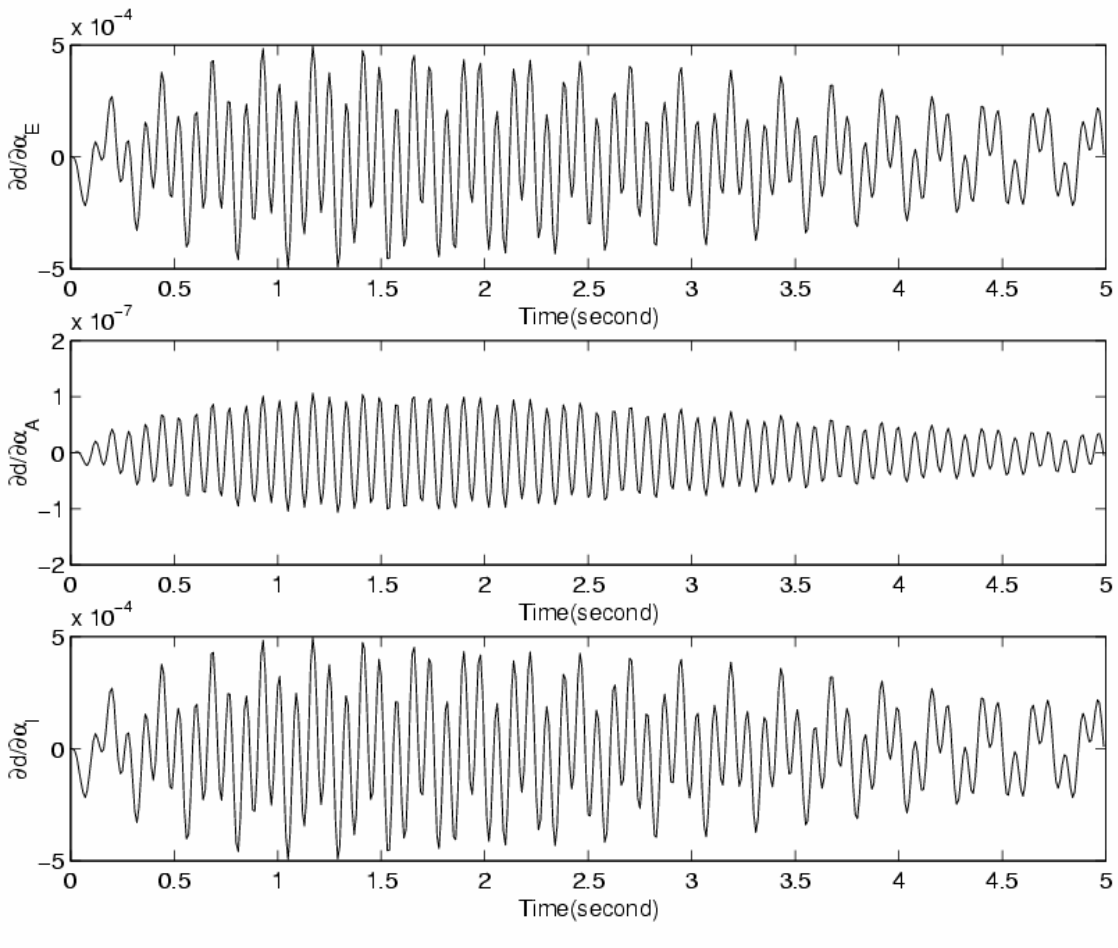

Figure 4-9- Sensitivities with respect to different damage indices

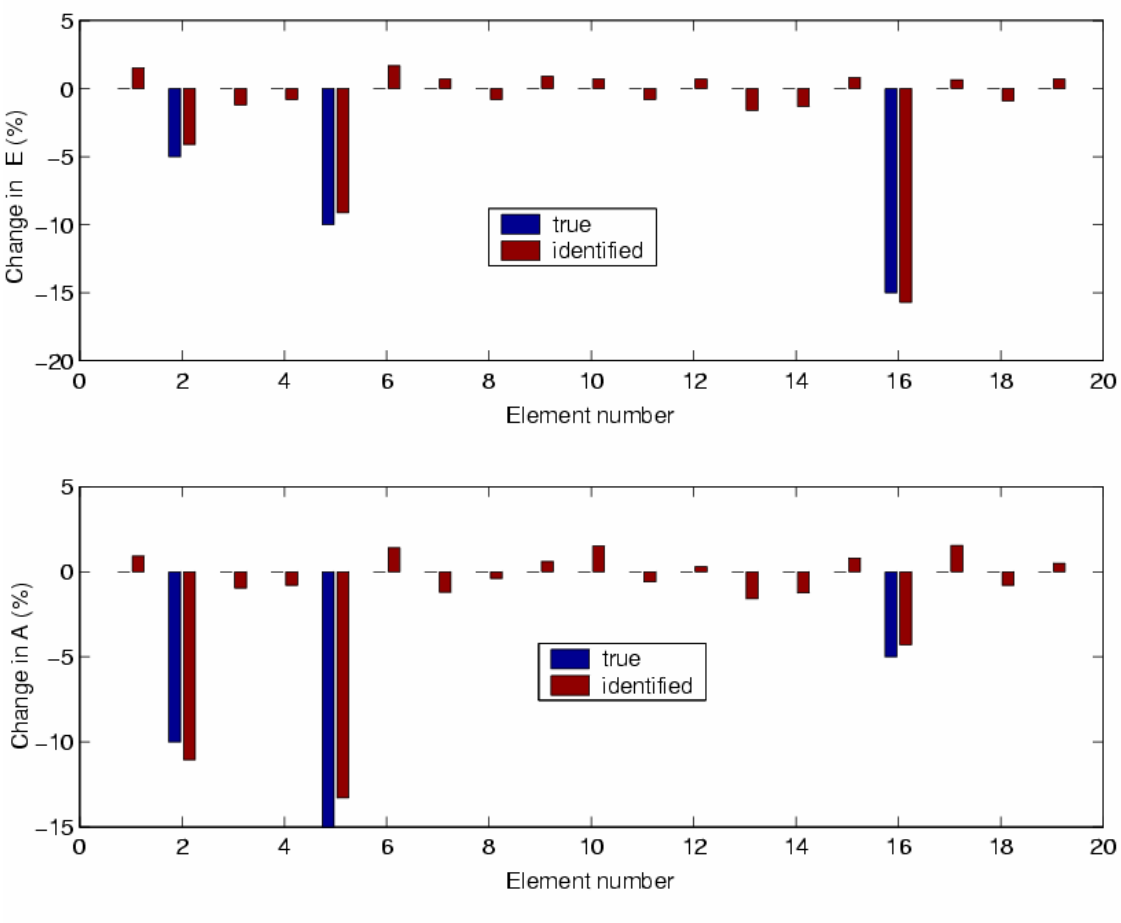

Figure 4-10- Identified results for Scenario 4

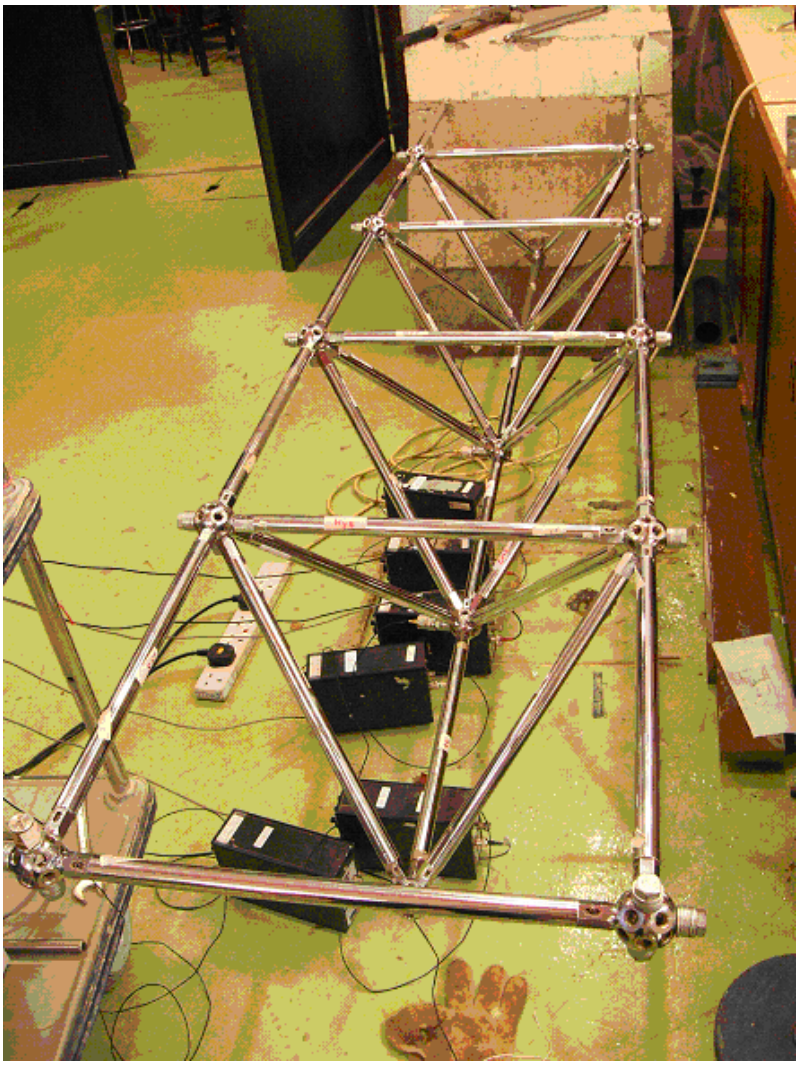

(a) The three-dimensional truss structure

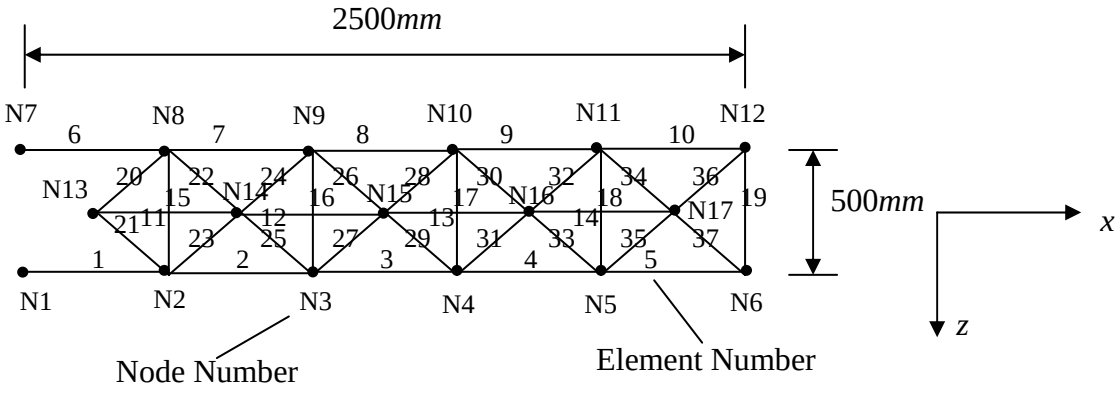

(b) Finite element model

Figure 4-11- The truss structure and its finite element model

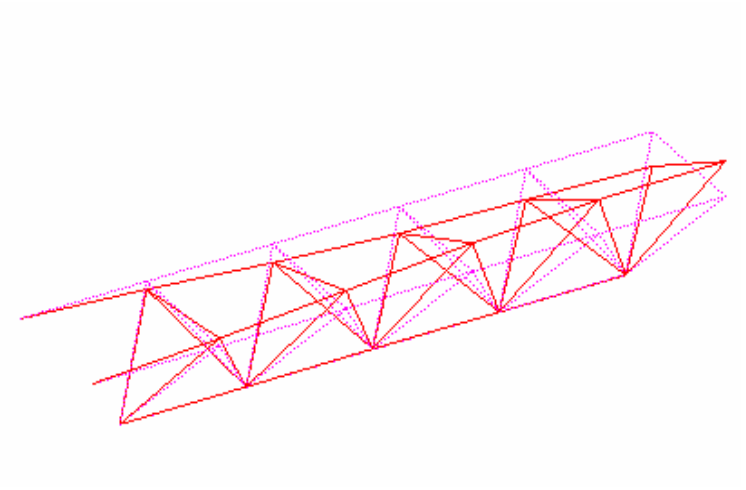

Mode 1 (torsion)

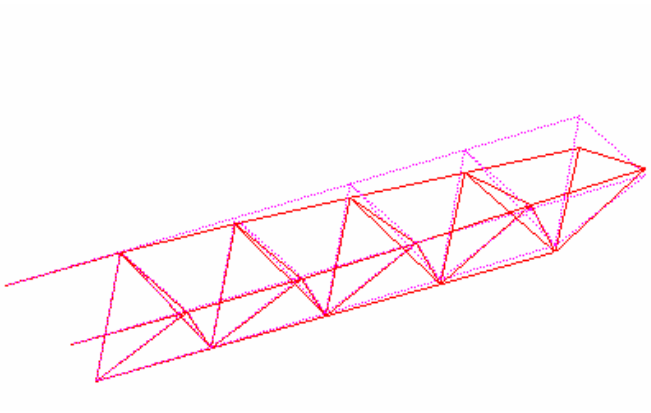

Mode 2 (torsion)

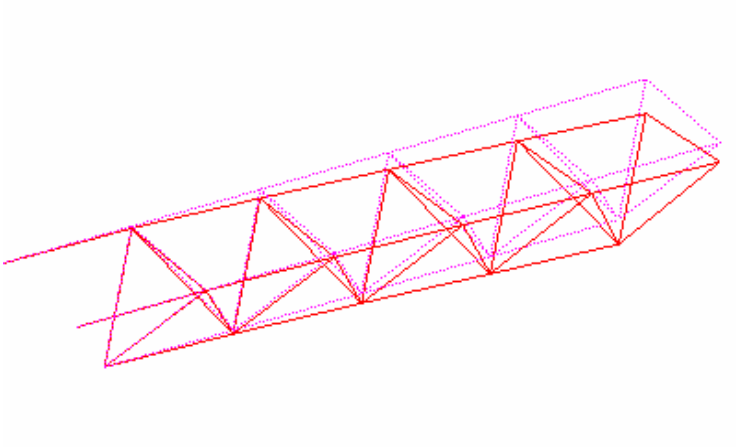

Mode 3 (bending)

(To be continued)

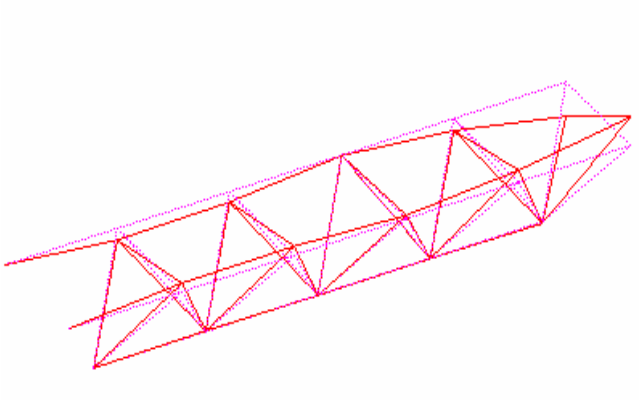

Mode 4 (torsion)

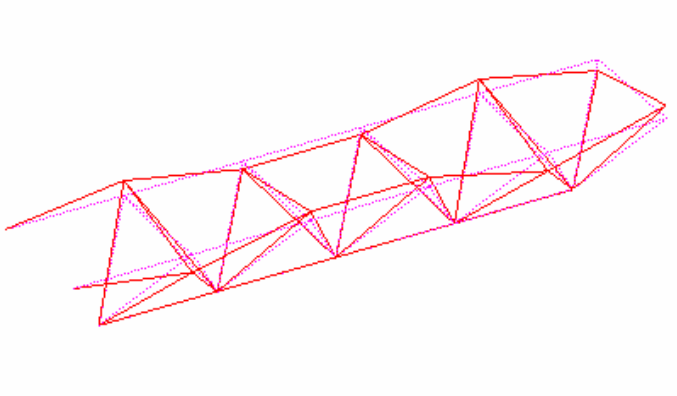

Mode 5 (torsion)

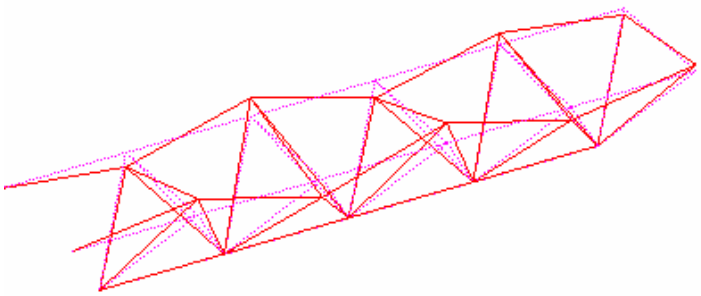

Mode 6 (torsion)

(To be continued)

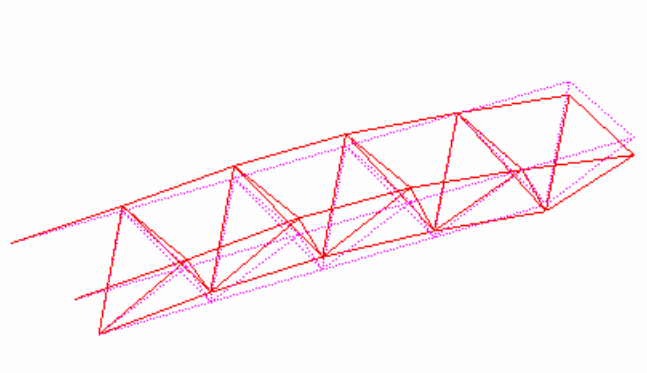

Mode 7 (bending)

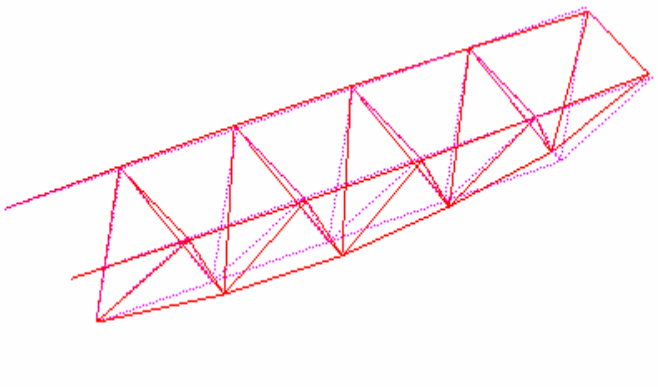

Mode 8 (bending)

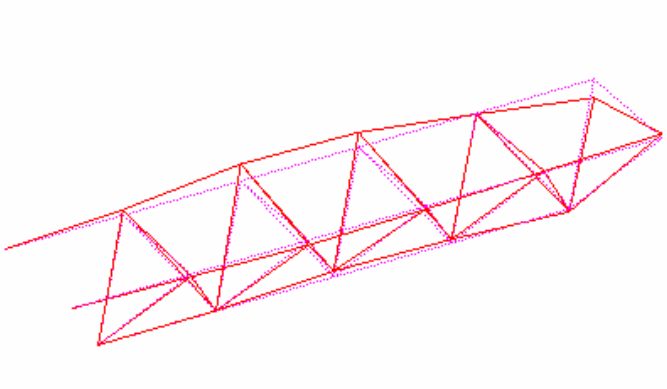

Mode 9 (torsion and bending)

(To be continued)

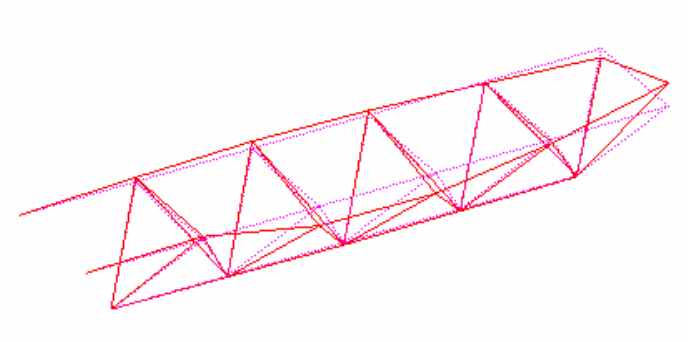

Mode 10 (torsion)

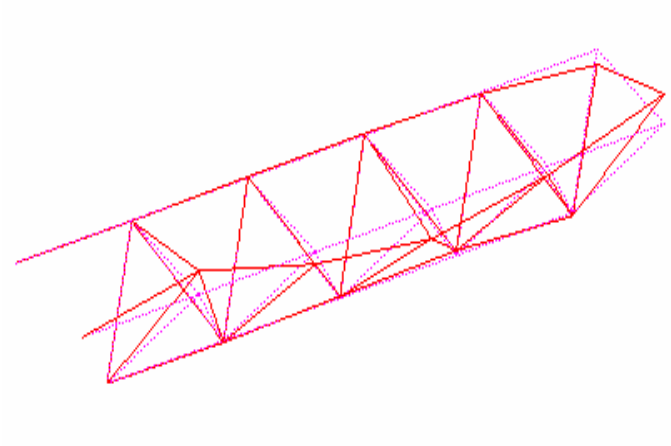

Mode 11 (torsion)

Figure 4-12 - The measured first 11 mode shapes of the structure

Figure 4-13– Detail of the first damaged member

Figure 4-14– Detail of the second damaged member

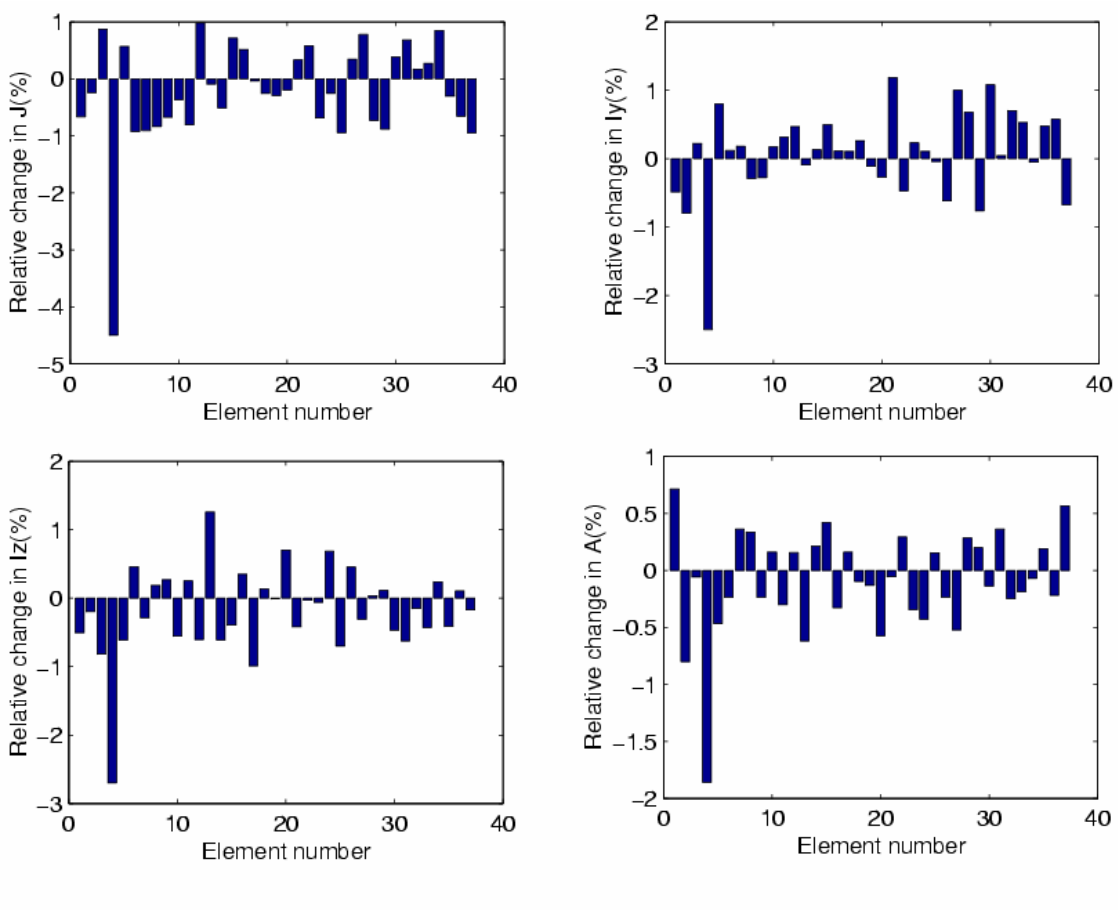

Figure 4-15– Identified percentage change in different physical parameters for Scenario E1

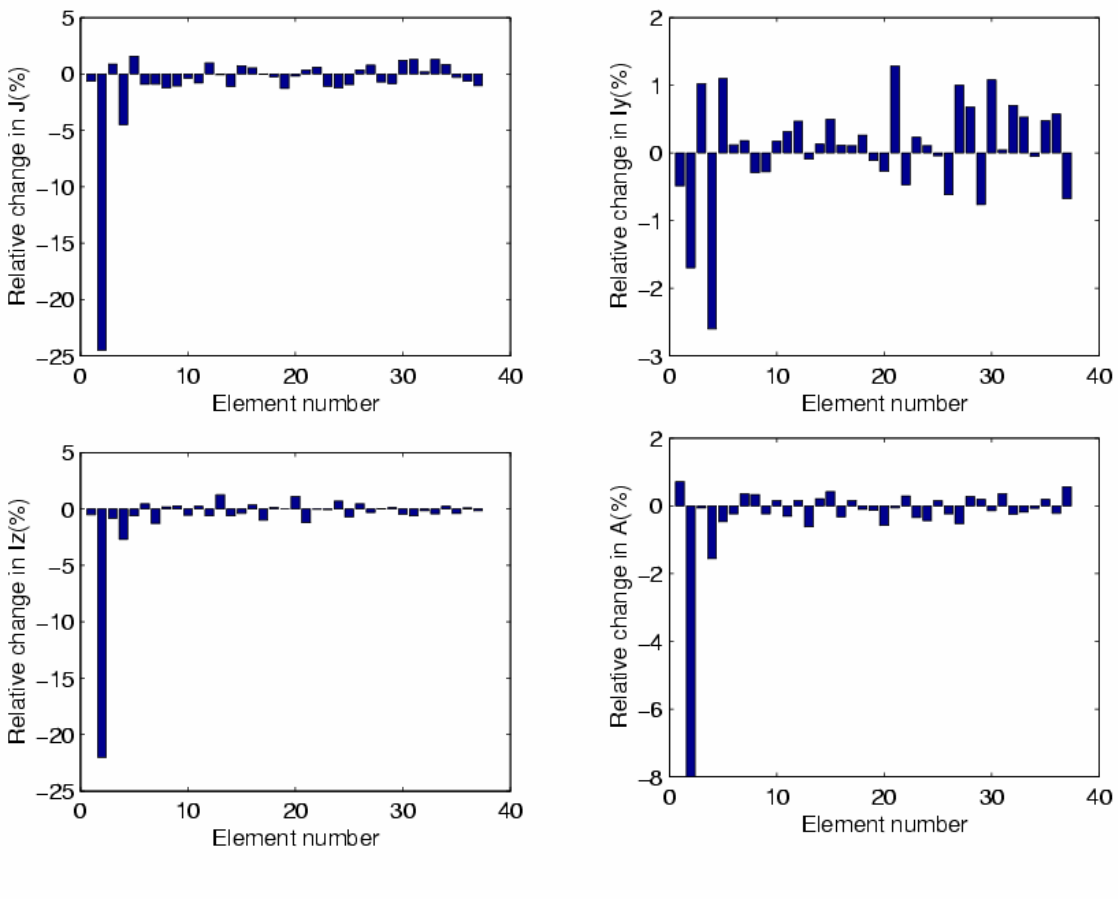

Figure 4-16- Identified percentage change in different physical parameters for Scenario E2

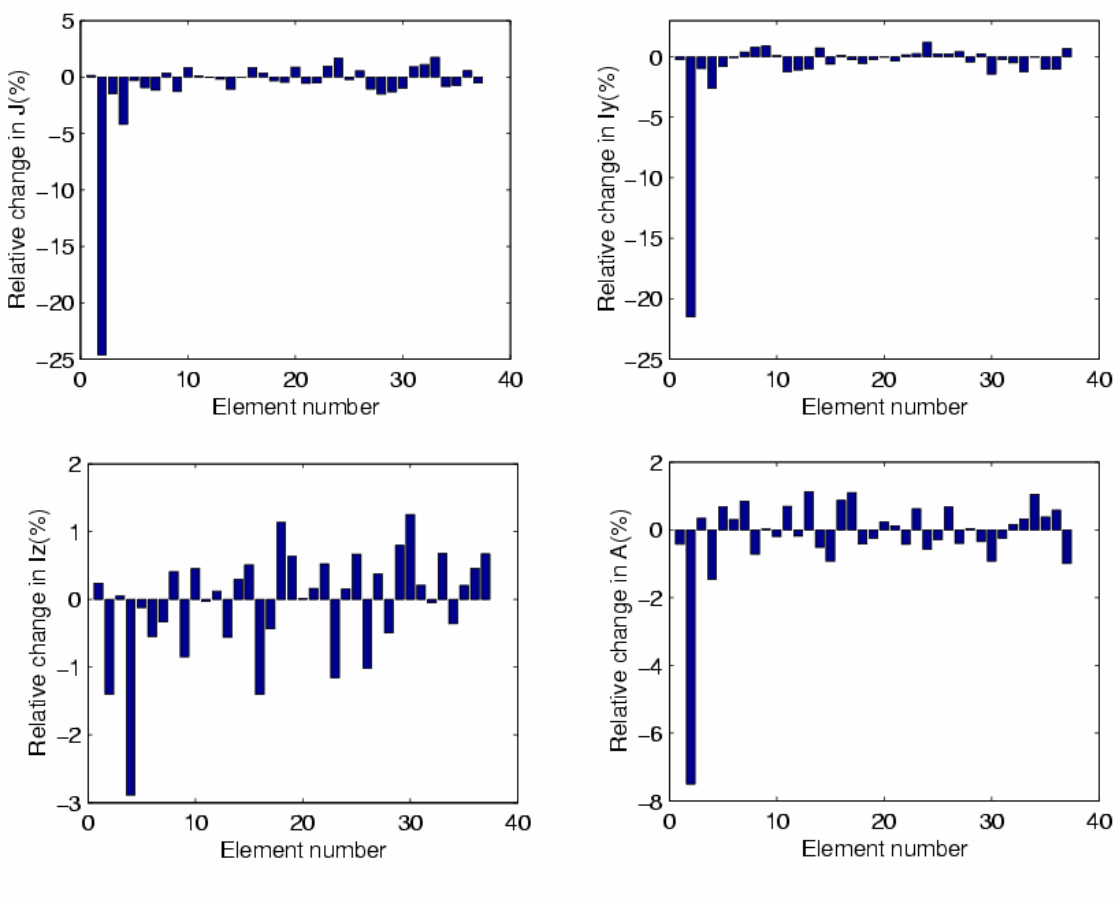

Figure 4-17- Identified percentage change in different physical parameters for Scenario E3

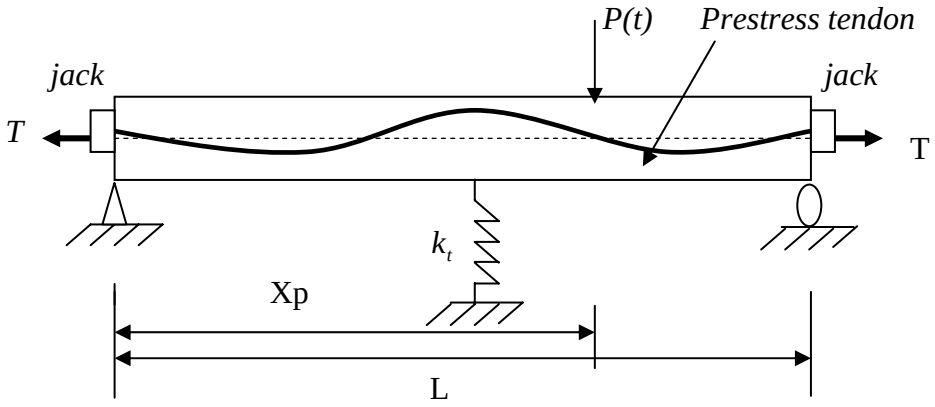

Figure 4-18- The multi-span prestressed bridge

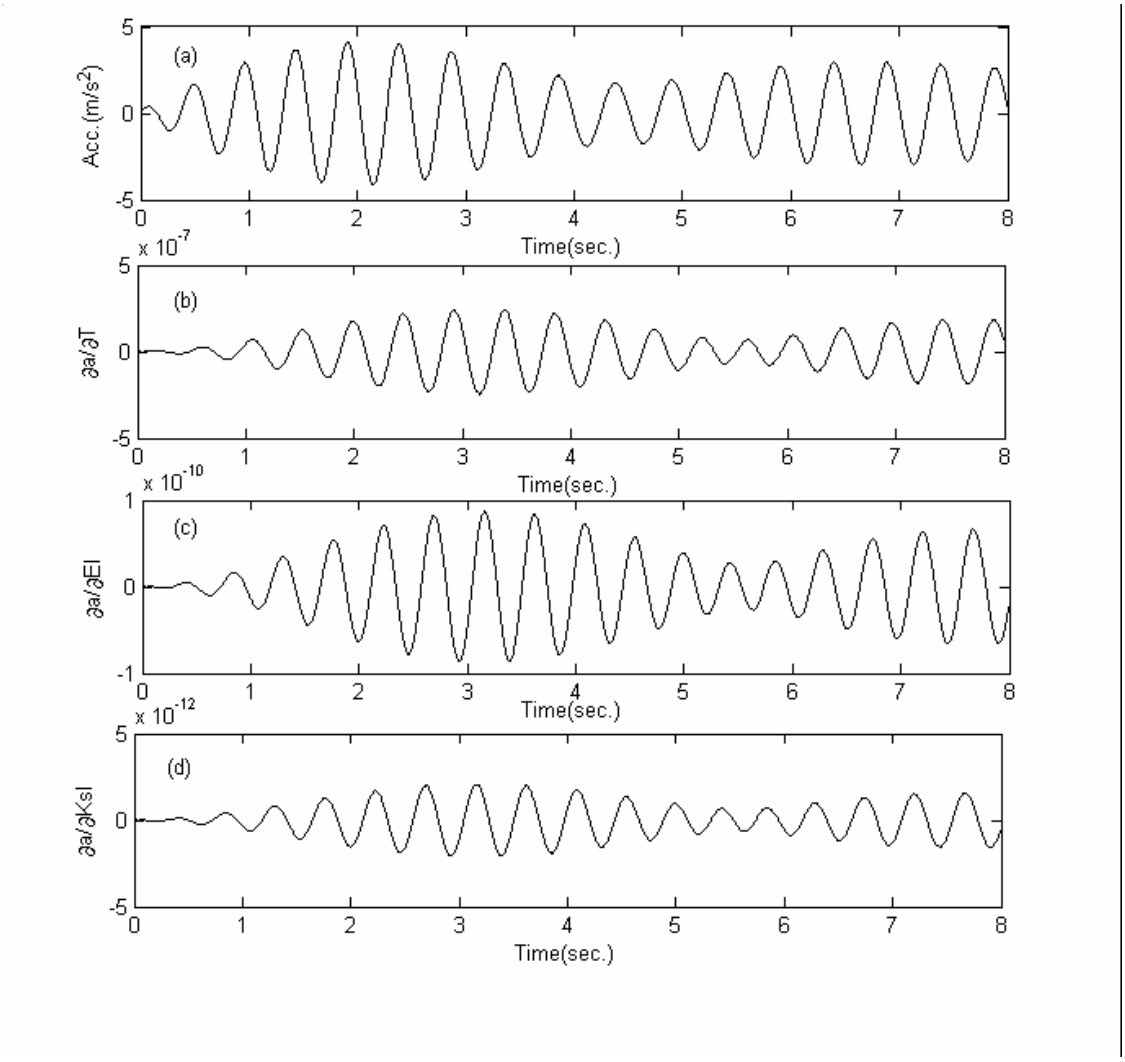

Figure 4-19- Acceleration sensitivity with respect to different parameters (a) Acceleration response; (b) Sensitivity w.r.t. prestress forece; (c) Sensitivity w.r.t. flexural rigidity; (d) Sensitivity w.r.t. stiffness of the support

(a)

(To be continued)

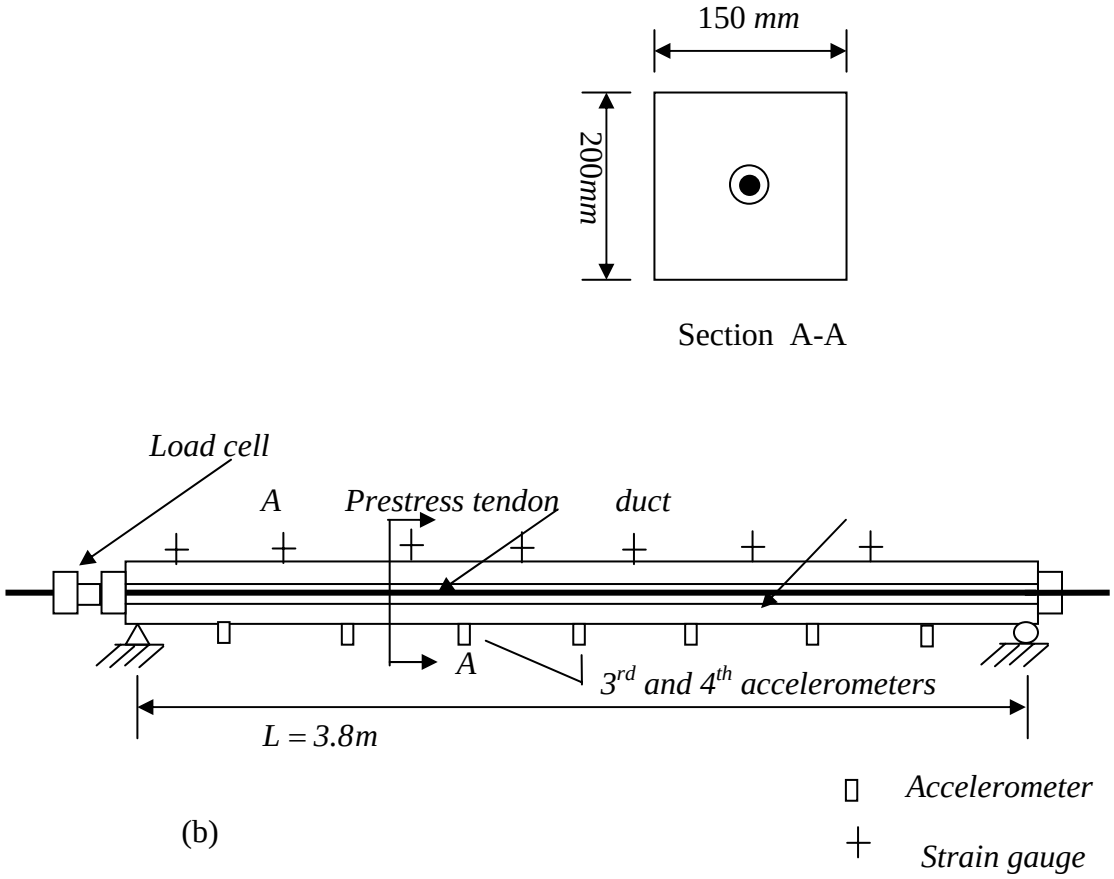

Figure 4-20- Test setup for the prestressed concrete beam

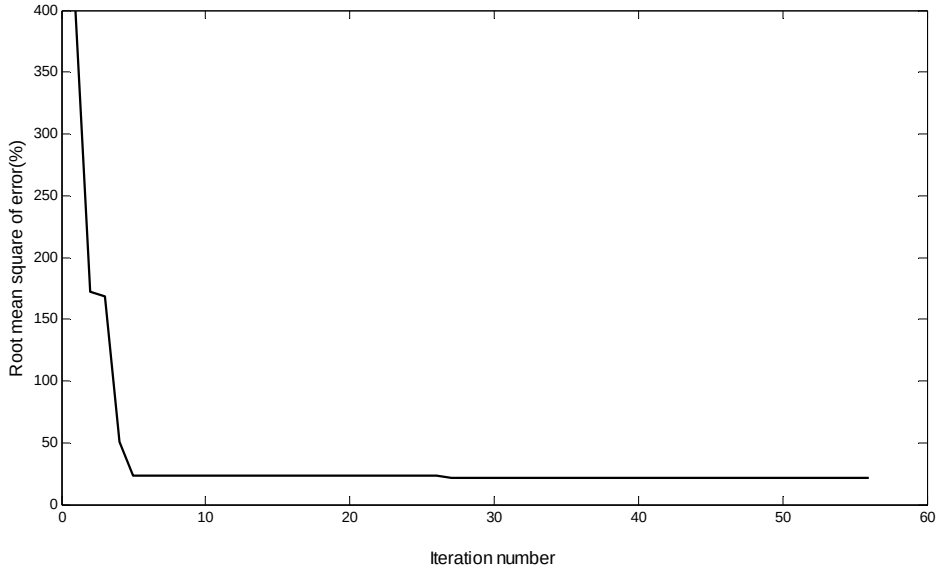

Figure 4-21– Curve of convergence of results

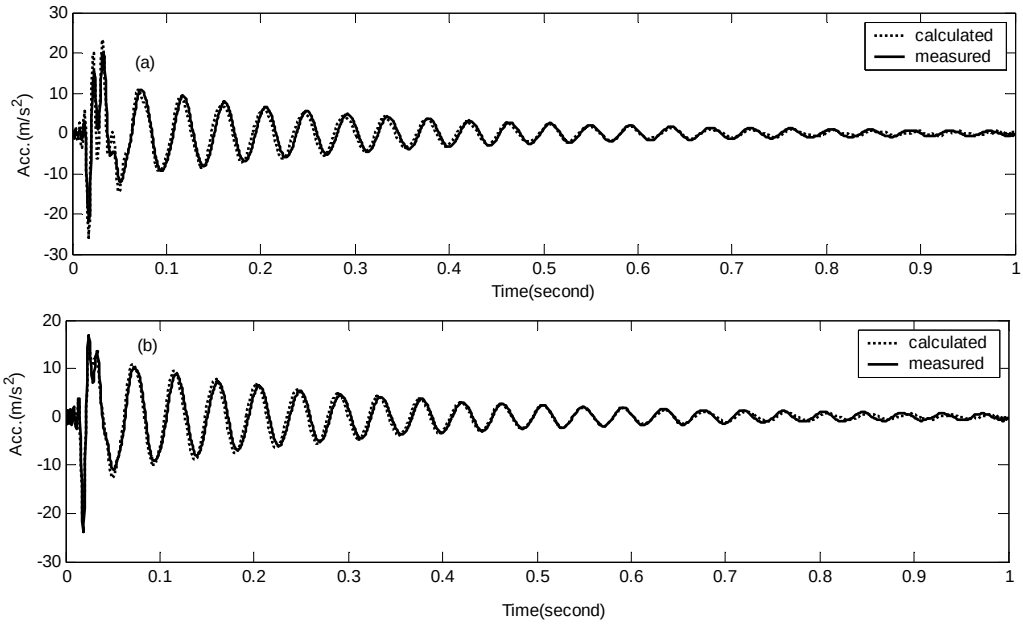

Figure 4-22– Time histories of measured and reconstructed acceleration responses. (a) the 3rd accelerometer; (b) the 4th accelerometer

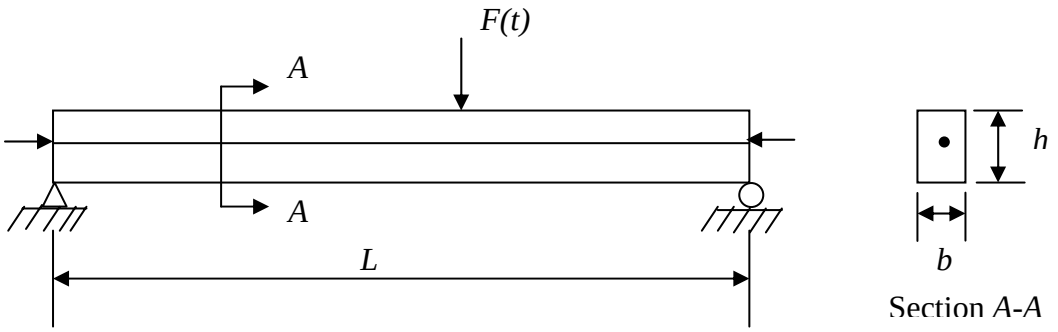

Figure 4-23- The prestressed beam model

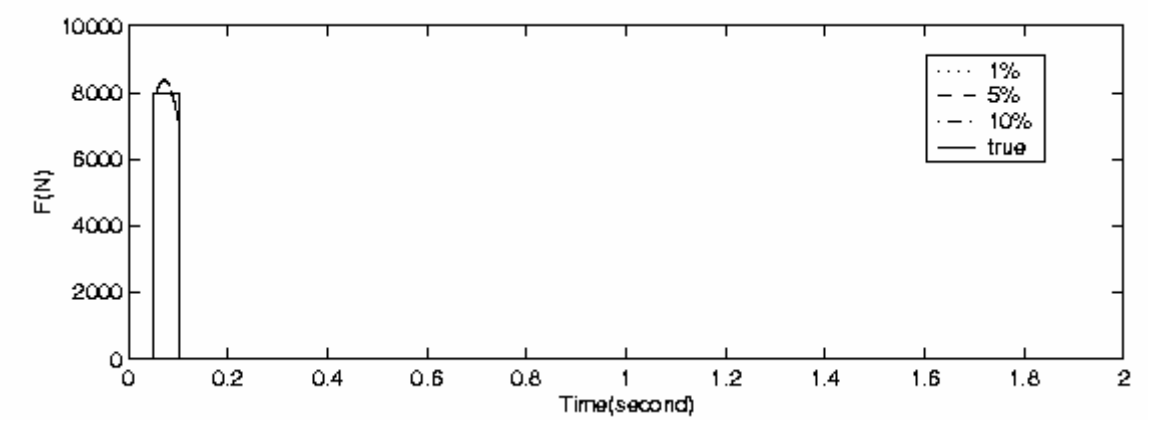

Figure 4-24– Identification of impulsive force with different noise levels

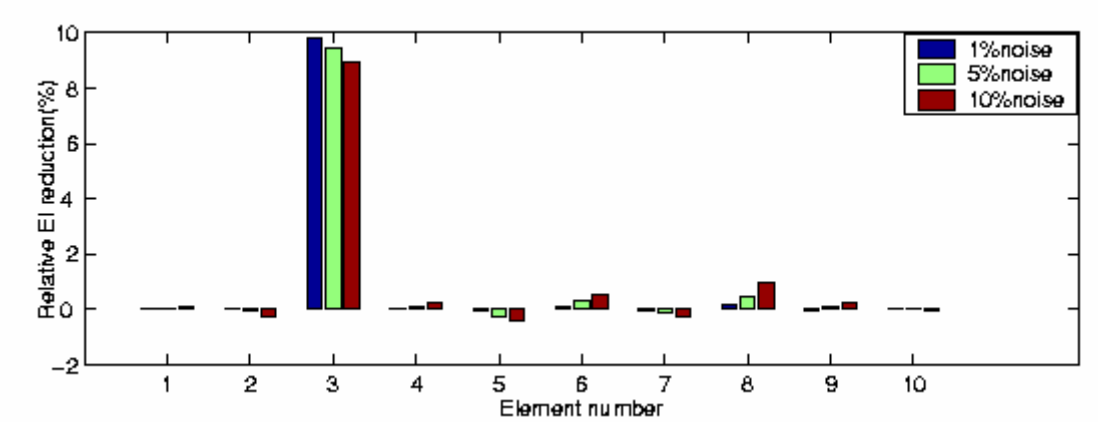

Figure 4-25– Identified damage for different noise levels

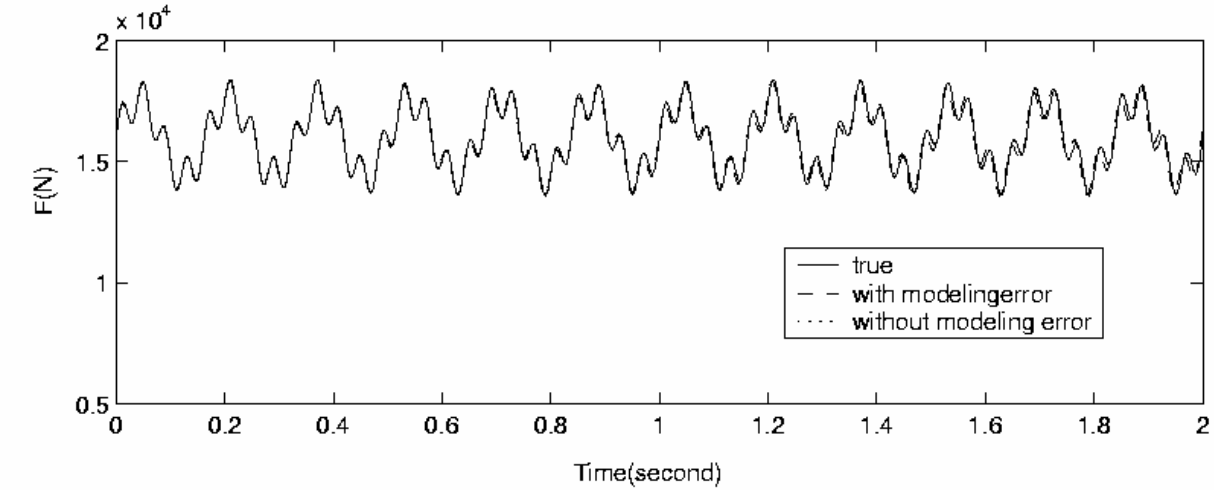

Figure 4-26– True and identified force histories after the second cycle of iterations

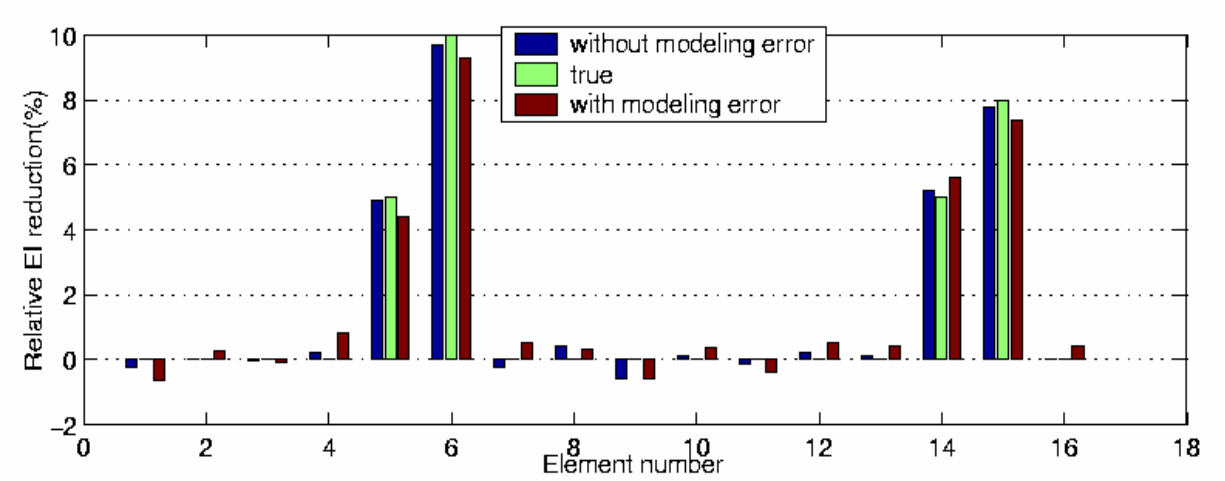

Figure 4-27– Identified damages after the second cycle of iterations

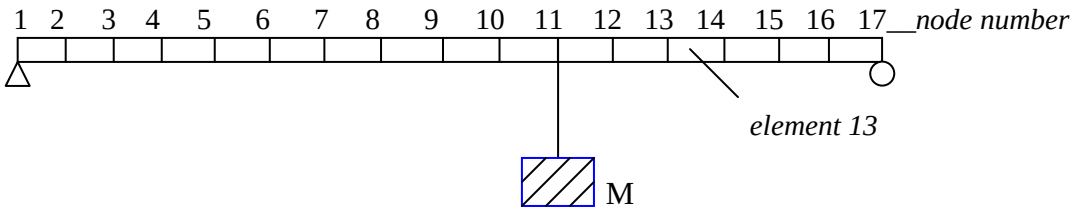

Figure 4-28- Experimental set-up

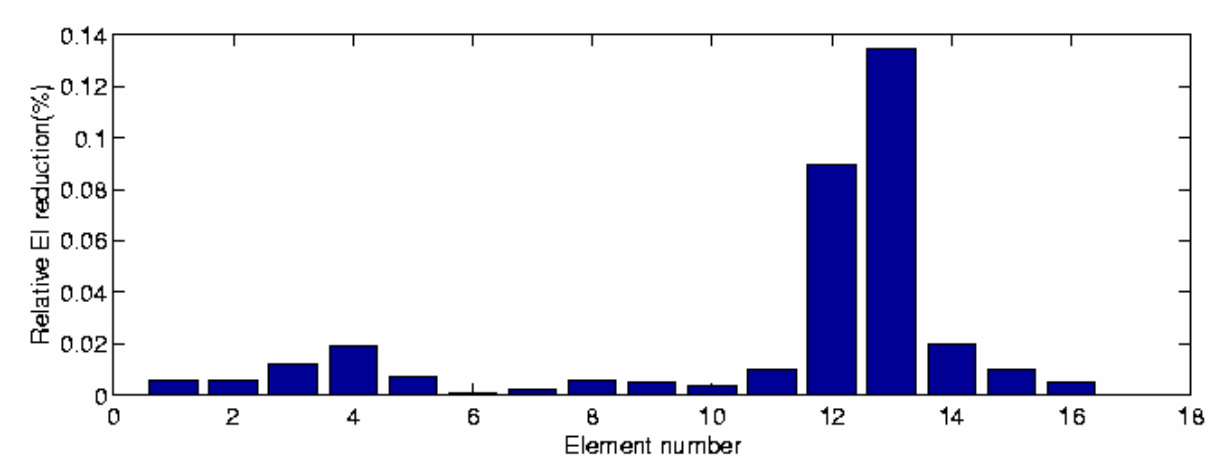

Figure 4-29– Final experimental identified damage

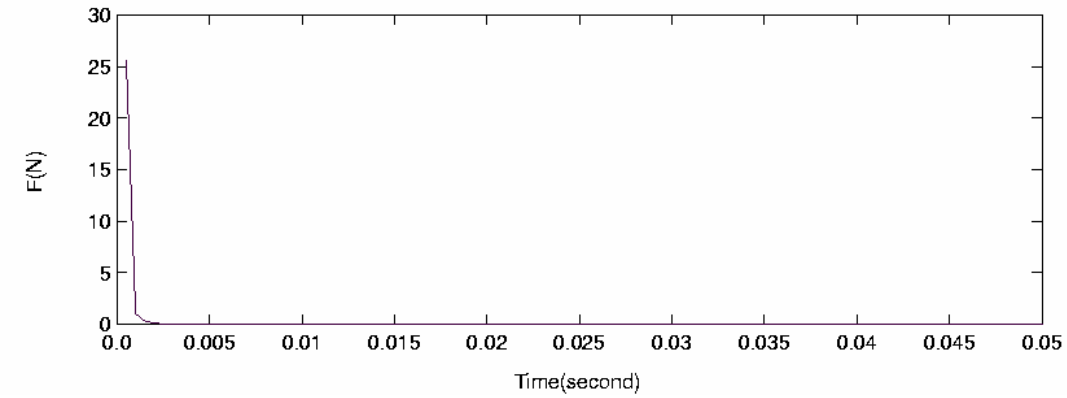

Figure 4-30– Identified force in experiment

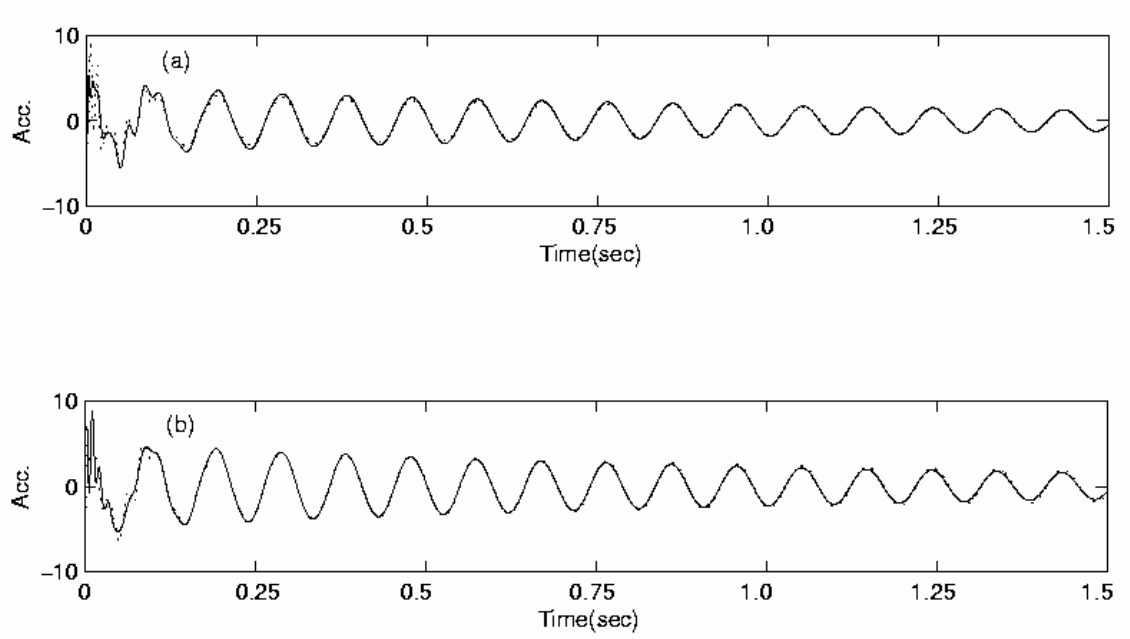

Figure 4-31– Experimental and calculated acceleration time histories from (a) node 7, (b) node 9; ___ calculated, …… experiment.

Chapter 5

OTHER DEVELOPMENTS OF THE THESIS

5.1 Crack Identification in Beam from Dynamic Responses

5.1.1 Introduction

Inspection of the structural components for damage is very important for making decision on the maintenance program of the structure. A lot of work has been published in the area of damage detection and many methods have been developed. These methods are mainly based on the relationship between the dynamic characteristics, such as the natural frequencies (Ibrahim et al., 1990; Cheng et al. 1999) or mode shapes (Rizos et al., 1990) and the damage parameters like the crack depth and its location.

A variety of crack models can be found in the literature as reviewed in Chapter 2, for instance, modeled as a spring (Adams et al., 1978; Ibrahim et al., 1990), a zone with a reduced Young's modulus (Joshi and Madhusudhan, 1991), and crack function models were also developed (Chondros et al., 1998) to model the crack in more details.

Most of the damage identification problems are solved in the frequency domain. Cawley and Adams (1979) are among the first ones to detect damage in elastic structure by using natural frequencies. Pandey et al. (1991) used complete mode shapes from the undamaged and damaged states to identify both the location and the extent of damage by solving a system of linear equations.

A crack with a constant depth is modeled with a Dirac delta function mathematically and a method is proposed to identify the crack parameters using the dynamic responses in this section. The method is developed based on the modal superposition and optimization technique in combination with regularization on the solutions to smooth out the large variations in the identified results. Either the displacement or the strain measurement can be used to identify the crack, and only the first few modes from several measuring points are required for the identification. Identification of both the single crack and multiple cracks are studied numerically with sinusoidal or impulsive excitation. The identification algorithm is further verified using experimental results from a beam with a single crack with different depths.

5.1.2 Direct Problem

5.1.2.1 *Equation of Motion*

A single-span uniform Euler-Bernoulli beam with a single-sided transverse crack subject to an excitation force $P(t)$ acting at x_p from the left support is shown in Figure 5-1. The crack is assumed to be fully opened and has a fixed depth h_c at a location distant x_c from the left support. The equation of motion of the beam can be written as

$$\rho A\frac{\partial^2 y(x,t)}{\partial t^2}+c\frac{\partial y(x,t)}{\partial t}+(EI_0-EI_c\delta(x-x_c))\frac{\partial^2}{\partial x^2}(\frac{\partial^2 y(x,t)}{\partial x^2})=P(t)\delta(x-x_p) \quad (5.1\text{-}1)$$

where ρ is the mass density of the beam, A is the cross-sectional area, c is the damping of the beam, E is the Young's modulus of material, I_0 is the moment of inertia of the beam cross-section, I_c is the reduction of the moment of inertia of beam cross-section at the crack defined as $\frac{b}{12}[h_0^3-(h_0-h_c)^3]$, h_0 is the depth of the beam, $y(x,t)$ is the

transverse displacement function of the beam, $\delta(x)$ is the Dirac delta function and *b* is the width of the beam. The beam is assumed to be at rest at the beginning of the identification, and the damping effect originated from the crack is not considered.

The kinetic energy T_E, the strain energy U_E, the work done W_c due to the viscous damping in the beam, and the work done W due to the external force can be expressed as

$$T_E = \frac{1}{2}\int_0^L \rho A(\frac{\partial y(x,t)}{\partial t})^2 dx \tag{5.1-2}$$

$$U_E = \frac{1}{2}\int_0^L EI(x)(\frac{\partial^2 y(x,t)}{\partial x^2})^2 dx = \frac{1}{2}\int_0^L [EI_0 - EI_c\delta(x-x_c)](\frac{\partial^2 y(x,t)}{\partial x^2})^2 dx \tag{5.1-3}$$

$$W_c = \int_0^L y(x,t)c\frac{\partial y(x,t)}{\partial t}dx \tag{5.1-4}$$

$$W = \int_0^L P(t)\delta(x-x_p)y(x,t)dx \tag{5.1-5}$$

Expressing the transverse displacement of the beam $y(x,t)$ in modal co-ordinates

$$y(x,t) = \sum_{i=1}^{n} Y_i(x)q_i(t) \tag{5.1-6}$$

where $Y_i(x)$ can be obtained from the assumed mode shapes. We have

$$T_E = \frac{1}{2}\int_0^L \rho A[\sum_{i=1}^{n} Y_i(x)\dot{q}_i(t)\sum_{j=1}^{n} Y_j(x)\dot{q}_j(t)]dx = \frac{1}{2}\sum_{i=1}^{n}\sum_{j=1}^{n}\dot{q}_i(t)m_{ij}\dot{q}_j(t) \tag{5.1-7}$$

$$U_E = \frac{1}{2}\int_0^L [EI_0 - EI_c\delta(x-x_c)](\sum_{i=1}^{n} Y_i''(x)q_i(t)\sum_{j=1}^{n} Y_j''(x)q_j(t))dx$$

$$= \frac{1}{2}\int_0^L EI_0\sum_{i=1}^{n} Y_i''(x)q_i(t)\sum_{j=1}^{n} Y_j''(x)q_j(t)dx$$

$$-\frac{1}{2}\int_0^L EI_c\delta(x-x_c)\sum_{i=1}^{n} Y_i''(x)q_i(t)\sum_{j=1}^{n} Y_j''(x)q_j(t)dx$$

$$= \frac{1}{2}\sum_{i=1}^{n}\sum_{j=1}^{n} q_i(t)k_{ij}q_j(t) - \frac{1}{2}\sum_{i=1}^{n}\sum_{j=1}^{n} q_i(t)k'_{ij}q_j(t)) \tag{5.1-8}$$

$$W_c = \int_0^L c \sum_{i=1}^{n} Y_i(x) q_i(t) \sum_{j=1}^{n} Y_j(x) \dot{q}_j(t) dx = \sum_{i=1}^{n} \sum_{j=1}^{n} q_i(t) c_{ij} \dot{q}_j(t) \qquad (5.1\text{-}9)$$

$$W = \int_0^L P(t) \delta(x - x_p) \sum_{i=1}^{n} Y_i(x) q_i(t) dx = \sum_{i=1}^{n} P(t) Y_i(x_p) q_i(t) = \sum_{i=1}^{n} f_i(t) q_i(t) \qquad (5.1\text{-}10)$$

and $\quad m_{ij} = \int_0^L \rho A Y_i(x) Y_j(x) dx, \qquad k_{ij} = \int_0^L EI_0 Y_i''(x) Y_j''(x) dx,$

$$k'_{ij} = \int_0^L EI_c \delta(x - x_c) Y_i''(x) Y_j''(x) dx = EI_c Y_i''(x_c) Y_j''(x_c),$$

$$c_{ij} = \int_0^L c Y_i(x) Y_j(x) dx, \quad f_i(t) = P(t) Y_i(x_p).$$

Substituting Equations (5.1-7) to (5.1-10) into the Lagrange equation

$$\frac{d}{dt}\left(\frac{\partial T_E}{\partial \dot{q}}\right) - \frac{\partial T_E}{\partial q} + \frac{\partial U_E}{\partial q} - \frac{\partial W_c}{\partial q} = \frac{\partial W}{\partial q} \qquad (5.1\text{-}11)$$

We obtain

$$\sum_{j=1}^{n} m_{ij} \ddot{q}_j(t) + \sum_{j=1}^{n} c_{ij} \dot{q}_j(t) + \sum_{j=1}^{n} (k_{ij} - k'_{ij}) q_j(t) = f_i(t) \qquad (i = 1,2,...,n) \qquad (5.1\text{-}12)$$

Writing Equation (5.1-12) in matrix form

$$[M]\{\ddot{q}(t)\} + [C]\{\dot{q}(t)\} + ([K] - [K'])\{q(t)\} = \{F(t)\} \qquad (5.1\text{-}13)$$

where

$$[M] = \{m_{ij}, i = 1,2,...,n; j = 1,2,...,n\}, \qquad [C] = \{c_{ij}, i = 1,2,...,n; j = 1,2,...,n\},$$

$$[K] = \{k_{ij}, i = 1,2,...,n; j = 1,2,...,n\}, \qquad [K'] = \{k'_{ij}, i = 1,2,...,n; j = 1,2,...,n\},$$

$$\{q(t)\} = \{q_1(t), q_2(t), ..., q_n(t)\}^T, \qquad \{F(t)\} = \{f_1(t), f_2(t), ..., f_n(t)\}^T \qquad (5.1\text{-}14)$$

The modal responses $\ddot{q}, \dot{q}, q$ of the beam can then be obtained by direct integration, say, Newmark method (1959).

5.1.2.2 *The Assumed Mode Shapes*

The general form of vibration mode for a uniform Euler beam can be written as

$$Y(x) = A_1 \cos \beta x + A_2 \sin \beta x + A_3 \cosh \beta x + A_4 \sinh \beta x \qquad (5.1\text{-}15)$$

where A_1, A_2, A_3, A_4 are constants and β is a frequency parameter. The vibration modes for an Euler beam with simply supported ends are obtained as

$$Y_i(x) = A_2 \sin \frac{i\pi x}{L} \tag{5.1-16}$$

where L is the length of the beam. It is noted that the effect of the crack on the vibration modes is very small (Fernandez-Saez et al., 1999) and it is not considered in this work.

5.1.2.3 *Accuracy of the Crack Model*

To validate the proposed crack model, the fundamental frequencies of the beam with the proposed crack model are compared with the results by Fernandaz-Saez, et al. (1999). They proposed a simplified method of evaluating the fundamental frequency for the bending vibrations of cracked Euler-Bernoulli beams with the crack in a beam modeled as an elastic spring. A closed form solution on the fundamental frequency was given for the simply supported cracked beam.

A 30 metres long simply supported Euler-Bernoulli beam with an open crack at 4 metres from the left support is studied. The parameters of the beam are: $\rho A = 5.0 \times 10^3 kg/m$, $E = 5 \times 10^{10} N/m^2$, $L = 30\ m$, $b = 0.6\ m$, and $h_0 = 1.0\ m$. Figure 5-2 shows the variation of the ratio of fundamental frequency with crack to the original frequency with no crack from different ratio of crack depth. The results from both models are close to each other except where the crack is at midspan, with the present model giving a slightly larger difference from those by Fernandaz-Saez et al. (1999).

Sinha et al. (2002) proposed an open crack model in an Euler-Bernoulli beam element with a modified local flexibility of the beam in the vicinity of the crack. The same beam for the above study is investigated here with an excitation force of

$P(t) = 40000[1 + 0.1\sin(10\pi t) + 0.05\sin(40\pi t)]$ N applied at 7 meters from the left support. The crack is at 4 metres from the left support with 0.25 m depth. The displacement responses at the 1/4 span and the middle point of the cracked beam were compared with the existing solution (Sinha et al., 2002) as shown in Figure 5-3. The responses obtained from both models are very close to each other indicating the accuracy of the proposed model.

5.1.3 Inverse Problem

5.1.3.1 *Identification from Measured Displacements*

Expressing the measured displacements $\tilde{y}(x_m, t)$ in modal co-ordinates

$$\tilde{y}(x_m, t) = \sum_{i=1}^{N} Y_i(x) q_i(t), \ (m = 1,2,..., N_m) \tag{5.1-17}$$

where N_m is the number of measurement locations; $\{\tilde{y}(x_m, t), m = 1,2,..., N_m\}$ are the displacements at x_m. Equation (5.1-17) can be re-written as

$$\{\tilde{y}\}_{N_m \times 1} = [Y]_{N_m \times N} \{q\}_{N \times 1} \tag{5.1-18}$$

where $\{\tilde{y}\}_{N_m \times 1}$ is the vector of displacements at N_m measurement locations. The vector of generalized co-ordinates can be written using the least-squares pseudo-inverse as

$$\{q\}_{N \times 1} = ([Y]^T{}_{N \times N_m} [Y]_{N_m \times N})^{-1} [Y]^T{}_{N \times N_m} \{\tilde{y}\}_{N_m \times 1} \tag{5.1-19}$$

The modal velocity and acceleration of the beam responses can be obtained from Equation (5.1-19) by numerical methods. However, if the central difference method is used to calculate the modal velocity and acceleration, it will lead to large approximation error. Therefore the generalized orthogonal polynomial (Law and Zhu, 2000) is used to model the displacement so as to avoid the approximation error,

$$\tilde{y}(x_j,t)=\sum_{i}^{Nf}a_iG_i(t) \tag{5.1-20}$$

where $\tilde{y}(x_j,t)$ is the approximated displacement at the *j*th measuring point, $G_i(t)$ is the orthogonal polynomial and the a_i is the coefficient. The velocity and acceleration are then approximated by the first and second derivatives of the orthogonal polynomial. The orthogonal polynomial used in this chapter is shown in Appendix B.

Writing in matrix form, we have,

$$\{\tilde{y}\}_{N_m\times 1}=[A]_{N_m\times Nf}\{G(t)\}_{Nf\times 1},\{\dot{\tilde{y}}\}_{N_m\times 1}=[A]_{N_m\times Nf}\{\dot{G}(t)\}_{Nf\times 1},\{\ddot{\tilde{y}}\}_{N_m\times 1}=[A]_{N_m\times Nf}\{\ddot{G}(t)\}_{Nf\times 1} \tag{5.1-21}$$

where $[A]_{N_m\times Nf}$, $\{G(t)\}_{Nf\times 1}$, $\{\dot{G}(t)\}_{Nf\times 1}$, $\{\ddot{G}(t)\}_{Nf\times 1}$ are the coefficient matrix of the polynomial, the orthogonal polynomial matrix, the first and second derivatives of the orthogonal polynomial variable matrix respectively. N_f is the order of the orthogonal polynomial. The coefficient matrix $[A]$ can be obtained by the least-squares method from Equation (5.1-21) as

$$[A]_{N_m\times Nf}=\{\tilde{y}\}_{N_m\times 1}\{G(t)\}^T_{1\times Nf}(\{G(t)\}_{Nf\times 1}\{G(t)\}^T_{1\times N_f})^{-1} \tag{5.1-22}$$

Substituting matrix $[A]$ into Equation (5.1-21), we can get $\{\dot{\tilde{y}}\}$ and $\{\ddot{\tilde{y}}\}$. And substituting $\{\tilde{y}\},\{\dot{\tilde{y}}\},\{\ddot{\tilde{y}}\}$ and the derivatives of { $G(t)$ } into Equation (5.1-19), we can obtain the modal displacement q , modal velocity $\dot{q}$ and modal acceleration $\ddot{q}$. Substituting further q , $\dot{q}$ and $\ddot{q}$ into Equation (5.1-13), we have

$$K'q=M\ddot{q}+C\dot{q}+Kq-F(t) \tag{5.1-23}$$

The elements of matrix K' are obtained as follows with the first order approximation

$$k'_{ij} = EI_c Y_i''(x_c) Y_j''(x_c) \approx \frac{Ebh_0^2 h_c}{4} Y_i''(x_c) Y_j''(x_c) \qquad (5.1\text{-}24)$$

The inverse problem here is how to find the crack location and the crack depth from Equation (5.1-23). When at time t_i, we have the following from Equations (5.1-23) and (5.1-24).

$$[K'] \begin{Bmatrix} q_1(t_i) \\ q_2(t_i) \\ \vdots \\ q_n(t_i) \end{Bmatrix} = [M] \begin{Bmatrix} \ddot{q}_1(t_i) \\ \ddot{q}_2(t_i) \\ \vdots \\ \ddot{q}_n(t_i) \end{Bmatrix} + [C] \begin{Bmatrix} \dot{q}_1(t_i) \\ \dot{q}_2(t_i) \\ \vdots \\ \dot{q}_n(t_i) \end{Bmatrix} + [K] \begin{Bmatrix} q_1(t_i) \\ q_2(t_i) \\ \vdots \\ q_n(t_i) \end{Bmatrix} - \begin{Bmatrix} f_1(t_i) \\ f_2(t_i) \\ \vdots \\ f_n(t_i) \end{Bmatrix} \qquad (5.1\text{-}25)$$

Rewriting Equation (5.1-25), and letting

$$J(x_c, h_c) = [K'] \begin{Bmatrix} q_1(t_i) \\ q_2(t_i) \\ \vdots \\ q_n(t_i) \end{Bmatrix} - \left[[M] \begin{Bmatrix} \ddot{q}_1(t_i) \\ \ddot{q}_2(t_i) \\ \vdots \\ \ddot{q}_n(t_i) \end{Bmatrix} + [C] \begin{Bmatrix} \dot{q}_1(t_i) \\ \dot{q}_2(t_i) \\ \vdots \\ \dot{q}_n(t_i) \end{Bmatrix} + [K] \begin{Bmatrix} q_1(t_i) \\ q_2(t_i) \\ \vdots \\ q_n(t_i) \end{Bmatrix} - \begin{Bmatrix} f_1(t_i) \\ f_2(t_i) \\ \vdots \\ f_n(t_i) \end{Bmatrix} \right] \qquad (5.1\text{-}26)$$

or

$$J(x_c, h_c) = A(p) - d \qquad (5.1\text{-}27)$$

where $J(x_c, h_c)$ is an error vector, and $A(p)$ represents the first term of the right-hand-side of Equation (5.1-26), and d represents the second term, the vector p contains the unknown crack location and depth parameters.

Now the problem becomes a nonlinear optimization problem with two unknown parameters: the crack depth h_c and the location x_c. This is equivalent to minimizing the error function

$$\min \left\| J(x_c, h_c) \right\|^2 = \min \left\| A(p) - d \right\|^2 \qquad (5.1\text{-}28)$$

Like many inverse problems, this is an ill-conditioned problem, and regularization method is adopted to provide bounds to the solution. A regularization term λ is introduced into the right-hand-side of Equation (5.1-28)

$$\min \left\| J(x_c, h_c) \right\|^2 = \min \{ \left\| A(p) - d \right\|^2 + \lambda \left\| p - p_0 \right\|^2 \} \qquad (5.1\text{-}29)$$

where $\lambda > 0$ and p_0 is the vector containing the *a priori* information on the crack location and depth at time t_i.

The following strategy is proposed to locate approximately the crack. It is known that when the identified crack location does not match the real location, the identified crack depth exhibits large fluctuations due to ill-conditioning in the solution. Therefore the variance of the identified crack depth time history from using different initial crack location in the calculation is taken as an indicator. The correct initial guess on the crack location should correspond to the smallest variance in the identified crack depth time history.

The crack identification can be realized through the following steps: the mode shapes $Y_i(x)$ are obtained from Equation (5.1-16). The modal displacement q, modal velocity $\dot{q}$ and modal acceleration $\ddot{q}$ are computed from Equation (5.1-21). Then by minimizing the error function J, we can get the crack location x_c and the crack depth h_c.

5.1.3.2 *Identification from Measured Strains*

The strain at the bottom of a rectangular beam with depth h_0 can be expressed in terms of the generalized co-ordinates as

$$\tilde{\varepsilon}(x_m, t) = -\frac{h_0}{2} \sum_{i=1}^{N} Y''(x_m) q_i(t) \qquad (m = 1,2,..., N_m) \qquad (5.1\text{-}30)$$

where N_m is the number of measurement locations; $\{\tilde{\varepsilon}(x_m,t), m=1,2,...,N_m\}$ are the strains at x_m. Equation (5.1-30) can be written as

$$\{\tilde{\varepsilon}\}_{N_m\times 1} = -\frac{h_0}{2}[Y'']_{N_m\times N}\{q\}_{N\times 1} \tag{5.1-31}$$

where $\{\tilde{\varepsilon}\}_{N_m\times 1}$ is the vector of strains at N_m measurement locations. Again the strain can be approximated by the orthogonal polynomial $G(t)$ as

$$\tilde{\varepsilon}(x_j,t) = \sum_{i}^{Nf} a_i G_i(t) \tag{5.1-32}$$

where $\tilde{\varepsilon}(x_j,t)$ is the strain at the *j*th measuring point. The rest of the computation in the identification is similar to those for identification from measured displacements mentioned above.

5.1.3.3 *Identification of Multiple Cracks*

The proposed formulation for single crack is extended to identify N_c single-sided transverse cracks in the beam, and Equation (5.1-1) becomes

$$\rho A\frac{\partial^2 y(x,t)}{\partial t^2} + c\frac{\partial y(x,t)}{\partial t} + (EI_0 - \sum_{k=1}^{Nc} E(I_c)_k \delta(x-(x_c)_k)\frac{\partial^2}{\partial x^2}(\frac{\partial^2 y(x,t)}{\partial x^2}) = P(t)\delta(x-x_p) \tag{5.1-33}$$

Matrix K' in Equation (5.1-14) becomes

$$K' = \sum_{k=1}^{Nc}(k'_{ij})_k, \qquad (i=1,2,...n;\ j=1,2,...,n) \tag{5.1-34}$$

where $(k'_{ij})_k$ is the matrix k'_{ij} in Equation (5.1-24) for the *kth* crack and Equation (5.1-25) becomes

$$\frac{Ebh_0^2}{4}\begin{bmatrix} \sum_{k=1}^{Nc} Y_1''((x_c)_k)Y_1''((x_c)_k)h_{ck} & \sum_{k=1}^{Nc} Y_1''((x_c)_k)Y_2''((x_c)_k)h_{ck} & \cdots & \sum_{k=1}^{Nc} Y_1''((x_c)_k)Y_n''((x_c)_k)h_{ck} \\ \sum_{k=1}^{Nc} Y_2''((x_c)_k)Y_1''((x_c)_k)h_{ck} & \sum_{k=1}^{Nc} Y_2''((x_c)_k)Y_2''((x_c)_k)h_{ck} & \cdots & \sum_{k=1}^{Nc} Y_2''((x_c)_k)Y_n''((x_c)_k)h_{ck} \\ \vdots & \vdots & \vdots & \vdots \\ \sum_{k=1}^{Nc} Y_n''((x_c)_k)Y_1''((x_c)_k)h_{ck} & \sum_{k=1}^{Nc} Y_n''((x_c)_k)Y_2''((x_c)_k)h_{ck} & \cdots & \sum_{k=1}^{Nc} Y_n''((x_c)_k)Y_n''((x_c)_k)h_{ck} \end{bmatrix}\begin{Bmatrix} q_1(t_i) \\ q_2(t_i) \\ \vdots \\ q_n(t_i) \end{Bmatrix}$$

$$= [M]\begin{Bmatrix} \ddot{q}_1(t_i) \\ \ddot{q}_2(t_i) \\ \vdots \\ \ddot{q}_n(t_i) \end{Bmatrix} + [C]\begin{Bmatrix} \dot{q}_1(t_i) \\ \dot{q}_2(t_i) \\ \vdots \\ \dot{q}_n(t_i) \end{Bmatrix} + [K]\begin{Bmatrix} q_1(t_i) \\ q_2(t_i) \\ \vdots \\ q_n(t_i) \end{Bmatrix} - \begin{Bmatrix} f_1(t_i) \\ f_2(t_i) \\ \vdots \\ f_n(t_i) \end{Bmatrix} \qquad (5.1\text{-}35)$$

The crack identification formulation will be similar to the single crack identification, and both the displacement and strain measurements can be used to identify multiple cracks in the beam.

5.1.4 Simulation and Results

5.1.4.1 *Single Crack Identification*

A 30 metres long simply supported Euler-Bernoulli beam with an open crack is studied. The first six natural frequencies of the uncracked beam are: 1.23, 4.94, 11.11, 19.75, 30.86 and 44.43 Hz. The damping ratios for these modes are all equal to 0.02. The excitation force is assumed to be $P(t) = 40000[1 + 0.1\sin(10\pi t) + 0.05\sin(40\pi t)]$ N, and it is applied at 7 metres from the left support. The dynamic components of the force are close to the second and fourth modal frequencies of the beam. The parameters of the beam are: $\rho A = 5.0 \times 10^3 kg/m$, $E = 5 \times 10^{10} N/m^2$, $L = 30\ m$, $b = 0.6\ m$, and $h_0 = 1.0\ m$. White noise is added to the calculated displacements and strains to simulate the polluted measurements as follows:

$$y = y_{calculated} + Ep \times N_{oise} \times \mathrm{var}(y_{calculated}) \qquad (5.1\text{-}26)$$

$$\varepsilon = \varepsilon_{calculated} + Ep \times N_{oise} \times \mathrm{var}(\varepsilon_{calculated}) \qquad (5.1\text{-}27)$$

where y and ε are the vectors of polluted displacement and strain respectively; Ep is the noise level ; N_{oise} is a standard normal distribution vector with zero mean and unit standard deviation; var(•) is the variance of the time history; $y_{calculated}$ and $\varepsilon_{calculated}$ are the vectors of calculated displacement and strain. 0%, 5% and 10% noise levels are studied in this paper. In the numerical simulation, the crack locates at 4 metres from the left support with the crack depth h_c equals 0.25m.

The first three modes are used in the calculation. Measured strains at *1/4L*, *1/2L* and *3/4L* are used in the identification. The sampling frequency is 100Hz, which is larger than two times the highest frequency of interest at 44.43 Hz.

Figure 5-4 shows the plot of variance of the identified crack depth time history against the initial crack location. The crack depth is taken as zero in the search for the crack location. The optimal regularization parameter λ was found different for different initial crack location, and it is taken equal to 200 for the preparation of Figure 5-4. The results confirm that the smallest variance corresponds to the correct crack location. In fact a wide range of λ from 20 to 200 gives results similar to Figure 3-4.

The initial crack location is then set at 4 metres as from Figure 3-4 with an initial zero crack depth. The regularization parameter is plotted against the variance of the identified crack location in Figure 5-5. The variance gradually increases with a reduction in the parameter until a point where there is a sudden jump in the variance. The value of λ corresponds to the point before this sudden jump (λ=20) is taken as the optimal regularization parameter.

Figures 5-6 shows the identified results from measured strains without any noise and with 10% noise respectively. There is little difference in the identified crack depth time histories from both cases. The polluted measurements have been approximated

with orthogonal polynomial functions with 20 terms, and the velocity and accelerations subsequently obtained by direct differentiating the functions are compared with those from the measurements in Figure 5-7, and they are found matching each other very well. Larger errors are only found in the accelerations.

The effect of modal truncation on the identification is also studied. Figure 5-8 shows the identified results from using the first three and six modes. And the number of measuring points is taken equal to the number of vibration modes with the measuring points evenly distributed on the beam. The sampling frequency is 100Hz, and 5% noise level is included in the measurement. It can be seen from the figure that the identification accuracy increases with increasing number of modes in the identification, but the curves obtained from using only three modes are still varying close to the true curves.

Large fluctuations are found in the identified crack depth within the first and final quarters of the time history in all the above cases. This can be explained by observing the acceleration and velocity obtained from the orthogonal polynomial functions in Figure 5-7. Errors are found in these time derivatives near the beginning and end of the time histories while those in the middle halve are well approximated by the polynomials. This is the major source of error in the identification and is due to the discontinuity of the time responses with the excitation force. The identification error is found to decrease when more modes are used.

5.1.4.2 *Multi-Cracks Identification*

The same simply supported Euler-Bernoulli beam with three open cracks is studied. The crack locations are at 4 m, 14 m and 24 m from the left support. The open crack depths are arbitrarily taken as $h_{c1} = 0.2m$, $h_{c2} = 0.25m$ and $h_{c3} = 0.2m$.

The first 6 modes and 6 displacement measurements are used in the identification, and 5% noise is included. The measuring points are evenly distributed on the beam, and the sampling frequency is 100 Hz. The same sinusoidal excitation force as for single crack identification is used in this study. The strategy for searching the optimal location for the single crack identification is not applicable for multiple cracks because of the existence of numerous local minima in the search for the global minimum variance. This strategy assumes that the desired locations are close to the nominal initial values and that there are no spurious solutions in the neighborhood of the correct solution. These assumptions are not valid in this case because the nominal initial values on the locations are not known. Hjelmstad (1996) has used a random starting point scheme in conjunction with the objective minimization algorithm to find all the multiple minima of the parameter estimation problem. Pothisiri and Hjelmstad (2002) have also proposed a method to find a near-optimal measurement set for parameter estimation. Both of these methods could be applied to the present problem to find solutions on the initial crack locations.

In this study, the true locations of the cracks are included in the identification, and the optimal regularization parameter is 100 in this study. Figure 5-9 shows the identification results on the three cracks, the first two are found almost overlapping with the true curve while the third one varies around the true curve. Large fluctuations are found at both ends of the time history similar to those found in the single crack identification.

5.1.4.3 *Crack Identification from an Impulsive Force*

A periodic impulsive force is applied on the same beam as for the above study with a period of 1 second, and the duration of the force is 0.1 second. The magnitude of the force is 9500 N simulating the impact excitation produced by a 125 kg weight free

falling for one metre on the beam. The effect of the falling mass after the impact is ignored. The force is applied at 7 metres from the left support and it can be expressed in the following form mathematically,

$$P(t) = \begin{cases} 190000(t - 0.05) & 0.05 \le t \le 0.1 \\ 190000(0.15 - t) & 0.1 \le t \le 0.15 \end{cases}$$

A Fourier series is used to simulate the force, i.e.

$$P(t) = \alpha_0 + \sum_{k=1}^{\infty} \alpha_k \cos\frac{2k\pi t}{T} + \sum_{k=1}^{\infty} \beta_k \sin\frac{2k\pi t}{T},$$

where $\alpha_0 = \frac{1}{T}\int_0^T P(t)dt$, $\alpha_k = \frac{2}{T}\int_0^T P(t)\cos\frac{2k\pi t}{T}dt$, and $\beta_k = \frac{2}{T}\int_0^T P(t)\sin\frac{2k\pi t}{T}dt$.

Forty terms in the series are used to include the higher frequency components in the force. The crack location and crack depth are the same as for the single crack identification. The regularization parameter is 20. The sampling frequency is 100 Hz, and the first 6 modes and 6 displacement measurements are used in the identification. 5% noise is included in the identification. The measuring points are evenly distributed on the beam. Figure 5-10 shows that the identified crack depth is close to the true one. Results not shown here indicate that the identified result is less dependent on the sampling rate. This is because the impulsive force consists of a wide spectrum of frequency components as an excitation force, but the majority of the responses come from the first few modes of the structure which can be easily collected using a low sampling rate.

5.1.4.4 *Comparison with Existing Method*

The accuracy of identification results is compared with those from Sinha et al. (2002) for the cases of single crack and multiple cracks under sinusoidal excitation and results from both methods are listed in Table 5-1. Since the parameters are identified in a time series, the data obtained from averaging the identified values

during the period 0.1s to 0.6 s are taken as the results. This is to avoid the errors close to the beginning and end of the time histories due to the discontinuity of the time response with the excitation force. The proposed method is found giving much better accuracy with 5% or 10% noise in the measurement than Sinha et al. (2002) without any measurement noise both in the location and crack depth. It is also noted that the crack parameters are identified in the time domain, and this means that the proposed method can be extended to identify breathing cracks in the beam with time varying parameters.

5.1.5 Laboratory Verification

Experimental results are used to verify the algorithm developed for the crack identification. The test steel beam was suspended with fine nylon rope at both ends. Figure 5-11 shows the experimental setup. The parameters of the test sample are: L= 2.1 *m*, b = 0.025 *m*, h_0 = 0.019 *m*, $E = 2.07\times10^{11}\ \ N/m^2$, $\rho = 7.832\times10^{3}\ \ kg/m^3$. The crack is at 1.72 *m* from the left free end, and is created using a machine saw with 1.3mm thick cutting blade. Five measured strains were used to identify the crack in the beam which were located at 0.6*m*, 0.9*m*, 1.1*m*, 1.4*m* and 1.95*m* from the left free end respectively. An impulsive force was applied with an impact hammer model B&K 8202 at 1.2 *m* from the left free end. The sampling frequency is 2000Hz, and the data record time duration is 1 minute. The data are re-sampled with a sampling frequency of 500 Hz in the identification in order to improve the computation efficiency. The first 5 natural frequencies of the intact and the damaged beam with the crack depth at 3*mm*, 6*mm* and 9*mm* are shown in Table 5-2. The frequencies do not change much with damage in the first two modes. Figure 5-12 shows a sample of the impulsive force and the five measured strains when the crack depth is 6 *mm*. Two hammer hits were

applied on the beam within this duration. It is noted that the measured strains from the beam are very small with a maximum of approximately 60 micron at 1.1 m.

Figure 5-13 shows the identified results for the different crack depths. The first 4 modes are used in the identification. And the regularization parameter λ is 100. Due to the limitation of the computer memory, only the first 7.0 seconds measured strains were used in the identification. The location of the crack can be obtained from a study of the variance of the identified results as what has been done in the simulation study, and therefore the true locations are used in the identification. The identified crack depth time history fluctuates close to the true value of the time history for all the cases. The identified crack depth for *9mm* crack is more accurate than those with smaller depth. It is noted that these results comes from two hammer hits on the beam with very low level of dynamic responses. The identified results are believed to improve significantly with longer duration in the identification or when more hammer hits are included within the time duration of computation.

5.1.6 Concluding Remarks

This section includes a method for crack identification in a beam structure. The crack with a constant depth is modeled with a Dirac delta function, and a method is proposed to identify the open crack in beam structures based on dynamic measurements in time domain. The proposed method is based on modal superposition and optimization technique with regularization on the solution. Only several displacement or strain measurements and the first few modes are required in the crack identification. An orthogonal polynomial function is used to approximate the measured strain or displacement for a practical application with noisy measurements.

But the acceleration measurement cannot be used for crack identification; this is because the displacement integrated twice from the acceleration will lead to a shift by using the orthogonal polynomial function. Computation simulations using sinusoidal and impulsive excitations on a beam with a single or multiple cracks show that the method is effective to identify cracks and is more accurate than the method by Sinha et al. (2002) from polluted measurements. Another advantage of the proposed method is that it can be easily extended to identify time-varying crack in the structures. This will be a further research topic for the authors. Experimental results also show that a few hammer hits could be used as the excitation source for the single crack identification. One limitation of the proposed crack identification method is that in the case of multiple damages, where the locations of the crack have to be known *a priori*.

5.2 Time Domain Responses of a Prestressed Beam and Prestress Identification

5.2.1 Introduction

Prestress force has been used very often with long span structure. The interest in the safety assessment of existing prestressed concrete bridges increases in recent years. Amongst the different physical parameters of the structural system, the prestress force is one of the most important parameters to describe the load-carrying capacity of the structure. A quick and non-destructive test method to assess the condition of existing structures is required by the industry for their maintenance programme.

Very few works have been reported on any successful method to identify directly or indirectly the prestress force of a beam. It is known that prestress force has very little effect on the mode shapes of the beam, and the higher modal frequencies do not change significantly with the prestress force. Saiidi et al. (1994) showed that the sensitivity of the modal frequency decreases with higher vibration modes, and the prestress force affects the first few lower modes more significantly than the higher ones. Consequently the prestress force would be difficult to identify from the modal frequencies. Also Abraham et al. (1995) reported that the mode shapes remain almost identical with different prestress force in the beam, and it will also be difficult to identify the force from the measured mode shapes.

The dynamic response of a prestressed beam under both fixed excitation force and moving force is studied in this section based on modal superposition, and the contribution from the higher modes is found less than that from lower modes. An

inverse problem to identify the prestress force is then formulated taking only the prestress force and both the prestress force and the flexural rigidity of the beam as variables in the identification with external excitation. A more general inverse problem is also studied with the identification of the prestress force, the moving force(s) and the flexural rigidity of the beam simultaneously. The damped least squares method with regularization is used for the solution. Orthogonal polynomial function (Law and Zhu, 2000) is used to approximate the measured strain responses to remove the measurement noise effect. The work presented in this section indicates that the identification of prestress force with normal modal testing technique is possible even with noisy data.

5.2.2 Forward Problem

5.2.2.1 *Equation of Motion*

The bridge deck is modeled as a single-span simply supported prestressed uniform rectangular Euler-Bernoulli beam subject to an external excitation force $P(t)$ acting at a distance x_p from the left support as shown in Figure 5-14. The equation of motion of the beam can be written as

$$\rho A\frac{\partial^2 y(x,t)}{\partial t^2}+c\frac{\partial y(x,t)}{\partial t}+T\frac{\partial^2 y(x,t)}{\partial x^2}+\frac{\partial^2}{\partial x^2}EI_0\frac{\partial^2 y(x,t)}{\partial x^2}=P(t)\delta(x-x_p) \qquad (5.2\text{-}1)$$

where ρ is the mass density of the beam, A is the cross-sectional area, c is the damping of the beam, E is the Young's modulus of material, $I_0=\frac{bh_0^3}{12}$ is the moment of inertia of the beam cross-section, b is the width of the beam, h_0 is the height of the beam, T is the externally applied compressive axial force (note that compressive is positive and

tension is negative), $y(x,t)$ is the transverse displacement function of the beam, and $\delta(x)$ is the Dirac delta function.

The prestress tendon is assumed unbonded with the concrete, and it is constant along the whole beam. The tendon eccentricity gives rise to a static moment effect on the beam section, but it has not any relationship with its dynamic properties. It is therefore not represented in Equation (5.2-1).

5.2.2.2 *Modal Responses*

On the basis of modal superposition, the dynamic deflection $y(x,t)$ of the beam can be expressed as:

$$y(x,t) = \sum_{i=1}^{\infty} Y_i(x) q_i(t) \tag{5.2-2}$$

where $Y_i(x)$ is the mode shape function of the *i*th mode and $q_i(t)$ is the *i*th modal amplitude.

Substituting Equation (5.2-2) into Equation (5.2-1), multiplying each term by $Y_j(x)$, integrating with respect to x between 0 and L and applying the modal orthogonality conditions, we have:

$$\ddot{q}_i(t) + 2\xi_i \overline{\omega}_i \dot{q}(t) + \overline{\omega}_i^2 q_i(t) = \frac{1}{m_i} f_i(t) \tag{5.2-3}$$

where $\overline{\omega}_i = \sqrt{(\frac{EI_0}{\rho A}(\frac{i\pi}{L})^4 - \frac{T}{\rho A}(\frac{i\pi}{L})^2)}$, ξ_i and m_i are the reduced modal frequency, the damping ratio and the modal mass of the *i*th mode; $f_i(t) = P(t)Y_i(x_p)$ is the modal force. The modal shape function of the prestressed beam resembles that of a beam

without prestress force (Abraham et al, 1995) and it is written in the normalized form as $Y_i(x) = \sqrt{\frac{2}{\rho AL}} \sin \frac{i\pi}{L} x$ for a simply supported beam, and

$$m_i = \int_0^L \rho A Y_i^2(x) dx = 1 \tag{5.2-4}$$

Writing equation (5.2-3) in matrix form

$$[I]\{\ddot{Q}(t)\} + [C]\{\dot{Q}(t)\} + ([K] - [K'])\{Q(t)\} = \{F(t)\} \tag{5.2-5}$$

where

$$[C] = diag(2\xi_i \omega_i); \quad [K] = diag(\frac{EI_0}{\rho A}(\frac{i\pi}{L})^4); \quad [K'] = diag(\frac{T}{\rho A}(\frac{i\pi}{L})^2);$$

$$\{Q(t)\} = \{q_1(t), q_2(t), ..., q_n(t)\}^T, \qquad \{F(t)\} = \{f_1(t), f_2(t), ..., f_n(t)\}^T$$

and $[I]$ is the unity matrix.

We can determine $\bar{\omega}_i$ for $T \le T_{cr}$ where $T_{cr} = \frac{\pi^2 EI_0}{L^2}$ is the critical buckling load of the beam. The dynamic response is computed in the time domain numerically using the Newmark's integration scheme.

5.2.3 Inverse Problem

5.2.3.1 *Prestress Force Identification from Measured Displacements*

Expressing the measured displacements $\tilde{y}(x_m, t)$ at a point x_m from the left support in modal co-ordinates

$$\tilde{y}(x_m, t) = \sum_{i=1}^{N} Y_i(x) q_i(t), \qquad (m = 1,2,..., N_m) \tag{5.2-6a}$$

or in matrix form as

$$\{\tilde{y}\}_{N_m \times 1} = [Y]_{N_m \times N} \{q\}_{N \times 1} \tag{5.2-6b}$$

where $\{\tilde{y}\}_{N_m \times 1}$ is the vector of displacements at N_m measurement locations, and *N* is the number of measured modes in the responses. The vector of generalized co-ordinates can be written using the least-squares pseudo-inverse

$$\{q\}_{N\times 1} = ([Y]^T{}_{N\times N_m}[Y]_{N_m\times N})^{-1}[Y]^T{}_{N\times N_m}\{\tilde{y}\}_{N_m\times 1} \tag{5.2-7}$$

The modal velocity and acceleration of the beam responses can be obtained from Equation (5.2-7) by numerical methods. However, when the measurements are polluted by noise, the use of central difference method to calculate the modal velocity and acceleration will lead to large computation error. Therefore the generalized orthogonal polynomial is used to model the measured displacement as

$$\tilde{y}(x_j, t) = \sum_{i}^{Nf} a_i G_i(t) \tag{5.2-8}$$

where $\tilde{y}(x_j, t)$ is the approximated displacement at the *j*th measuring point. N_f is the order of the orthogonal polynomial function. The velocity and acceleration are then approximated by the first and second derivatives of the orthogonal polynomial. It is note that the order of the orthogonal polynomial function, N_f, has large effects on the accuracy of velocity and acceleration approximated by the first and second derivatives of the orthogonal polynomial. Study in the present paper found that $N_f = 20$ is the optimal order such that the velocity and acceleration can be obtained accurately.

Substituting Equation (5.2-8) into (5.2-6) and writing in matrix form, we have,

$$\begin{aligned}
\{\tilde{y}\}_{N_m\times 1} &= [A]_{N_m\times Nf}[G]_{Nf\times 1} \\
\{\dot{\tilde{y}}\}_{N_m\times 1} &= [A]_{N_m\times Nf}[\dot{G}]_{Nf\times 1} \\
\{\ddot{\tilde{y}}\}_{N_m\times 1} &= [A]_{N_m\times Nf}[\ddot{G}]_{Nf\times 1}
\end{aligned} \tag{5.2-9}$$

where $[A]_{N_m \times Nf}$, $[G]_{Nf \times 1}$, $[\dot{G}]_{Nf \times 1}$, $[\ddot{G}]_{Nf \times 1}$ are the coefficient matrix of the polynomial, the orthogonal polynomial matrix, the first and second derivatives of the orthogonal polynomial variable matrix respectively. The coefficient matrix [A] can be obtained by the least-squares method from Equation (5.2-9)

$$[A]_{N_m \times Nf} = \{\tilde{y}\}_{N_m \times 1}[G]^T_{1 \times Nf}([G]_{Nf \times 1}[G]^T_{1 \times N_f})^{-1} \tag{5.2-10}$$

Substituting matrix [A] and the derivatives of [G] into Equation (5.2-9), we can get $\{\tilde{y}\}$ and $\{\ddot{\tilde{y}}\}$. And substituting $\{\tilde{y}\},\{\dot{\tilde{y}}\},\{\ddot{\tilde{y}}\}$ into Equation (5.2-7), we can obtain the modal displacement q, modal velocity $\dot{q}$ and modal acceleration $\ddot{q}$. Substituting further q, $\dot{q}$ and $\ddot{q}$ into Equation (5.2-5), and after transformation, we have

$$[K']\{Q(t)\} = [I]\{\ddot{Q}(t)\} + [C]\{\dot{Q}(t)\} + [K]\{Q(t)\} - \{F(t)\} \tag{5.2-11}$$

Matrix [K'] contains the prestress force T, which is assumed constant throughout the length of the beam. Matrix [C] contains the modal damping ξ_i and modal frequency ω_i which are assumed unchanged, and matrix [K] contains the system parameters of the beam which are also assumed unchanged. The inverse problem is to solve Equation (5.2-11) in time domain to get the prestress force T. Rewriting Equation (5.2-11)

$$\{B\}_{N \times 1} T = \{\bar{F}\}_{N \times 1} \tag{5.2-12}$$

where

$$\{B\} = \begin{bmatrix} (\frac{\pi}{L})^2 \frac{1}{\rho A} & 0 & 0 & 0 \\ 0 & (\frac{2\pi}{L})^2 \frac{1}{\rho A} & 0 & 0 \\ 0 & 0 & \ddots & 0 \\ 0 & 0 & 0 & (\frac{N\pi}{L})^2 \frac{1}{\rho A} \end{bmatrix}_{N \times N} \begin{Bmatrix} q_1(t) \\ q_2(t) \\ \vdots \\ q_N(t) \end{Bmatrix}_{N \times 1}$$

and vector $\{\bar{F}\}$ contains all the terms on the right-hand-side of Equation (5.2-11). From Equation (5.2-12) one can see, the equation number is N but the unknown is

only one, T, so the prestress force T can be calculated directly by the simple least-squares method

$$T = (\{B\}^T \{B\})^{-1} \{B\}^T \{\overline{F}\} \tag{5.2-13}$$

In order to have bounds on the ill-conditioned solution, the damped least-squares method (DLS) is used and singular value decomposition is used in the pseudo-inverse computation. Equation (5.2-13) is written in the following form using the DLS method.

$$T = (\{B\}^T \{B\} + \lambda I)^{-1} \{B\}^T \{\overline{F}\} \tag{5.2-14}$$

where λ is the non-negative damping coefficient governing the contribution of the least-squares error in the solution. The solution of Equation (5.2-14) is equivalent to minimizing the function

$$J(T, \lambda) = \min(\left\| \{B\}T - \{\overline{F}\} \right\|^2 + \lambda \left\| T \right\|^2) \tag{5.2-15}$$

with the second term in Equation (5.2-15) providing bounds to the solution.

5.2.3.2 *Identification from Measured Strains*

The strain at the bottom of the beam at a point x_m from the left support can be expressed similar to Equation (5.2-6) in terms of the generalized co-ordinates as

$$\tilde{\varepsilon}(x_m, t) = -\frac{h_0}{2} \sum_{i=1}^{N} Y''(x_m) q_i(t) \qquad (m = 1,2,..., N_m) \tag{5.2-16}$$

where h_0 is the depth of the beam. Equation (5.2-16) can be written as

$$\{\tilde{\varepsilon}\}_{N_m \times 1} = [Y'']_{N_m \times N} \{q\}_{N \times 1} \tag{5.2-17}$$

where $\{\tilde{\varepsilon}\}_{N_m \times 1}$ is the vector of strains at N_m measurement locations. Again the strain at the *j*th measuring point can be approximated by the orthogonal function $G(t)$ as

$$\tilde{\varepsilon}(x_j, t) = \sum_{i}^{Nf} a_i G_i(t) \tag{5.2-18}$$

The rest of the computation in the identification is similar to that for identification from measured displacements mentioned above.

5.2.3.3 *Identification of both Prestress Force and the Flexural Rigidity of the Beam*

Other variables in the system should also be included in the identification for a real application. Since the dimensions of the beam can be measured accurately, and the modal damping can be estimated from a preliminary spectral analysis before the identification, the only variable with uncertainty is the flexural rigidity EI_0 of the beam section. If we have a uniform uncracked beam, we have both T and EI_0 as the two variables in the identification. Rewriting Equation (5.2-11) as

$$\left(T \begin{bmatrix} (\frac{\pi}{L})^2 \frac{1}{\rho A} & 0 & 0 & 0 \\ 0 & (\frac{2\pi}{L})^2 \frac{1}{\rho A} & 0 & 0 \\ 0 & 0 & \ddots & 0 \\ 0 & 0 & 0 & (\frac{N\pi}{L})^2 \frac{1}{\rho A} \end{bmatrix}_{N\times N} - EI_0 \begin{bmatrix} (\frac{\pi}{L})^4 \frac{1}{\rho A} & 0 & 0 & 0 \\ 0 & (\frac{2\pi}{L})^4 \frac{1}{\rho A} & 0 & 0 \\ 0 & 0 & \ddots & 0 \\ 0 & 0 & 0 & (\frac{N\pi}{L})^4 \frac{1}{\rho A} \end{bmatrix}_{N\times N} \right) \begin{Bmatrix} q_1(t) \\ q_2(t) \\ \vdots \\ q_N(t) \end{Bmatrix}$$

$$= \begin{bmatrix} 1 & 0 & 0 & 0 \\ 0 & 1 & 0 & 0 \\ 0 & 0 & \ddots & 0 \\ 0 & 0 & 0 & 1 \end{bmatrix}_{N\times N} \begin{Bmatrix} \ddot{q}_1(t) \\ \ddot{q}_2(t) \\ \vdots \\ \ddot{q}_N(t) \end{Bmatrix}_{N\times 1} + \begin{bmatrix} 2\xi_1\omega_1 & 0 & 0 & 0 \\ 0 & 2\xi_2\omega_2 & 0 & 0 \\ 0 & 0 & \ddots & 0 \\ 0 & 0 & 0 & 2\xi_N\omega_N \end{bmatrix}_{N\times N} \begin{Bmatrix} \dot{q}_1(t) \\ \dot{q}_2(t) \\ \vdots \\ \dot{q}_N(t) \end{Bmatrix}_{N\times 1} - \begin{Bmatrix} f_1(t) \\ f_2(t) \\ \vdots \\ f_N(t) \end{Bmatrix}_{N\times 1} \tag{5.2-19}$$

The inverse problem is to solve Equation (5.2-19) in time domain at each time step to get the prestress force T and the flexural rigidity EI_0. Rewriting Equation (5.2-19) in a simple form

$$[B]\{X\} = \{\overline{F}\}_{N\times 1} \tag{5.2-20}$$

where

$$[B]=\begin{bmatrix} B_T & 0 \\ 0 & B_{EI} \end{bmatrix},\ \{X\}=\begin{Bmatrix} T \\ EI_0 \end{Bmatrix},$$

$$\{B_T\}=\begin{bmatrix} (\frac{\pi}{L})^2\frac{1}{\rho A} & 0 & 0 & 0 \\ 0 & (\frac{2\pi}{L})^2\frac{1}{\rho A} & 0 & 0 \\ 0 & 0 & \ddots & 0 \\ 0 & 0 & 0 & (\frac{N\pi}{L})^2\frac{1}{\rho A} \end{bmatrix}_{N\times N} \begin{Bmatrix} q_1(t) \\ q_2(t) \\ \vdots \\ q_N(t) \end{Bmatrix}_{N\times 1},$$

$$\{B_{EI}\}=\begin{bmatrix} (\frac{\pi}{L})^4\frac{1}{\rho A} & 0 & 0 & 0 \\ 0 & (\frac{2\pi}{L})^4\frac{1}{\rho A} & 0 & 0 \\ 0 & 0 & \ddots & 0 \\ 0 & 0 & 0 & (\frac{N\pi}{L})^4\frac{1}{\rho A} \end{bmatrix}_{N\times N} \begin{Bmatrix} q_1(t) \\ q_2(t) \\ \vdots \\ q_N(t) \end{Bmatrix}_{N\times 1},$$

Again the prestress force T and the flexural rigidity EI_0 can be calculated directly by the simple least-squares method

$$\{X\}=([B]^T[B])^{-1}[B]^T\{\overline{F}\} \tag{5.2-21}$$

or in the following form using the DLS method.

$$\{X\}=([B]^T[B]+\lambda[I])^{-1}[B]^T\{\overline{F}\} \tag{5.2-22}$$

Both the prestress force and the flexural rigidity of the beam are identified at each time step. The dimension of the variable $\{X\}$ is $2nt\times 1$, where nt is the total time steps. The variable vector $\{X\}$ is defined with these two variables appearing in alternative order, i.e. the prestress force takes up the odd terms of the vector $\{X\}$ while the flexural rigidity takes up the even terms.

5.2.3.4 *Simultaneous Identification of Prestress Force and Moving Loads*

The equation of motion of a beam subject to a set of moving forces $P_l\ (l=1,2,...,N_p)$ can be written as

$$\rho A\frac{\partial^2 y(x,t)}{\partial t^2}+c\frac{\partial y(x,t)}{\partial t}+T\frac{\partial^2 y(x,t)}{\partial x^2}+\frac{\partial^2}{\partial x^2}EI_0\frac{\partial^2 y(x,t)}{\partial x^2}=\sum_{l=1}^{N_p}P_l(t)\delta(x-x_l(t)) \quad (5.2\text{-}23)$$

The identification equation can be expressed as the following,

$$[K']\{Q(t)\}+\{F(t)\}=[I]\{\ddot{Q}(t)\}+[C]\{\dot{Q}(t)\}+[K]\{Q(t)\} \quad (5.2\text{-}24)$$

The vector of generalized force $\{F(t)\}$ can also be found from

$$\{F(t)\}=[L]\{P(t)\} \quad (5.2\text{-}25)$$

where $\{P(t)\}$ are the set of moving forces on the beam and

$$[L]=\begin{bmatrix} Y_1(x_1(t)) & Y_1(x_2(t)) & \dots & Y_1(x_{N_p}(t)) \\ Y_2(x_1(t)) & Y_2(x_2(t)) & \dots & Y_2(x_{N_p}(t)) \\ \vdots & \vdots & \cdots & \vdots \\ Y_N(x_1(t)) & Y_N(x_2(t)) & \cdots & Y_N(x_{N_p}(t)) \end{bmatrix} \quad (5.2\text{-}26)$$

where $Y_i(x_1(t))=\sqrt{\frac{2}{\rho AL}}\sin(\frac{i\pi x_1(t)}{L})$ is the value of *ith* mode shape function at the location of $x_1(t)$, etc.

Rewriting Equation (5.2-24) in a simple form

$$\{B_T\}_{N\times 1}T+[L]_{N\times N_p}\{P(t)\}_{N_p\times 1}=\{r\}_{N\times 1} \quad (5.2\text{-}27)$$

where vector $\{r\}$ contains all the terms on the right-hand-side of Equation (5.2-24). In Equation (5.2-27) T is the unknown prestress force of the beam and $\{P(t)\}$ is the unknown moving force vector to be identified.

The inverse problem is to solve Equation (5.2-13) in time domain. Since both T and $\{P(t)\}$ are uncoupled, Equation (5.2-27) can be further simplified into

$$[B_d]X=\{r\} \quad (5.2\text{-}28)$$

where $[B_d]=[\{\mathbf{B}_T\},[L]]$, $X=\begin{Bmatrix} T \\ \{P\} \end{Bmatrix}$.

The prestress force T and the moving force $\{P\}$ can be calculated directly by the damped simple least-squares method (DLS)

$$\{X\} = ([B_d]^T[B_d] + \lambda I)^{-1}[B_d]\{r\} \tag{5.2-29}$$

5.2.3.5 *Identification of the Prestress and Moving Forces and the Flexural Rigidity of the Beam*

Other variables in the system should also be included in the identification for a real application. If we have a uniform uncracked beam in the problem, we have prestress force T, flexural rigidity EI_0 and moving force $P(t)$ as the three variables in the identification. Rewriting Equation (5.2-24) as

$$\{\boldsymbol{B}_T\}_{N\times 1}T + [L]_{N\times N_p}\{P(t)\}_{N_p\times 1} - \{B_{EI}\}EI_0 = \{r'\}_{N\times 1} \tag{5.2-30}$$

where

$$\{r'\} = [I]\{\ddot{Q}(t)\} + [C]\{\dot{Q}(t)\} \tag{5.2-31}$$

or in a simple form

$$[B_d]\{X\} = \{r'\}_{N\times 1} \tag{5.2-32}$$

where

$$B_d = \left[\{B_T\},[B],\{B_{EI}\}\right], \quad X = \begin{Bmatrix} T \\ P \\ EI_0 \end{Bmatrix},$$

Again the vector of variables X can be calculated directly by the simple least-squares method or using the DLS method.

5.2.4 Simulation and Results

5.2.4.1 *The Prestress Beam*

A 30 metres long simply supported Euler-Bernoulli beam with an axial prestress force of $0.3T_{cr} = 8.2247 \times 10^6$ N is studied. The first six natural frequencies of the beam are: 1.03, 4.75, 10.11, 19.56, 30.67 and 44.25 Hz. The damping ratios for these six modes are all equal to 0.02. The prestress force is constant along the beam. The external exciting force is $f(t) = 12000[1 + 0.1\sin(10\pi t) + 0.05\sin(40\pi t)]$ N and it is applied at 7 metres from the left support. The parameters of the beam are: $\rho A = 5.0 \times 10^3 kg/m$, $E = 5 \times 10^{10} N/m^2$, $L = 30m$, $b = 0.6m$, and $h_0 = 1.0\ m$. The flexural rigidity EI_0 of the beam is calculated as 2.5×10^9 Nm^2.

5.2.4.2 *Effect of Prestress on the Modal Frequency and Responses*

Table 5-3 shows the modal frequencies of the first five modes of the above beam when $T = 0.1T_{cr}$, $T = 0.3T_{cr}$ and $T = 0.5T_{cr}$ respectively, and the lower modal frequencies are seen more affected by the axial compression than the higher modes. The frequency of the beam decreases with an increase in the axial compression and vice versa. This is due to the "compression softening" effect (Tse, 1978) from the prestress force.

Figures 5-15 and 5-16 show the effect of the prestress force on the responses of the beam when $T = 0.1T_{cr}$ and $T = 0.3T_{cr}$ respectively when only three modes are included. It is seen that the effect of prestress is most significant with the displacement responses and the acceleration responses are least affected and such effect increases with larger prestress in the beam.

5.2.4.3 *Case 1- Prestress Force Identification from Measured Strains*

White noise is added to the calculated displacements and strains to simulate the polluted measurements as follows:

$$y = y_{calculated} + Ep \times N_{oise} \times \mathrm{var}(y_{calculated}) \qquad (5.2\text{-}33)$$

$$\varepsilon = \varepsilon_{calculated} + Ep \times N_{oise} \times \text{var}(\varepsilon_{calculated}) \qquad (5.2\text{-}34)$$

where y and ε are the vectors of polluted displacements and strains respectively; Ep is the noise level ; N_{oise} is a standard normal distribution vector with zero mean and unit standard deviation; var(•) is the variance of the time history; $y_{calculated}$ and $\varepsilon_{calculated}$ are the vectors of calculated displacements and strains. 5% and 10% noise levels are included in the study in this section.

The above beam with $T = 0.3T_{cr}$ axial force is studied. The first three modes are used in the calculation. Measured displacements at *1/4L*, *1/2L* and *3/4L* are used in the identification. The sampling frequency is 1000Hz, which is larger than 20 times the highest frequency of interest at 44.25 Hz. The beam is assumed at rest initially.

Figure 5-17 shows the identified results from measured strains with 5% and 10% noise with the corresponding optimal regularization parameter equals to 3.4×10^{-6} and 6.1×10^{-6} respectively. There is only a slight difference in the time histories of the identified prestress from both cases. This is because the measurements have been approximated with 20 terms of the orthogonal functions and the velocities and accelerations are subsequently obtained by directly differentiating the functions. This shows that the orthogonal function approach is effective in eliminating the noise in the measured data.

Large responses are found close to the start and end of the time histories while those in the middle halve vary closely around the true value. This is because the response is a discontinuous function of time at these two time instances. The second term in Equation (5.2-22) provides bounds to the solution. When the regularization parameter λ approaches zero, the estimated vector $\{\overline{F}\}$ approaches the solution obtained from the least squares method. In practice, the expected value of λ is not

known, and the error between the true and the estimated forces is minimized for a specific range of λ. The optimal λ is determined from the L-curve method (Hansen, 1992).

5.2.4.4 *Case 2- Identification using Impulsive Excitation*

An impulsive force is also used to identify the prestess force, which acts on the beam from t = 0.05s to 0.15s. The magnitude of the force is 9500 N simulating the impact excitation produced by a 125 kg weight free falling for one meter on the beam. The weight is assumed bounced off the beam after impact, and the effect of the falling mass after the impact is ignored. The force is applied at 7 metres from the left support and it can be expressed in the following form

$$P(t) = \begin{cases} 190000(t - 0.05)\ N & (0.05 \le t \le 0.1) \\ 190000(0.15 - t)\ N & (0.1 \le t \le 0.15) \end{cases} \quad \text{(5.2-35)}$$

The sampling frequency is 1000 Hz, and the first three modes and three displacement measurements evenly distributed along the beam are used in the identification. Five percent noise is included in the identification. Figure 5-18 shows that the identified prestress force obtained from using an optimal regularization parameter of 4.1×10^{-6} and it is found fluctuating closely around the true value except close to the two ends.

5.2.4.5 *Case 3- Identification of Both Prestress Force and the Flexural Rigidity of the Beam*

The same system as for the last study is used here, and the flexural rigidity EI_0 of the beam is $2.5\times10^9\ Nm^2$. The sampling frequency is 1000 Hz, and the first three modes and three evenly distributed displacement measurements are used in the

identification. Also 5% noise is included in the identification. All other parameters remain unchanged.

Figure 5-19 shows that both the identified prestress force and the flexural stiffness are fluctuating around the true values except close to the two ends. The corresponding optimal regularization parameter is 2.7×10^{-6}. This shows further the effectiveness of the proposed method with multiple parameters identification.

5.2.4.6 *Case 4- Identification of Both Prestress Force and One Moving Force*

The same system as for the last study is used here. The moving force is taken as $P(t) = 40000[1 + 0.5\sin(2\pi t) + 0.3\sin(10\pi t)]$ *N*, which moves along the axial direction of the beam at a velocity of 30 *m/s* from the left support to the right support.

The effect of the number of modes used on the results of prestress force identification is studied. The first three to six modes and measured strains are used in the calculation. The number of measurement location is equal to the number of modes, and the measurement locations are evenly distributed on the beam. The damping ratio is equal to 0.02 for all modes. The sampling frequency is 1000Hz, which is larger than twenty times the highest frequency of interest at 44.25 Hz.

Table 5-4shows the errors in the identified single moving force and the prestress force from using different number of vibration modes. The following conclusions can be made:

- The identification errors decrease with the increase in the number of the vibration modes used in the identification.
- The errors in the moving force identification is much less than the error in the prestress force identification, this may be due to the reason that the response is not sensitive to the prestress force.

- The identification errors are not sensitive to the noise level in the response measurements used in the identification.

Figures 5-20 shows the identified results from measured strains with 5% and 10% noise. There is only a slight difference in the time histories of the identified moving force from the two noise levels. This is because the measurements have been approximated with 20 terms of the orthogonal functions and the velocities and accelerations are subsequently obtained by directly differentiating the functions. The effect of measurement noise has been substantially removed. The identified prestress force also gives close to true value in the middle portion of the time history.

The large fluctuations in the response at the start and end of the time histories are typically ill-solutions in the problem due to the discontinuity of the solution in time at these two moments. The optimal value of parameter λ is 4.85×10^{-6}.

5.2.4.7 *Case 5- Identification of a Single Moving Force, the Pretress Force and the Flexural Rigidity of the Beam*

The same system as for the previous study is used here, and the flexural rigidity EI_0 of the beam is calculated as $2.5\times10^{9}\ \ Nm^2$. The sampling frequency is 500 Hz, and the first four modes and four displacement measurements are used in the identification. The measured points are evenly distributed along the beam. The damping ratio is equal to 0.02 for all modes. 5% random noise is included in the identification. All other parameters remain unchanged.

Figure 5-21 shows that both the identified prestress force and the flexural stiffness are fluctuating around the true values while the identified moving force varies closely to the true force. This demonstrates further the effectiveness of the proposed method for multiple parameters identification.

5.2.4.8 *Case 6- Identification of Two Moving Forces and the Prestress Force*

Again the single span simply supported prestressed beam is considered. The parameters of the beam are the same as those for Case 1 study. The two moving forces are

$$P_1(t) = 20000[1 + 0.5\sin(2\pi t) - 0.3\sin(10\pi t)] \quad N,$$

$$P_2(t) = 20000[1 + 0.5\sin(2\pi t) + 0.2\sin(10\pi t)] \quad N.$$

and they are moving as a group at 4 metres spacing at 30 m/s from left to right. Again, the effect of the number of measured modes used in the identification is studied. The first three to eight vibration modes and measured strains are used in the calculation. The number of measured strain is taken equal to the number of vibration modes, and the measurement locations are evenly distributed on the beam. The damping ratio is equal to 0.02 for all modes. The sampling frequency is 500 Hz. Table 5-5 gives the errors in the identified moving forces and the prestress force from using different number of vibration modes. Figure 5-22 shows the identified results from measured strains with 5% and 10% random noise. The following observations are made:

- The errors in the identified moving forces and the prestress force are larger than those for single force identification.
- Errors in the identified prestress force are larger than the errors in the identified moving forces. This is due to the same reason as the single moving force identification.
- The errors decrease with the increase in the number of the vibration modes used in the identification. This observation is the same for Case 5 study.
- When the noise level is relatively small and below 5%, and the number of vibration modes is more than four, the errors do not vary too much with different combinations of mode numbers and noise level. This indicates little improvements in the identified results despite an increase in the

number of vibration modes and sensors. The errors in the results would mainly come from the large fluctuations at the beginning and end of the time histories. Similar observation can be found for Case 5 study.

5.2.4.9 *Case 7 - Identification of Two Moving Forces, the Prestress Force and the Flexural Rigidity of the Beam*

The same system as for Case 1 is studied here and the two moving forces to be identified are the same as for Case 6 study. Again, the sampling frequency is 500 Hz, and the first four modes and four evenly distributed strain measurements are used in the identification. Also 5% noise is included in the identification. Other parameters remain unchanged.

Figure 5-23 shows that the identified prestress force, two moving forces and the flexural stiffness are fluctuating around the true values. The moving forces are more accurately identified than the system parameters with the latter ones being more accurately identified only over the middle half of the time histories.

5.2.4.10 *Sensitivity of the Proposed Method to Prestress Force Magnitude*

In most cases of construction with prestress, the prestress force in a beam component is relatively small. A study is therefore made to study the errors involved in the identification of different magnitude of prestress force with different noise levels. The same beam and excitation for the last study is used. Five prestress levels and three noise levels are studied and the summation of error of the identified force according to Equation (7-36) is shown in Table 5-6. The time histories of the identified prestress force which are $0.01T_{cr}$, $0.1T_{cr}$ and $0.3T_{cr}$ under 10% noise level are shown in Figure 5-24 obtained from using an optimal regularization parameter of 6.1×10^{-6}.

$$error = \frac{\left\| T_{pid} - T_{ptrue} \right\|}{\left\| T_{ptrue} \right\|} \times 100\% \tag{5.2-36}$$

The noise level is not important to the identification except for the case of a small prestress force of 0.01 T_{cr}. However detail inspection of Figure 5-24 shows that all the curves are fluctuating around their corresponding true values. The sum of squares error or the variance of the identified forces is of the same order for all the cases studied indicating same order of accuracy in all the identifications. This also shows that the proposed method is insensitive to the level of prestress force. The large percentage error for a small prestress force arises from a small denominator as calculated from Equation (5.2-36). Furthermore, over ninety percent of the force time history in the middle gives close to true values of the force with smaller fluctuations indicating the good accuracy of the proposed method.

5.2.5 Experimental Verification

The proposed method is further verified with a simply supported prestress concrete beam in the laboratory. The same experimental setup as Figure 4.3-20 is used, and the test procedure is the same as the experiment verification in Section 4.3.

5.2.5.1 *Identification of Prestress Force*

Impulsive force is applied with the impact hammer at node 7 of the beam. The sampling rate is 2000 Hz. Time histories of both the excitation force and the strains are recorded, and data obtained from the third and fourth strain gauges are used in the prestress force identification.

The flexural rigidity of the beam before prestressing is calculated as 3.13×10^3 $kN\text{-}m^2$. The beam is assumed to be simply supported. Rayleigh damping model is adopted

in calculating the structural response, and the measured modal damping ratios for the first three modes are respectively 0.028, 0.15 and 0.11. The analytical modal frequencies are shown in Table 7-5.

After the beam is prestressed, the flexural rigidity of the beam section is calculated to be $3.20\times10^3\ kN\text{-}m^2$. The prestress force is identified using data from 0 second to 1.0 second after the hammer impact. Measured strains from the 3rd and the 4th strain gauges were used for prestress force identification. Figure 5-25 shows the measured time history from the two strain gauges. The orthogonal polynomial function is used to remove the measurement noise. The measured modal damping ratios for the first three modes are 0.022, 0.14 and 0.08 respectively. The load cell at the end of the strand shows that the prestress force is 66.7 KN. The identified magnitude of the prestress force is 45.3 KN, the relative error is 32.1%. The optimal regularization parameter is1.6×10^{-5}. The large percentage error may come from the assumption that the beam is rigidly supported.

5.2.6 Concluding Remarks

A method is proposed to identify the prestress force in a prestressed concrete beam in this section. All the system parameters are assumed to be time-inrariant. The prestress force in a beam has been identified successfully with or without including the flexural rigidity of the beam in the inverse analysis. And it is further extend to identify both moving force and prestress force simultaneously. Several numerical simulation studies show that it is possible to identify these two parameters from measured dynamic responses. The noise effect is improved using the orthogonal polynomial function. Both the sinusoidal and impulsive excitation could give good results from the

lower three measured modes and strain or displacement obtained from only three measuring points. Both displacement response and strain response can be used for prestress force identification. Work in this section indicates that indirect measurement of the prestress force in a beam is feasible.

Table 5-1- Comparison with existing method

	Single crack		Depth of crack (m)		
	Location (m)	Depth (m)	crack 1	crack 2	crack 3
True value	4.0	0.25	0.20	0.25	0.20
Sinha et al. (2002).	4.16/4%	0.31/24%	0.235/17.5%	0.21/-16%	0.237/17.5%
Proposed method	4.03/0.75%	0.23/-8%	0.195/-2.5%	0.254/1.6%	0.182/-9%

Note: •/• denotes the identified value and percentage of error.

Table 5-2– Experimental Modal frequencies (Hz) of the cracked beam

Crack depth and location	Mode Number				
	1	2	3	4	5
No crack	22.868	62.763	123.049	203.236	303.452
h_c = *3mm at 1720mm*	22.797	62.622	122.559	202.271	302.490
h_c = *6mm at 1720mm*	22.766	62.378	121.704	201.050	301.514
h_c = *9mm at 1720mm*	22.766	61.890	119.995	198.486	299.500

Table 5-3– Modal frequencies corresponding to different prestress force

Prestress force	Frequency(Hz)				
	1st	2nd	3rd	4th	5th
$T = 0$	1.23	4.94	11.11	19.75	30.86
$T = 0.1T_{cr}$	1.17	4.88	11.05	19.69	30.80
$T = 0.3T_{cr}$	1.03	4.75	10.92	19.56	30.67
$T = 0.5T_{cr}$	0.87	4.62	10.80	19.44	30.55

Table 5-4- Errors in the identified single moving force and prestress force (%)

Number of vibration modes	Noise level		
	1%	5%	10%
3	5.8/27.2	6.0/28.9	7.6/36.0
4	5.1/26.3	5.0/28.2	6.3/34.8
5	5.1/26.1	5.1/28.0	5.7/34.2
6	4.8/25.8	4.9/27.6	5.4/32.7

Note: •/• denotes errors for the moving force and the prestress force respectively.

Table 5-5- Errors in the two identified moving forces and prestress force (%)

Number of vibration modes	Noise level		
	1%	5%	10%
3	15.3/18.1/29.7	24.8/23.9/56.0	29.2/28.1/70.8
4	10.0/12.4/25.0	12.5/12.9/50.4	17.1/15.8/68.3
5	7.8/8.4/22.9	9.2/8.7/45.8	12.1/10.4/66.3
6	7.2/6.7/19.3	7.7/7.5/43.6	9.8/7.8/65.0
7	6.6/6.2/21.8	6.8/6.8/43.5	8.1/7.1/64.8
8	5.7/5.4/23.5	6.1/5.7/42.4	7.0/6.2/64.0

Note: •/•/• denotes errors for the first and second moving forces and the prestress force respectively.

Table 5-6- Error percentage (%) and sum of squares error in the Identified Prestress Force for different noise level

Prestress Force	*1% noise*	*5% noise*	*10% noise*
$0.01T_{cr}$	$173/(7.77\text{x}10^{7})$	$218.3/(1.1\text{x}10^{8})$	$237.88/(1.37\text{x}10^{8})$
$0.05T_{cr}$	$75.53/(1.79\text{x}10^{8})$	$81.46/(2.16\text{x}10^{8})$	$86.46/(2.53\text{x}10^{8})$
$0.1T_{cr}$	$46.37/(2.19\text{x}10^{8})$	$48.33/(2.48\text{x}10^{8})$	$50.29/(2.8\text{x}10^{8})$
$0.3T_{cr}$	$31.02/(3.03\text{x}10^{8})$	$31.86/(3.30\text{x}10^{8})$	$32.8/(3.66\text{x}10^{8})$
$0.5T_{cr}$	$21.6/(3.43\text{x}10^{8})$	$21.62/(3.48\text{x}10^{8})$	$22.91/(3.56\text{x}10^{8})$

Note: (•) denotes the sum of squares error.

Table 5-7– Experimental modal frequencies (Hz) of the non-prestressed and prestressed beam

	unprestressed		*prestressed*	
	Calculated	*Experimental*	*Calculated*	*Experimental*
1st Mode	23.64	23.21	23.87	23.31
2nd Mode	89.82	86.17	90.64	87.98
3rd Mode	195.33	183.29	197.82	185.93

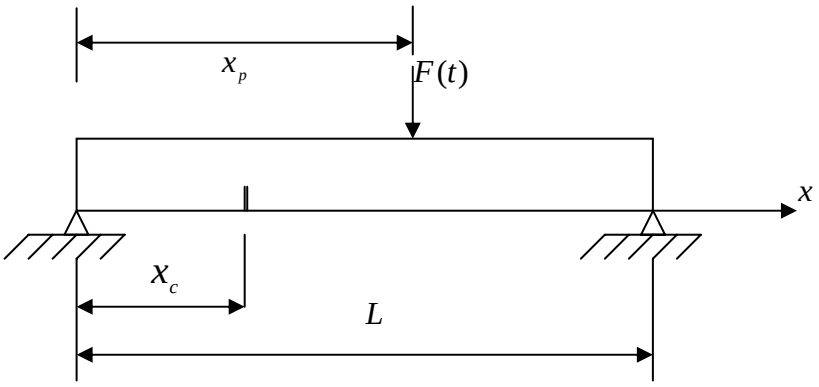

Figure 5-1 - The cracked beam model

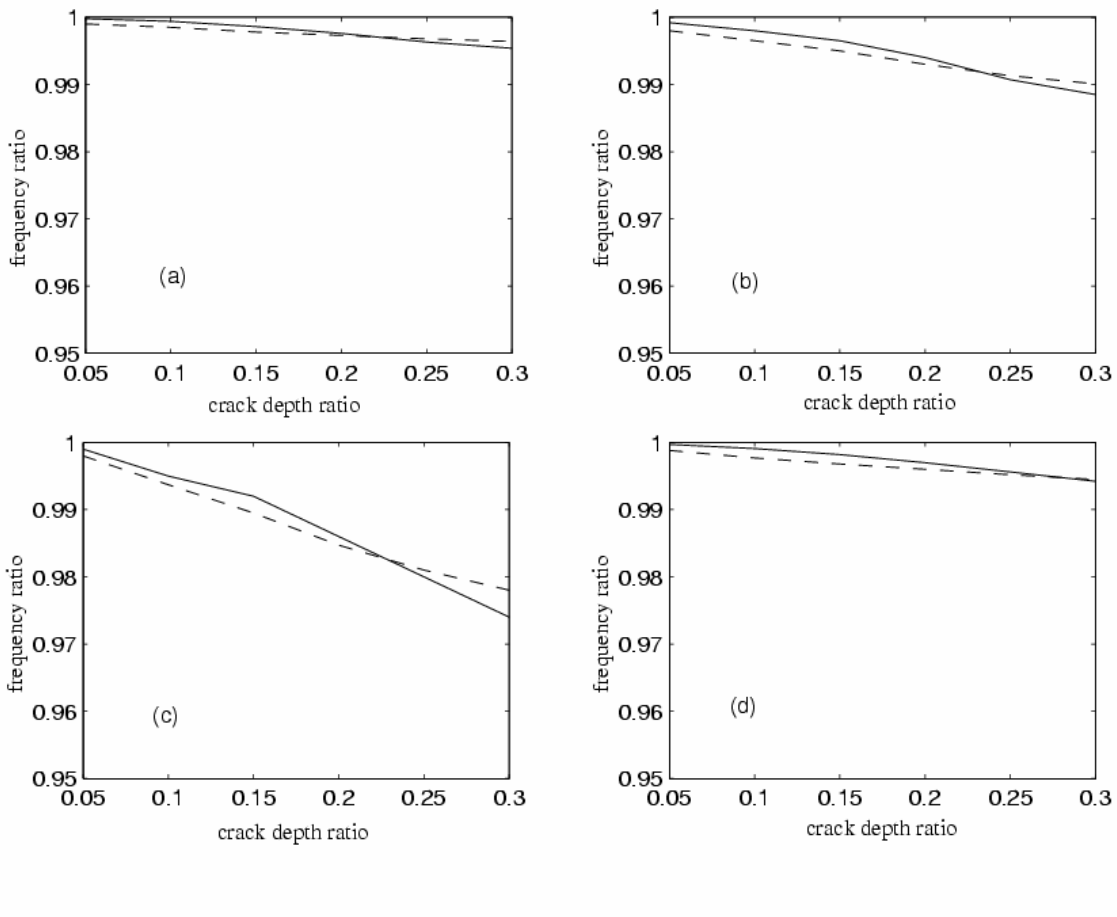

Figure 5-2- The variation of the fundamental frequency corresponding to different crack location

(___Fernandaz-Saez et al (1999), ---Proposed, (a) x_c =4m, (b) x_c =7m, (c) x_c =15m, (d) x_c =25 m)

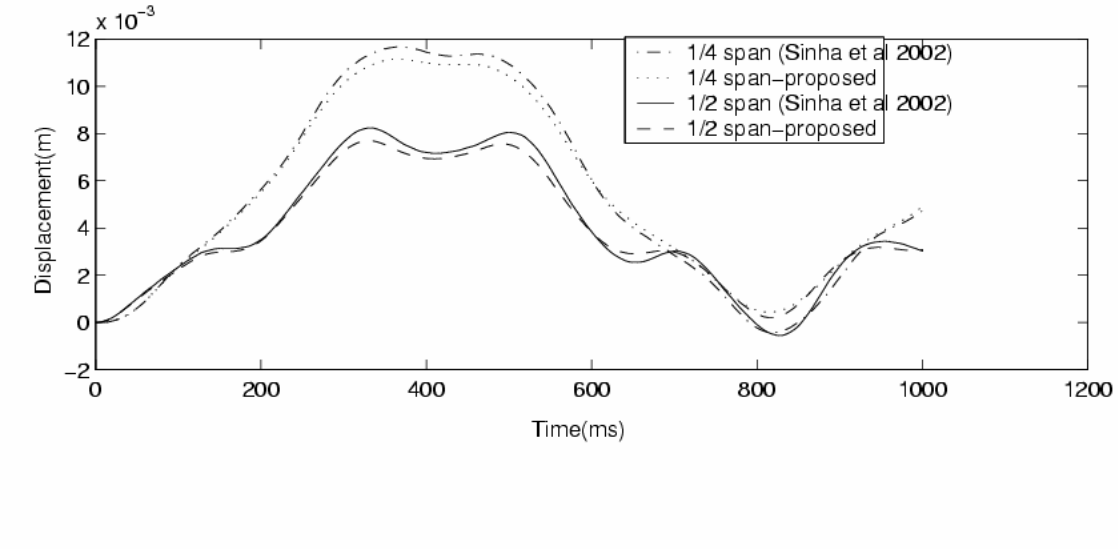

Figure 5-3– The displacement responses of cracked beam for different crack model

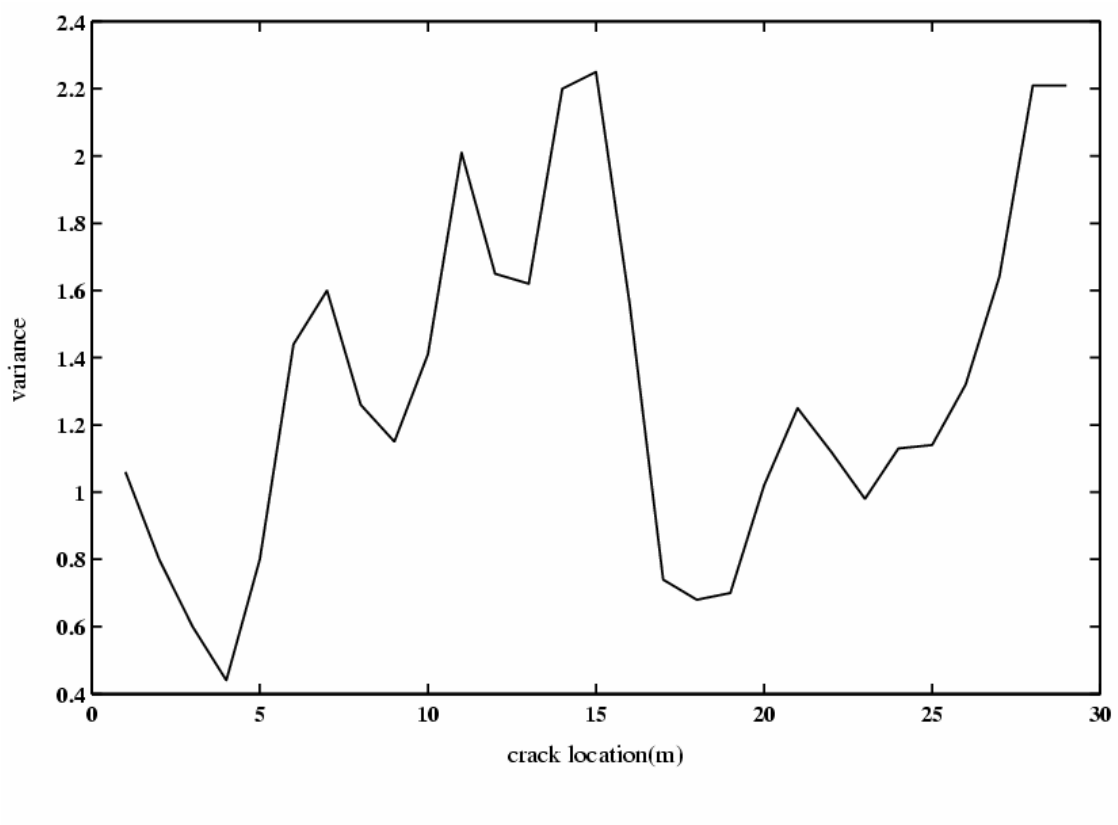

Figure 5-4– The variance of the identified crack location (5% noise)

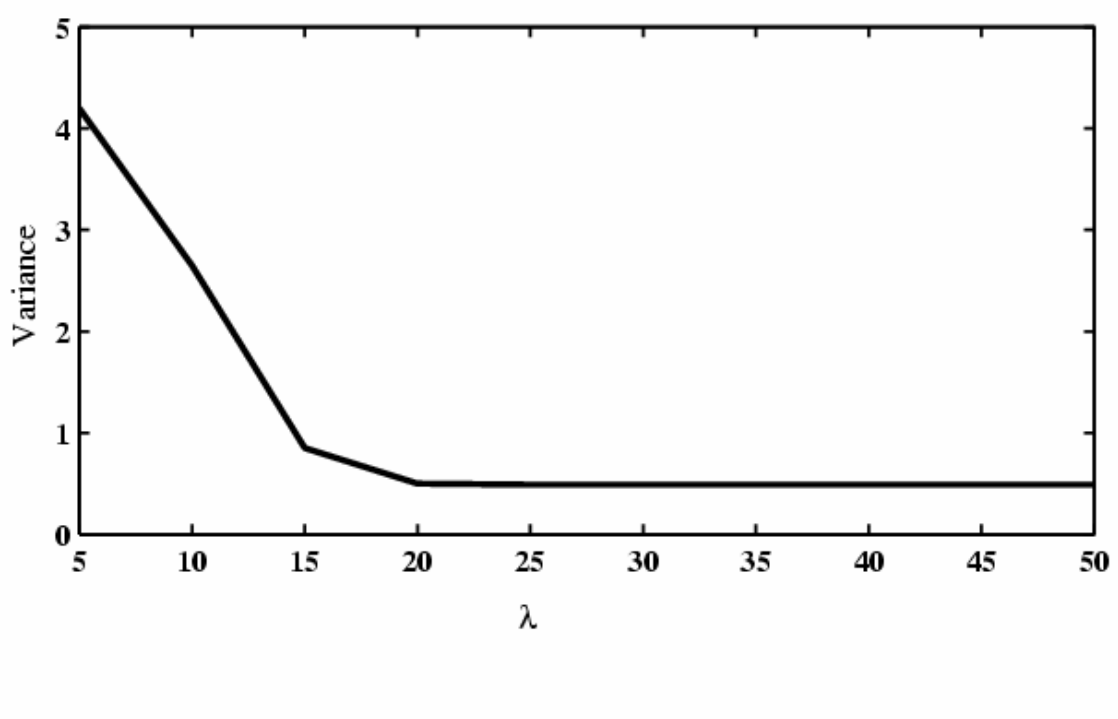

Figure 5-5– The optimal regularization parameter (corresponding to crack location at 4 m and 5% noise)

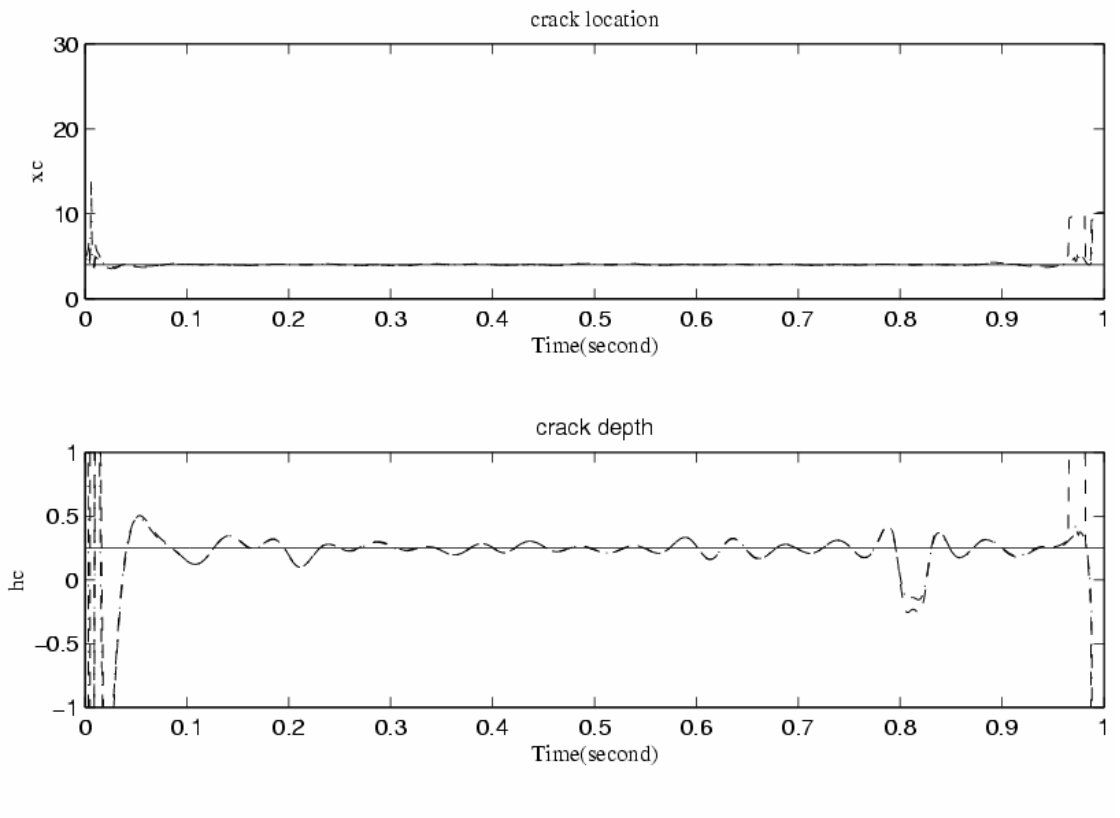

Figure 5-6– Crack identification from different noise level

(___ True; -.-.-. no noise; ---10% noise)

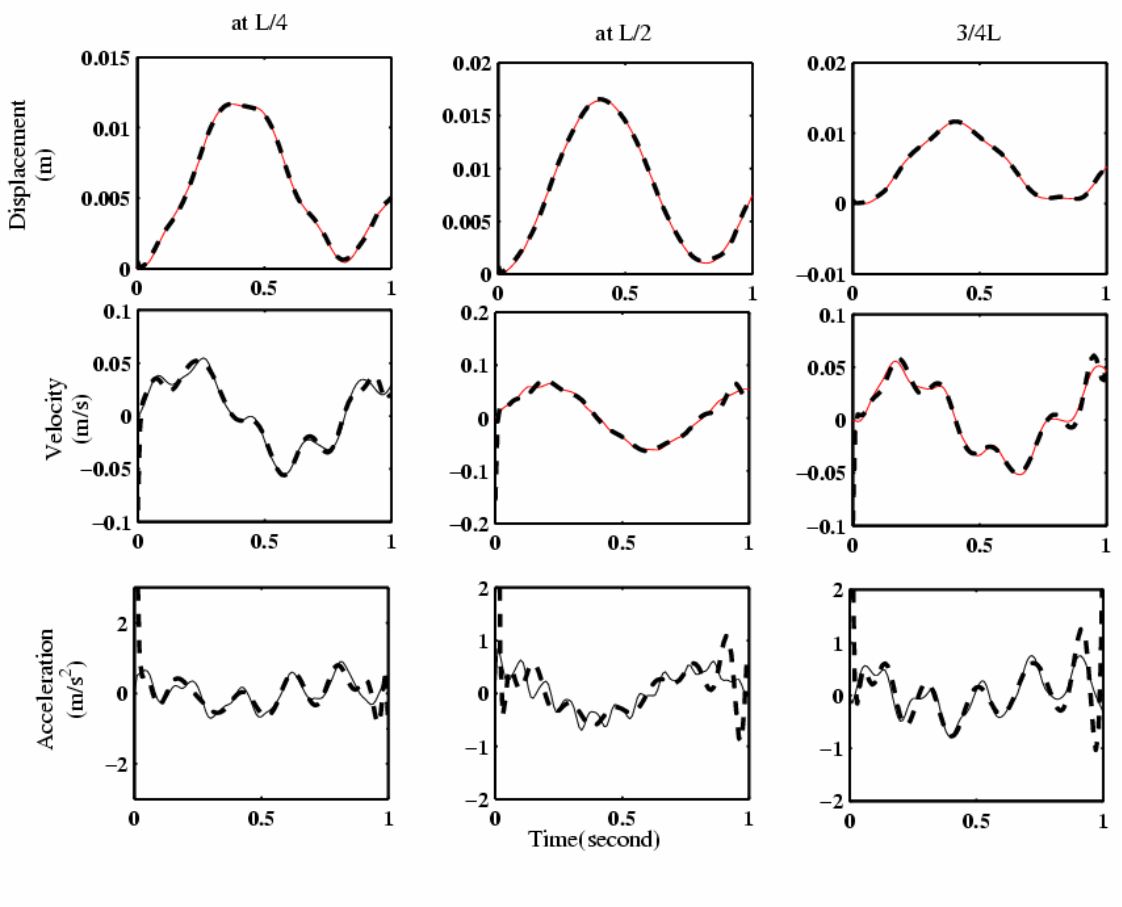

Figure 5-7– Response at the measuring points (___ from simulation; ---- from orthogonal function)

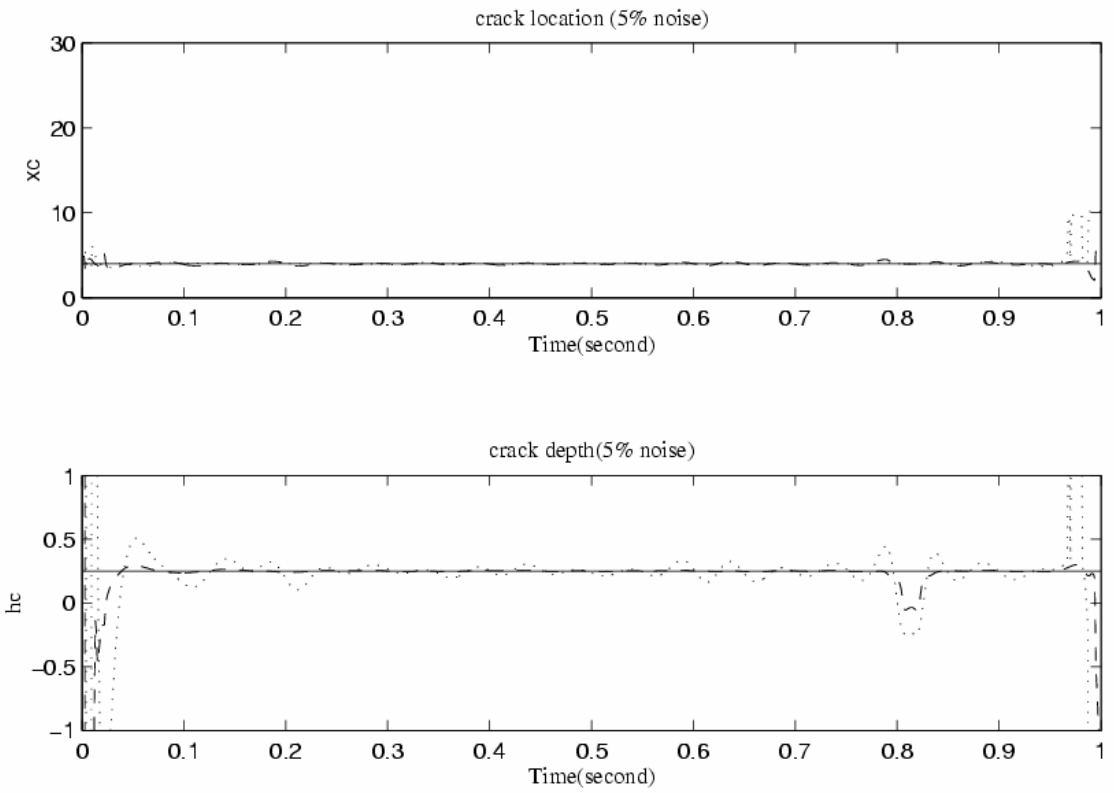

Figure 5-8– Crack identification from 3 and 6 modes (___ True; …. 3 modes; ---- 6 modes)

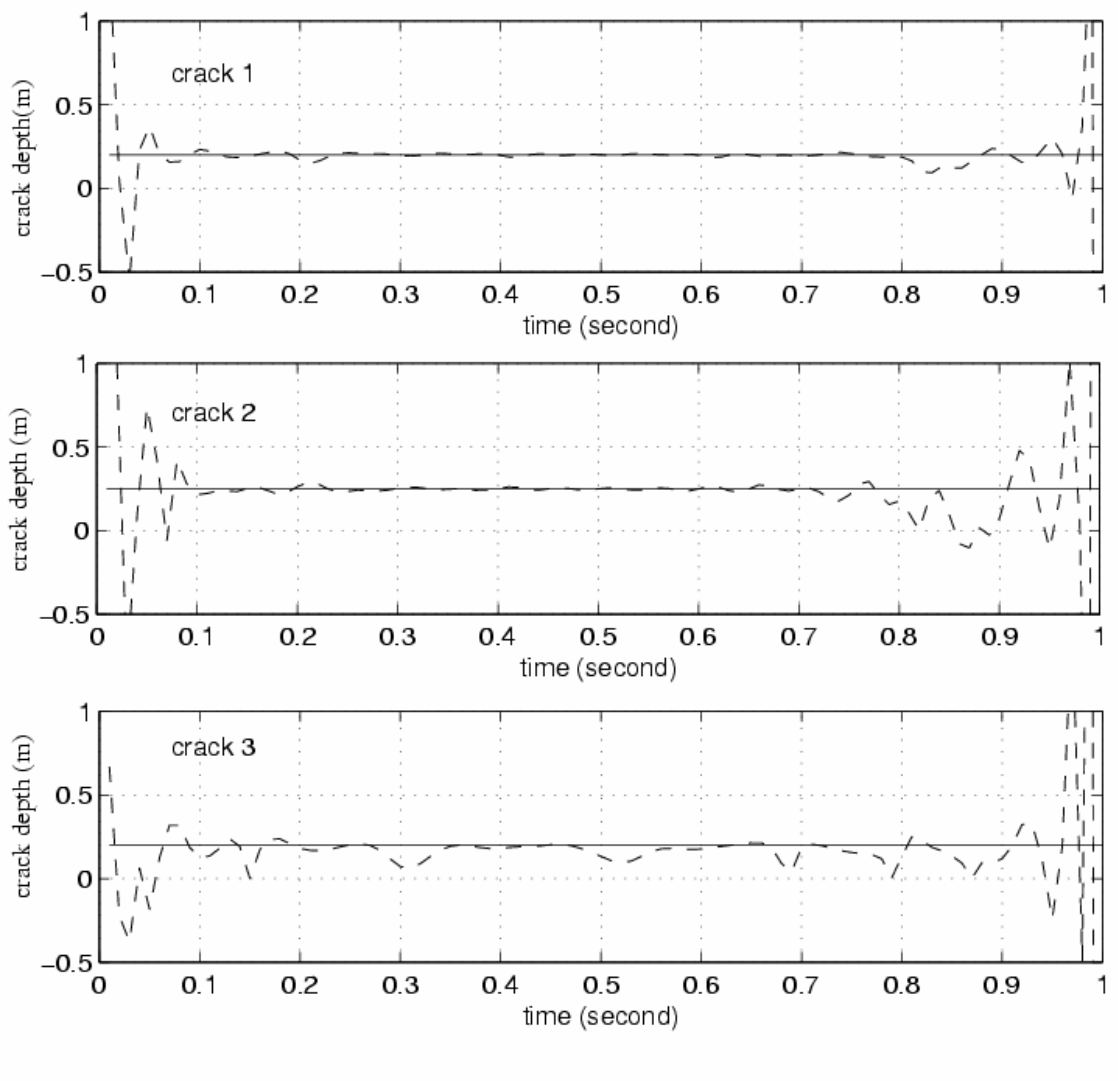

Figure 5-9– Identified crack depth for the three cracks (5% noise)

(___ True; ---- Identified)

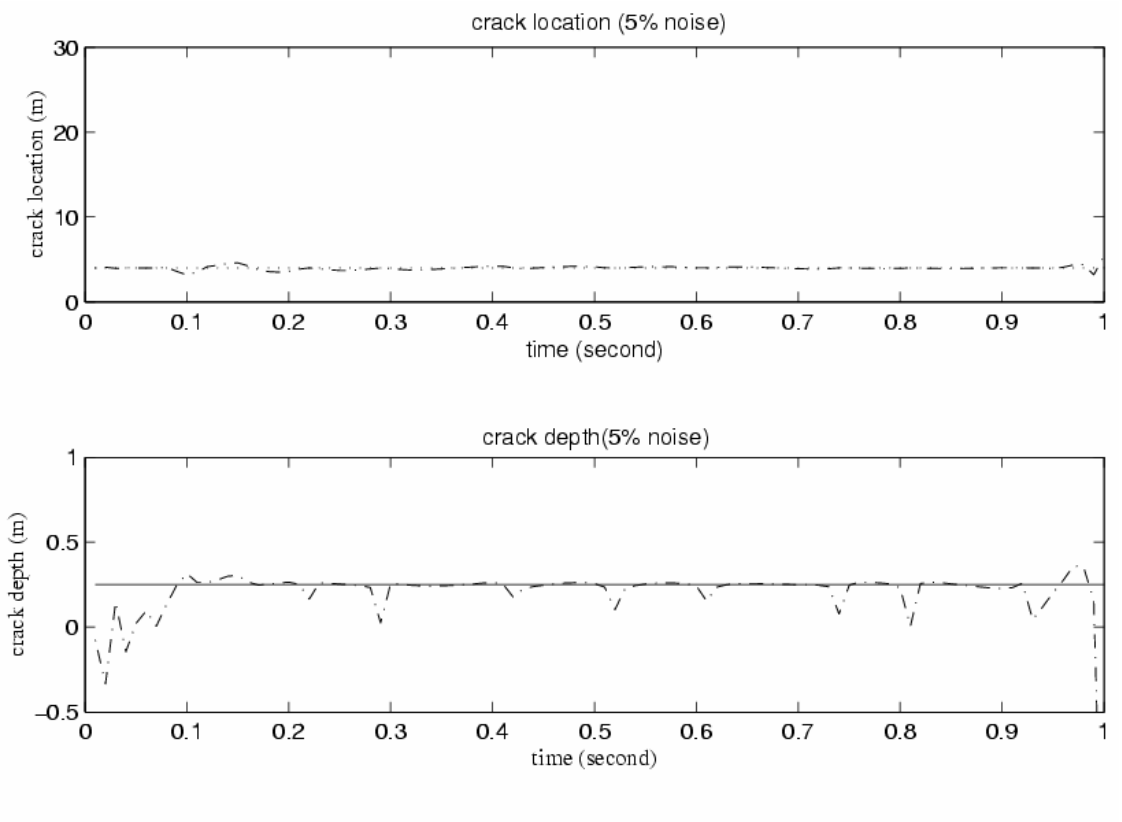

Figure 5-10 – Crack identification from impulsive force (___ True; -.-.-. Identified)

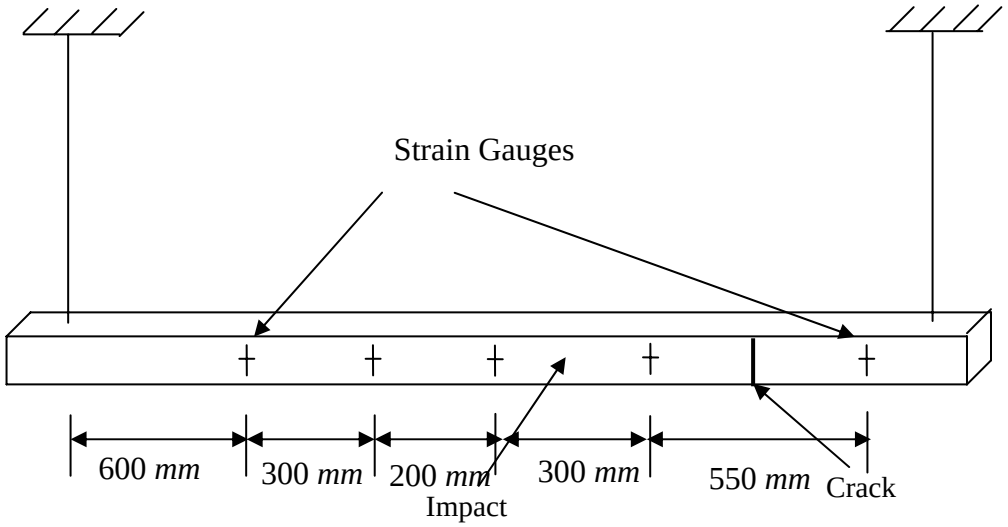

Figure 5-11- The experiment setup

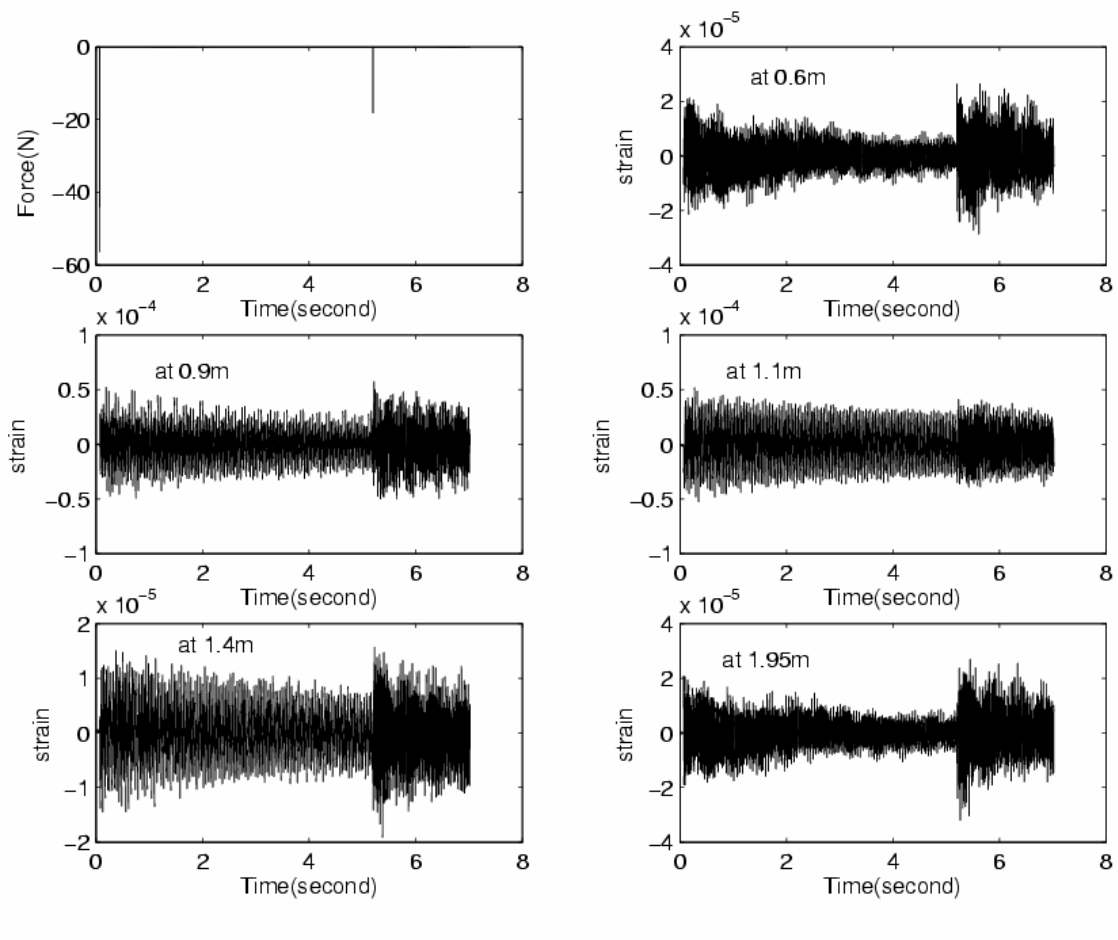

Figure 5-12– The impulsive force and five measured strains

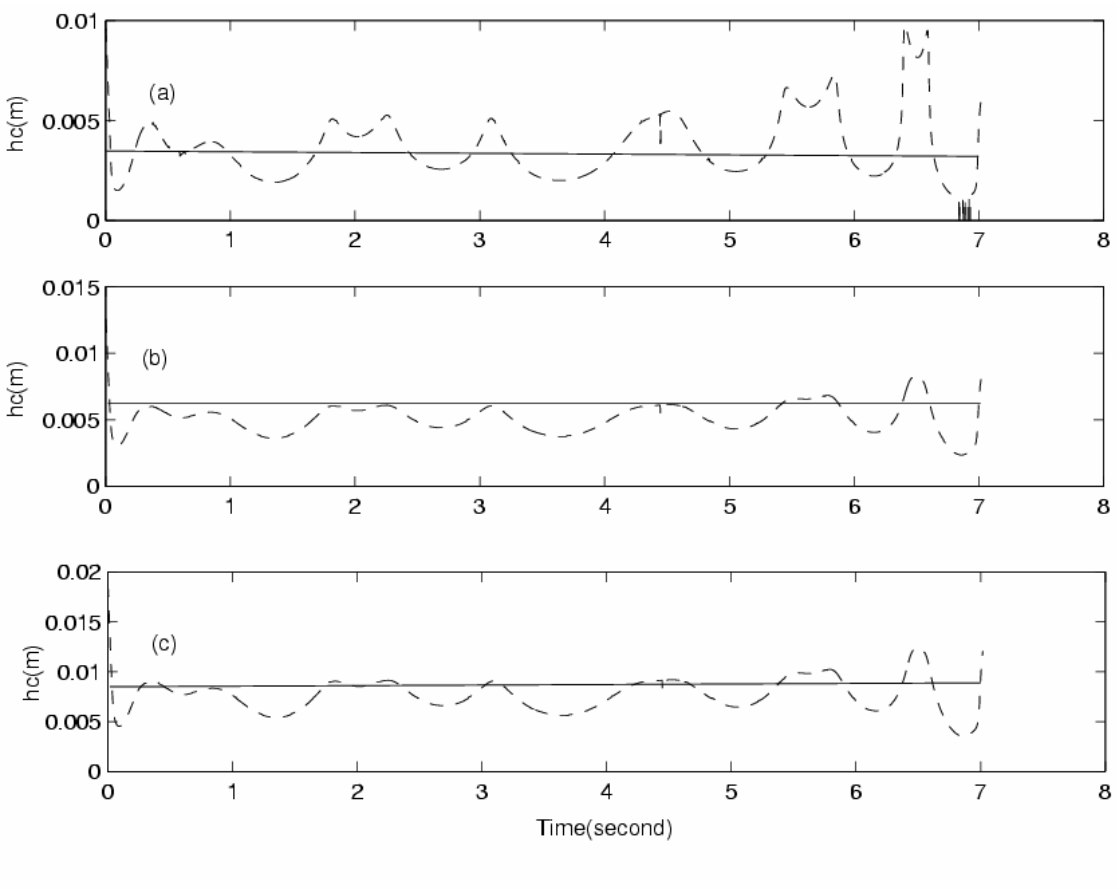

Figure 5-13– Crack identification from measured strains
(a) hc=3mm, (b) hc=6mm, (c) hc=9mm,; (___ True, ---- Identified)

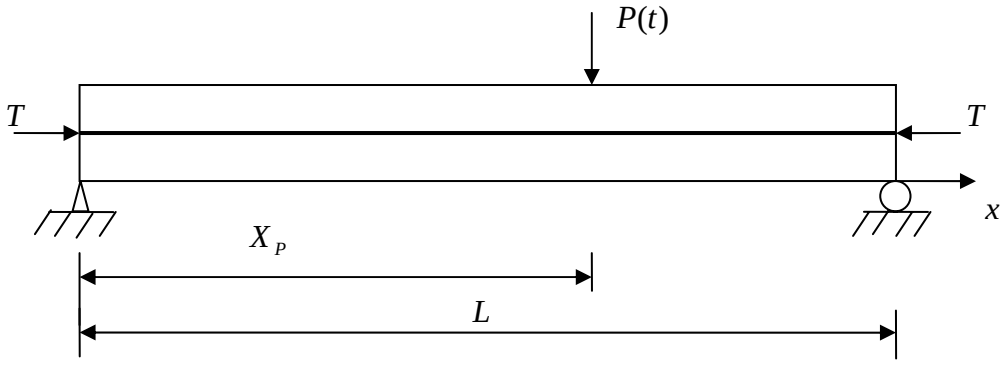

Figure 5-14- The prestressed beam model

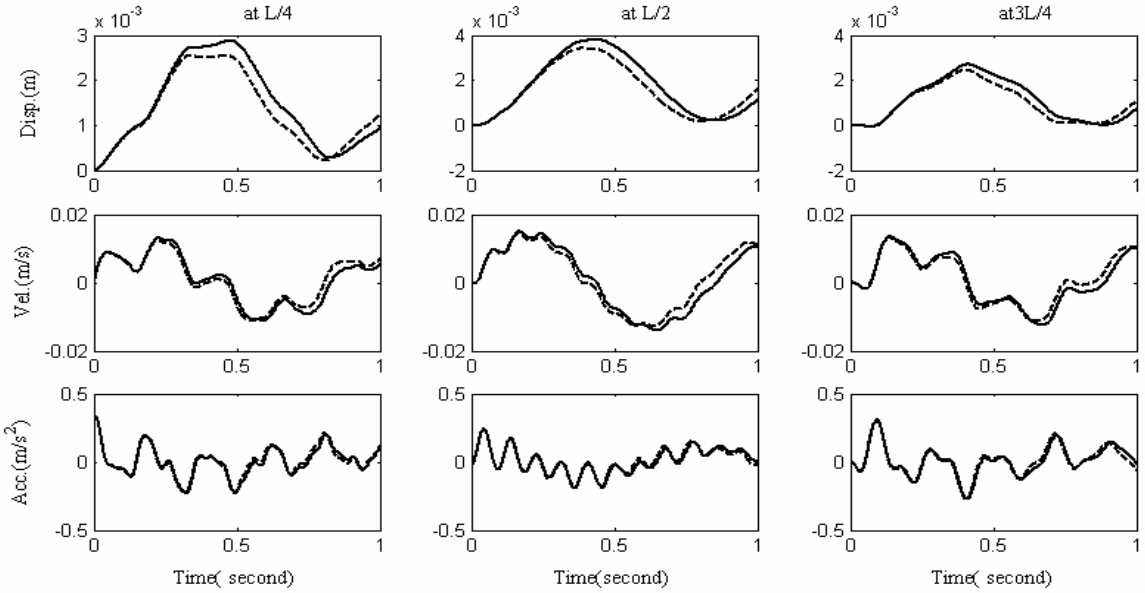

Figure 5-15 – Comparison of response with and without prestress force (T =0.1T_{cr} ; ___ With Prestress force; ---- Without prestress force)

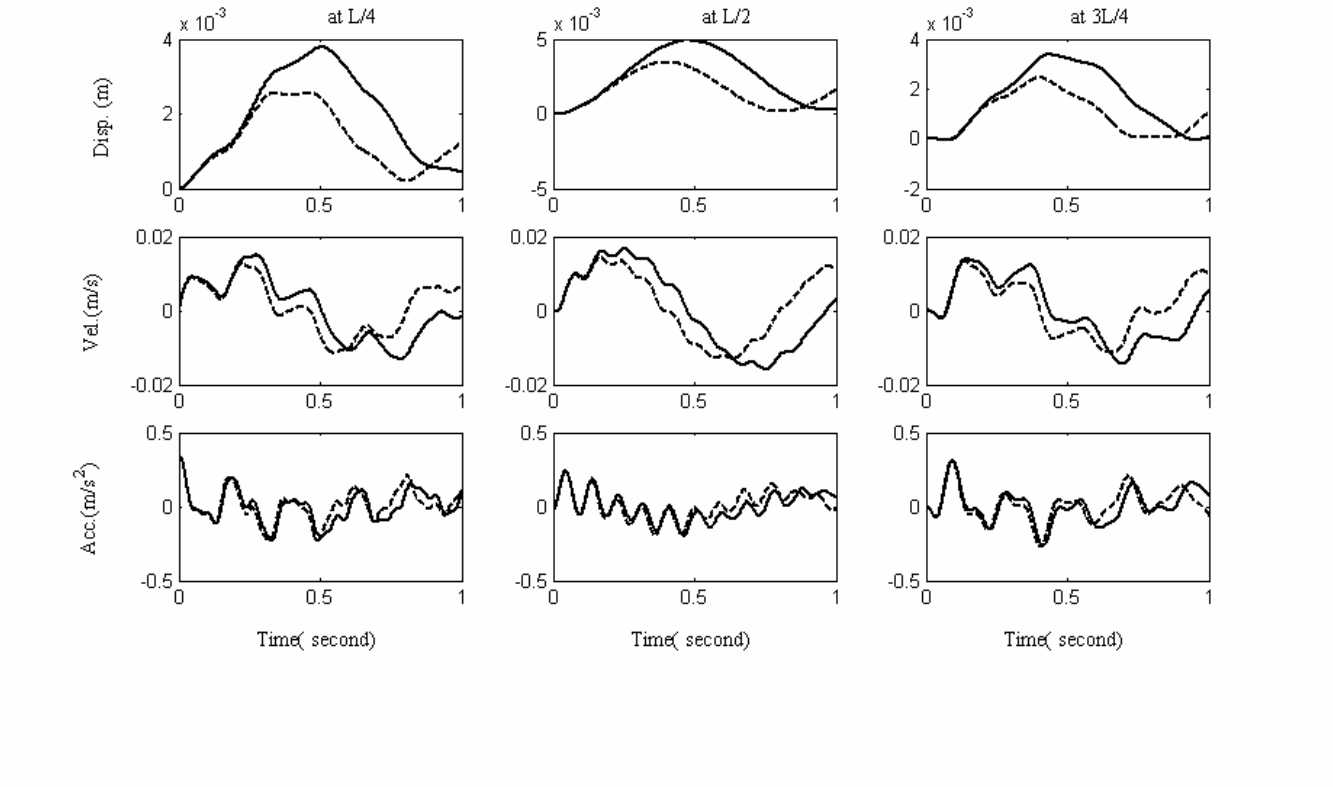

Figure 5-16 – Comparison of response with and without prestress force
(T =0.3T_{cr} ; ___ With Prestress force; ---- Without prestress force)

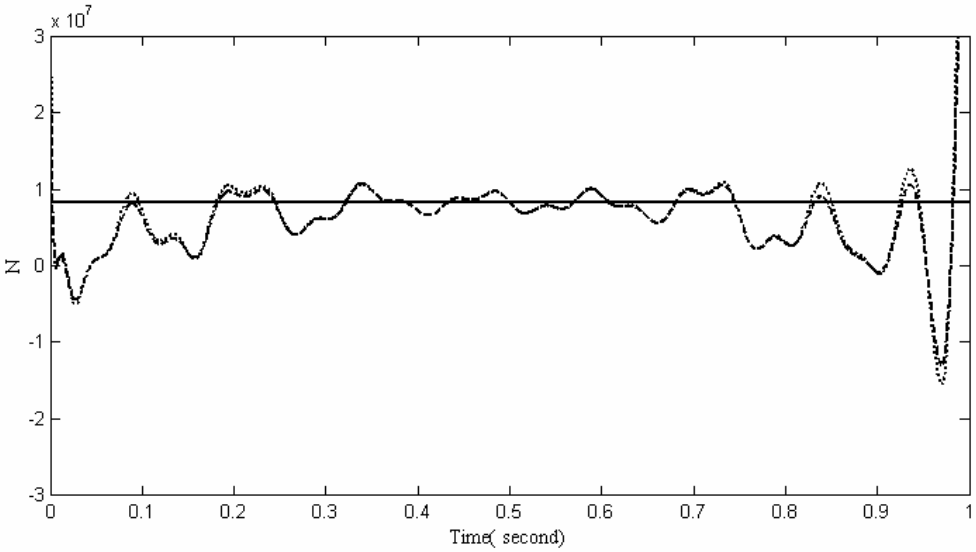

Figure 5-17 – Prestress force identified from the first three mode (__ True; --- 5% noise; … 10% noise)

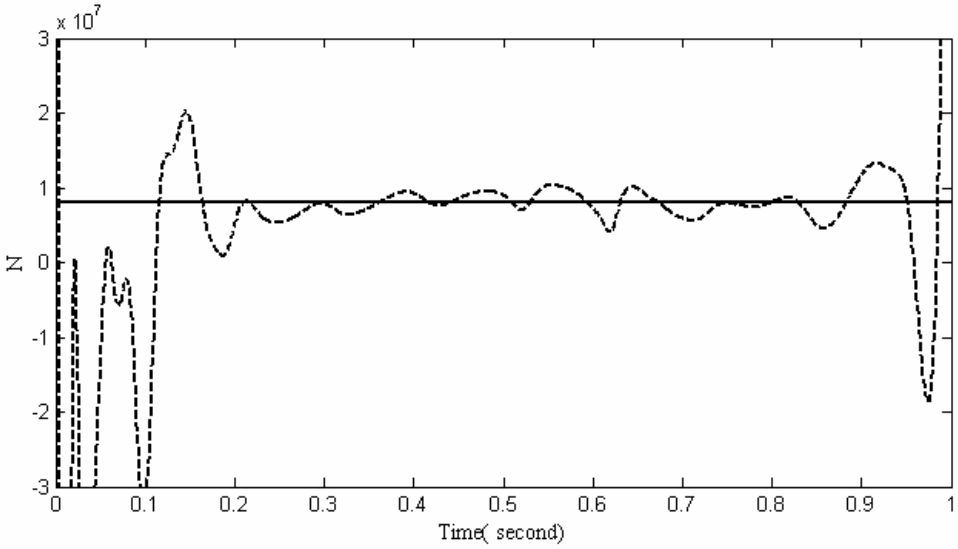

Figure 5-18 – Prestress force identified from impulsive force (__ True; --- Identified)

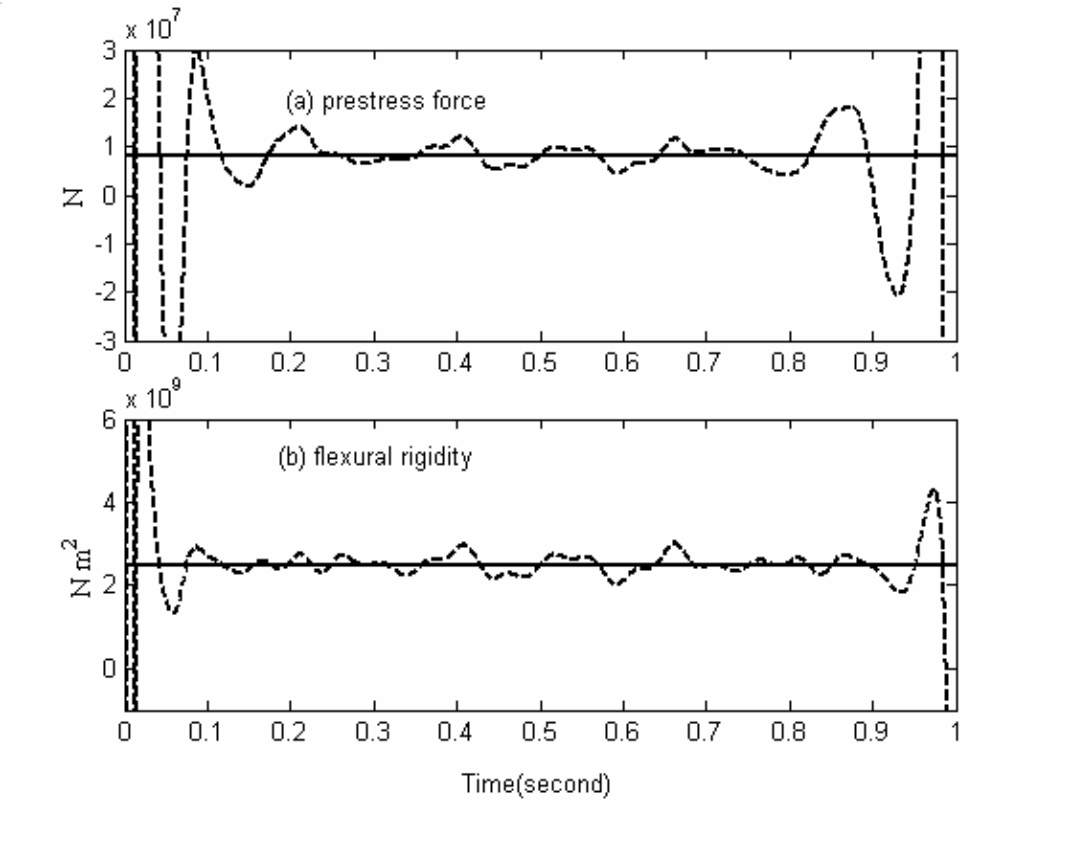

Figure 5-19 – Identification of prestress force and flexural rigidity (__ True; --- Identified)

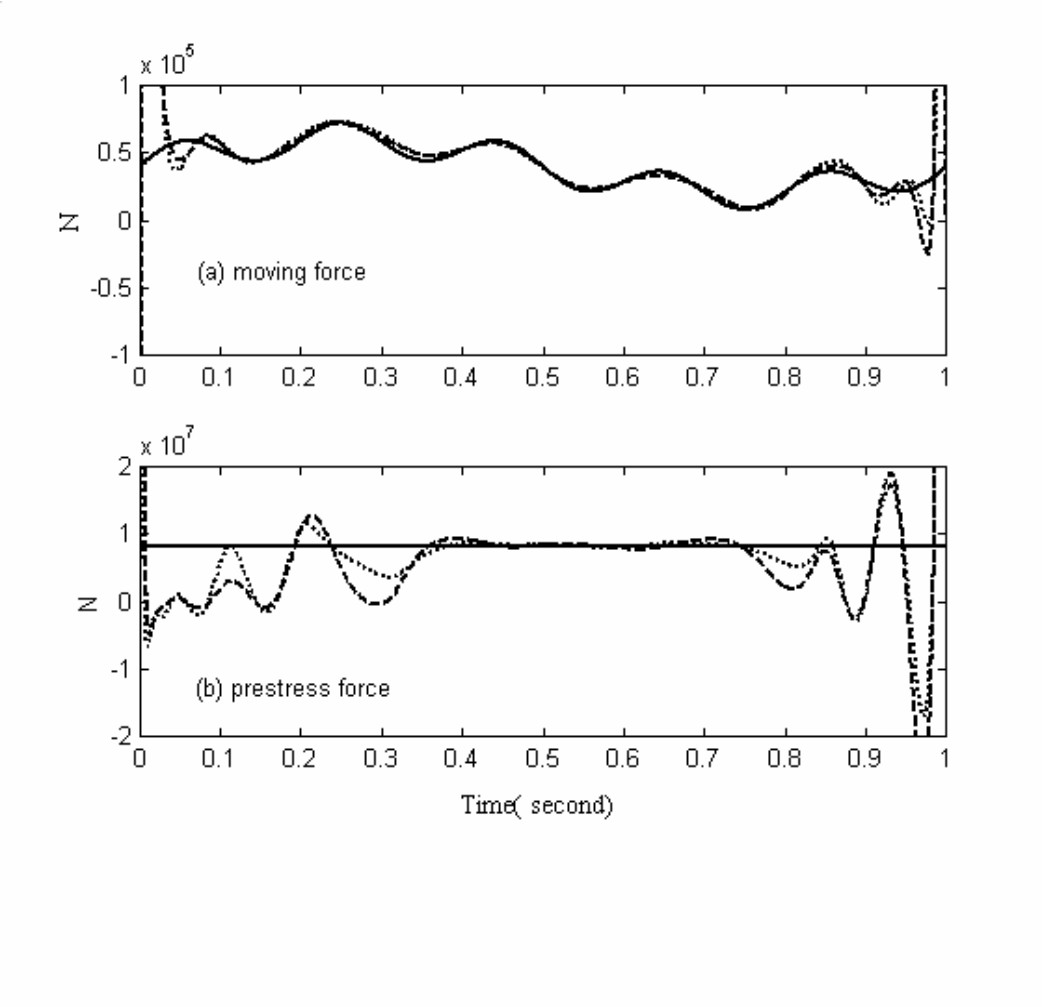

Figure 5-20 – Identification of single moving force and prestress force with different noise levels (__ True; … 5% noise; 10% noise)

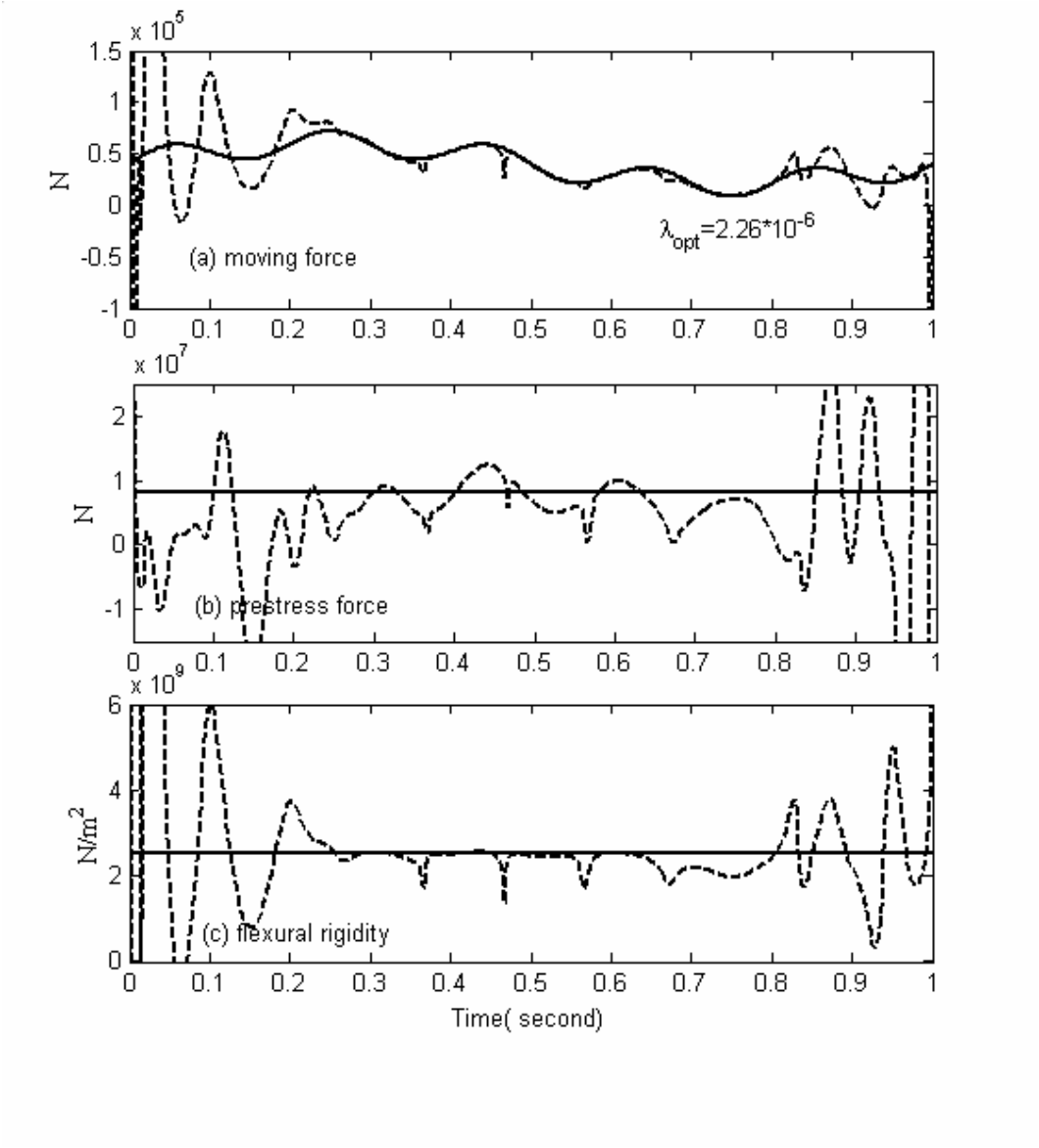

Figure 5-21 – Identification of moving force, prestress force and flexural rigidity of beam (__ True; --- Identified)

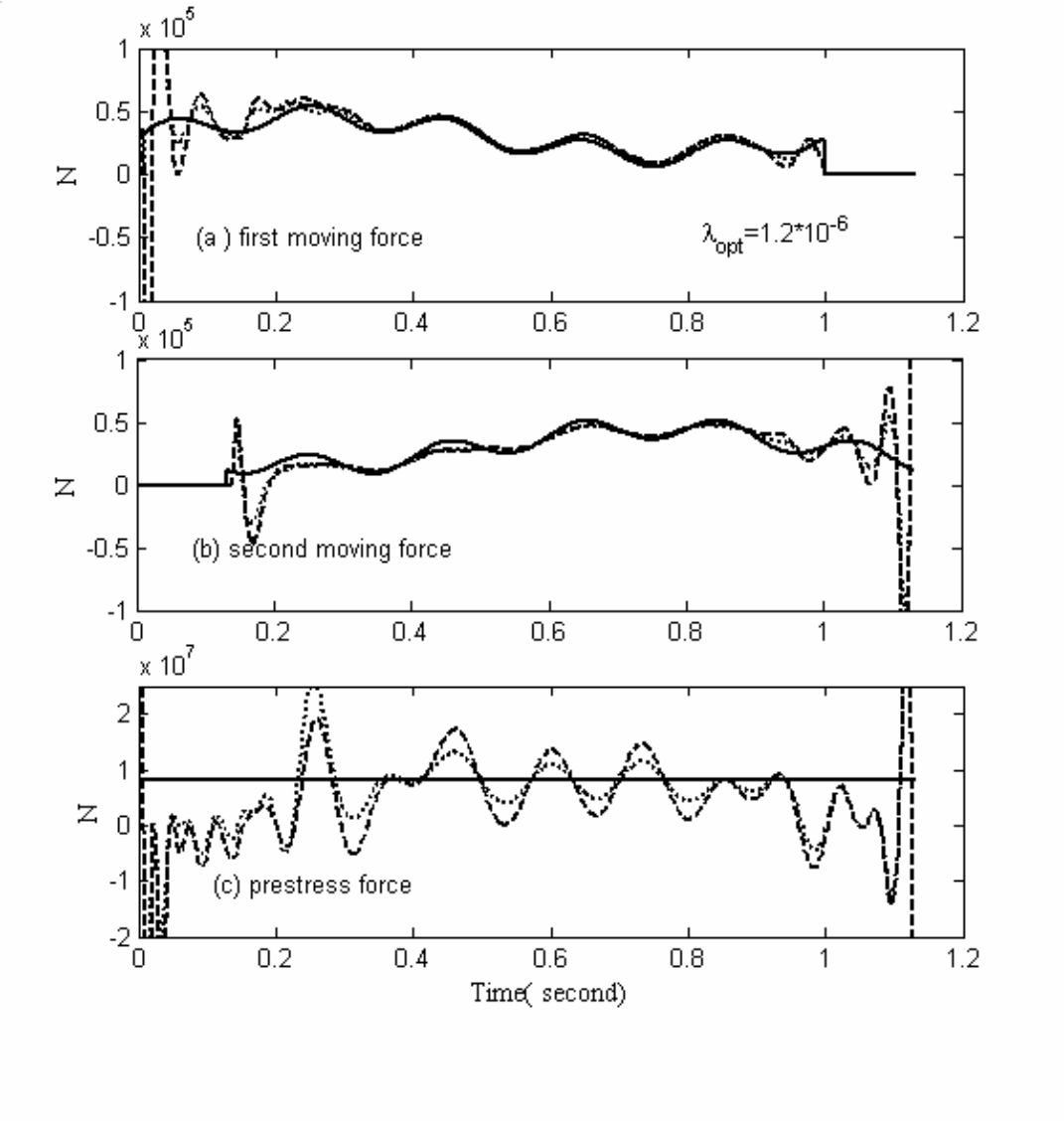

Figure 5-22 – Identification of two moving force and prestress force (__ True; … 5% noise; --- 10% noise)

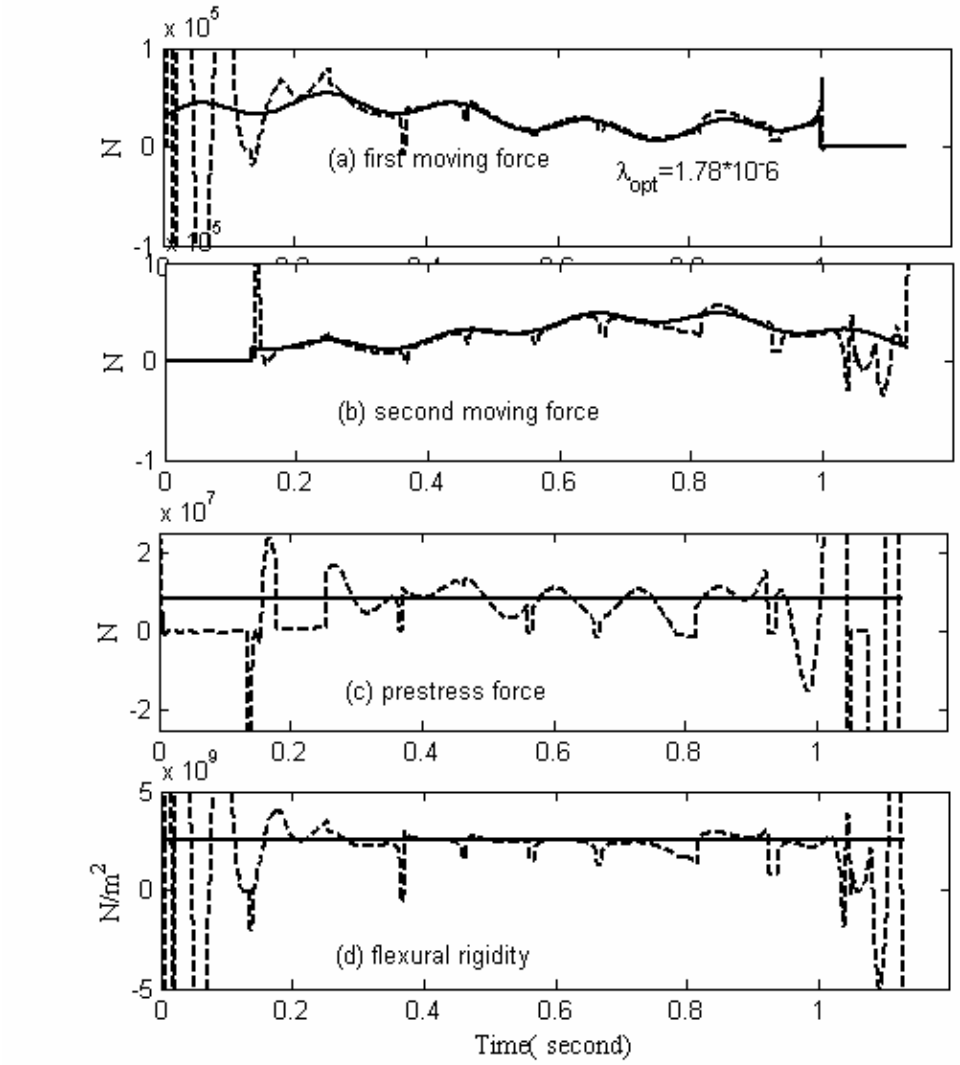

Figure 5-23 – Identification of two moving forces, prestress force and flexural rigidity of beam (__ True; --- Identified)

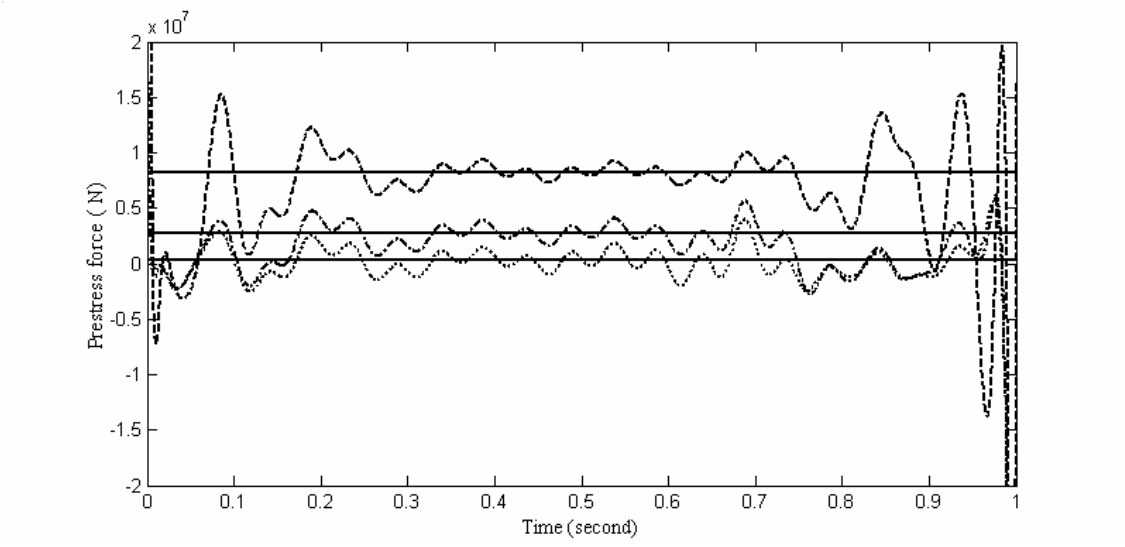

Figure 5-24 – Identification of different magnitude of prestress force

(__ True; --- $T = 0.3T_{cr}$; -.-.-. $T = 0.1T_{cr}$; … $T = 0.01T_{cr}$)

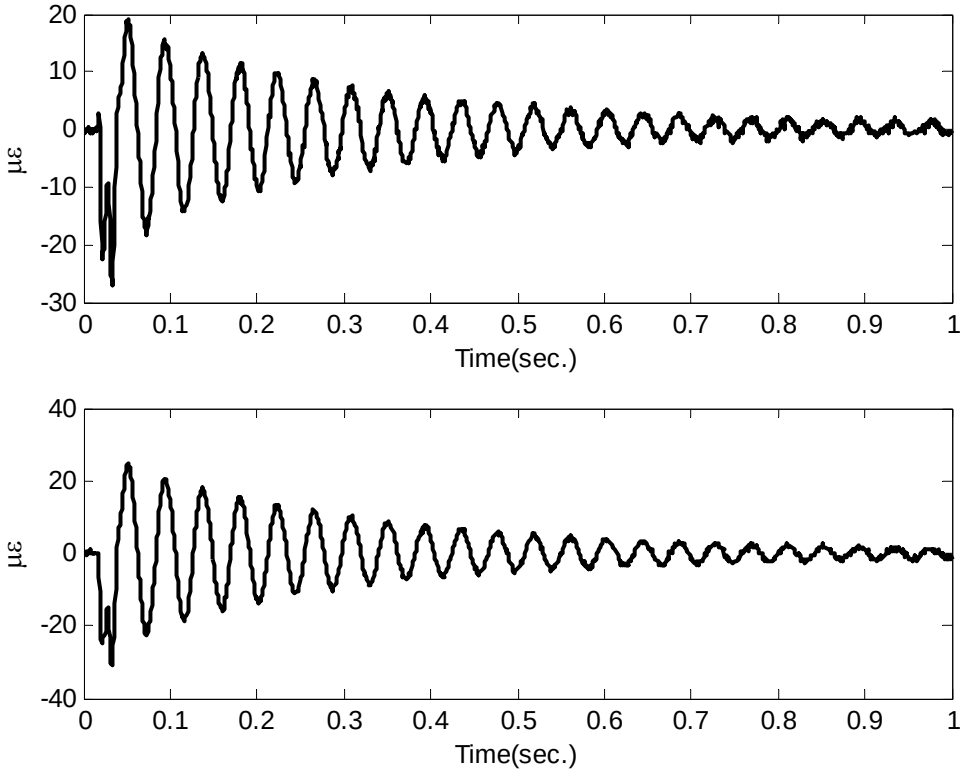

Figure 5-25 - Time histories of the measured two strains, (a) the 3rd; (b) the 4th

Chapter 6

CONCLUSIONS AND RECOMMENDATIONS

6.1 Conclusions on the Present Study

This dissertation aims to develop a simple, economical and yet sophisticated vibration-based evaluation procedure to assess damage as well as prestress force in existing structures using the measured structural dynamic responses. Some useful conclusions are drawn as shown in the following paragraphs.

A novel damage identification method based on dynamic response sensitivity is proposed in Chapter 3. The dynamic response sensitivities with respect to the physical parameters have been derived numerically. Only one response measurement is used for the updating of a large number of system parameters theoretically, because the plenty measured data in time domain can be used directly in the solution. When more measurements are taken in the identification, the identified results can be improved as shown in this chapter. The advantages of this approach for damage identification are: the number of measurements can be very small; the identification process is fast and the identified results are accurate; and finally, the number of identification equation can be adjusted according to the duration of time. And this indicates that the identification equation can always be over-determined. This method is further studied with other problems in the broad topic of damage assessment, such as, taking into account the temperature effect, differentiating different types of damage for structures consisting of isotropic material, identification of prestress force in prestressed concrete

structures and the identification of the system parameters including the load environment in Chapters 4.

In Chapter 5 Section 1, a method is proposed for crack identification in a beam structure. The crack with a constant depth is modeled with a Dirac delta function, and a method is proposed to identify the open crack in beam structures based on dynamic measurements in time domain. Only several displacement or strain measurements and the first few vibration modes of the beam are required in the crack identification. Computation simulations using sinusoidal and impulsive excitations on a beam with a single crack show that the method is effective to identify cracks and is more accurate than the method by Sinha et al. (2002) from polluted measurements.

Chapter 5 Section 2 proposed a method based on modal superposition in combination with optimization and regularization methods to identify the prestress force in time domain. The prestress force in a beam has been identified successfully with or without including the flexural rigidity of the beam in the inverse analysis whereas many other methods based on modal frequencies fail. And the proposed method can be further extended to identify both moving force and prestress force simultaneously. Identification of prestress force based on the response sensitivity method is also included in this section. The presented work indicates that indirect measurement of the prestress force in a beam is feasible.

As a conclusion, the major contribution of this desertation lies in: the dynamic response sensitity with respect to system parameters has been derived numerically and analytically. And the response sensitivity-based finite element updating is used for damage and prestress force identification. The proposed method can take into account the temperature effect in the identification which is neglected by other existing damage

detection methods. In this thesis, an iterative algorithm is proposed to identify structural damage including the load environment; both the excitation force and the structural damage can be identified successfully. The proposed method has been used successfully to beam structures, plane frame and space frame structures subjected to damage of different types. The presented method is not sensitive to measurement noise, modeling errors as shown in the numerical studies and the laboratory work, and thus, it has the potention for real application for damage and prestress force identification. Theoretically speaking, the methodology can be extended and applied to more complex structures. But how to successfully apply the method in a real structure is still difficult because a practical structure usually has a huge number of DOFs, and according to the number of unknowns, the measurement data sets requirement would be many times larger than what has been studied in this thesis.

6.2 Recommendations

Further studies related to the vibration-based damage and prestress force identification are recommended. The present work in this dissertation provides some exploratory experiences and suggestions in the following aspects:

1. The algorithm proposed for damage detection with the removal of temperature effect (Chapter 4, Section 1) was only validated by numerical simulations. An experimental verification or a real application to a large-scale civil engineering structure is needed for further verification.
2. The crack model proposed in Chapter 5 is assumed permanent open. However, in practice, the crack may open and close under the normal traffic. Therefore, it is

more practical to extend this time-invariant crack to time-variant crack model for further investigation.

3. With regards to long-term health monitoring of structures such as bridges, offshore platforms, etc., the need to reduce the dependence on measurable excitation forces should be noted. The ability to use the vibrations from ambient or operating loads for assessment of structural damage is an area that highly merits further research.

4. Theoretically, measurement from only one sensor is need for damage detection. But computation simulation shows that measurements from multiple sensor combinations will result not only in a reduction in iteration steps but also an improvement in the identified results. Therefore, the issues on optimal sensor number and the optimal sensor location for the damage detection worth further research.

5. In this dissertation, only the vibration of translational degree-of-freedom is used. Although it is still difficult to measure the vibration of rotational degree-of-freedom in most practical structures, it is suggested that both simulation study and the laboratory techniques to measure vibration of rotational degree-of-freedom and the related damage detection methods may worth further research.

6. The proposed method based on response sensitivity has been utilized for damage detection applications on skeletal structures (such as beams, plane frame and space frame) in this dissertation. Further investigations aim to extend this method for damage detection in plate-like structures are expected.

7. The proposed method based on response sensitivity has been utilized for both damage detection and prestress force identification in structures. Further

investigations should extend this approach to identify damage and prestress force simultaneously in prestressed structures.

8. In this dissertation, Rayleigh damping model is used. And the damping is assumed to remain unchanged before and after the damage occurrence. But in fact, the damping may change after the occurrence of damage; therefore, further research should identify the damping coefficients as well as the structural damage.

APPENDIX A

ELEMENTAL MASS MATRIX AND STIFFNESS MATRIX

Elemental Consistent Mass Matrix of 3-D Finite Element

$$m=\rho Al\begin{bmatrix}
1/3 & 0 & 0 & 0 & 0 & 0 & 1/6 & 0 & 0 & 0 & 0 & 0\\
0 & 13/35 & 0 & 0 & 0 & 11*l/210 & 0 & 9/70 & 0 & 0 & 0 & -13*l/420\\
0 & 0 & 13/35 & 0 & -11*l/210 & 0 & 0 & 0 & 9/70 & 0 & 13*l/420 & 0\\
0 & 0 & 0 & J/(3A) & 0 & 0 & 0 & 0 & 0 & J/(6A) & 0 & 0\\
0 & 0 & -11*l/210 & 0 & l^2/105 & 0 & 0 & 0 & -13*l/420 & 0 & -l^2/140 & 0\\
0 & 11*l/210 & 0 & 0 & 0 & l^2/105 & 0 & 13*l/420 & 0 & 0 & 0 & l^2/140\\
1/6 & 0 & 0 & 0 & 0 & 0 & 1/3 & 0 & 0 & 0 & 0 & 0\\
0 & 9/70 & 0 & 0 & 0 & 13*l/420 & 0 & 13/35 & 0 & 0 & 0 & -11*l/210\\
0 & 0 & 9/70 & 0 & -13*l/420 & 0 & 0 & 0 & 13/35 & 0 & 11*l/210 & 0\\
0 & 0 & 0 & J/(6A) & 0 & 0 & 0 & 0 & 0 & J/(3A) & 0 & 0\\
0 & 0 & 13*l/420 & 0 & -l^2/140 & 0 & 0 & 0 & 11*l/210 & 0 & l^2/105 & 0\\
0 & -13*l/420 & 0 & 0 & 0 & l^2/140 & 0 & -11*l/210 & 0 & 0 & 0 & l^2/105
\end{bmatrix}$$

Elemental Stiffness Matrix of 3-D Finite Element

$$k^e = \rho Al \begin{bmatrix}
EA/l & 0 & 0 & 0 & 0 & 0 & -EA/l & 0 & 0 & 0 & 0 & 0 \\
0 & 12EI_z/l^3 & 0 & 0 & 0 & 6EI_z/l^2 & 0 & -12EI_z/l^3 & 0 & 0 & 0 & 6EI_z/l^2 \\
0 & 0 & 12EI_y/l^3 & 0 & -6EI_y/l^2 & 0 & 0 & 0 & -12EI_y/l^3 & 0 & -6EI_y/l^2 & 0 \\
0 & 0 & 0 & GJ/l & 0 & 0 & 0 & 0 & 0 & -GJ/l & 0 & 0 \\
0 & 0 & -6EI_y/l^2 & 0 & 4EI_y/l & 0 & 0 & 0 & -6EI_y/l^2 & 0 & 2EI_y/l & 0 \\
0 & 6EI_z/l^2 & 0 & 0 & 0 & 4EI_z/l & 0 & -6EI_z/l^2 & 0 & 0 & 0 & 2EI_z/l \\
-EA/l & 0 & 0 & 0 & 0 & 0 & EA/l & 0 & 0 & 0 & 0 & 0 \\
0 & -12EI_z/l^3 & 0 & 0 & 0 & -6EI_z/l^2 & 0 & 12EI_z/l^3 & 0 & 0 & 0 & -6EI_z/l^2 \\
0 & 0 & -12EI_y/l^3 & 0 & 6EI_y/l^2 & 0 & 0 & 0 & 12EI_y/l^3 & 0 & 6EI_y/l^2 & 0 \\
0 & 0 & 0 & -GJ/l & 0 & 0 & 0 & 0 & 0 & GJ/l & 0 & 0 \\
0 & 0 & -6EI_y/l^2 & 0 & 2EI_y/l & 0 & 0 & 0 & 6EI_y/l^2 & 0 & 4EI_y/l & 0 \\
0 & 6EI_z/l^2 & 0 & 0 & 0 & 2EI_z/l & 0 & -6EI_z/l^2 & 0 & 0 & 0 & 4EI_z/l
\end{bmatrix}$$

APPENDIX B

THE ORTHOGONAL POLYNOMIAL FUCTION

$$G_1(t) = \frac{1}{\sqrt{\pi}},$$

$$G_2(t) = \sqrt{\frac{2}{\pi}}(\frac{2}{T}t - 1),$$

$$G_3(t) = \sqrt{\frac{2}{\pi}}(2(\frac{2}{T}t - 1)^2 - 1),$$

……

$$G_{j+1}(t) = 2(\frac{2}{T}t - 1)G_j(t) - G_{j-1}(t).$$

REFERENCES

A

Aalami, B.O.(2000) “Structural modeling of posttentioned members.” *Journal of Structural Engineering*, ASCE, **126**(2), 157-162.

Abdel, Wahab M., De Roeck, G. and Peeters (1999) “Parameterization of damage in reinforced concrete structures using model updating.” *Journal of Sound and Vibration*, **228**(4), 717-730.

Abdel Wahab, M. M. (2001). “Effect of modal curvatures in damage detection using model updating.” *Mechanical Systems and Signal Processing*, **15**(2), 439-445.

Abdo, M. A. B. and Hori, M. (2002). “A numerical study of structural damage detection using changes in the rotation of mode shapes.” *Journal of Sound and Vibration*, **251**(2), 227-239.

Abraham, O.N.L and Brandon, J.A.(1995). “The modeling of the opening and closure of a crack.” *Journal of Vibration and Accoustics* ASCE, **117**, 370-377.

Abraham, M.A., Park, S.Y. and Stubbs, N. (1995b). “Loss of prestress prediction on nondestructive damage location algorithms.” *SPIE, Smart Structures and materials*, Vol. 2446, 60-67.

Adams, R. D., Cawley, P., Pye, C. J. and Stone, B. J. (1978). “A vibration technique for non-destructive assessing the integrity of structures.” *Journal of Mechanical Engineering Science*, **20**, 93-100.

Araujo Dos Santos J.V., Mota Soares, C.M., Mota Soares, C.A. and Pana, H.L.G.(2000). “Development of a numerical model for the damage identification on composite plate structure.” *Composite Structures*, **48**, 59-65.

Arrunda, J.R.F., Sun, F. and Mitchell, L.D. (1992). “Spatial domain techniques for modal analysis using a laser Doppler velocimeter.” *Proceedings of the 10th IMAC*, 656-664.

B

Ballo, I.(1998) “Non-linear effects of vibration of a continuous transverse cracked slender shaft.” *Journal of Sound and Vibration*, **217**(2), 321-333.

Baruch. M. (1978). “Optimization procedure to correct stiffness and flexibility matrices using vibration tests.” *AIAA Journal*, **16**(11), 1208-1210.

Bathe, K. J. (1982). Finite Element Procedures in Engineering Analysis. Prentice Hall, New Jersey.

Berman, A. (1979). “Comment on ‘Optimal weighted orthogonalization of measured modes’.” *AIAA Journal,* **17**, 927-928.

Berman A. and Flannely, W. G. (1971). “Theory of incomplete models of dynamic structures.” *AIAA Journal*, **9**, 1481-1487.

Berman, A. and Nagy, E. J. (1983). “Improvement of large analytical model using test data.” *AIAA Journal,* **21**(8), 1168-1173.

Bicanic, N. and Chen, H.P.(1997). “Damage identification in framed structures using natural frequencies.” *International Journal for Numerical Methods in Engineering*, **40**, 4451-4468.

Biswas, M., Pandey, A. K. and Samman, M. M. (1990). “Diagnostic experimental spectral/modal analysis of a highway bridge.” *International Journal of Analytical and Experimental Modal Analysis*, **5**, 33-42.

Bovsunovsky, A.P. and Matveev, V.V.(2000)” Analytical approach to determination of dynamic characteristics of a beam with a closing crack.” *Journal of Sound and Vibration*, **235**(3), 415-434.

Brandon J.A. and Abraham O.N.L.(1995). “Counter-intuitive quasi-periodic motion in the autonomous vibration of cracked Timoshenko beams.” *Journal of Sound and Vibration*, **185**(3), 415-430.

Brandon, J.A. and Mathias, M.H. (1998). “Complex oscillatory behavior in a cracked beam under sinusoidal excitation.” *Journal of Sound and Vibration*, **186**(2), 350-354.

Brandon J.A., Stepheno A.E., Lopes E.M.O. and Kwan A.S.K.(1999). “Spectral indicators in structural damage identification: A case study.” *Proc. Instn. Mech. Engrs. Part C*, 213, 411-415.

Brock, J. E. (1968). “Optimal matrices describing linear systems.” *AIAA Journal*, **6**(7), 1292-1296.

Bueckner, H.F. (1958).“ The propagation of cracks and the energy of elstic deformation.” *Trans. ASME*, **80**, 1225-1229.

C

Carneiro, S.H.S. and Inman, D.J.(2002). “Continuous model for the transverse vibration of cracked Timoshenko beams.” *Journal of Vibration and Accoustics* ASME, **124**, 310-320.

Cattarius, J. and Inmanm D. J. (1997). “ Time domain analysis for damage detection in smart structures.” *Mechanical Systems and Signal Processing*, **11**(3), 409-423.

Cawley, P. and Adams, R. D. (1979). “The location of defects in structures from measurements of natural frequencies.” *Journal of Strain Analysis*, **14**(2), 49-57.

Chance, J., Tomlinson, G. R. and Worden, K. (1994). “A simplified approach to the numerical and experimental modeling of the dynamics of a cracked beam.” *Proceeding of the 12th International Modal Analysis Conference*, 778-785.

Chen, H.P. and Bicanic, N. (2000) “Assessment of damage in continuum structures based on incomplete modal information.” *Computers and Structures*, **74**, 559-570.

Chen J. and Li J.(2004). “Simultaneous identification of structural parameters and input time history from output-only measurements.” *Computational Mechanics*. **33**(5), 365-374.

Chen, J. C. and Garba, J. A. (1980). “Analytical model improvement using modal testing results.” *AIAA Journal*, 12(2), 684-690

Chen, J. C. and Garba, J. A. (1988). “On-orbit damage assessment for large space structures.” *AIAA Journal*, **26**(9), 1119-1126.

Chen, J. C. et al. (1983). “Direct structural parameter identification by modal test results.” *AIAA Paper*, 83-0812.

Cheng, S.M., Swamid, A.S. J., Wu, X.J. and Wallace, W. (1999). “Vibrational response of a beam with a breathing crack.” *Journal of Sound and Vibration*, **225**,201-208.

Chondros, T.G., Dimarogonas, A.D, and Yao, J.(1998). “A continuous cracked beam vibration theory.” *Journal of Sound and Vibration*, **215**(1), 17-34.

Christides, S. and Barr, A.D.S. (1984) “One-dimensional theory of cracked Bernoulli-Euler beams.” *International Journal of Mechanical Science*, **26(**11-12**)**, 639-648.

Cobb, R. G. and Liebst, B. S. (1997). “Structural damage identification using assigned partial eigenstructure.” *AIAA Journal*, **35**(1), 152-158.

Collins, J. D., Young, J. and Kiefling, L. (1972). “ Methods and applications of system identification in shock and vibration.” *Annual Meeting of ASME*, 45-71.

Collins, J. D., Hart, G. C., Hasselman, T. K. and Kennedy, B. (1974). “Statistical identification of structures.” *AIAA Journal*, **12**(1), 185-190.

Contursi, T., Messina, A. and Williams, E. J. (1998). “A multiple damage location assurance criterion based on natural frequency changes.” *Journal of Vibration and Control*, **4**(5), 619-633.

Cooley, J. W. and Tukey, J. W. (1965). “An algorithm for the machine calculation of complex Fourier series.” *Mathematics of Computation*, **19**, 297-301.

Creed, S. G. (1987). “Assessment of large engineering structures using data collected during in-service loading.” in *Structural Assessment: The Use of Full and Large Scale Testing* (edited by Garas, F. K., Clarke, J. K. and Armer, G. S. T.), Butterworths, London, 55-62.

Cunha, J.,Cogan, S. and Berthod, C. (1999). “Application of genetic algorithm for the identification of elastic constrains of composite materials form dynamic tests.” *International Journal for Numerical Methods in Engineering*, **45**, 891-900.

D

Dailey, R. L. (1988). “Eigenvector derivatives with repeated eigenvalues.” *AIAA Journal*, **27**, 486-491.

Dascotte, E. (1990). “Practical applications of finite element tuning using experimental modal data.” *Eighth IMAC*, 1032-1037.

Doebling, S. W. (1996). “Damage detection and model refinement using elemental stiffness perturbations with constrained connectivity.” *In Proc. Of the AIAA/ASME/AHS Adaptive Structures Forum*, 360-370, AIAA-96-1037.

Doebling, S. W., Farrar, C. R. and Prime, M. B. (1998). “A summary review of vibration-based damage identification methods.” *The Shock and Vibration Digest*, **30**(2), 91-105.

Doebling, S. W., Hemez, F. M., Peterson, L. D. and Farhat, C. (1997). “Improved damage location accuracy using strain energy-based model selection criteria.” *AIAA Journal*, **35**, 693-699.

Doherty, J. E. (1993). “Nondestructive evaluation.” *In Handbook on Experimental Mechanics, 2nd ed.*, New York: VCH; Bethel: Society for Experimental Mechanics, 527-556.

Drdacky, M. (1992). Lesons from Structural Failures: *Proceedings of the Second International Conference on Lessons From Structural Failures*, Telc [Czechoslovakia]: Aristocrat.

E

Eugene, J.O. and Andrew, S.D. (1995) Reinforced and prestressed concrete design - The complete process. New York: John Wiley & Sons.

F

Farrar, C. R., Doebling, S. W. and Nix, D. A. (2001). "Vibration-based structural damage identification." *Philosophical Transactions of the Royal Society of London Series A-Mathematical Physical and Engineering Sciences*, **359**(1778), 131-149.

Farrar, C.R. and Jauregui, D.V. (1996). "Damage detection algorithm applied to experimental and numerical modal data from the I-40 bridge." *Los Alamos National Lab report*, LA-13074-MS.

Fernandez-Saez, J., Ruvio, L. and Navarro, C. (1999). "Approximate calculation of the fundamental frequency for bending vibrations of cracked beams." *Journal of Sound and Vibration*, **225**(2), 345-352.

Farhat, C. and Hemez, F.M.(1993). "Updating finite element dynamic models using an element-by-element sensitivity methodology." *AIAA Journal*, **31**, 1702-1711.

Fox, C. H. J. (1992). "The location of defects in structures: a comparison of the use of natural frequency and mode shape data." *Proceeding of the 10th International Modal Analysis Conference*, 522-528.

Fox, R. L. and Kapoor, M. P. (1968). "Rates of Change of Eigenvalues and Eigenvectors." *AIAA Journal*, **6**, 2426-2429.

Friswell, M. I. (1989). "The adjustment of structural parameters using minimum variance estimatior." *Mechanical System and Signal Processing*, **3**, 143-155.

Friswell, M. I., Penny, J. E. T. and Wilson, D. A. L. (1994). "Using vibration data and statistical measures to locate damage in structures." *Modal Analysis: The*

International Journal of Analytical and Experimental Modal Analysis, **9**(4), 239-254.

Friswell, M. I. and Mottershead, J. E. (1995). *Finite element model updating in structural dynamics*, Kluwer Academic Publishers.

Fritzen, C. P., Jennewein, D. and Kiefer, T. (1998). "Damage detection based on model updating methods." *Mechanical systems and signal processing*, **12**(1), 163-186.

G

Grossman, D.T. (1982). "An automated technique for improving modal test/analysis correlation." *23rd Structural Dynamic and Material Conference*, **2**, 68-76.

Gudmundson, P. (1982). "Eigenfrequency changes of structures due to cracks, notches, or other geometrical changes." *J. Mech. Physics Solids*, **30**(5), 339-353.

Gudmundson, P. (1983). "The dynamic behaviour of slender structures with cross-sectional cracks." *Journal of Mechanics and Physics of Solids*, **31**(4), 329-345.

H

Haisty, B.S. and Springer, W.T. (1988) " A general beam element for use in damage assessment of complex structures." *Journal of Vibration and Acoustics* ASME, **110**(3), 389-394.

Hall, B. M. (1970). "Linear estimation of structural parameters from dynamic test data." *Proceedings of AIAA/ASME 11th Structures, Structural Dynamics, and Materials Conference*, 193-197.

Hansen, P.C. (1992). Regularization Tools---- A Matlab Package for Analysis and Solution of Discrete Ill-Posed Problem, Version 3.0.

Hassiotis, S. and Jeong, G.D. (1993). “Assessment of structural damage from natural frequency measurements.” *Computers and Structures*, **49**, 679-691.

Hemez, F. M. (1993). “Theoretical and experimental correlation between finite element models and modal tests in the context of large flexible space structures.” Ph.D. dissertation, University of Colorado, Boulder.

Hemez, F. M. and Farhat, C. (1995). “Structural damage detection via a finite element model updating methodology.” *Modal Analysis: The International Journal of Analytical and Experimental Modal Analysis*, **10**(3), 152-166.

Hern, G. and Testa, R. B. (1991). “ Modal analysis for damage detection in structures.” *Journal of Structural Engineering*, **117**(10), 3042-3063.

Hjelmstad, K.D.(1996). “On the uniqueness of modal parameter estimation.” *Journal of Sound and Vibration*, **192**. 581-598.

I

Ibrahim, A., Ismail, F. and Martin, H.R. (1987) “ Modelling of the dynamics of continuous beam including nonlinear fatigue crack.” *Journal of Analytical, Experimental Modal Analysis*, **2,** 76-82.

Ibrahim, A., Ismail, F and Martin, H. K. (1990). “Identification of fatigue cracks from vibrating testing.” *Journal of Sound and Vibration***, 140**, 305-317.

Irwin, G.R. (1957) “Analysis of stresses and strains near the end of a crack transversing a plate.” *Journal of Applied Mechanics*, **24,** 361-364.

J

Jahn, H. A. (1948). “Improvement of an Approximate Set of Latent Roots and Modal Columns of a Matrix by Methods akin to Those of Classical Perturbation Theory.” *Quarterly Journal of Mechanics and Applied Mathematics*, **1**, 132-144.

Jin, S., Livingston, R. A. and Marzougui, D. (2000). “Energy index approach for damage detection in nonlinear highway structures.” *Proceedings of SPIE - The International Society for Optical Engineering*, v3995, *Nondestructive Evaluation of Highways, Utilities, and Pipelines IV*, Newport Beach, CA, USA, 52-63.

Jones, D. R. H. (1998). Failure Analysis Case Studies: *a sourcebook of case studies selected from the pages of Engineering failure analysis 1994-1996*, Elsevier, Amsterdam.

Jones, D. R. H. (2001). Failure Analysis Case Studies II: *a sourcebook of case studies selected from the pages of Engineering failure analysis 1997-1999*, Elsevier, Amsterdam.

Joshi, A and Madhusudhan, B.S.(1991). “A unified approach to free vibration of locally damaged beams having various homogeneous boundary conditions.” *Journal of Sound and Vibration* **147**,475-488.

Jung, H. and Ewins, D. J. (1992). “Error Sensitivity of the Inverse Eigensensitivity Method for Model Updating.” *Proceedings of the 10th International Modal Analysis Conference, San Diego*, 992-998.

K

Kabe, A. M. (1985). “Stiffness matrix adjustment using mode data.” *AIAA Journal.* **23**(9), 1431-1436.

Kaouk, M. and Zimmerman, D. C. (1994a). “Assessment of damage affecting all structural properties.” *Proceedings of the 9th VPI and SU Symposium on Dynamics and Control of Large Structures*, 445-455.

Kaouk, M. and Zimmerman, D. C. (1994b). “Structural damage assessment using a generalized minimum rank perturbation theory.” *AIAA Journal*, **32**(4), 836-842.

Kaouk, M. and Zimmerman, D. C. (1994c). “Structural damage detection using measured modal data and no original analytical model.” *Proceedings of the 12th International Modal Analysis Conference*, 731-737.

Kaouk, M. and Zimmerman, D. C. (1995). “Structural health assessment using a partition model update technique.” *Proceedings of the 13th International Modal Analysis Conference*, 445-455.

Kashangaki, T. A. L., Smith, S. W. and Lim, T. W. (1992). “Underlying modal data issues for detecting damage in truss structures.” *Proceeding of the AIAA/ASME/ASCE/AHS/ASC/ 33rd Structures, Structural Dynamics, and Materials Conference*, Washington, D.C., AIAA paper 92-2264.

Kim, J. H., Jeon, H. S. and Lee, C. W. (1992). “Application of the modal assurance criteria for detecting and locating structural faults.” *Proceedings of the 10th International Modal Analysis Conference*, 536-540.

Kim, J.T. and Stubbs, N. (1995). “Model uncertainty impact and damage-detection accuracy in plate girder.” *Journal of Structural Engineering*, ASCE, **121**(10), 1409-1417.

Kim, J.T. and Stubbs, N. (2002). “Improved damage identification method based on modal information.” *Journal of Sound and Vibration*, **252(**2), 223-238.

Kim, J.T., Ryu, Y.S., Cho, H.M. and Stubbs, N. (2003). “Damage identification in beam-type structures: frequency-based method vs mode-shape-based method.” *Engineering Structures*, **25**, 57-67.

Kim, J.T., Yun C. B., Ryu, Y.S. and Cho, H.M. (2004). Identification of prestress-loss in PSC beams using modal information. *Structural Engineering and Mechanics*. **17**(3-4), 467-482.

Kisa, M., and Brandon, J.A. (2000). “ The effects of closure of cracks on the dynamics of a cracked cantilever beam.” *Journal of Sound and Vibration*, **238**, 1-18.

Kochersbergen, K., Mitchell, L.D. and Wicks, A. L. (1992). “ An efficient method for determining magnitude and phase from laser velocimeter.” *Proceedings of the 10th IMAC*, 375-381.

Koh, C. G., See, L. M. and Balendra, T. (1995). “Damage detection of buildings: numerical and experimental studies.” *Journal of Structural Engineering —ASCE*, **121**(8), 1155-1160.

Krawczuk, M and Ostachowitz, W.M. (1992) “ Parameteric vibrations of beam with crack.” *Archive of Applied Mechanics*, **62**(7), 463-473.

Krawczuk, M and Ostachowitz, W.M. (1993a) “Transverse natural vibration of a cracked beam loaded with a constant axial force.” *Journal of Vibration and Acoustics ASCE*, **115(**4), 428-524.

Krawczuk, M. (1993b). “A rectangular plate finite element with an open crack.” *Computers and Structures*, **46**, 487-493.

L

Lancaster, J. (2000). *Engineering catastrophes: Causes and effects of major accidents*, Abington Publishing and CRC Press.

Law, S. S., Chan, T. H. T. and Wu, D. (2001). “Efficient numerical model for the damage detection of large scale structure.” *Engineering Structures*, **23**, 436-451.

Law, S. S., Shi, Z. Y. and Zhang, L. M. (1998). “Structural damage detection from incomplete and noisy modal test data.” *Journal of Engineering Mechanics*, **124**(11), 1280-1288.

Law, S.S. and Zhu, X.Q.(2000). “Study on different beam models in moving force identification.” *Journal of Sound and Vibration* **234**,661-679.

Law, S.S. and Zhu, X.Q. (2004). “Damage detection in concrete bridge structures under moving vehicular loads.” *Journal of Vibration and Acoustics*, ASME, (under review).

Lee, I. W. and Jung, G. H. (1997). “An efficient algebraic method for the computation of natural frequency and mode shape sensitivities-Part II: Multiple natural frequencies.” *Computers and structures*, **62**(3), 437-443.

L

Li, J. and Chen, J.(1999). “A statistical average algorithm for the dynamic compound inverse problem.” *Computational Mechanics*, **30**(2), 88-95.

Lieven, N. A. J. and Ewins, D. J. (1988). “Spatial correlation of mode shapes, the Coordinate Modal Assurance Criterion (COMAC).” *Proceedings of the 6th International Modal Analysis Conference* **1**, 690-695.

Lifshiz, J. M. and Rotem, A. (1969). “Determination of reinforcement unbonding of composites by a vibration technique.” *Journal of Composite Materials*, **3**, 412-423.

Lim, K. B., Junkins, J. L. and Wang, B. P. (1987). “Ere-examination of eigenvector derivatives.” *Journal of Guidance, Control and Dynamics*, **10**(6), 581-587.

Lim, T. W. (1994). “Structural damage detection of a planar truss structure using a constrained eigenstructure assignment.” *Proceedings of the 35th AIAA/ASME/ASCE/AHS/ASC Structures, Structural Dynamics and Materials Conference*, AIAA-94-1715-CP, 336-346.

Lim, T. W. (1995). “Structural damage detection using constrained eigenstructure assignment.” *Journal of Guidance, Control, and Dynamics*, **18**(3), 411-418.

Lim, T. W. and Kashangaki, T.A.L. (1994). “Structural damage detection of space truss structure using best achievable eigenvectors.” *AIAA Journal,* **32**(5), 1049-1057.

Lin, C. S. (1990). “Location of model errors using modal test data.” *AIAA journal*, **28**, 1650-1654.

Lin, T.Y.(1963). Design of Prestressed Concrete Structures, John Wiley & Sons, USA.

Lin, R.M., Lim, M.K., and Du, H. (1995). “Improved inverse eigensensitivity method for structural analytical model updating.” *ASME Journal of Vibration and Acoustics*, **117,** 192-198.

Lindner, D. K. and Goff, R. (1993). “Damage detection. Location and estimation for space trusses.” *SPIE Smart Structures and Intelligent Systems: Smart Structures and Materials*, 1028-1039.

Ling, X. L. and Haldar, A. (2004). “Element level system identification with unknown input with Rayleigh damping.” *Journal of Engineering Mechanics*, ASCE, **130**(8), 877-885.

Liu, G.R. and Chen S.C.(2001). “Flaw detection in sandwich plates based on time-harmonic response using genetic algorithm.” *Computer Methods in Applied Mechanics and Engineering*, **190**, 5505-5514.

Liu, G.R. and Chen, S.C. (2002). “A novel technique for inverse identification of distributed stiffness factor in structures.” *Journal of Sound and Vibration* **254**(5), 823-835.

Livingston, R. A., Jin, S. and Marzougui, D. (2001). “Application of nonlinear dynamics analysis to damage detection and health monitoring of highway structures.” *Proceedings of SPIE - The International Society for Optical Engineering*, v4337, *Health Monitoring and Management of Civil Infrastructure Systems*, Newport Beach, CA, 402-410.

Lu, Q., Ren, G. and Zhao, Y. (2002). “Multiple damage location with flexibility curvature and relative frequency change for beam structures.” *Journal of Sound and Vibration*, **253**(5), 1101-1114.

M

Majumder, L. and Manohar, C. S. (2003). “ A time-domain approach for damage detection in beam structures using vibration data with moving oscillator as an excitation source.” *Journal of Sound and Vibration*, **268**, 699-716.

Matveer, V.V. and Bovsunousky, A.P. (2002) “ Vibration based diagnostics of fatigue damage of beam-like structures.” *Journal of Sound and Vibration*, **249**(1), 23-40.

Mayes, R. L. (1992). “Error localization using mode shapes: An application to a two link robot arm.” *Proceedings of the 10th International Modal Analysis Conference*, 886-891.

McGowan, P. E., Smith, S. W. and Javeed, M. (1990). “Experiments for locating damage members in a truss structure.” *Proceedings of the 2nd USAF/NASA Workshop on System Identification and Health Monitoring of Precision Space Structures*, 571-615.

Messina, A., Williams, E. J. and Contursi, T. (1998). “Structural damage detection by a sensitivity and statistical-based method.” *Journal of Sound and Vibration*, **216**(5), 791-808.

Messina, A., Jones, I. A. and Williams, E. J. (1996). “Damage detection and localization using natural frequency changes.” *Proceedings of conference on Identification in Engineering Systems*, Swansea, U. K., 67-76.

Minas, C. and Inman, D. J. (1990). “Matching finite element models to modal data.” *Transactions of the ASME, Journal of Vibration and Acoustics*, **112**(1), 84-92.

Miyamoto, A., Tei, K., Nakamura, H. and Bull, J. W. (2000), “Behavior of prestressed beam strngthed with external tendons.” *Journal of Structural Engineering*, ASCE, **126**(9), 1033-1044.

Morassi, A. and Rovere, N. (1997). “Localizing a notch in a steel frame from frequency measurements.” *Journal of Engineering Mechanics —ASCE*, 123(5), 422-432.

Mottershead, J. E. and Friswell, M. I. (1993). “Model updating in structural dynamics: a survey.” *Journal of Sound and Vibration*, **167**(2), 347-375.

Mottershead, J. E. and James, S. (1997). “ The modeling of a three-story aluminium space frame and updating of finite element parameter at joints.” *Proceedings of the Third International Conference on Modern Practice in Stress and Vibration* Analysis, Dublin, Ireland. 227-232.

N

Narkis, Y. (1994) " Identification of crack location in vibrating simply supported beams." *Journal of Sound and Vibration*, **172**(4), 549-558.

Nelson, R. B. (1976). "Simplified calculations of eigenvector derivatives." *AIAA Journal* **14**, 1201-1205.

Neild, S.A.(2001). "Using non-linear vibration technique to detect damage in concrete bridges." Ph. D dissertation, University of Oxford, Department of Engineering Science, United Kingdom.

Neild, S.A., Mcfadden, P.D. and Williams, M.S. (2001) "A discrete model for a vibrating beam using a time-stepping approach." *Journal of Sound and Vibration*, **239**(1),99-121.

Newmark, N.W. (1959). "A method of computation for structural dynamics." *Journal of Engineering Mechanics Division* ASCE. **85**(3), 67.

O

Ostanchowicz, W. and Krawczuk, M. (1990) " Vibration analysis of cracked beam." *Computers and Structures*, **36**, 245-250.

Ostanchowicz, W. and Krawczuk, M. (1991) "Analysis of the effects of cracks on the natural frequencies of a cantilever beam." *Journal of Sound and Vibration*, **36**, 245-250.

Owen, J.S., Tan, C.M. and Choo, B.S.(2002) "Empirical model of the non-linear vibration of cracked reinforced concrete beams." *Proceedings of 1st European Workshop on Structural Health Monitoring*, Paris, France, 195-202.

P

Pandy, A. K. and Biswas, M. (1995). “Experimental verification of flexibility difference method for locating damage in structures.” *Journal of Sound and Vibration*, **184**(2), 311-328.

Pandy, A. K. and Biswas, M. (1994). “ Damage detection in structures using changes in flexibility.” *Journal of Sound and Vibration*, **169**(1), 3-17.

Pandy, A. K., Biswas, M. and Samman, M. M. (1991). “Damage detection from changes in curvature mode shapes.” *Journal of Sound and Vibration*, **145**(2), 321-332.

Penny, J. E. T., Wilson, D. and Friswell, M. I. (1993). “Damage location in structures using vibration data.” *Proceedings of the 11th International Modal Analysis Conference* **1**, 861-867.

Pothisiri, P and Hjelmstad, K. D. (2002). “Strategy for finding a near-optimal measurement set for parameter estimation from modal response.” *Journal of Sound and Vibration*, **257**(1), 89-106.

Q

Qian, G.L., Gu, S.N. and Jiang, J.S. (1990). “ The dynamic behavior and crack detection of a beam with a crack.” *Journal of Sound and Vibration*,**138**(2), 233-243.

R

Raghavendrachar, M. and Aktan, A.E. (1992). “Flexibility of multi-reference impact testing for bridge diagnostics.” *Journal of Structural Engineering* **118**, 2186-2203.

Ratcliffe, C. P. (1997). “Damage detection using a modified Laplacian operator on mode shape data.” *Journal of Sound and Vibration*, **204**(3), 505-517.

Rizos, P. F., Aspragathos, N. and Dimarogonas, A. D. (1990). “Identification of crack location and magnitude in a cantilever from the vibration modes.” *Journal of Sound and Vibration*, **138**(3), 381-388.

Rodden, W. P. (1967). “A method for deriving structural influence coefficients from ground vibration tests.” *AIAA Journal*, **5**, 991-1000.

Ross, R. G. Jr. (1971). “Synthesis of stiffness and mass matrices from experimental vibration modes.” *SAE Conference paper* 710787, 2627-2635.

Rytter, A. (1993). *Vibration based inspection of civil engineering structures*, Doctoral Dissertation, Department of Building Technology and Structural Engineering, University of Aalborg.

S

Saiidi, M., Douglas, B. and Feng. S. (1994). “Prestress Force Effect on Vibration Frequency of Concrete Bridges.” *Journal of Structural Engineering*, ASCE, **120(7),** 2233-2241.

Saiidi, M., Shield, J., O’Connor, D. and Hutchens, E. (1996). “Viriation of prestress force in a prestressed concrete bridge during the first 30 months.” *PCI Journal*, **41**(5), 66-72.

Saiidi, M., Hutchens, E., and Gardella, D. (1998). “Bridge prestress losses in dry climate.” *Journal of Bridge Engineering*, ASCE, **3**(3), 111-116.

Salawu, O. S. (1997a). “Detection of structural damage through changes in frequency: A review.” *Engineering Structures*, **19**(9), 718-723.

Salawu, O. S. (1997b). “An integrity index method for structural assessment of engineering structures using modal testing.” *Insight: The journal of the British Institute of Non-Destructive Testing*, **39**(1).

Salawu, O. S. (1995). “Non-destructive assessment of structures using the integrity index method applied to a concrete highway bridge.” *Insight: The journal of the British Institute of Non-Destructive Testing*, **37**(1), 875-878.

Salawu, O. S. and Williams, C. (1994). “Damage location using vibration mode shapes.” *Proceedings of the 12th International Modal Analysis Conferencd*, 933-939.

Sanayei, M. and Onipede, O. (1991). “Damage assessment of structures using static test data.” *AIAA Journal*, **29**(7), 1174-1179.

Sanayei, M. and Saletnik, M. J. (1996a) “Parameter estimation of structures from static strain measurements, Part I: Formulation.” *Journal of Structural Engineering, ASCE*, **122**(5), 555-562.

Sanayei, M. and Saletnik, M. J. (1996b) “Parameter estimation of structures from static strain measurements, Part II: Error sensitivity analysis.” *Journal of Structural Engineering, ASCE*, **122**(5), 563-572.

Schultz, M.J., Pai, P.F. and Abdelnaser, A.S. (1996). “ Frequency response function assignment technique for structural damage identifiction.” *In Proc. of the 14th International Modal Analysis Conference*, 105-111.

Seibold, S. and Weinert, K. (1996). “ A time domain method for the localization of cracks in rotors.” *Journal of Sound and Vibration*, **195**(1), 57-73.

Shen, M.H.H. and Chu, Y.C. (1992). “Vibration of beams with a fatigue crack.” *Computers and Structures*, **45**(1), 79-93.

Shen, M. H. H. and Pierre, C. (1990). “Natural modes of Bernoulli-Eiler beams with symmetric cracks.” *Journal of Sound and Vibration*, **138**,115-134.

Shen M.H.H. and Pierre C. (1994). “ Free-vibrations of beams with a single-edged crack.” *Journal of Sound and Vibration*, **170(**2), 237-259.

Shi, T. H., Jones, N. P. and Ellis, J. H.(2000). “Simultaneous estimation of system and input parameters from output measurements.” *Journal of Engineering Mechanics*, ASCE, **126**(7), 746-753.

Shi, Z. Y., Law, S. S. and Zhang, L. M. (1998). “Structural damage localization from modal strain energy change.” *Journal of Sound and Vibration*, **218**(5), 825-844.

Shi, Z. Y., Law, S. S. and Zhang, L. M. (2000a). “Damage location by directly using incomplete mode shapes.” *Journal of Engineering Mechanics*, **126**(6), 656-660.

Shi, Z. Y., Law, S. S. and Zhang, L. M. (2000b). “Structural damage detection from modal strain energy change.” *Journal of Engineering Mechanics*, **126**(12), 1216-1223.

Shi, Z. Y., Law, S. S. and Zhang, L. M. (2002). “Improved damage quantification from elemental modal strain energy change.” *Journal of Engineering Mechanics*, **128**(5), 521-529.

Shifrin, E.I. and Ruotolo, R. (1999) “ Natural frequencies of a beam with an arbitrary number of cracks.” *Journal of Sound and Vibration*, **222**(3), 409-423.

Sinha, J. K., Friswell M. I. and Edwards S. (2002). “Simplified models for the location of cracks in beam structures using measured vibration data.” *Journal of Sound and Vibration*, **251**(1), 13-38.

Skjaeraek, P. S., Nielsen, S. R. K. and Cakmak, A. S. (1996). “Identification of damage in reinforced concrete structures from earthquake records: Optimal location of sensors.” *Soil Dynamics and Earthquake Engineering*, **15**(6), 347-358.

Smith, S. W.(1992). “Iterative use of direct matrix updates: connectivity and convergence. ” *Proc. Of 33rd AIAA Structures, Structural Dynamics and Materials Conference*, 1797-1806.

Smith, S. W. and Beattie, C. A. (1991). “Model correlation and damage location for large space truss structures: Secant method development and evaluation.” *NASA Report* NASA-CR-188102.

Stubbs, N. and Kim, J. T. (1996). “Damage localization in structures without baseline modal parameters.” *AIAA journal*, **34**(8), 1644-1649.

Stubbs, N., Kim, J. T. and Topole, K. (1992). “An efficient and robust algorithm for damage localization in offshore platforms.” Proceedings of the ASCE 10th Structures Congress, 543-546.

Stubbs, N. and Osegueda, R. (1990). “Global damage detection in solids: Experimental verification.” *Modal analysis: The International Journal of Analytical and Experimental Modal Analysis*, **5**(2), 81-97.

Sundermeyer, J.N. and Weaver, R.L. (1995). “On crack identification and characterization in a beam by nonlinear vibration analysis.” *Journal of Sound and Vibration*, **183** (5), 857-871.

T

Tada, H., Paris, P.C. and Olmstead, J.L.D. (1985) The Stress Analysis of Cracks Handbook. Del Research Corporation, Hellertown, Pennsylvania, U.S.A.

Tarantola, A.(1987). *Inverse Problem Theory – methods for data fitting and model parameter estimation.* Elsevier Science Publishers B.V., Netherlands.

Ting, T. (1992). “Accelerated sub-space iteration for eigenvector derivatives.” *AIAA Journal*, **30**(8), 2114-2118.

Tikhonov, A.M. (1963). “On the solution of ill-posed problems and the method of regularization.” *Soviet Mathematics*, **4**, 1035-1038.

Toksoy, T. and Aktan, A. E. (1995), “Bridge-condition assessment by modal flexibility.” *Workshop on Instrumentation and Vibration Analysis of Highway Bridges*, University of Cincinati, Ohio.

Topole, K. G. and Stubbs, N. (1995). “Nondestructive damage evaluation of structure from limited modal parameters.” *Earthquake Eng. Struct. Dyn.* **24**(11), 1427-1436.

Topole, K. G. and Tzvetkova, G. (1996). “Damage detection of highly nonlinear structures from response measurements.” *Proceedings of SPIE (V2719): Smart Structures and Materials 1996: Smart Systems for Bridges, Structures, and Highways*, San Diego, CA, USA, 170-179.

Tracy, K. G. and Pardoen, G. C. (1989). “Effect of delamination on the natural frequencies of composite laminates.” *Journal of Composite Materials*, **23**, 1200-1215.

Tse, F.S., Morse, I.E. and Hinkle, R.T. (1978). *Mechanical Vibrations, Theory and Applications*. Allyn and Bacon, Inc. Boston, Mass.

U

Uzgider, Z., Sanli, A.K., Piroglu, F. and Caglayan, D.B. (1993). " Identification of railway bridges using locomotive-induced vibrations." *Bridge Management,* **2**, 833-841, London: Thomas Telford.

V

Van De Abeele K. and De Visscher, J.(2000). "Damage assessement in reinforced concrete using spectral and temporal nonlinear vibration techniques." *Cement and Concrete Research*, **30**, 1453-1464.

Vanlanduit, S., Parloo, E., Guillaume, P. and De Vos, W. (2002). "Validation of on-line linear and nonlinear fatigue crack detection techniques." *Proceedings of 1st European Workshop on Structural Health Monitoring*, Paris, France, 219-226.

Viola, E., Nobile, L. and Federici, L. (2002). " Formulation of cracked beam element for structural analysis." *Journal of Engineering Mechanics* ASCE, **128**(2), 220-230.

W

Wang, W. and Zhang, A. (1987). "Sensitivity analysis in fault vibration diagnosis of structures." *Proceedings of the 5th International Modal Analysis Conference*, 496-501.

West, W. M. (1984). "Illustration of the use of modal assurance criterion to detect structural changes in an orbiter test specimen." *Proceedings of the Air Force Conference on Aircraft Structural Integrity*, 1-6.

Westmann, R.A. and Yang, W.H. (1967) "Stress analysis of cracked rectangular beams." *Journal of Applied Mechanics,* **32**, 693-701.

Williams, E. J., Contursi, T. and Messina, A. (1996). "Damage detection and localization using natural frequencies sensitivity." *Proceedings of Conference on Identification in Engineering Systems*, Swansea, U. K., 368-376.

Wu, D. and Law, S. S. (2004a). “Damage Localization in Plate Structures from Uniform Load Surface Curvature.” *Journal of Sound and Vibration*. **276**(1-2), 227-244.

Wu, D. and Law, S. S. (In press). “Sensitivity of ULS Curvature for Damage Identification in Plate Structures.” *Journal of Vibration and Acoustics*.

Wu, D. and Law, S. S. (2004c). “Model error correction from truncated modal flexibility sensitivity and generic parameters. I: Simulation” *Mechanical System and Signal Processing*, **18**(6), 1381-1399.

Wu, D. and Law, S. S. (2004d). “Model error correction from truncated modal flexibility sensitivity and generic parameters. II: Experimental Verification” *Mechanical System and Signal Processing*, **18**(6), 1401-1419

Wu, D. and Law, S. S. (2004). “Anisotropic damage model for an inclined crack in thick plate and sensitivity study for its detection.” *International Journal of Solids and Structures*. **41**(16-17), 4321-4336.

Wu, D. and Law, S. S., (2002). “Differentiating structural damage using truncated modal flexibility.” *Proceedings of the 2nd International Conference on Structural Stability and Dynamics*, Singapore, 749-754.

Y

Yu, M., Liu, Z. S. and Wang, D. J. (1996). “ Comparison of several approximate modal methods for computing mode shape derivatives.” *Computers and Structures*, **62**(2), 381-393.

Yuen, M. M. F. (1985). “A numerical study of the eigen-parameters of a damaged cantilever.” *Journal of sound and Vibration*, **103**, 301-310.

Z

Zak, M. (1983). “Discrete model improvement by eigenvector updating.” *Journal of Engineering Mechanics, ASCE*, **109**(6), 1437-1444.

Zhang, K. Y., Gu, A. J. and Li, J. W. (1992). “Diagnosis of a slot fault on a frame structure.” *Proceedings of 10th International Modal Analysis Conference* **1**, San Diego, California, 549-553.

Zhang, K. Y., Cheng, L. J. and Jin, T. X. (1993). “Research on the diagnosis of defect on a building foundation piles.” *Proceedings of 11th International Modal Analysis Conference* **1**, Kissimmee, Florida, 690-695.

Zhang, Q., Lallement, G., Fillod, R. and Piranda, J. (1987). “A Complete Procedure for the Adjustment of a Mathematical Model from the Identified Complex Modes.” *Proceedings of the 5th International Modal Analysis Conference*, London, U.K., 1183-1190.

Zhang, W.Z. and Testa, R.B. (1999) “Closure effects on fatigue crack detection.” *Journal of Engineering Mechanics* ASCE, **125**(10), 1125-1132.

Zhang, Z and Aktan A. E. (1998). “Application of modal Flexibility and its derivatives in structural identification.” *Research in Nondestructive Evaluation*, **10**(1), 43-61.

Zhang, Z. and Aktan, A. E. (1995). “The damage indices for constructed facilities.” *Proceedings of the 13th International Modal Analysis Conference*, 1520-1529.

Zhao, J., and Dewolf, J. T. (1999). “Sensitivity Study for Vibrational Parameters Used in Damage Detection.” *Journal of Structural Engineering*, **125**(4), 410-416.

Zimmerman, D. C. and Kaouk, M. (1992). “Eigenstructure assignment approach for structural damage detection.” *AIAA Journal*, **30**(7), 1848-1855.

Zimmerman, D. C. and Kaouk, M. (1994). “Structural damage detection using a minimum rank update theory.” *Journal of Vibration and Acoustics*, **116**, 222-230.

Zimmerman, D. C., Kaouk, M. and Simmermacher, T. (1995). “Structural damage detection using frequency response functions.” *Proceedings of the 13th International Modal Analysis Conference*, 179-184.

Zimmerman, D. C. and Widengren, M. (1990). “Correcting finite element models using a symmetric eigenstructure assignment technique.” *AIAA Journal*, **28**(9), 1670-1676.

Zimmerman, D. C. and Smith, S.W. (1992). “Model refinement and damage location for intelligent structures.” *Intelligent Structural Systems*. Tzou, H.S. and Anderson, G.L. Eds., Kluwer Academic Publishers, 403-452.